BORISLAV GEORGIEV PENEV

ADVANCED TWO-DIMENSIONAL PROPORTIONAL-DERIVATIVE COMMAND TO LINE-OF-SIGHT GUIDANCE LAWS

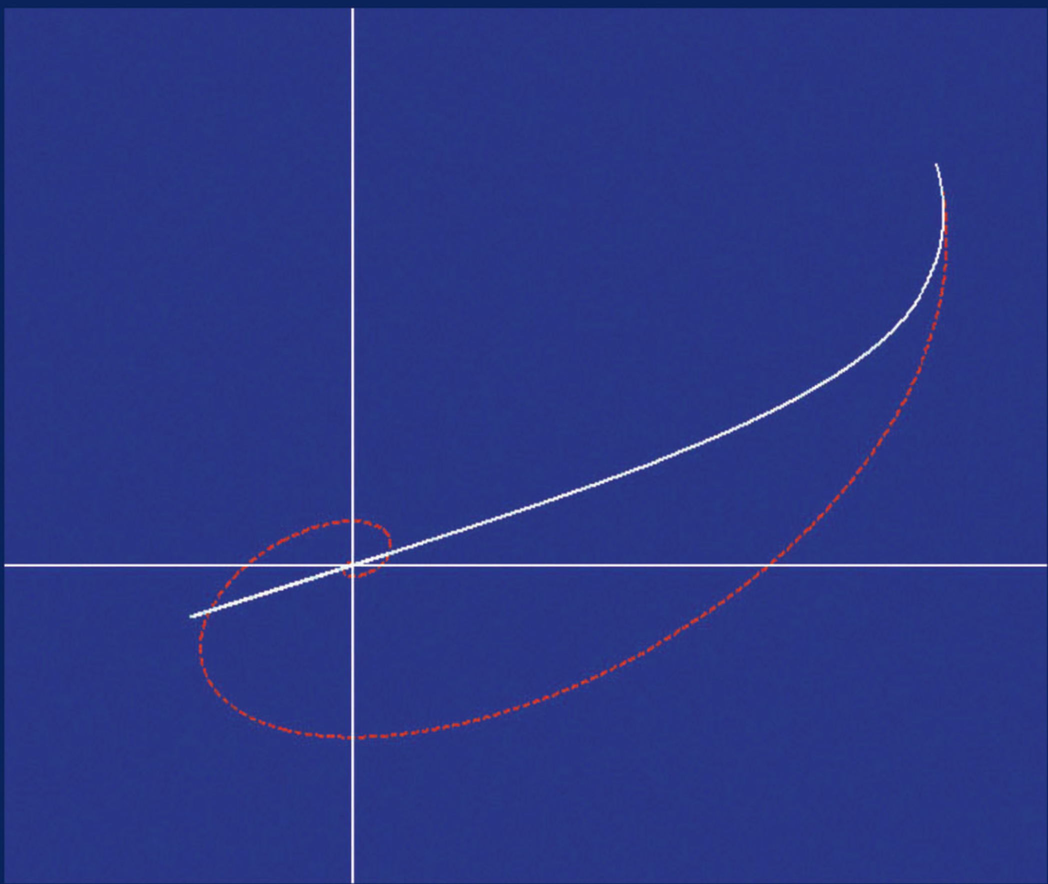

IIIT ACADEMIC PUBLISHING HOUSE

PLOVDIV

2021

BORISLAV GEORGIEV PENEV

ADVANCED TWO-DIMENSIONAL PROPORTIONAL-DERIVATIVE COMMAND TO LINE-OF-SIGHT GUIDANCE LAWS

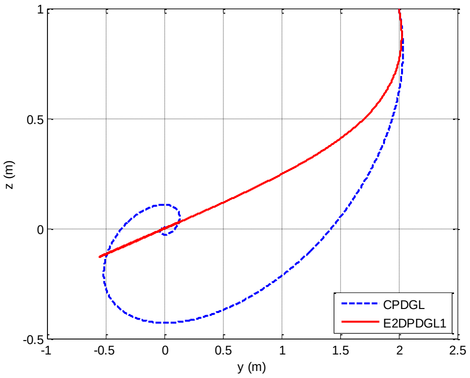

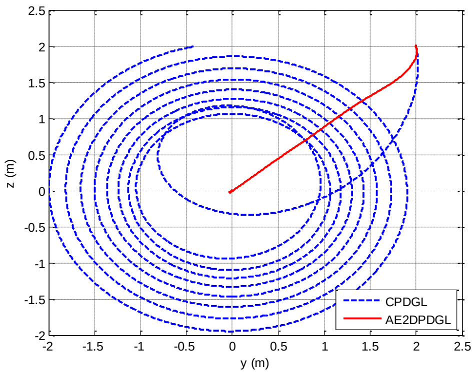

IIIT ACADEMIC PUBLISHING HOUSE
INSTITUTE OF INFORMATICS AND INNOVATIVE TECHNOLOGIES
PLOVDIV
2021

First published 2021

by the Academic Publishing House of the Institute of Informatics and Innovative Technologies - IIIT Academic Publishing House.

Institute of Informatics and Innovative Technologies – IIIT

14, Valko Shopov St., Plovdiv 4023, BULGARIA, http://iiit.bg

Author: Borislav Georgiev Penev, Assoc. Prof. PhD, email: bpenev@tu-plovdiv.bg

Monograph's title: Advanced Two-Dimensional Proportional-Derivative Command to Line-of-Sight Guidance Laws

There is usually seen a trajectory not lying on a straight line but a spiral type trajectory in the plane perpendicular to the line-of-sight (LOS) called also the picture plane during the transient process of putting a command to line-of-sight (CLOS) anti-tank guided missile (ATGM) from the initial deviations in both vertical and horizontal planes onto the LOS implementing the CLOS guidance even though the target is non-maneuvering. This occurrence worsens the performance indicators of the ATGM system. In order to modernize the synthesis of the classical spatial closed loop guidance and control systems with new guidance laws which overcome the classical immutable but unfavorable characteristics a set of several new nonlinear guidance laws has been developed. The new guidance laws fight effectively the spiraling trajectories in the picture plane due to the phase coupling between the horizontal and vertical channels and/or existence of non-proportional to each other initial conditions. They improve drastically the performance of the spatial closed loop guidance and control system and provide theoretically established system stability.

ISBN 978-619-91382-1-2 (papersoft)

ISBN 978-619-91382-2-9 (ebook)

The monograph is published upon the decision of the extended council of the Department of Systems and Control of the Faculty of Automatics of the Technical University - Sofia taken on June 10, 2021.

Reviewed by:

1. Prof. Dr. Petko Hristov Petkov, PhD and DSc;
2. Prof. Dr. Chavdar Ivanov Damyanov, PhD and DSc;
3. Assoc. Prof. Dr. Valentin Nenkov Penev, PhD.

ACKNOWLEDGEMENTS

I would like to express my gratitude to my long-term friends – Professor Dr. Habil. Nicolai Christov and Associated Professor Dr. Dimitar Penev, PhD, who have encouraged my perseverance in finalizing this project.

Thank you to Kayla Friedman and Malcolm Morgan of the Centre for Sustainable Development, University of Cambridge, UK for producing the Microsoft Word thesis template used to produce this document.

This monograph is peer reviewed. Thank you to the reviewers Prof. Dr. Petko Petkov, PhD and DSc, Prof. Dr. Chavdar Damyanov, PhD and DSc, and Assoc. Prof. Dr. Valentin Penev, PhD, for their excellent suggestions for improving this manuscript.

CONTENTS

1 INTRODUCTION

1.1 General problem statement and formulation

The command to line-of-sight (CLOS) guidance, also called three-point guidance, is a classical guidance method [1] (Chap. 8, 8-3, 8-4, pp. 273-284), [2] (Chap. 2, § 2.2, pp. 76-82), [3] (Chap. 4, 4.2.2, pp. 162-174), and [4] (Chap. 2, pp. 11-46). The simplicity of the idea of CLOS guidance to keep by a closed loop system the missile as closely as possible to the line-of-sight (LOS) joining the ground tracker and the target is implemented in many anti-tank guided missile (ATGM) systems. In [5] it is mentioned that “the performance of CLOS guidance for short range engagements is known to be typically good” but the improvement of the CLOS guidance law techniques and control schemes in order to achieve better performance meeting the contemporary challenges drives the research flow in this field. As mentioned also there “Recent advances in beam-pointing technology have led to renewed interest in CLOS guidance”.

Let us consider from the above point of view an occurrence which worsens the performance indicators of a CLOS ATGM guidance and control system. There is seen usually a trajectory not lying on a straight line but a spiral type trajectory in the plane perpendicular to the LOS, i.e. in the picture plane represented in Figure 1.1, which corresponds to Fig. 2.5 in [2], or the $Y_L Z_L$-plane represented in Figure 1.2 corresponding to Fig. 2 in [5], during the transient process of putting the ATGM from the initial deviations in both vertical and horizontal planes onto the LOS implementing the CLOS guidance even though the target is non-maneuvering. The design of the ATGM guidance and control system based on symmetric channels for control in vertical and horizontal planes is aimed at eliminating the vertical and horizontal deviations respectively in the plane perpendicular to the LOS. Despite taking into consideration the cross-coupling between the two orthogonal channels, the proposed design does not eliminate the spiral type trajectory. Furthermore, this pattern is observed even in the case of ideal and symmetric decoupled control channels. Thus it appears that the traditionally acclaimed application of two identical guidance laws for each pitch and yaw channel does possess the immutable spiral type trajectory characteristic. It further makes sense how to enhance the traditionally implemented guidance laws in order to fight successfully this occurrence in a way which also enables an easy practical realization. In [6], [7], and [8] some techniques to deal with this occurrence employing the polar coordinates and a kind of pseudo-polar coordinates are proposed. The features of the approach include forming the guidance law based on polar or the pseudo-polar presentations of the vector pointing the missile position in the plane perpendicular to the LOS, a feedback linearization there, and proportional-derivative (PD) control regarding the polar radius in [6] or the pseudo-polar radius in [7] and [8]. This enables a spatial guidance and control closed loop system organized in a new way with decoupled new control channels. The accepted there approach faces up theoretical issues but shows promising simulation results. So the goal is to keep the core of the original idea for a spatial CLOS guidance law synthesis in polar coordinates but to overcome the obstacles imposed by the initially accepted approach.

1.2 Survey of the field of the CLOS guidance laws synthesis

The survey of the field of the CLOS guidance laws synthesis shows an enormous number of papers. There could be seen the strong position of the Journal of Guidance, Control, and Dynamics. The intensive researchers' activity involves powerful modern control theory techniques from the fields of the back-stepping control, predictive control, adaptive control, feedback linearization, optimal control, fuzzy logic control, fuzzy sliding mode control, game theory approach, and etc. to deal with different engagement scenarios including also highly maneuvering targets [9] for overcoming specific disadvantages of the CLOS guidance and to improve the performance of the CLOS based systems [5], [9], [10], [11], [12], [13], [14], [15], [16], [17], [18], [19], [20], [21], [22], [23], and [24].

In [10] a CLOS guidance law based on an adapted to the guidance predictive control law is proposed. A predictive functional control for the midcourse phase and a predictive functional control for the terminal phase of the guidance are described. The authors mention the better performance of the proposed control techniques in comparison with the classical proportional-integral-derivative control with regard to the relative miss distance in engagement scenarios with a different types of maneuvering targets where “the superiority of the predictive guidance control is obvious in the case of fast maneuvering targets”, especially by adding the terminal phase control. The assumptions made include treating of the guidance problem “in two independent planes by neglecting cross-coupling between the two orthogonal components” and a relative simple internal model for the predictive law “constituted from a transfer function which represents very approximatively the missile for a given flight time, the total time delay in the guidance loop and a double integration” where “the parameters are considered time invariant”.

A CLOS guidance law is obtained by feedback linearization in [5] and further developed in [11]. In [5] the authors mention that “the key idea lies in converting the three-dimensional CLOS guidance problem to the tracking problem of a time varying nonlinear system” and their “result may shed new light on the role of the feedforward acceleration terms used in the conventional CLOS guidance laws”. It could be seen there that in case of non-maneuvering target the guidance law for managing with the horizontal and vertical components of the tracking error of the missile position in the LOS frame contains one and the same PD control law.

CLOS guidance laws implementing accordingly fuzzy logic control, fuzzy sliding-mode control, adaptive fuzzy sliding-mode control, and a model-based feedback linearization guidance law are proposed in [12], where a control laws comparison based on two engagement scenarios is also made.

In [20] a “sliding mode control algorithm combined with a fuzzy control scheme is developed for the trajectory control of a command guidance system”. It is mentioned that “the proposed controller is used to compensate for the influence of unmodeled dynamics" and "chattering phenomena has been alleviated", which "problem may result in performance degradation and/or excite the missile body bending dynamics (elastic modes)". The missile model there is a medium range surface-to-air missile, while both engagement scenarios examined involve highly maneuvering targets. The assumptions made include a rolling stabilized missile with axis symmetry around its vertical and horizontal axes, decoupled pitch and yaw missile dynamics, and second order lag system autopilot dynamics. One of the proposed control technique benefits is the smoothness of the control signals shown in both engagements. The research carried out in [20] has been practically repeated in [21] where the results confirm the conclusions already made in [20] regarding the effectiveness of the proposed fuzzy sliding mode control.

For CLOS guidance law design a fuzzy adaptive learning method is developed in [22]. To determine weights of the adaptive mechanism a negative gradient method is applied. A feedback linearization guidance law is presented also. A comparison between two control laws is made against one engagement scenario. The authors emphasize that the fuzzy adaptive guidance law can achieve smaller miss distance and smoother control efforts than the feedback linearization one. It could be seen there that the feedback linearization guidance law yields two separate stable linear homogeneous differential equations of second order regarding the horizontal and vertical deviations of the missile position in the LOS frame and practically the control law for each of both errors represents a PD control law.

A CLOS guidance law based on fuzzy sliding mode control but using continuous ant colony system "to optimize the parameters of a pre-constructed fuzzy sliding mode controller" is proposed in [14]. "The cost function is defined based on the average performance obtained over 10 randomly generated engagement scenarios". The optimal set of parameters obtained is examined against two other engagements. The simulations include also a missile and target maneuvering limiters. The results show the proposed guidance law successfully drives the tracking error to zero. The authors claim that the continuous ant colony system has the ability "to solve practical optimization problems such as guidance and control systems design" and emphasize on the simplicity of the continuous ant colony system having only the number of ants as a parameter, whose setting is "easier than many other optimization methods", against other meta-heuristics such as Genetic Algorithm. The authors develop further the idea to utilize the continuous ant colony system for optimization of fuzzy sliding mode control at the CLOS guidance in [15]. They propose a two-phase guidance scheme. The guidance in the first midcourse phase includes a lead angle with respect to the LOS on the base of a PD fuzzy sliding mode controller with a supervisory controller coupled to guarantee the missile flight within the beam. The second terminal phase guidance is pure CLOS guidance based on a proportional-integral-derivative fuzzy sliding mode controller. An extended to multi-objective optimization problems continuous ant colony system algorithm is applied for the optimization of the pre-constructed fuzzy sliding model controllers. The authors claim that among the advantages of the proposed control scheme in tested engagements in comparison with the model-based feedback control scheme is the relatively better performance in the presence of measurement noise and the fact that the "proposed methodology does not require any information obtained from the inertial navigation system".

A modified guidance and control sliding mode controller for the three-dimensional CLOS guidance "formulated as a tracking error problem for a time-varying nonlinear system" is proposed in [23]. The authors claim the guidance law provides robustness and better performance compared to the proportional navigation method regarding chattering, miss-distance and finite time in simulated engagement scenarios where the target performs a variety of maneuvers. The proposed modified sliding mode control depends on a state feedback controller of second order where the values of the coefficients of the state feedback gain determine the increase or decrease of the chattering against the conventional sliding mode control. It is mentioned that "for this reason, the missile does not need to generate a high value of command to track the target; it only needs to generate the appropriate command to ensure that the missile will be close to the sliding line or line of sight".

In [24] for the CLOS guidance law design Back-stepping control technique is applied after formulating the CLOS guidance problem as a three-dimensional tracking problem. The authors emphasize on the effectiveness of the guidance control law design in terms of the miss distance achieved on the base of three engagement scenarios, two anti-aircraft and one anti-missile scenarios. The modeling includes a maneuvering limiter to limit the missile's maneuverability and a measurement noise at providing the ground tracker data. It could be noticed that the control technique adopted for the study comprises identical PD parts regarding the vertical and horizontal missile errors in the LOS frame.

In [16] the authors propose an "approach to the three-player guidance law" and a novel guidance law which "can be classified as a three-point guidance" but is "similar to the proportional navigation (PN)". The guidance law "manipulates two LOS rates associated with three vehicles and has benefits over the conventional three-point guidance law in two major aspects: 1) a simple form with one gain for two LOS rates, and 2) high sensitivity to an attacking missile's maneuvers in the proximity of the attacking missile, but low sensitivity to the attacking missile's maneuvers in the proximity of the protected aircraft". According to the authors "The "three points" in the three-point guidance usually means a missile, a target, and a reference point from which the target LOS is drawn or the target is observed. In this study, the protected aircraft is selected as one of the three points instead of the reference point." Thus, the guidance law that is proposed "can be classified as a three-point guidance" but is "similar to the proportional navigation (PN)". The authors derive the guidance law "using optimal control theory" based on five assumptions where the first assumption is that "The three vehicles are moving in a plane". Thus, the problem formulation and respective solution called "the airborne-CLOS" guidance law differ wholly from the considered here problem - the spiral type trajectory in the plane perpendicular to the LOS of the spatial ATGM CLOS closed loop system which worsens the performance indicators of the system in the transient process of putting a CLOS ATGM onto the LOS. This conclusion could be applied also to [17]. There a similar "three-body interception scenario is considered where an aircraft launches a defending missile as a counter weapon against an incoming attacking missile".

"A new three-point trajectory-shaping guidance concept against stationary targets is presented" in [18]. The authors employ the geometric "principle of constant inscribed angles in a circle, which enables the imposition of a required impact angle by traversing specific circular paths." The publication includes also a survey of the guidance laws which allow one to impose the impact angle. The work features the two top levels of the guidance process, “namely, formulating a new geometric guidance concept/rule and then proposing a guidance law that implements this new geometric rule.” It should be mentioned that “the proposed guidance concept can be viewed as a generalization of the classical line-of-sight guidance concept.” The consideration is made in the planar case. The controller design is “performed using linearization around a nominal circular trajectory” and the guidance loop block diagram is provided. The authors carry out also a performance analysis based on numerical simulations as well as considering implementation possibilities of the guidance concept. It could be concluded that the focus of the work differs from the problem stated here although the work considers a three-point trajectory-shaping guidance concept and a respective guidance law.

In [19] “a three-dimensional nonlinear guidance law for path-following is proposed using differential geometry of space curves.”

In [13] “an optimal pursuit-evasion problem between two-aircraft including a realistic weapon envelope is analyzed using differential game theory”. The authors optimize a performance index which consists of time of flight together with a realistic weapon envelope for the pursuing aircraft in a form of “a linear combination of flight time and the square of the vehicle acceleration”. “The weapon envelope considered is an arbitrary three-dimensional manifold with its origin at the center of gravity” which “manifold may be specified as a function of the angle between the LOS vector and the vehicle velocity vector”. Although the paper does not consider an ATGM CLOS guidance law synthesis but a pursuit-evasion problem which is practically a homing guidance problem the publication could serve as illustration of combining different techniques in order to obtain an effective guidance law solution. Thus, in [13] a closed form solution in a form of feedback guidance law is obtained “using differential game theory and the theory of feedback linearization”. The authors also claim that the “nonlinear guidance law is useful for onboard implementation” “because of its modest computational requirements”.

It should be mentioned that the scope of the studies is rather global. Thus a CLOS ATGM trajectory spiraling into the target in the initial transient phase of the controlled flight, even though the target is non-maneuvering, is not considered a problem or even presented as far as the resulting missile trajectories are solutions of CLOS guidance problems with a rather quite different focus.

With regard to the above mentioned problem concerning the enhancement of an implemented guidance law which enables a prospective easy practical realization, we could also consider the opinion of the author of [25], in which the topic discusses a class of guidance laws including proportional navigation law, who in opposition to the enthusiasm of many authors for the newly developed guidance laws which “improve the effectiveness of the proportional navigation (PN) law against maneuvering targets” and “can be easily realized in practice” criticizes very consistently the guidance laws based on some results of the control theory. The author considers the sliding mode control, some types of variable structure control, guidance laws obtained as a solution of an optimization problem, and guidance laws as a result of the game approach. Regarding the guidance laws based on the sliding mode control the existence of chattering limits the practical realization of such systems and a related simplification of the control law needs “rigorous justification and testing”. “Also, in the presence of a maneuvering target the sliding mode area depends on the target acceleration, and for small LOS derivatives the sliding mode can disappear”. Regarding the solutions of the guidance problem defined as an optimal control problem it is usually assumed “the trajectory of a maneuvering target as well as time-to-go and/or the intercept point are known. In practice, such information is unknown and can only be evaluated approximately”, while the game approach “deals mostly with models of engagement too simple to be recommended for practical applications”.

So in order to narrow the survey let us suppose the target is non-maneuvering and the trajectory of a CLOS ATGM in the plane perpendicular to the LOS from its initial deviations from the LOS in the transient phase of the controlled flight while putting the missile onto the LOS represents a non-spiraling curve which in the ideal case is a straight segment joining the initial point and the origin of the considered plane. Such type of trajectory looks like a very much desired trajectory of a missile. So forming by the CLOS guidance law pitch and yaw acceleration commands in the above way it looks very attractive to improve the performance of a CLOS ATGM.

On the other hand the techniques proposed to deal with the presented here occurrence of spiraling into target CLOS ATGM in [6], [7], and [8] include the proportional-derivative (PD) guidance law. This is within the channel regarding the polar radius in [6] or the pseudo-polar radius in [7] and [8] of the polar or pseudo-polar presentations of the vector pointing the missile position in the plane perpendicular to the LOS. The radius is a coordinate of the organized in a new way spatial closed loop system structure of the CLOS ATGM there. Let us also take into account that the proportional-derivative (PD) guidance law still appears as a workhorse of the CLOS guidance [4] (Chap.2, 2.4, pp. 31-38), [26], [27], [28], [29], and [30].

In [29] a replacement of the warhead of an existing old generation semi-automatic CLOS anti-tank guided missile (ATGM) with thrust vector control by two new warhead modifications is proposed in order to increase the efficiency of the missile against explosive reactive armor. The authors mention that "the modification of the missile warhead is related to the front part of the missile, while the rear part with the motor and the missile control system remain the same for all modified missiles". Because of the change of the shape, the weight and the center of mass of the modified missile a technique is developed to obtain similar to the original closed loop guidance system performance while keeping all of the original existing control system elements. The research involves obtaining new derivatives of the aerodynamic coefficients, tuning by guidance loop stability analysis, redesigning of the aerodynamic configuration by a semi-empirical method, computer simulations and wind tunnel experiments, and finally carried out flight tests. It can be seen from the analysis of the guidance loop stability in the vertical plane that the control system comprises a first order phase-lead compensator which realizes a real PD control law.

In the patent [26] the elevation and azimuth lateral accelerations (latax) commands are produced on the basis of PD control law applied on the each of the "components of the projected miss distance in orthogonal reference planes" with a further modification by a scaling gain "stored in a look up table for implementation in the guidance loop". The author mentions that "the technique enables missile longax (longitudinal acceleration) coupling to be compensated without a requirement to measure the missile body angle relative to the line of sight".

The method proposed in [28] "comprises launching and moving missile in control field with rudders folded inside airframe in lengthwise grooves, opening radiation receiver and changing rudders in outside position". "Deviations of rudders after missile start is performed inside missile airframe grooves" and after specifically determined time interval "extending rudders outside of airframe is executed". The method "allows to reduce the time of the transition process in the missile closed loop control system on the stage of putting onto the beam axis and significantly to decrease the near-field boundary of missile operational range". Here the closed loop control system includes a real PD controller and the authors practically fight the undesired effect of the step response of the controller on the above mentioned stage of guidance.

The effect of the patent [27] is an "increased rocket aiming accuracy due to elimination of phase coupling of control channels". The method forms the "rocket control signals in yaw and pitch channels respectively" for fighting the phase coupling between the channels of the missile "due to inertia of its rudders' actuators". The technique is based also on two identical real PD controllers, one for the horizontal channel and the other one for the vertical channel, which are traditionally applied for providing stability of both the control channels as well as the whole spatial closed loop system. It should be mentioned here that the phase coupling of the missile control channels leads to un-proportional to one another processes in the horizontal and the vertical planes, which results in a rotation of the vector pointing the missile position in the picture plane spiraling into the origin of the picture plane. But the technique proposed in the patent is not based on the closed loop control of the angular velocity of rotation of the vector pointing the missile position in the picture plane in contrast to the proposed techniques in [6], [7], and [8]. It should be also mentioned that the techniques in [6], [7], and [8] employ the fundamental principle of feedback control to fight with the system's output deviation no matter what the cause at the core of such a deviation is.

"A new type of training flight simulator for manual command to line-of-sight guidance, which realization is based on simulation of the missile silhouette over the pre-recorded videos of the background with fixed or moving target, is given in the paper" [30]. The guidance laws for both horizontal and vertical channels represent two identical real PD guidance laws. It is said in Section 4 "Mathematical model of the missile flight" with regard to the "4.3. Compensator" that "the stability of the guidance loop of the command to line-of-sight guidance is realized by differential compensator in the forward loop (phase lead compensator). Since the same type of the compensator is used for both vertical and horizontal planes, only the pitch channel compensator is considered here".

Straightening the system's trajectory in the picture plane means decoupling alongside with proportionality. So the idea is to enhance the PD based guidance law in [6], [7], and [8] in a way which apart from straightening the missile trajectory in the plane perpendicular to the LOS, the picture plane, as proposed there also provides the stability of the spatial closed loop system which is not justified theoretically in [7] and [8].

The frame of the above proposal, in order to place it properly, addresses a survey of the fields of the STT/BTT missile control and the missile integrated guidance and control (IGC).

In [31] the authors propose a new nonlinear control method "used to design a full-envelope, hybrid bank-to-turn (BTT)/skid-to-turn (STT) autopilot for an air-breathing air-to-air missile". They employ the so called theta – D approximation method in order to design the inner/outer autopilot loop, in which based on the "approximate solution to the Hamilton-Jacobi-Bellman (HJB) equation" technique avoids the need of "online computation of the algebraic Riccati equation at each sample time". The design is based on the "accepted results of the flight mechanics that the flight control problem is structured in two layers. The motion of the center of gravity is addressed in the outer loop while the angular motion around the center of gravity is taken care of by the inner loop". The design scheme shows that guidance law acceleration commands as a guidance system's output are considered as an input for the inner loop. "A hybrid BTT/STT autopilot command logic is used to convert the commanded accelerations from the guidance laws to reference angle commands for the autopilot". So the benefits that come along with the autopilot design with its both "basic modes of controlling the attitude of a missile to achieve the acceleration commanded by the guidance law: skid-to-turn (STT) and bank-to-turn (BTT)" yield "excellent tracking response over a large region of the operating envelope".

From the point of view of the considered in this monograph idea of guidance and control it could be mentioned here that the assumption the autopilot provides ideal tracking response one more time shows the responsibility of the guidance law in each phase of the controlled missile flight to the target. Even more, apart from providing stability the acceleration commands formed by the guidance law in a way to straighten the missile trajectory in the plane perpendicular to the LOS could also significantly contribute to the performance of a CLOS ATGM.

The survey of the field of IGC shows an early paper [32] from the same time period as [6], [7], and [8]. The comparison between [32] and [6], [7], and [8] shows that driven from different reasons the authors of [32] employ the polar coordinates in order to solve the planar proportional guidance problem in a closed form while the authors of [6], [7], and [8] employ the polar coordinates in order to compensate the spiral type trajectory into the target of a CLOS ATGM in its spatial variant, also in a closed form. It turns out that all the authors entirely independent of one another propose formally one and the same crucial initial technique for avoidance coupling between the control channels with regard to the polar radius and the polar angle known now as feedback linearization irrespective of the difference in the their initial approach to the topic due to considering different problems and implied meaning of the introduced polar coordinates. After this cross point [32] continues within the scope of the proportional navigation guidance while [6], [7], and [8] continue within the scope of the CLOS ATGM guidance. As mentioned above, the part of the proposed in [6] guidance law with regard to the polar radius also includes the traditional for this type of guidance PD law neglecting knowingly in conclusions the nature of the polar radius which cannot be negative. A kind of pseudo-polar coordinates which also allows negative values of the polar radius is presented in [7] and [8] in order to have a smooth transition through the origin of the plane perpendicular to the LOS at the CLOS guidance by keeping the smoothness of the solution of the system of differential equations at the CLOS guidance in its spatial case. The allowance of negative values for the polar radius stems from Euler's complex number presentation. Note that $r(t)e^{j\varphi_0}$ where $r(0) > 0$, $\varphi_0 = const.$ and $r(t) \in (-\infty, \infty)$ represents a movement alongside a straight line in the complex plane, so there is no need at all to exclude negative values of the variable $r(t)$. Note also that there is no reason to avoid concerning the function $r(t)e^{j\varphi(t)}$ without any constrains of the sign of the variable $r(t)$. The technique accepted in [7] and [8] for modeling the spatial closed loop system also includes keeping the kinematics of CLOS guidance in Cartesian coordinates with further conversion into polar coordinates but treated in the above more common way as pseudo-polar coordinates for providing smooth transition of $r(t)$ through the origin. It is shown there that during this transition the polar angle stays constant. By this technique the use of the inverse trigonometric arctangent function yet exists. Thus the development in the chosen direction shows promising simulation results including also an autopilot design idea but the increased number of nonlinear issues and the lack of a rigorous stability justification cause further development in this way to be abandoned. However, the attractive idea of how to fight the spiral type trajectory of the CLOS ATGM in the transient phase of putting the missile onto the LOS is not forgotten.

Now new techniques to deal with the considered here in the monograph problem on the basis of the reborn author's idea are proposed. There are no pseudo-polar coordinates, there are not any concerns with the inverse trigonometric arctangent function at all. The closed-form solutions for the guidance laws are now comprehensive and relatively simple. All five guidance laws of the new set of guidance laws are nonlinear where four of them are variable structure controls, but not sliding mode control laws. They represent complex expansion of both classical PD guidance laws for the horizontal and vertical planes and include additional nonlinear components connected with the derivatives of the missile position vector in the plane perpendicular to the LOS, the picture plane. The global stability of the spatial closed loop system of the CLOS ATGM with the new guidance laws is theoretically justified. An improved transient process performance of the spatial closed loop system of the CLOS ATGM is achieved while putting the missile onto the LOS fighting effectively the spiral type trajectory in the picture plane. The synthesized new guidance laws could also be considered as a foundation for turning a symmetrical CLOS ATGM into one with improved efficiency.

Due to the fact that the considered technique in [6], [7], and [8] for fighting the spiral type trajectory of a CLOS ATGM intersects with one of the features of [32] “recognizing the importance of polar coordinates” the track of the citations of [32] shows that five other papers [33], [34], [35], [36], and [37] refer to it. These papers do not concern problems similar to the spiral type trajectory into the target of a CLOS ATGM in the plane perpendicular to the LOS, the picture plane, during the transient process of putting the missile onto the LOS.

Thus in [33] the emphasis of the paper is on a proposed there three-dimensional design approach on the basis of a robust design inversion control and dynamic surface control for a class of BTT aircraft “in order to improve the matching relationship between the guidance subsystem and control subsystem”. It is claimed that the designed guidance law “guarantees the stable flight and accurate guidance”. It “also satisfies the constrained condition of terminal flight angles, which adequately reflects the validation and the effectiveness” of the scheme proposed alongside with “strong robust property against system uncertainties”. It could be seen there that the simulation examples with engagement scenarios and the design scope differ from the considered here technique.

In [34] “the performance of the three guidance laws is evaluated and compare via a thrust vector control missile” where one is based on the separated approach but the rest two are based on the IGC concept with all the states fed back. One of the considered IGC schemes features a single-loop guidance system while the second one features the two-loop scheme. From the performance point of view the authors’ decision is in favor of the IGC. In order to make the difference with regard to the proposed here technique which is an upgrade of the presented in [6], [7], and [8] techniques and their intersection with the [32] it is very useful to cite the perception of [32] by the authors. They say literally that in [32] “a class of PN guidance laws has been obtained in closed form by the decoupling of the radial and tangential coordinates. Then, a typical transverse acceleration component of the PN guidance laws’ family was combined with the airframe dynamics to derive an autopilot control law.” This could serve as an illustration of the way the authors considering the guidance law problems do percept the role of the polar coordinates combined with decoupling by feedback linearization.

Regarding the rest three papers [35], [36], and [37] which refer to [32] it could be seen that [35] and [36] represent practically one and the same material. From the point of view of the considered here problem the scope of all three is different.

The more thorough survey of the field of the missile guidance laws shows the existence of the publication [38], published a year after [32] of the same author as the first author of [32] who says that "the central idea here is that the polar coordinates present a natural coordinate system for a missile engagement". The author states also that "The decoupling of the coordinates leads also to a two-point boundary problem with linear time-varying coefficients. However, with a time-varying transformation, a class of closed form solutions are obtained that yield several proportional guidance laws."

The authors of the state of the art book [39] appearing also as authors of [32], [35], [36], and [38] deal with the design and implementation of a CLOS guidance system (Chap. 14), where "the approach presented here is based on the linear quadratic Gaussian (LQG) formalism."

In [40] within the scope of homing guidance the author "first drive a new 2-D nonlinear guidance law based on the RHE angle in Cartesian coordinates but to extend the nonlinear guidance strategy to 3-D space for any initial missile and target direction in the polar coordinate system for simplicity by using the theory of feedback linearization". The author taking into consideration the publication [5] with regard to the feedback linearization with CLOS scope comments that "To date, the feedback linearization method has been applied to derive the exact command to the LOS guidance law". Turning once again to [5] it could be seen once again that the scope of the authors' study is global. By a feedback linearization they achieve decoupling but from the point of view of the proposed here idea they do not consider or even mention the spiraling into the target in case of already decoupled pitch and yaw channels and non-maneuvering target. The engagement scenarios in the examples show also the different emphasis of their paper.

The paper [41] is a recent publication in the journal "Gyroscopy and Navigation" where the authors employ the presentation of the missile movement in the plane perpendicular to LOS, the picture plane, in polar coordinates for the synthesis of a guidance law based only on the polar radius coordinate. Practically, this is a repetition of the approach proposed first in [6], [7], and [8] regarding the use of the polar coordinates for an ATGM CLOS guidance law synthesis.

In order to cope with the "intertwining" between the missile onboard coordinate system and the tracker's beam coordinate system the authors of [41] try to achieve CLOS control based only on the polar radius coordinate in the picture plane ignoring the control of the polar angle coordinate. They say: "The gyro coordinator stores the position of the missile body fixed coordinate system coinciding with the vehicle's measurement coordinate system (the beam coordinate system). During maneuvering, the coordinate systems of the vehicle and missile turn relative to each other ('intertwine'). Thus, missile position in the beam is misrepresented, which adversely affects the MCS stability and targeting accuracy" (the authors abbreviate the missile control system as MCS).

The authors of [41] propose a classical linear proportional-integral-derivative control of the polar radius which plays the role of the single controlled coordinate. It is important to them when "the control equipment becomes simpler and more reliable". The integral component of the classical linear control law is introduced in order to achieve higher accuracy taking into consideration the inclusion of the gravity force into the system's model. The simulation results show unsatisfactory performance indicators of the closed loop process in the $Y_L Z_L$-plane, the picture plane, as well as the processes' time evolution.

The comparison between [6], [7], and [8] and the recent publication [41] is in favor of the author's technique [6], [7], and [8]. In [6], [7], and [8] two new decoupled control channels in reference to the polar radius and the polar angle based on a feedback linearization are synthesized while in [41] a very simple linear control of the polar radius is only implemented neglecting the control of the polar angle. The authors of [41] concede the unsatisfactory performance indicators due to the simplicity of the control law. They say: "It is expected that oscillations will be damped after the introduction of some changes in the control law without using any additional control channel." Thus, because of the lack of control of the polar angle and the very simple control technique the authors of [41] claim another benefit:

"There is no need in a gyro coordinator and there is no 'intertwining' of the coordinate systems".

It should be also mentioned that both the early [7] and [8] and the recent [41] employ for the model of the kinematic relations of the spatial closed loop system the ideal simplest linear presentation in a form of a pair of double integrators. This fact confirms once again the relevance of this classic presentation of the kinematic relations for considering a model of a CLOS closed loop system. This form of the kinematic relations is used here as well (1.1).

Despite the unsatisfactory performance indicators of the closed loop the publication [41] shows once again the importance of the development of ATGM CLOS guidance law techniques and control schemes. It also emphasizes the "beginning" of the recognition of the importance of the ATGM motion presentation in the plane perpendicular to the LOS, the picture plane, in the terms of the polar coordinates for the CLOS guidance law synthesis by the research community despite the fact that the first real public recognition of this approach is made by the author in [6], [7], and [8] dating back more than 20 years.

It could be concluded that the author's early publications [6], [7], and [8] and the recent publication [41] are practically the very few publications in the field of CLOS ATGM guidance law synthesis based on the motion presentation of the ATGM in the plane perpendicular to the LOS in polar coordinates. It should also be acknowledged that this approach is provoked by the pursuit of improvement of the spatial closed loop control system transient process performance indicators of putting an ATGM onto the LOS.

Let us summarize in order to appreciate the benefits of the proposed here technique. In the aspect of non-maneuvering target, the spiral type trajectory of a CLOS ATGM in the plane perpendicular to the LOS in the transient process of putting the missile onto the LOS deteriorates the performance indicators of the spatial closed loop system. The first idea – [6], [7], and [8] – of fighting this effect by simultaneous application of polar coordinates and a feedback linearization technique dates back more than 20 years. The approach achieves decoupling the spatial closed loop system of a CLOS ATGM into two separate linear looking control channels regarding the polar radius and polar angle but in the plane perpendicular to the LOS. This technique allows negative values for the polar radius as well. This hybrid technique features also simultaneous employment of both Cartesian and polar coordinates for resolving the missile kinematics.

Unfortunately, the proposed technique has been overlooked by the research community in the field of CLOS ATGM. One of the reasons could be the initial development direction of the original idea of [6] shown in [7] and [8]. The development of the idea there within one control structure and the way chosen to deal with the inverse arctangent function caused more issues than solutions. These obstacles are now avoided by the new enhanced technique getting even more hybrid by involvement also of the variable structure control but no sliding mode control, and still staying comprehensible and for that reason reliable. The inertia in the field of CLOS ATGM development augmented perhaps by the success on the basis of the implementation of the beam riding technology could be pointed as second reason. It could be noted that the initial idea presentation was at several Eastern European science conferences in Bulgaria and consequently published in the following proceedings. Now the author’s idea considered and developed in new ways from a modern point of view could serve effectively the CLOS ATGMs.

1.3 Formulation of the problem

1.3.1 Decoupled case of the spatial guidance loop

Let us consider the ideal most simple linear symmetric and decoupled case of the spatial guidance loop of a CLOS ATGM regarding the horizontal and vertical components of the ATGM in the plane perpendicular to the LOS, the $Y_L Z_L$-plane represented in Figure 1.2 or the picture plane shown in Figure 1.1, (1.1) with identical PD guidance law in each pitch and yaw channel (1.3) assuming the target is non-maneuvering and ignoring the gravity acceleration.

$\begin{bmatrix}\ddot{y}\\ \ddot{z}\end{bmatrix}=\begin{bmatrix}a_{yc}\\ a_{zc}\end{bmatrix},\qquad \begin{bmatrix}a_{yc}\\ a_{zc}\end{bmatrix}\triangleq\begin{bmatrix}u_y\\ u_z\end{bmatrix}$	(1.1)
$\begin{bmatrix}y(0)\\ z(0)\end{bmatrix}=\begin{bmatrix}y_0\\ z_0\end{bmatrix},\qquad \begin{bmatrix}\dot{y}(0)\\ \dot{z}(0)\end{bmatrix}=\begin{bmatrix}y_{10}\\ z_{10}\end{bmatrix}$	(1.2)

$u_y = \frac{-1}{a_0}(y + a_1\dot{y})\,,$ $u_z = \frac{-1}{a_0}(z + a_1\dot{z})\,,$ $a_0 > 0, a_1 > 0$	(1.3)
$a_0\ddot{y} + a_1\dot{y} + y = 0\,,$ $a_0\ddot{z} + a_1\dot{z} + z = 0$	(1.4)
$f(s) = a_0s^2 + a_1s + 1$	(1.5)

It is easily seen that the PD controls u_y and u_z (1.3) provide asymptotic stability of the closed loop system (1.1) - (1.3) and both separate y and z-channels have identical dynamics (1.4) based on one and the same characteristic polynomial (1.5). Although the processes in each channel are based on one and the same characteristic polynomial, they are a function of the initial conditions (1.2), for the y-channel – the pair $(y_0\,, y_{10})$ and respectively for the z-channel – the pair $(z_0\,, z_{10})$. So the processes do not look symmetric or proportional to one another in the common case, which results in a spiral trajectory to the point of origin of the Y_LZ_L-plane.

To illustrate this effect, let us consider all three cases with respect to the roots of the characteristic polynomial (1.5).

1.3.1.1 Case of a pair complex conjugate roots

Let the pair complex conjugate roots be (s_1, s_2) (1.6) represented there by the time constant T $(T > 0)$ and the damping ratio ξ ($\xi \in (0,1)$). Then the coefficients of the characteristic polynomial (1.5) represented also by T and ξ are (1.7). The closed loop system (1.4) represents the equations (1.8) with initial conditions (1.2) and (1.8) solved analytically [42] (Chap. 2, § 7, Examples) determine the processes (1.9) for y and z respectively. Suppose at least one of the four initial conditions (1.2) is non-zero, for example let $y_0 \neq 0$, and define a coefficient k as (1.10) and express $z(t)$ from (1.9) in form (1.11). The condition (1.12) is satisfied if (1.13) is valid, which results in the condition (1.14). So the processes in the y and z-channels are proportional to one another only in case that this ratio is already provided at the initial conditions, which is impossible in the common case and illustrated in Figure 1.3.

$$s_1 = -\frac{\xi}{T} + i\Omega, \quad s_2 = -\frac{\xi}{T} - i\Omega, \quad T > 0, \quad \xi \in (0,1), \quad \Omega = \frac{\sqrt{1-\xi^2}}{T}$$	(1.6)
$$a_0 = T^2, \quad a_1 = 2\xi T$$	(1.7)
$$T^2\ddot{y} + 2\xi T\dot{y} + y = 0\,, \quad T^2\ddot{z} + 2\xi T\dot{z} + z = 0$$	(1.8)
$$y(t) = c_{y1}e^{-\frac{\xi}{T}t}\cos\Omega\, t + c_{y2}e^{-\frac{\xi}{T}t}\sin\Omega\, t\,, \quad z(t) = c_{z1}e^{-\frac{\xi}{T}t}\cos\Omega\, t + c_{z2}e^{-\frac{\xi}{T}t}\sin\Omega\, t\,, \quad c_{y1} = y_0\,, \quad c_{y2} = \frac{y_{10} + \frac{\xi}{T}y_0}{\Omega}\,, \quad c_{z1} = z_0\,, \quad c_{z2} = \frac{z_{10} + \frac{\xi}{T}z_0}{\Omega}$$	(1.9)
$$k = \frac{z_0}{y_0}\,, y_0 \neq 0$$	(1.10)
$$z(t) = ky(t) + \frac{\left(z_{10} + \frac{\xi}{T}z_0\right) - k(y_{10} + \frac{\xi}{T}y_0)}{\Omega}e^{-\frac{\xi}{T}t}\sin\Omega\, t$$	(1.11)
$$z(t) = ky(t)\ \forall\ t \geq 0$$	(1.12)
$$\frac{\left(z_{10} + \frac{\xi}{T}z_0\right) - k(y_{10} + \frac{\xi}{T}y_0)}{\Omega} = 0$$	(1.13)
$$z_{10} = ky_{10}$$	(1.14)
$$T = 0.2\ (s), \qquad \xi = 0.4$$	(1.15)
$$y_0 = 2, \quad y_{10} = 0, \quad z_0 = 1, \quad z_{10} = 0$$	(1.16)
$$y_0 = 2, \quad y_{10} = 2, \quad z_0 = 1, \quad z_{10} = -5$$	(1.17)

1.3.1.2 Case of a pair negative and different roots

Let the pair negative and different roots be (s_1, s_2) (1.18) represented there by the different time constants $T_1 > 0$ and $T_2 > 0$. The coefficients of the characteristic polynomial (1.5) represented also by T_1 and T_2 are (1.19). The closed loop system (1.4) represents here the equations (1.20) with initial conditions (1.2) and (1.20) solved analytically [42] (Chap. 2, § 7, Theorem 4) determine the processes (1.21) for y and z respectively. Analogically with the previous case, suppose at least one of the four initial conditions (1.2) is non-zero, for example let $y_0 \neq 0$, and define a coefficient k as (1.10) and express $z(t)$ from (1.21) in form (1.22). The condition (1.12) with respect to (1.22) is satisfied if (1.14) is valid. So analogically with the previous case the processes in the y and z-channels are proportional to one another only in case that this ratio is already provided at the initial conditions, which is impossible in the common case and illustrated in Figure 1.4.

$s_1 = -\dfrac{1}{T_1}, \quad s_2 = -\dfrac{1}{T_2},$ $T_1 > 0, T_2 > 0, T_1 \neq T_2$	(1.18)
$a_0 = T_1 T_2\,, \quad a_1 = (T_1 + T_2)$	(1.19)
$T_1 T_2 \ddot{y} + (T_1 + T_2)\dot{y} + y = 0\,,$ $T_1 T_2 \ddot{z} + (T_1 + T_2)\dot{z} + z = 0$	(1.20)
$y(t) = c_{y1} e^{-\frac{t}{T_1}} + c_{y2} e^{-\frac{t}{T_2}}\,,$ $z(t) = c_{z1} e^{-\frac{t}{T_1}} + c_{z2} e^{-\frac{t}{T_2}}\,,$ $c_{y1} = \dfrac{-\frac{y_0}{T_2} - y_{10}}{-\frac{1}{T_2} + \frac{1}{T_1}}\,, \quad c_{y2} = \dfrac{y_{10} + \frac{y_0}{T_1}}{-\frac{1}{T_2} + \frac{1}{T_1}}\,,$ $c_{z1} = \dfrac{-\frac{z_0}{T_2} - z_{10}}{-\frac{1}{T_2} + \frac{1}{T_1}}\,, \quad c_{z2} = \dfrac{z_{10} + \frac{z_0}{T_1}}{-\frac{1}{T_2} + \frac{1}{T_1}}$	(1.21)
$z(t) = ky(t) - \dfrac{(z_{10} - ky_{10})}{\left(-\frac{1}{T_2} + \frac{1}{T_1}\right)}\left(e^{-\frac{t}{T_1}} - e^{-\frac{t}{T_2}}\right)$	(1.22)
$T_1 = 0.25\ (s), \qquad T_2 = 0.35\ (s)$	(1.23)

1.3.1.3 Case of double negative root

Let the double negative root be s_1 (1.24) represented there by the time constant $T_1 > 0$. The coefficients of the characteristic polynomial (1.5) represented also by T_1 are (1.25). The closed loop system (1.4) represents here the equations (1.26) with initial conditions (1.2) and (1.26) solved analytically [42] (Chap. 2, § 8, Theorem 5) determine the processes (1.27) with respect to y and z respectively. Analogically with the previous two cases, suppose at least one of the four initial conditions (1.2) is non-zero, for example let $y_0 \neq 0$, and define a coefficient k as (1.10) and express $z(t)$ from (1.27) in form (1.28). The condition (1.12) with respect to (1.28) is satisfied if (1.14) is valid. So analogically with the previous two cases the processes in the y and z-channels are proportional to one another in case that this ratio is already provided at the initial conditions, which is impossible in the common case and illustrated in Figure 1.5.

$s_{1,2} = -\dfrac{1}{T_1}, \quad T_1 > 0$	(1.24)
$a_0 = {T_1}^2\,, \quad a_1 = 2T_1$	(1.25)
${T_1}^2\ddot{y} + 2T_1\dot{y} + y = 0\,,$ ${T_1}^2\ddot{z} + 2T_1\dot{z} + z = 0$	(1.26)
$y(t) = c_{y1}e^{-\frac{t}{T_1}} + c_{y2}te^{-\frac{t}{T_1}}\,,$ $z(t) = c_{z1}e^{-\frac{t}{T_1}} + c_{z2}te^{-\frac{t}{T_1}}\,,$ $c_{y1} = y_0\,,\;\; c_{y2} = y_{10} + \dfrac{y_0}{T_1}\,,$ $c_{z1} = z_0\,,\;\; c_{z2} = z_{10} + \dfrac{z_0}{T_1}$	(1.27)
$z(t) = ky(t) + (z_{10} - ky_{10})te^{-\frac{t}{T_1}}$	(1.28)
$T_1 = 0.3\;(s)$	(1.29)

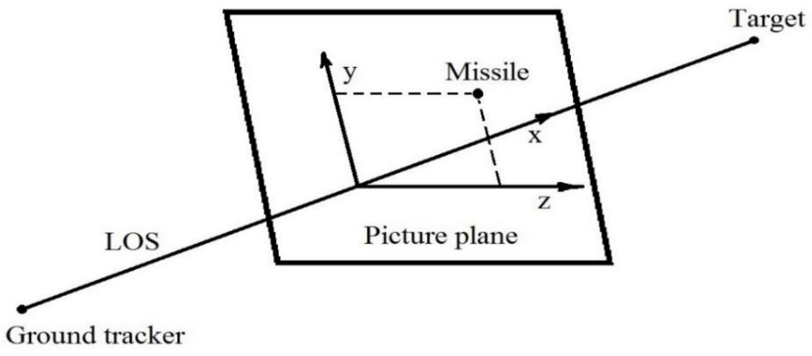

Figure 1.1 Picture plane representation in three-point guidance.

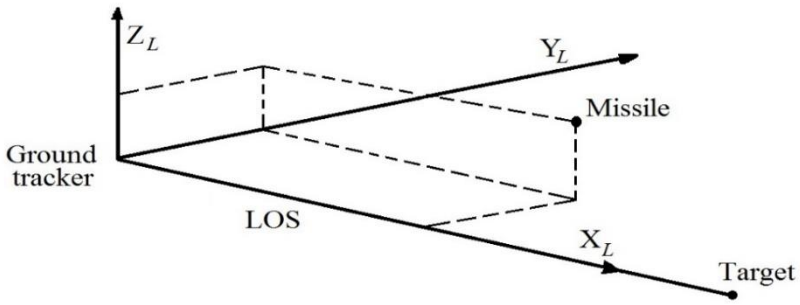

Figure 1.2 The LOS frame (X_L, Y_L, Z_L) in CLOS guidance.

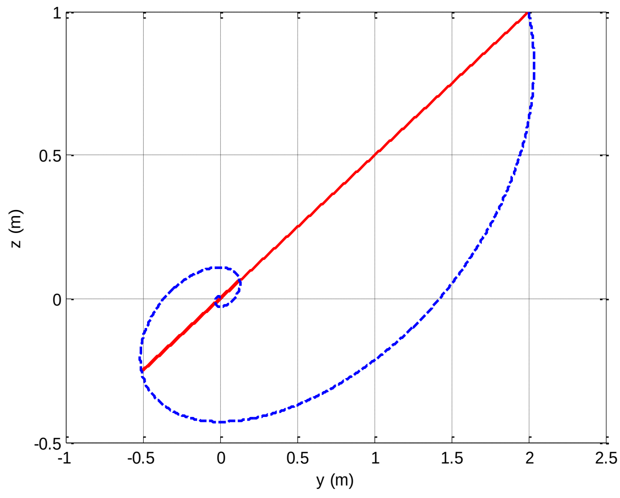

Figure 1.3 Processes in the $Y_L Z_L$-plane, the picture plane, of the closed loop system (1.1), (1.3) with identical classical PD guidance law in each channel in case (1.7) - (1.8) with parameters (1.15) at initial conditions (1.16) proportional to one another (solid line) and at initial conditions (1.17) non-proportional to one another (dashed line).

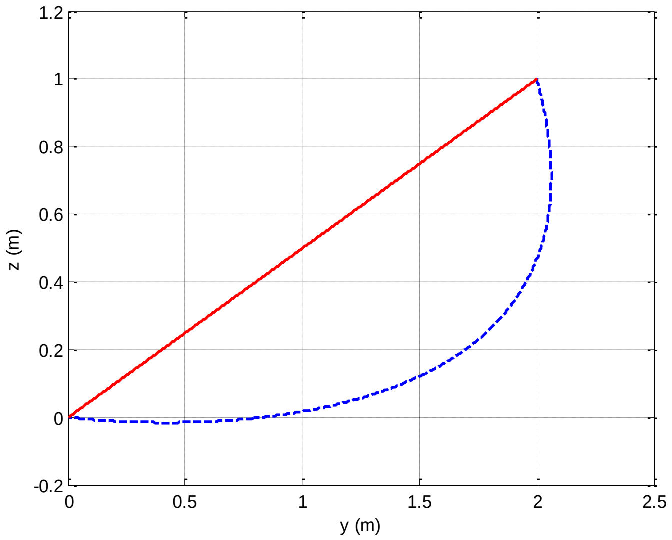

Figure 1.4 Processes in the $Y_L Z_L$-plane, the picture plane, of the closed loop system (1.1), (1.3) with identical classical PD guidance law in each channel in case (1.19) - (1.20) with parameters (1.23) at initial conditions (1.16) proportional to one another (solid line) and at initial conditions (1.17) non-proportional to one another (dashed line).

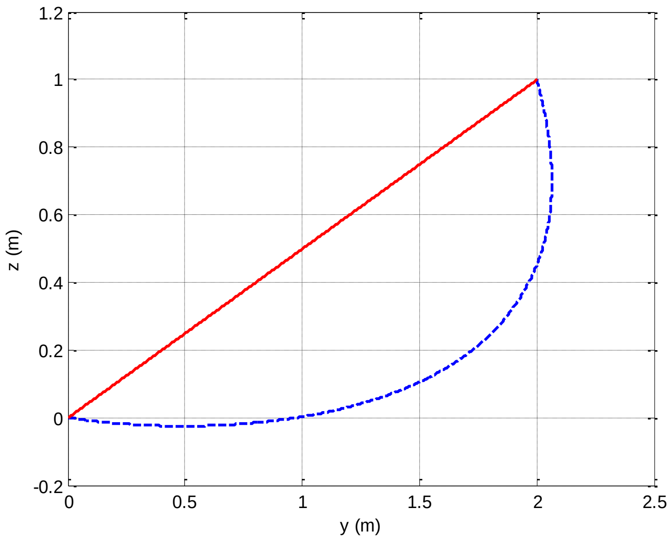

Figure 1.5 Processes in the $Y_L Z_L$-plane, the picture plane, of the closed loop system (1.1), (1.3) with identical classical PD guidance law in each channel in case (1.25) - (1.26) with parameters (1.29) at initial conditions (1.16) proportional to one another (solid line) and at initial conditions (1.17) non-proportional to one another (dashed line).

1.3.1.4 Conclusions

The employment of identical classical PD guidance law in each channel of the spatial two-channel closed loop system of CLOS ATGM even in the ideal and most simple symmetric case with no coupling between the channels results in rotation of the vector pointing out the missile position in the $Y_L Z_L$-plane the picture plane. The classical approach to the synthesis of the spatial closed loop system by splitting the system into two separate independent linear channels with provided stability in each channel and identical characteristic polynomial in both of them does not guarantee a missile trajectory lying on a straight line in the $Y_L Z_L$-plane, the picture plane. This in the common case spiral type trajectory of the transient process of putting the missile onto the LOS in the $Y_L Z_L$-plane perpendicular to the LOS represents an immutable characteristic of such type of guidance law application. This typical effect worsens the performance of the spatial guidance and control system in the initial phase of the controlled missile flight.

So in order to improve the transient process performance while putting the missile onto the LOS the idea is to expand the above classical PD guidance law in a way to provide straightening the system trajectory in the $Y_L Z_L$-plane, the picture plane, as it is already commented in the previous Section 1.1 and Section 1.2.

1.3.2 Case with phase coupling between two channels

Let γ be a parameter (1.31) and consider the following case (1.30) with phase coupling, cross-links, between two y and z-channels:

$\ddot{y} = a_y(t)$, $\ddot{z} = a_z(t)$, $a_y = u_y \cos\gamma + u_z \cos\left(\frac{\pi}{2} + \gamma\right)$, $a_z = u_y \sin\gamma + u_z \sin\left(\frac{\pi}{2} + \gamma\right)$.	(1.30)
$\gamma = \gamma_0 = const\ (rad)$	(1.31)

In case of (1.32) the system (1.30) turns into system (1.1). Let us do the synthesis in the way considered in the previous Section 1.3.1 with identical PD guidance law in each channel (1.3) supposing (1.33).

$\gamma_0 = 0$	(1.32)
$\cos\gamma_0 \approx 1 \; and \; \sin\gamma_0 \approx 0$	(1.33)

The analysis of the stability of the closed loop system (1.30) - (1.31) with control (1.3) in function of the parameter γ is done in Appendix – Section 8.1 "Analysis of the stability of the closed loop system (1.30) - (1.31) with control (1.3) in function of the parameter γ" (page 185). According to the "General conclusion on the stability of the closed loop system" obtained in Section 8.1.3 the system (1.30) - (1.31) with control law (1.3) is asymptotically stable if γ_0 satisfies (8.56). The closed loop system becomes neutrally stable at the boundaries (8.57) of (8.56) and becomes unstable at (8.58). The critical crossover value of $|\gamma_0|$ – γ_{cr} represents (8.55) where the gain crossover frequency ω_{cg_0} is calculated according to (8.29).

Let us employ the results of Section 8.1.4 "Example" (page 195). Note that the initial conditions (1.16) are proportional to one another with a ratio of $k = 0.5$ for (1.10). The processes on y and z are proportional to one another only in the decoupled case when $\gamma_0 = 0$ shown in Figure 8.4. There is loss of proportionality between the processes on y and z at $\gamma_0 \neq 0$. The increase of the parameter γ_0 within the stability interval of γ_0 (8.56) leads to a clockwise spiral trajectory to the origin of the picture plane as shown in Figure 8.6 and Figure 8.8, while the decrease of γ_0 within the stability interval (8.56) leads to a counter clockwise spiral trajectory to the origin of the picture plane – Figure 8.5 and Figure 8.7. The processes outside the stability interval (8.56) at $\gamma_0 = \gamma_{cr}$ and $\gamma_0 > \gamma_{cr}$ evolve clockwise in the $Y_L Z_L$-plane, the picture plane, as shown in Figure 8.10 and Figure 8.12, while at $\gamma_0 = -\gamma_{cr}$ and $\gamma_0 < -\gamma_{cr}$ evolve counter clockwise – Figure 8.9 and Figure 8.11.

So the existence of phase coupling between the channels in spite of the fact that the processes start evolving at proportional to one another initial conditions leads to loss of symmetry and proportionality between the processes in both channels. The system's transition process trajectory in the $Y_L Z_L$-plane, the picture plane, in the common case does not lie on a straight line and represents a spiral one. The phase coupling defeats system's stability and symmetry. It worsens the performance indices of the spatial closed loop system of the CLOS ATGM concerning the settling time and overshooting/falling of the transition process of putting the missile onto the LOS from the initial deviations from the LOS at the beginning of the missile controlled flight to the target.

1.4 Monograph's main goals

Summarizing the conclusions made in the survey and the consideration of both cases without and with phase coupling between the channels, the main goals of this monograph are formulated as synthesis of new command to line-of-sight – CLOS guidance laws which should:

- Effectively fight the anti-tank guided missile's – ATGM's spiraling and provide straightening the system's trajectory in the plane perpendicular to the line-of-sight – LOS, the $Y_L Z_L$-plane, the picture plane, regardless of the disproportionality of the initial conditions and phase coupling between the horizontal and vertical missile channels during the transition process of putting the missile onto the line-of-sight – LOS which worsen the performance and stability of the spatial closed loop anti-tank guided missile – ATGM system;
- Provide theoretically proven stability of the new spatial closed loop guidance and control system;
- Despite obvious complexity be presented in a form which is relatively comprehensible and reliable consistent to the designers of anti-tank guided missile – ATGM guidance and control systems with ability for future realization;
- Complement and upgrade the accepted command to line-of-sight – CLOS anti-tank guided missile – ATGM guidance and control systems design schemes.

The current review of the topic and the presented here goals acknowledge the complexity of the problems regarding the command to line-of-sight – CLOS anti-tank guided missile – ATGM guidance and control systems, which are still a matter for discussion in the scientific fields. Therefore it is definitely worth the challenge of studying them.

2 EXPANDED TWO-DIMENSIONAL PD CLOS GUIDANCE LAW FOR THE CASE WITH NO COUPLING BETWEEN THE CHANNELS

2.1 Guidance law formulation

An expanded two-dimensional (2D) PD CLOS guidance law is proposed in (2.2), which practically acts as a classical PD control law within a small predetermined area around the LOS while at missile deviations pointing a position outside this area the guidance law includes additional components connected with the derivatives of the missile position vector in the $Y_L Z_L$-plane. In (2.2) $\varepsilon_r > 0$ represents a positive parameter while $\dot{r}$ and $\dot{\varphi}$ are the derivatives of the magnitude and the argument employing the presentation (2.1).

$p = y + iz = re^{i\varphi}$, $r = \lvert p \rvert = \sqrt{y^2 + z^2}\,,\ \ \varphi = \arg(p)$	(2.1)
$u_y = \begin{cases} -\dfrac{1}{a_0}(y + a_1\dot{y}) & if\ r \le \varepsilon_r\,, \\ -\dfrac{1}{a_0}\big(y + a_1(\dot{y} + z\dot{\varphi})\big) - y\dot{\varphi}^2 - 2\dot{r}\dot{\varphi}\sin\varphi + \dfrac{1}{T_\varphi}z\dot{\varphi} & if\ r > \varepsilon_r\,, \end{cases}$ $u_z = \begin{cases} -\dfrac{1}{a_0}(z + a_1\dot{z}) & if\ r \le \varepsilon_r\,, \\ -\dfrac{1}{a_0}\big(z + a_1(\dot{z} - y\dot{\varphi})\big) - z\dot{\varphi}^2 + 2\dot{r}\dot{\varphi}\cos\varphi - \dfrac{1}{T_\varphi}y\dot{\varphi} & if\ r > \varepsilon_r\,, \end{cases}$	(2.2)

The closed loop system (1.1), (2.2) could be described as (2.3). According to the switching condition in (2.2) in Case 1 (2.4) the closed loop system decomposes into two independent and separate linear channels for y and z (2.5) and represents practically the system (1.4).

In Case 2 (2.6) the system (2.3) represents (2.7). Having in mind (2.8), (2.7) results into (2.9). Based on (2.9) the closed loop system (2.3) could be described also in the form (2.10). On the other hand the comparison of the second derivative of p (2.11) with (2.9) results into (2.12) and (2.13). The last could be represented by (2.10) also in form (2.14) as a model of the system in Case 2 (2.6) in an implicit form. From (2.13) we obtain (2.15) which is actually a linear system with independent and separate differential equations on each variable r and $\dot{\varphi}$ with initial conditions calculated according to the relations (2.16). It is easily seen that the system (2.15) is asymptotically stable on r and $\dot{\varphi}$. The equation on r provides dynamics determined by the characteristic polynomial (1.5). The analytical solution of (2.15) regarding $\dot{\varphi}$ is (2.17) where the time constant T_{φ} determines how fast we desire the process on $\dot{\varphi}$ to strive exponentially towards zero, in other words how fast we desire to "straighten" the system trajectory in the $Y_L Z_L$-plane.

$\ddot{p} = u_p\,,$ $u_p = u_y + iu_z$	(2.3)
Case 1. $r = \sqrt{y^2 + z^2} \leq \varepsilon_r$	(2.4)
$\ddot{y} = -\dfrac{1}{a_0}(y + a_1\dot{y})\,,$ $\ddot{z} = -\dfrac{1}{a_0}(z + a_1\dot{z})$	(2.5)
Case 2. $r = \sqrt{y^2 + z^2} > \varepsilon_r$	(2.6)

$$
\begin{gathered}
\ddot{p} = \ddot{y} + i\ddot{z} = \\
= \left(-\frac{1}{a_0}\big(y + a_1(\dot{y} + z\dot{\varphi})\big) - y\dot{\varphi}^2 - 2\dot{r}\dot{\varphi}\sin\varphi + \frac{1}{T_\varphi} z\dot{\varphi}\right) + \\
+i\left(-\frac{1}{a_0}\big(z + a_1(\dot{z} - y\dot{\varphi})\big) - z\dot{\varphi}^2 + 2\dot{r}\dot{\varphi}\cos\varphi - \frac{1}{T_\varphi} y\dot{\varphi}\right)
\end{gathered}
\tag{2.7}
$$

$$
\begin{aligned}
&y = r\cos\varphi \ , \\
&z = r\sin\varphi \ , \\
&\dot{y} = \dot{r}\cos\varphi - r\dot{\varphi}\sin\varphi \ , \\
&\dot{z} = \dot{r}\sin\varphi + r\dot{\varphi}\cos\varphi
\end{aligned}
\tag{2.8}
$$

$$
\begin{gathered}
\ddot{p} = \ddot{y} + i\ddot{z} = \\
= \left(\begin{gathered} -\frac{1}{a_0}\Big(r\cos\varphi + a_1\big((\dot{r}\cos\varphi - r\dot{\varphi}\sin\varphi) + r\sin\varphi\,\dot{\varphi}\big)\Big) - \\ -r\cos\varphi\,\dot{\varphi}^2 - 2\dot{r}\dot{\varphi}\sin\varphi + \frac{1}{T_\varphi} r\sin\varphi\,\dot{\varphi} \end{gathered}\right) + \\
+i\left(\begin{gathered} -\frac{1}{a_0}\Big(r\sin\varphi + a_1\big((\dot{r}\sin\varphi + r\dot{\varphi}\cos\varphi) - r\cos\varphi\,\dot{\varphi}\big)\Big) - \\ -r\sin\varphi\,\dot{\varphi}^2 + 2\dot{r}\dot{\varphi}\cos\varphi - \frac{1}{T_\varphi} r\cos\varphi\,\dot{\varphi} \end{gathered}\right)
\end{gathered}
$$

$$
\begin{gathered}
\ddot{p} = \ddot{y} + i\ddot{z} = \left(\begin{gathered} -\frac{1}{a_0}(r\cos\varphi + a_1\dot{r}\cos\varphi) - \\ -r\cos\varphi\,\dot{\varphi}^2 - 2\dot{r}\dot{\varphi}\sin\varphi + \frac{1}{T_\varphi} r\sin\varphi\,\dot{\varphi} \end{gathered}\right) + \\
+i\left(\begin{gathered} -\frac{1}{a_0}(r\sin\varphi + a_1\dot{r}\sin\varphi) - \\ -r\sin\varphi\,\dot{\varphi}^2 + 2\dot{r}\dot{\varphi}\cos\varphi - \frac{1}{T_\varphi} r\cos\varphi\,\dot{\varphi} \end{gathered}\right)
\end{gathered}
$$

$$
\begin{gathered}
\ddot{p} = \ddot{y} + i\ddot{z} = \\
= \left(\begin{gathered} -\frac{1}{a_0}\big((r\cos\varphi + ir\sin\varphi) + a_1(\dot{r}\cos\varphi + i\dot{r}\sin\varphi)\big) - \\ -(r\cos\varphi + ir\sin\varphi)\dot{\varphi}^2 + 2\dot{r}\dot{\varphi}(-\sin\varphi + i\cos\varphi) - \frac{1}{T_\varphi} r\dot{\varphi}(-\sin\varphi + i\cos\varphi) \end{gathered}\right)
\end{gathered}
$$

$\ddot{p} = \ddot{y} + i\ddot{z} =$ $= -\frac{1}{a_0}\big(r(\cos\varphi + i\sin\varphi) + a_1\dot{r}(\cos\varphi + i\sin\varphi)\big) - r(\cos\varphi + i\sin\varphi)\dot{\varphi}^2 +$ $+2\dot{r}\dot{\varphi}\left(\cos(\varphi + \frac{\pi}{2}) + i\sin(\varphi + \frac{\pi}{2})\right) - \frac{1}{T_\varphi}r\dot{\varphi}\left(\cos\left(\varphi + \frac{\pi}{2}\right) + i\sin\left(\varphi + \frac{\pi}{2}\right)\right)$	
$\ddot{p} = \ddot{y} + i\ddot{z} =$ $= -\frac{1}{a_0}\left(re^{i\varphi} + a_1\dot{r}e^{i\varphi}\right) - r\dot{\varphi}^2e^{i\varphi} + 2\dot{r}\dot{\varphi}e^{i\left(\varphi+\frac{\pi}{2}\right)} - \frac{1}{T_\varphi}r\dot{\varphi}e^{i\left(\varphi+\frac{\pi}{2}\right)} =$ $= \left(-\frac{1}{a_1}(r + a_1\dot{r}) - r\dot{\varphi}^2\right)e^{i\varphi} + \left(2\dot{r}\dot{\varphi} - \frac{1}{T_\varphi}r\dot{\varphi}\right)ie^{i\varphi}$	
$\ddot{p} = \ddot{y} + i\ddot{z} = e^{i\varphi}\left(\left(-\frac{1}{a_0}(r + a_1\dot{r}) - r\dot{\varphi}^2\right) + i\left(2\dot{r}\dot{\varphi} - \frac{1}{T_\varphi}r\dot{\varphi}\right)\right)$	(2.9)
$\ddot{p} = u_p$, $u_p = e^{i\varphi}\left(u_r + iu_\varphi\right)$, $u_r = -\frac{1}{a_0}(r + a_1\dot{r}) - r\dot{\varphi}^2$, $u_\varphi = 2\dot{r}\dot{\varphi} - \frac{1}{T_\varphi}r\dot{\varphi}$	(2.10)
$\ddot{p} = e^{i\varphi}\big((\ddot{r} - r\dot{\varphi}^2) + i(2\dot{r}\dot{\varphi} + r\ddot{\varphi})\big)$	(2.11)
$e^{i\varphi}\big((\ddot{r} - r\dot{\varphi}^2) + i(2\dot{r}\dot{\varphi} + r\ddot{\varphi})\big) =$ $= e^{i\varphi}\left(\left(-\frac{1}{a_0}(r + a_1\dot{r}) - r\dot{\varphi}^2\right) + i\left(2\dot{r}\dot{\varphi} - \frac{1}{T_\varphi}r\dot{\varphi}\right)\right)$	(2.12)
$\ddot{r} - r\dot{\varphi}^2 = -\frac{1}{a_0}(r + a_1\dot{r}) - r\dot{\varphi}^2$, $2\dot{r}\dot{\varphi} + r\ddot{\varphi} = 2\dot{r}\dot{\varphi} - \frac{1}{T_\varphi}r\dot{\varphi}$	(2.13)
$\ddot{r} - r\dot{\varphi}^2 = u_r$, $2\dot{r}\dot{\varphi} + r\ddot{\varphi} = u_\varphi$	(2.14)
$a_0\ddot{r} + a_1\dot{r} + r = 0$, $T_\varphi\ddot{\varphi} + \dot{\varphi} = 0$	(2.15)

$\dot{r} = \dot{y}\cos\varphi + \dot{z}\sin\varphi = \dfrac{y\dot{y} + z\dot{z}}{\sqrt{y^2 + z^2}}$, $\dot{\varphi} = \dfrac{\dot{z}\cos\varphi - \dot{y}\sin\varphi}{r} = \dfrac{\dot{z}y - \dot{y}z}{y^2 + z^2}$	(2.16)
$\dot{\varphi} = \dot{\varphi}_0 e^{-\frac{t}{T_\varphi}}$	(2.17)

Summarizing, the considered here guidance law is practically a nonlinear variable structure control. In case the missile is within the ε_r area around the LOS in the $Y_L Z_L$-plane, the picture plane, the guidance law turns into the classical PD control law regarding the horizontal and vertical components of the missile position in the $Y_L Z_L$-plane while outside this ε_r area the guidance law practically decouples the spatial guidance loop and transforms it into two separate linear channels regarding the polar coordinates of the missile position in the $Y_L Z_L$-plane. These benefits for the closed loop system are achieved by the special design of the guidance law based on a feedback linearization technique accompanied with a special pre-coupling between the channels aimed to straighten the missile trajectory in the $Y_L Z_L$-plane, the picture plane.

2.2 Global stability of the closed loop system

The nonlinear variable structure expanded 2D PD CLOS guidance law (2.2) turns the closed loop system (1.1), (2.2) into a nonlinear variable structure one. In order to prove its stability we employ the specially synthesized function $V(y, z, \dot{y}, \dot{z})$ (2.18). Because of its specific form designed to take into account the nonlinear variable structure control law (2.2) we investigate $V(y, z, \dot{y}, \dot{z})$ (2.18) around the switching boundary (2.20) in order to show its continuity there. Thus investigating the cases (2.21) and (2.23) we obtain (2.22) and (2.24), which show that the function $V(y, z, \dot{y}, \dot{z})$ (2.18) is continuous at the boundary (2.20) and represents there (2.25). Having in mind also (2.19), we consider the function $V(y, z, \dot{y}, \dot{z})$ (2.18) as a positive definite function – a Lyapunov-candidate-function for proving the stability of the closed loop system (1.1), (2.2) according to [43] (Chap. 17, § 17.2), [44] (Chap. 3)

	$V(y,z,\dot{y},\dot{z}) = \\ = \begin{cases} \dfrac{1}{a_0}y^2 + \dfrac{1}{a_0}z^2 + \dot{y}^2 + \dot{z}^2 & if \quad r \le \varepsilon_r\ , \\ \dfrac{1}{a_0}(y^2+z^2) + \left(\dfrac{y\dot{y}+z\dot{z}}{\sqrt{y^2+z^2}}\right)^2 + {\varepsilon_r}^2\left(\dfrac{\dot{z}y-\dot{y}z}{y^2+y^2}\right)^2 & if \quad r > \varepsilon_r \end{cases}$	(2.18)
	$V(y,z,\dot{y},\dot{z}) > 0$ for all $(y,z,\dot{y},\dot{z}) \neq (0,0,0,0)$, $V(0,0,0,0) = 0$	(2.19)
	$r = \sqrt{y^2+z^2} = \varepsilon_r.$	(2.20)
Case 1	$\sqrt{y^2+z^2} \to {\varepsilon_r}^-$	(2.21)
	$\lim\limits_{\sqrt{y^2+z^2}\to{\varepsilon_r}^-} V(y,z,\dot{y},\dot{z}) = \lim\limits_{\sqrt{y^2+z^2}\to{\varepsilon_r}^-}\left(\dfrac{1}{a_0}y^2 + \dfrac{1}{a_0}z^2 + \dot{y}^2 + \dot{z}^2\right) =$	
	$= \dfrac{1}{a_0}{\varepsilon_r}^2 + \dot{y}^2 + \dot{z}^2$	(2.22)
Case 2	$\sqrt{y^2+z^2} \to {\varepsilon_r}^+$	(2.23)
	$\lim\limits_{\sqrt{y^2+z^2}\to{\varepsilon_r}^+} V(y,z,\dot{y},\dot{z}) = \\ = \lim\limits_{\sqrt{y^2+z^2}\to{\varepsilon_r}^+}\left(\dfrac{1}{a_0}(y^2+z^2) + \left(\dfrac{y\dot{y}+z\dot{z}}{\sqrt{y^2+z^2}}\right)^2 + {\varepsilon_r}^2\left(\dfrac{\dot{z}y-\dot{y}z}{y^2+z^2}\right)^2\right) =$	
	$= \dfrac{1}{a_0}{\varepsilon_r}^2 + \\ + \lim\limits_{\sqrt{y^2+z^2}\to{\varepsilon_r}^+}\left(\left(\dfrac{y^2\dot{y}^2 + 2y\dot{y}z\dot{z} + z^2\dot{z}^2}{y^2+z^2}\right) + {\varepsilon_r}^2\left(\dfrac{\dot{z}^2y^2 - 2\dot{z}y\dot{y}z + \dot{y}^2z^2}{(y^2+z^2)^2}\right)\right) =$	
	$= \dfrac{1}{a_0}{\varepsilon_r}^2 + \lim\limits_{\sqrt{y^2+z^2}\to{\varepsilon_r}^+}\dfrac{(y^2+z^2)(\dot{y}^2+\dot{z}^2)}{{\varepsilon_r}^2} =$	
	$= \dfrac{1}{a_0}{\varepsilon_r}^2 + \dot{y}^2 + \dot{z}^2$	(2.24)
	$\lim\limits_{\sqrt{y^2+z^2}\to\varepsilon_r} V(y,z,\dot{y},\dot{z}) = \dfrac{1}{a_0}{\varepsilon_r}^2 + \dot{y}^2 + \dot{z}^2$	(2.25)

By the relations (2.16) $V(y,z,\dot{y},\dot{z})$ is presented in form (2.26) and for $\dot{V}$ we obtain (2.27) having in mind that in Case 1 (2.4) for $\ddot{y}$ and $\ddot{z}$ the obtained expressions are (2.5) and in Case 2 (2.6) the expressions for $\ddot{r}$ and $\ddot{\varphi}$ are obtained from (2.15). By substitution of $\dot{r}$ and $\dot{\varphi}$ in (2.27) for their expressions according to (2.16), we obtain (2.28) from which it follows (2.29). Thus, the closed loop system (1.1), (2.2) is globally asymptotically stable.

$V(y,z,\dot{y},\dot{z}) = \begin{cases} \frac{1}{a_0}y^2 + \frac{1}{a_0}z^2 + \dot{y}^2 + \dot{z}^2 & if \quad r \le \varepsilon_r\,, \\ \frac{1}{a_0}r^2 + \dot{r}^2 + {\varepsilon_r}^2\dot{\varphi}^2 & if \quad r > \varepsilon_r\,, \end{cases}$ where $\dot{r}$ and $\dot{\varphi}$ are according to (2.16)	(2.26)
$\dot{V}(y,z,\dot{y},\dot{z}) = \begin{cases} \frac{1}{a_0}2y\dot{y} + \frac{1}{a_0}2z\dot{z} + 2\dot{y}\ddot{y} + 2\dot{z}\ddot{z} & if \quad r \le \varepsilon_r\,, \\ \frac{1}{a_0}2r\dot{r} + 2\dot{r}\ddot{r} + 2{\varepsilon_r}^2\dot{\varphi}\ddot{\varphi} & if \quad r > \varepsilon_r\,. \end{cases}$	
$\dot{V}(y,z,\dot{y},\dot{z}) = \\ = \begin{cases} \left(\begin{array}{c} \frac{1}{a_0}2y\dot{y} + \frac{1}{a_0}2z\dot{z} + \\ +2\dot{y}\left(-\frac{1}{a_0}(y + a_1\dot{y})\right) + 2\dot{z}\left(-\frac{1}{a_0}(z + a_1\dot{z})\right) \end{array} \right) & if\ r \le \varepsilon_r\,, \\ \frac{1}{a_0}2r\dot{r} + 2\dot{r}\left(-\frac{1}{a_0}(r + a_1\dot{r})\right) + 2{\varepsilon_r}^2\dot{\varphi}\left(-\frac{1}{T_\varphi}\dot{\varphi}\right) & if\ r > \varepsilon_r\,. \end{cases}$	
$\dot{V}(y,z,\dot{y},\dot{z}) = \\ = \begin{cases} \left(\begin{array}{c} \frac{1}{a_0}2y\dot{y} - \frac{1}{a_0}2\dot{y}y - \frac{1}{a_0}2a_1\dot{y}^2 + \\ + \frac{1}{a_0}2z\dot{z} - \frac{1}{a_0}2\dot{z}z - \frac{1}{a_0}2a_1\dot{z}^2 \end{array} \right) & if\ r = \sqrt{y^2 + z^2} \le \varepsilon_r\,, \\ \frac{1}{a_0}2r\dot{r} - \frac{1}{a_0}2\dot{r}r - \frac{1}{a_0}2a_1\dot{r}^2 - \frac{2{\varepsilon_r}^2}{T_\varphi}\dot{\varphi}^2 & if\ r = \sqrt{y^2 + z^2} > \varepsilon_r\,. \end{cases}$	
$\dot{V}(y,z,\dot{y},\dot{z}) = \begin{cases} -\frac{2a_1}{a_0}(\dot{y}^2 + \dot{z}^2) & if\ r = \sqrt{y^2 + z^2} \le \varepsilon_r\,, \\ -\frac{2a_1}{a_0}\dot{r}^2 - \frac{2{\varepsilon_r}^2}{T_\varphi}\dot{\varphi}^2 & if\ r = \sqrt{y^2 + z^2} > \varepsilon_r\,, \end{cases}$	(2.27)

$$\dot{V}(y,z,\dot{y},\dot{z}) = \\ = \begin{cases} -\dfrac{2a_1}{a_0}(\dot{y}^2+\dot{z}^2) & if\ r=\sqrt{y^2+z^2}\le\varepsilon_r\ , \\ -\dfrac{2a_1}{a_0}\left(\dfrac{y\dot{y}+z\dot{z}}{\sqrt{y^2+z^2}}\right)^2-\dfrac{2\varepsilon_r{}^2}{T_\varphi}\left(\dfrac{\dot{z}y-\dot{y}z}{y^2+z^2}\right)^2 & if\ r=\sqrt{y^2+z^2}>\varepsilon_r\ . \end{cases}$$	(2.28)
$\dot{V}(y,z,\dot{y},\dot{z})<0$ for all $(y,z,\dot{y},\dot{z})\neq(0,0,0,0)$, $\dot{V}(0,0,0,0)=0$.	(2.29)

2.3 Simulations

In order to show the effectiveness of the new guidance law simulations are carried out for both types of the closed loop systems – the classic linear system (1.1), (1.3) and the system (1.1), (2.2) with identical pairs (a_0, a_1) of guidance laws parameters (1.3) and (2.2), and with one and the same initial conditions (1.17). All three cases with respect to the roots of the characteristic polynomial (1.5) are studied and illustrated by the three different pairs (a_0, a_1) corresponding to the illustrative examples of 1.3.1 Decoupled case of the spatial guidance loop: Section 1.3.1.1 "Case of a pair complex conjugate roots" – ((1.7), (1.15)) (page 19), Section 1.3.1.2 "Case of a pair negative and different roots" – ((1.19), (1.23)) (page 21), and Section 1.3.1.3 "Case of double negative root" – ((1.25), (1.29)) (page 22). The parameter ε_r of the guidance law (2.2) is chosen for the illustrations as (2.30). The time constant T_φ of the guidance law (2.2) is chosen consequently as (2.31) and (2.32).

$\varepsilon_r = 0.2\ m$	(2.30)
$T_\varphi = 0.1\ s$	(2.31)
$T_\varphi = 0.05\ s$	(2.32)

For convenience the guidance law of the closed loop linear system (1.1), (1.3) – the classical (C) PD guidance (G) law (L) is named CPDGL, while the guidance law of the closed loop system (1.1), (2.2) – the expanded (E) 2D PD guidance (G) law (L) is named E2DPDGL. The acronyms E2DPDGL1 and E2DPDGL2 represent respectively the version of the E2DPDGL with the value of time constant T_φ (2.31) and the version of the E2DPDGL with the value the time constant T_φ (2.32).

2.3.1 Performance of the E2DPDGL in case the pair (a_0, a_1) defines a pair complex conjugate roots of the characteristic polynomial $f(s)$ (1.5)

2.3.1.1 Performance comparison of the guidance loop with CPDGL and the guidance loop with E2DPDGL

Figure 2.1 - Figure 2.5 show some simulation results for the closed loop linear system (1.1), (1.3) with the CPDGL compared with the processes of the closed loop nonlinear system (1.1), (2.2) with the E2DPDGL1 in case the pair (a_0, a_1) represents ((1.7), (1.15)). The E2DPDGL1 fights effectively the spiraling trajectory in the $Y_L Z_L$-plane, the picture plane, as shown in Figure 2.1 and improves the closed loop performance in the phase of the transient process of putting the missile onto the LOS from the initial deviations from the LOS. The spatial overshooting/falling with regard to the LOS is better as well as the settling time while the control costs are similar - Figure 2.4. Figure 2.5 shows the zoomed control $u_z(t)$ from Figure 2.4 in the time interval $[0.3, 0.6]$ (s). It is well seen the E2DPDGL is a variable structure control (but not a sliding mode one) as well as the switching over to the CPDGL mode of the E2DPDGL when the polar radius is in the predetermined ε_r area around the plane origin and the system trajectory crosses trough this area in the $Y_L Z_L$-plane, the picture plane.

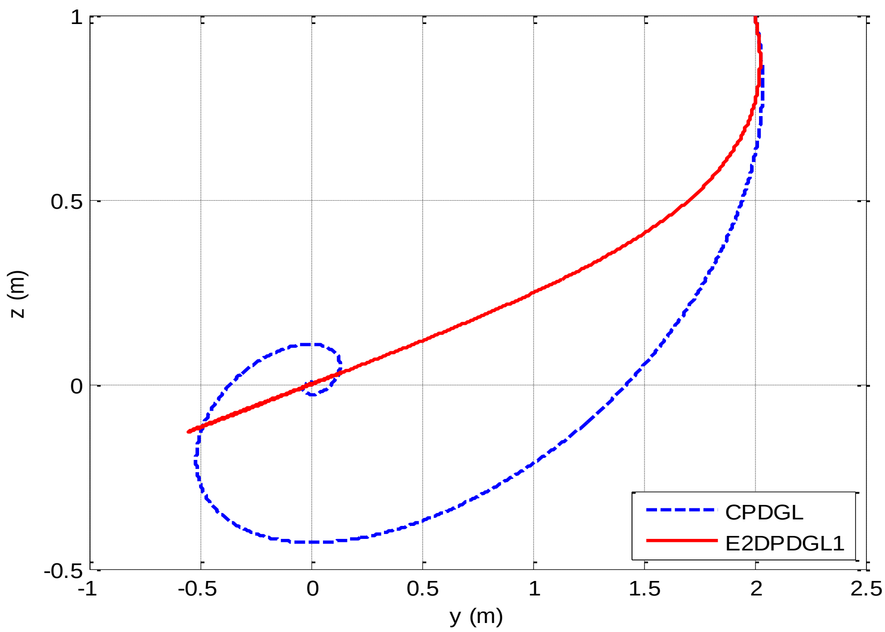

Figure 2.1 Performance comparison in the $Y_L Z_L$-plane, the picture plane, of the guidance loop with CPDGL and the guidance loop with E2DPDGL.

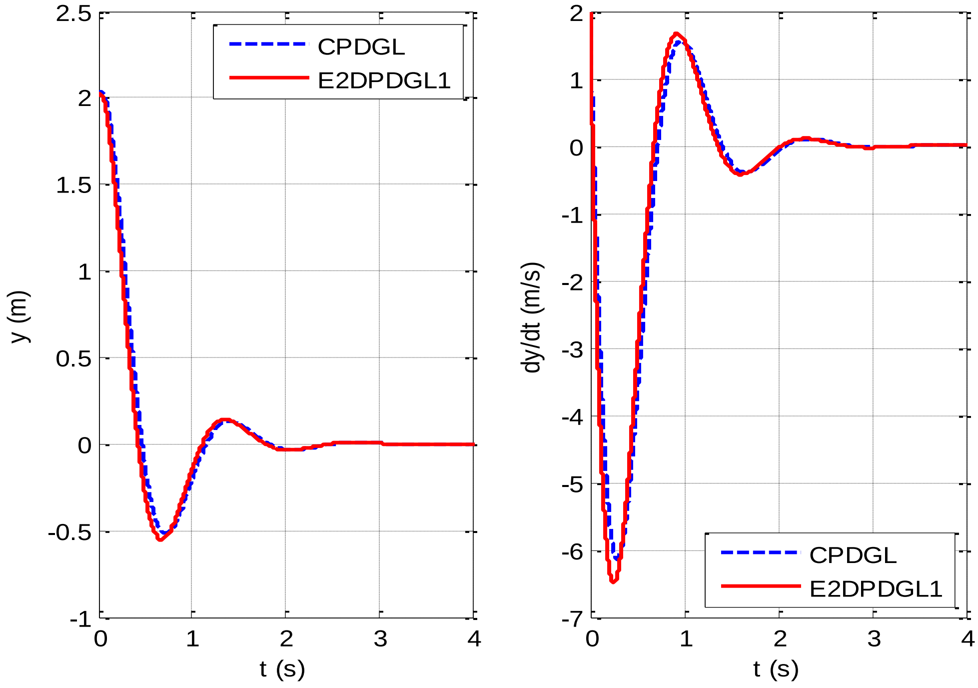

Figure 2.2 Comparison of the processes on y and the first derivative of y in the guidance loop with CPDGL and in the guidance loop with E2DPDGL.

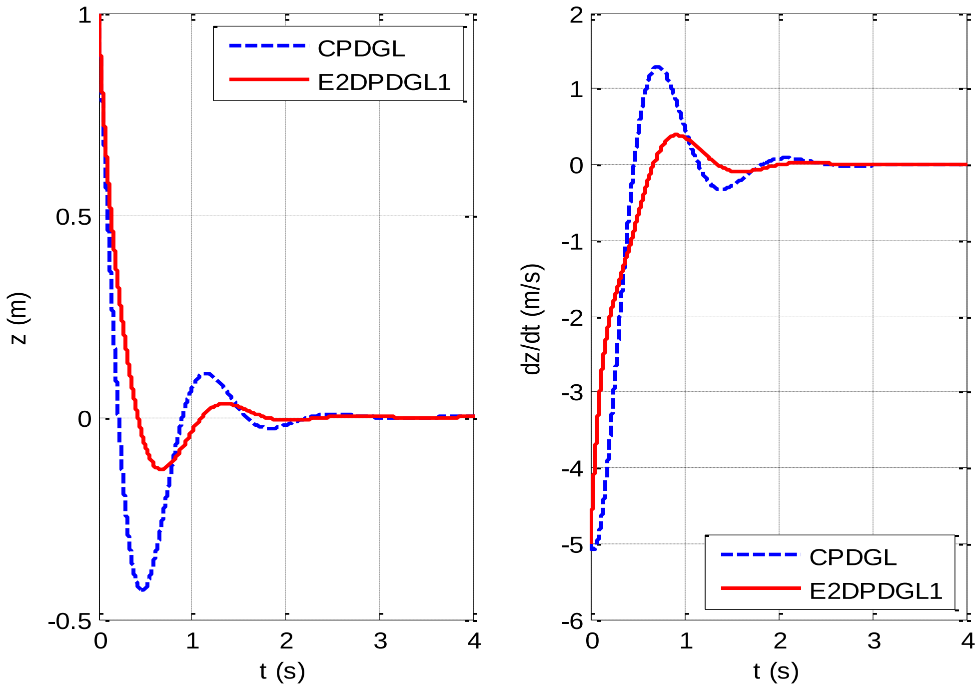

Figure 2.3 Comparison of the processes on z and the first derivative of z in the guidance loop with CPDGL and in the guidance loop with E2DPDGL.

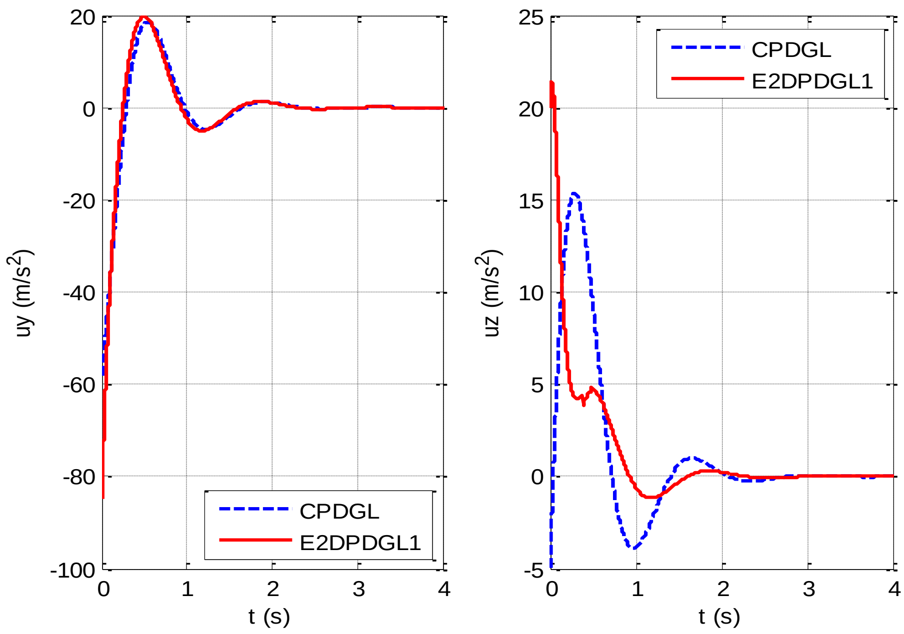

Figure 2.4 Comparison of the controls u_y and u_z in the guidance loop with CPDGL and in the guidance loop with E2DPDGL.

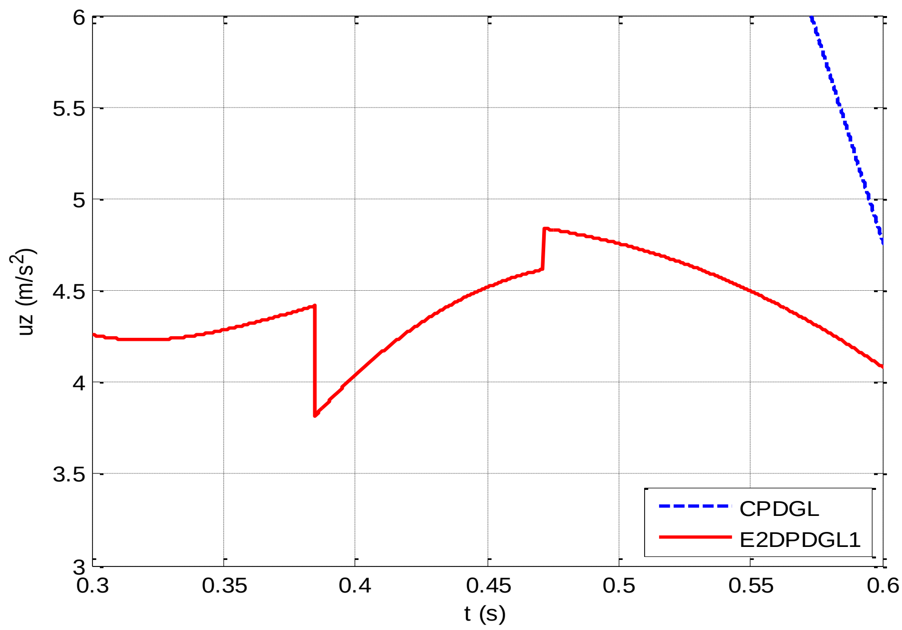

Figure 2.5 The zoomed control $u_z(t)$ from Figure 2.4 in the time interval $[0.3, 0.6]$ s. It is well seen the E2DPDGL is a variable structure control (but not a sliding mode one) as well as the switching over to the CPDGL mode of the E2DPDGL when the polar radius is in the predetermined ε_r area around the plane origin and the system trajectory crosses trough this area.

2.3.1.2 Performance comparison of the guidance loop with E2DPDGL1 and the guidance loop with E2DPDGL2

In order to show the effectiveness of straightening the missile trajectory in the $Y_L Z_L$-plane, the picture plane, by the new E2DPDGL Figure 2.6 - Figure 2.11 show a comparison between the processes of the closed loop system with the E2DPDGL at two values of T_φ (2.31) and (2.32). According to the design of the E2DPDGL the time constant T_φ determines how fast the polar angle velocity $\dot{\varphi}(t)$ strives exponentially towards zero. Thus the decreased value of T_φ (2.32) provides faster trajectory straightening in the $Y_L Z_L$-plane, the picture plane, as shown in Figure 2.11 while the control costs increase in the initial phase of the transient process as shown in Figure 2.9 and zoomed in in Figure 2.10. Figure 2.10 shows also that the E2DPDGL2 in the considered case provides a balanced and similar distribution of the control costs in both channels.

It should be mentioned once again here that the new E2DPDGL due to its special design has the ability to straighten effectively the ATMG CLOS trajectory. The CPDGL lacks such capability at all while the new E2DPDGL enables a way to achieve an ATGM CLOS system design based on system dynamics symmetry and proportionality.

2.3.2 Performance of the guidance loop with E2DPDGL in case the pair (a_0, a_1) defines negative roots of the characteristic polynomial $f(s)$ (1.5)

The simulation results of both cases ((1.19), (1.23)) and ((1.25), (1.29)) with negative roots of the characteristic polynomial $f(s)$ (1.5) which correspond to Section 1.3.1.2 “Case of a pair negative and different roots” (page 21) and Section 1.3.1.3 “Case of double negative root” (page 22) are very similar. Therefore the comparison between the CPDGL and the E2DPDGL shown in Figure 2.12 - Figure 2.15 as well as the comparison between E2DPDGL1 and the E2DPDGL2 presented in Figure 2.16 - Figure 2.19 when the pair (a_0, a_1) ((1.19), (1.23)) defines a pair negative and different roots of $f(s)$ (1.5) could also serve as illustration of the other case ((1.25), (1.29)) of double negative root of $f(s)$ (1.5).

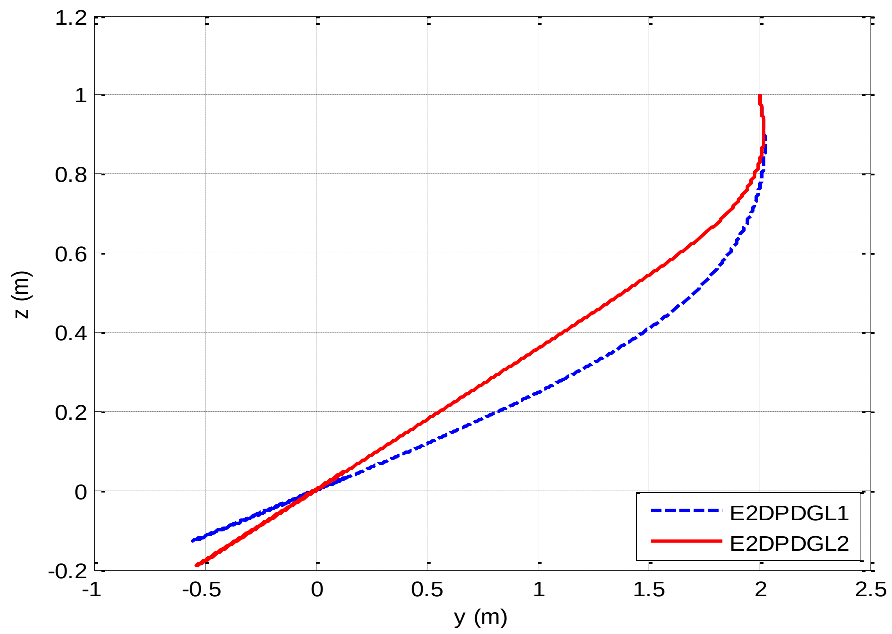

Figure 2.6 Performance comparison in the $Y_L Z_L$-plane, the picture plane, of the guidance loop with E2DPDGL1 and the guidance loop with E2DPDGL2.

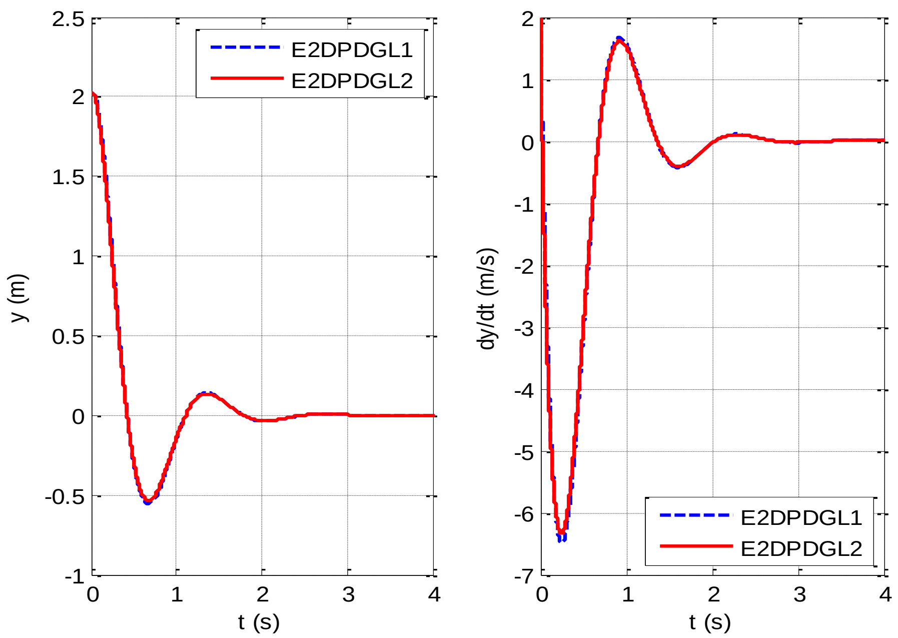

Figure 2.7 Comparison of the processes on y and the first derivative of y in the guidance loop with E2DPDGL1 and the guidance loop with E2DPDGL2.

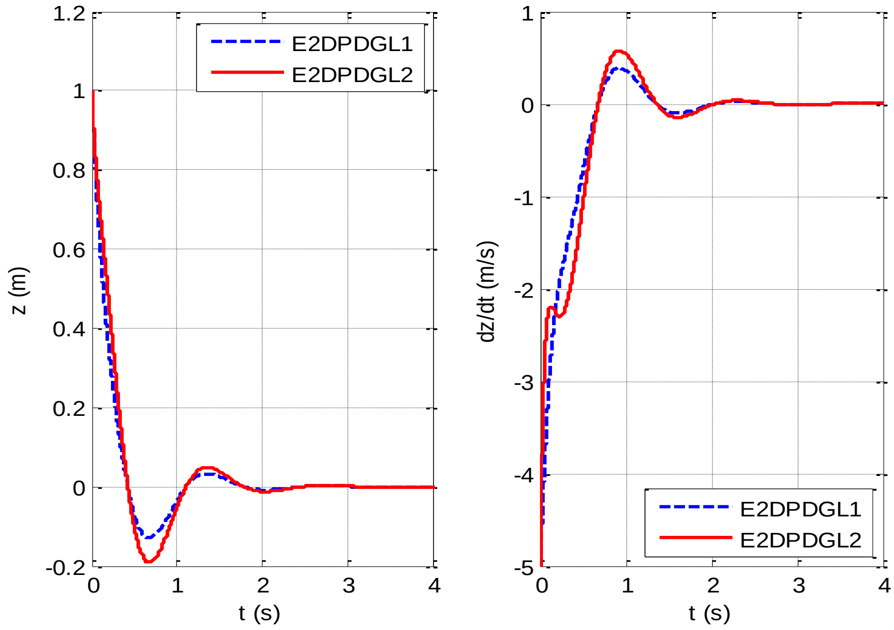

Figure 2.8 Comparison of the processes on z and the first derivative of z in the guidance loop with E2DPDGL1 and the guidance loop with E2DPDGL2.

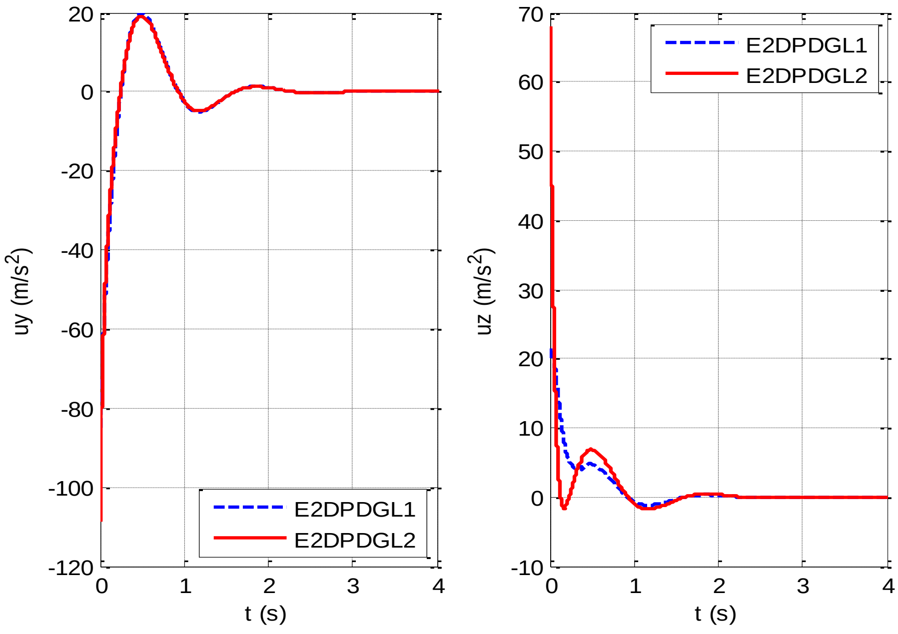

Figure 2.9 Comparison of the controls u_y and u_z in the guidance loop with E2DPDGL1 and the guidance loop with E2DPDGL2.

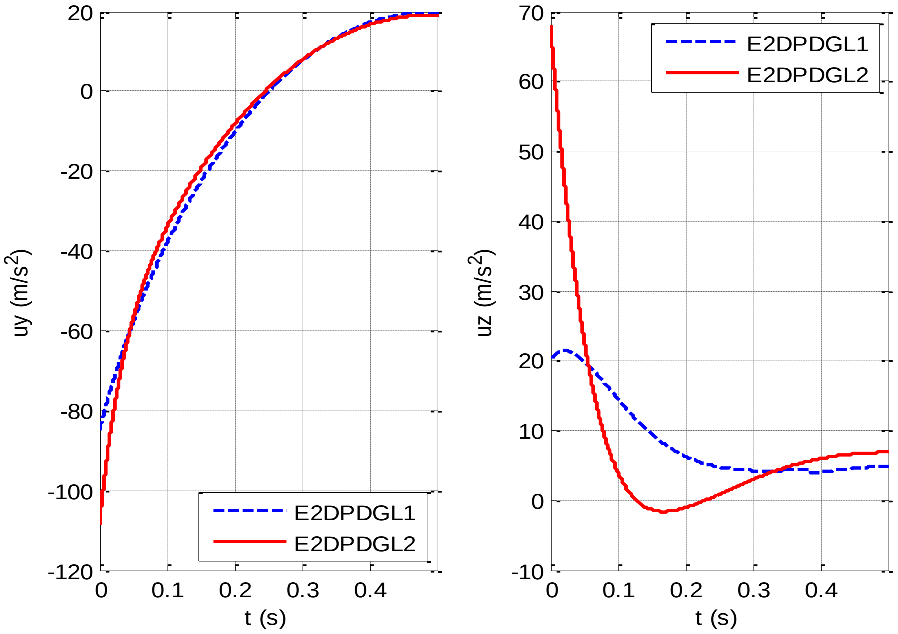

Figure 2.10 Comparison of the zoomed controls u_y and u_z from Figure 2.9 in the time interval $[0, 0.5]$ s.

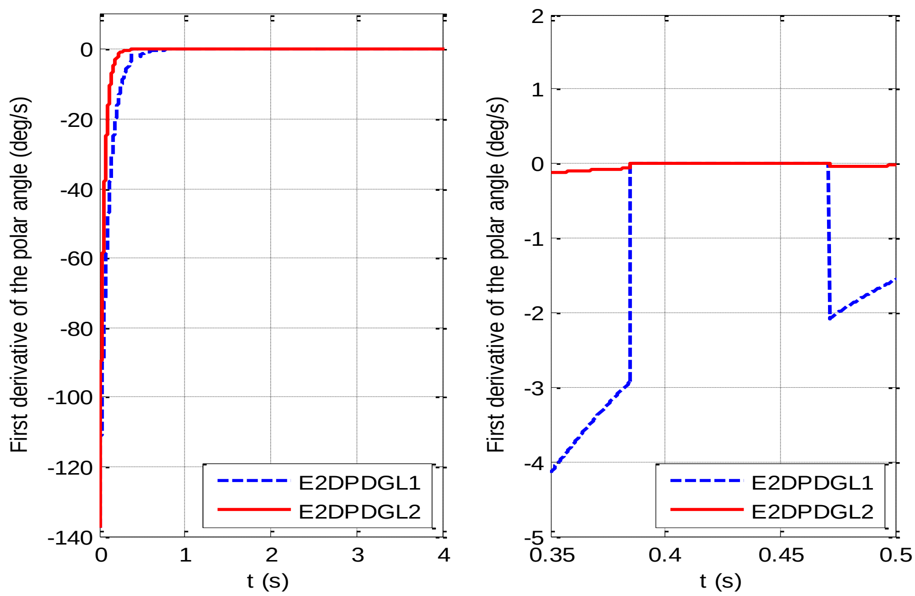

Figure 2.11 Comparison of the polar angle velocity in the guidance loop with E2DPDGL1 and the guidance loop with E2DPDGL2. The right picture shows the switching over to the CPDGL mode of the E2DPDGL when the polar radius is in the predetermined ε_r area around the plane origin and the system trajectory crosses trough this area in the $Y_L Z_L$-plane, the picture plane.

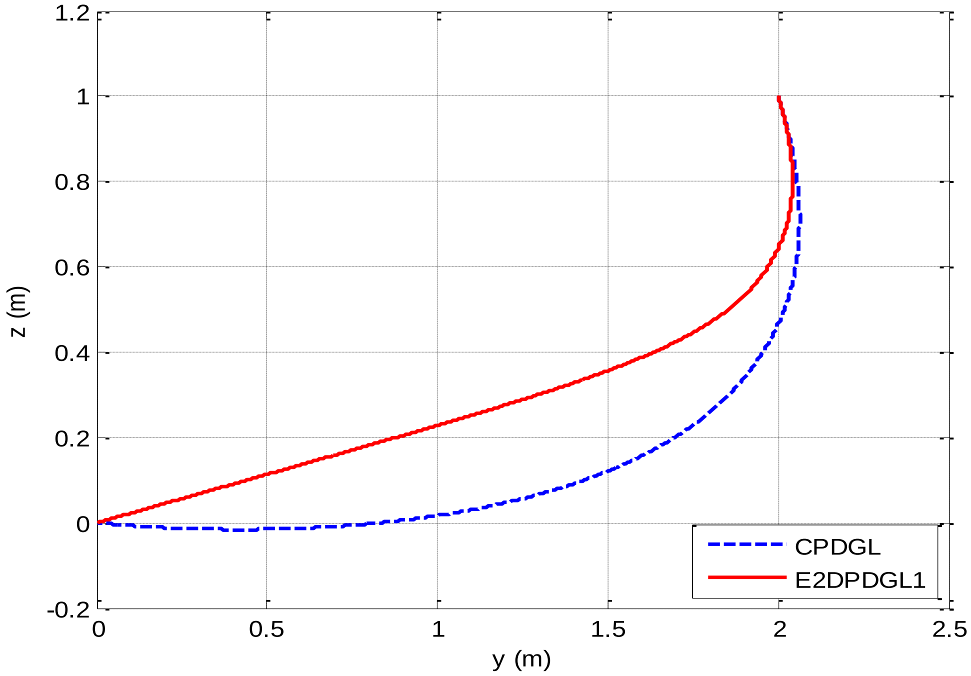

Figure 2.12 Performance comparison in the $Y_L Z_L$-plane, the picture plane, of the guidance loop with CPDGL and the guidance loop with E2DPDGL.

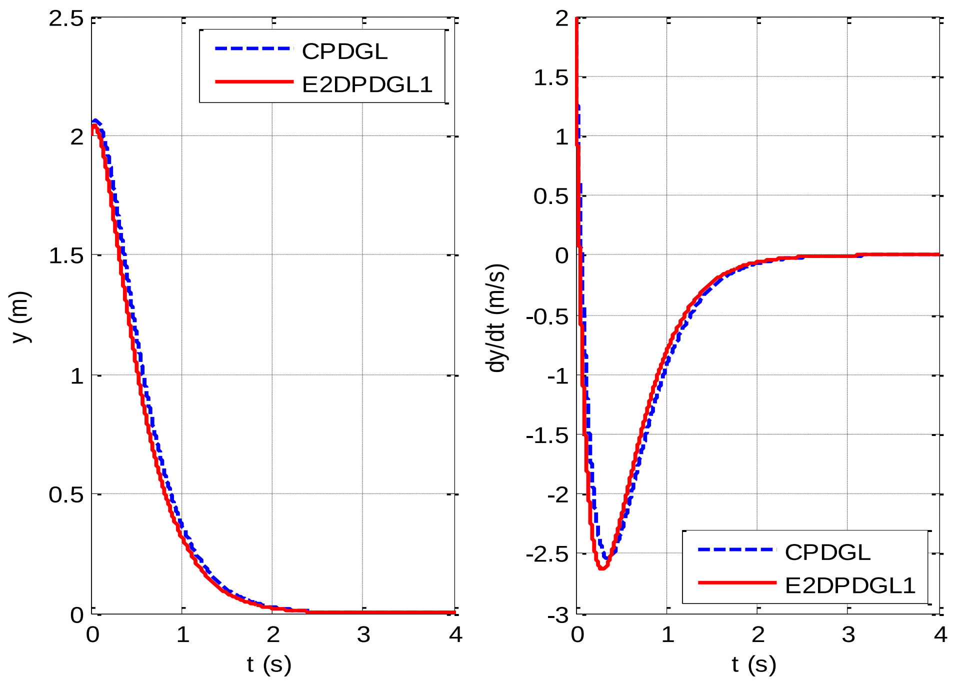

Figure 2.13 Comparison of the processes on y and the first derivative of y in the guidance loop with CPDGL and in the guidance loop with E2DPDGL.

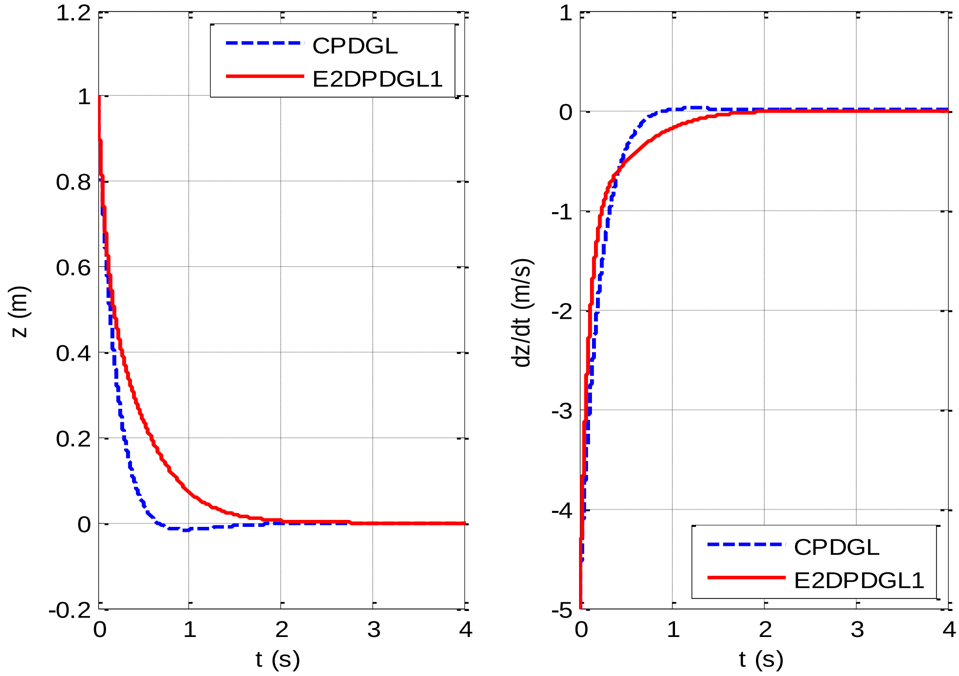

Figure 2.14 Comparison of the processes on z and the first derivative of z in the guidance loop with CPDGL and in the guidance loop with E2DPDGL.

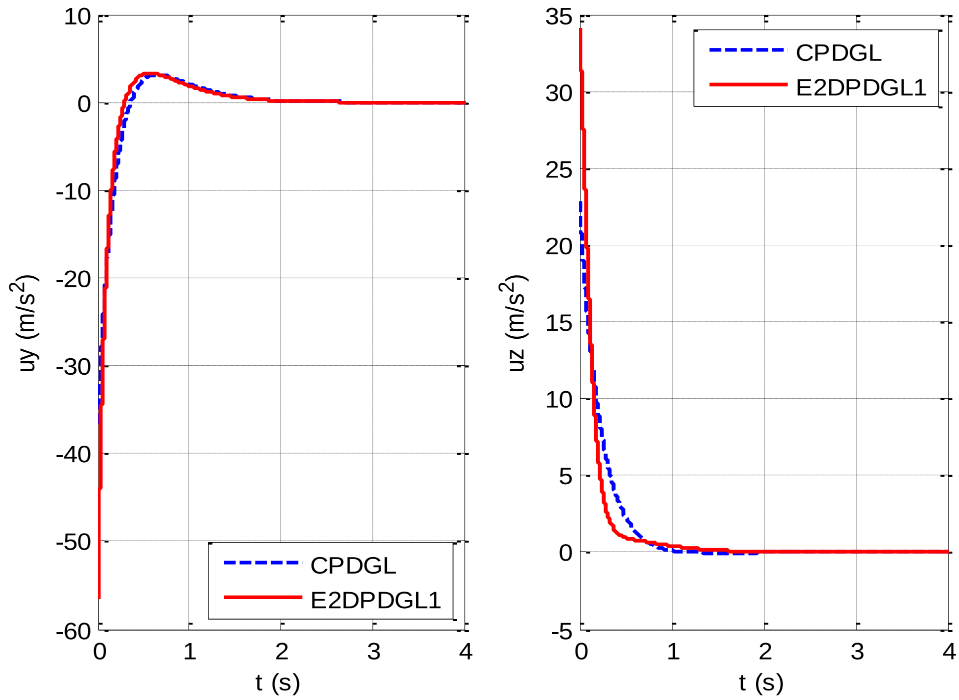

Figure 2.15 Comparison of the controls u_y and u_z in the guidance loop with CPDGL and in the guidance loop with E2DPDGL.

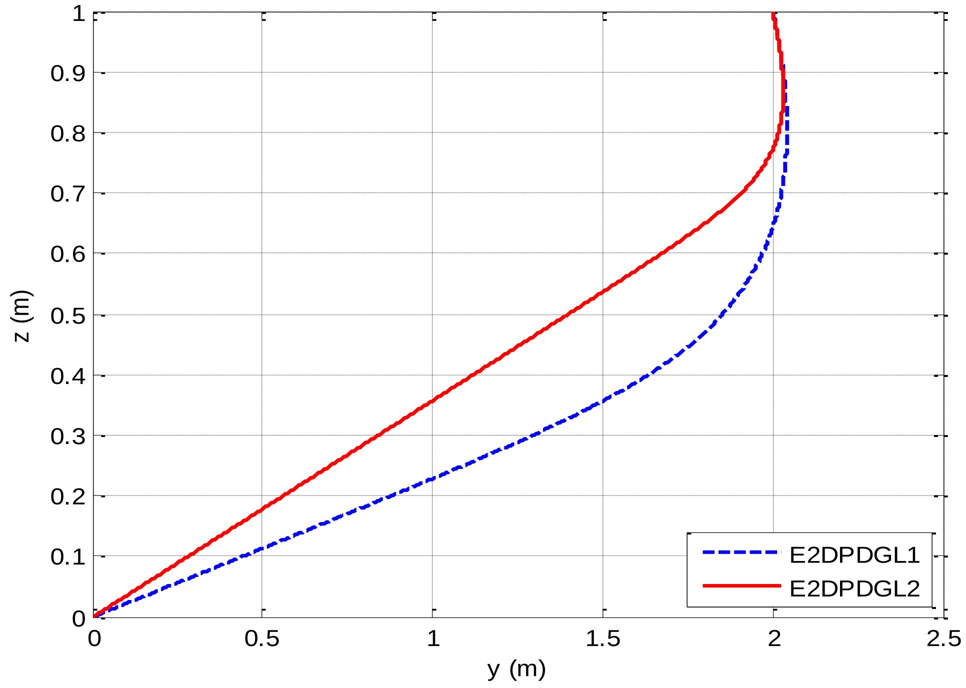

Figure 2.16 Performance comparison in the $Y_L Z_L$-plane, the picture plane, of the guidance loop with E2DPDGL1 and the guidance loop with E2DPDGL2.

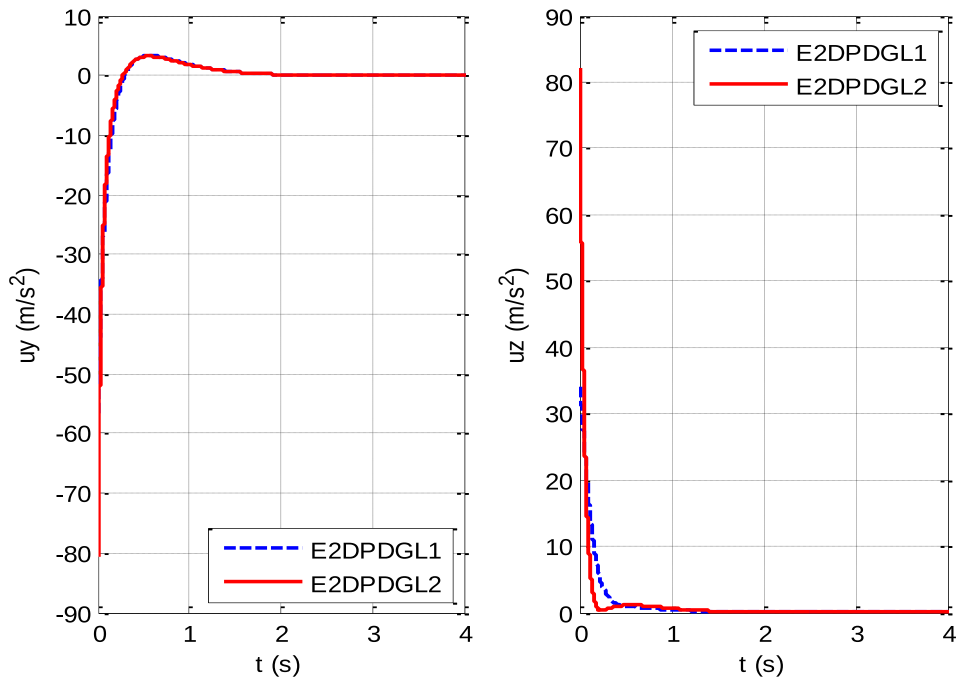

Figure 2.17 The controls u_y and u_z in the guidance loop with E2DPDGL1 and the guidance loop with E2DPDGL2.

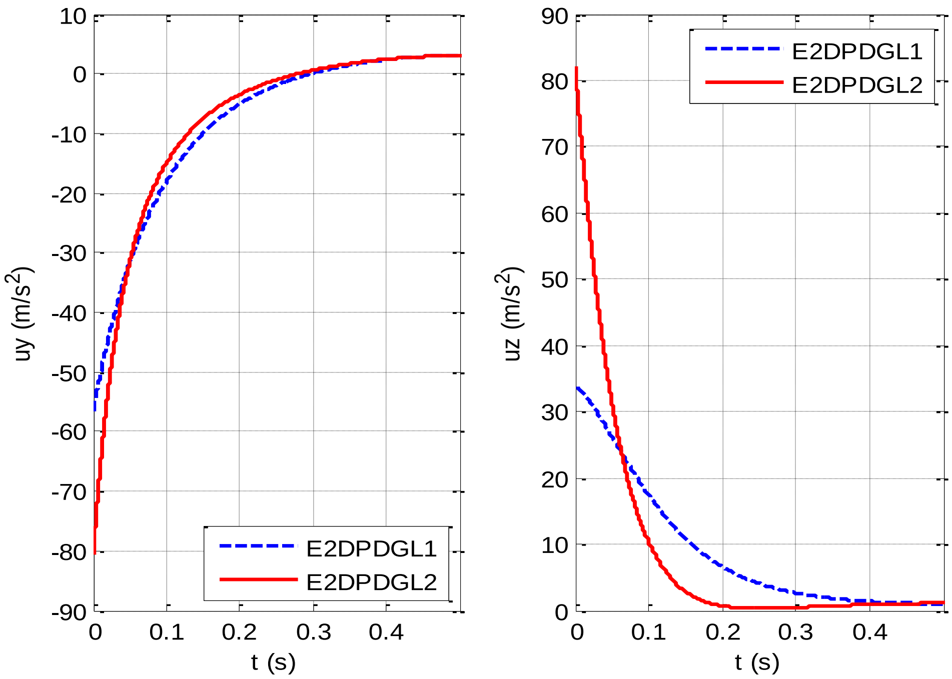

Figure 2.18 The zoomed controls u_y and u_z from Figure 2.17 in the time interval $[0, 0.5]$ s.

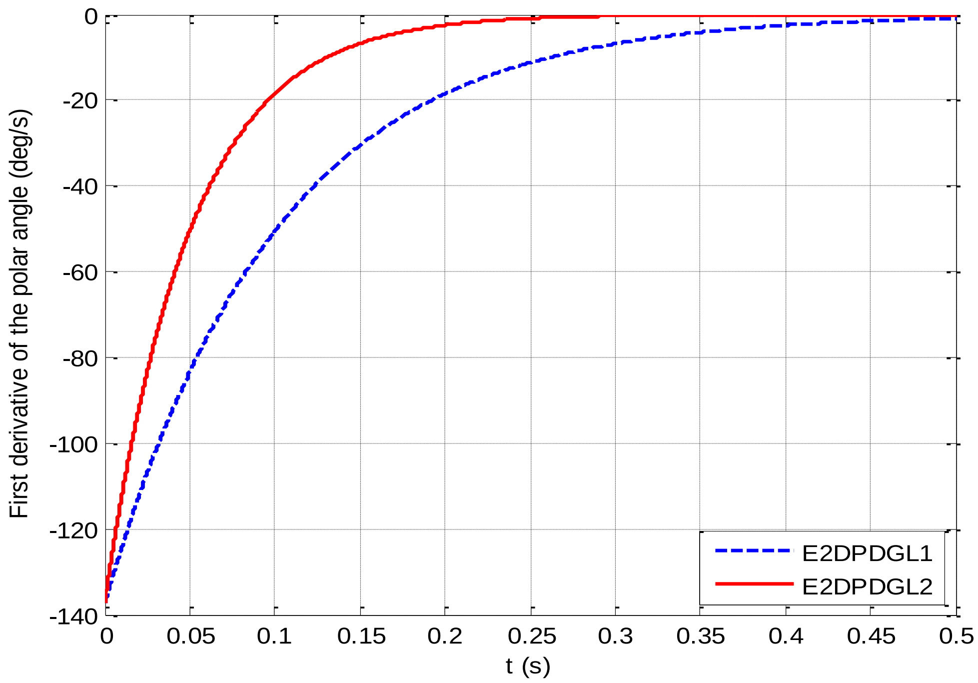

Figure 2.19 The polar angle velocity in the guidance loop with E2DPDGL1 and the guidance loop with E2DPDGL2 in the time interval $[0, 0.5]$ s.

Because of the fact the roots of $f(s)$ (1.5) of the closed loop linear system (1.1), (1.3) with the CPDGL are negative the processes with the CPDGL do not have oscillations as shown in Figure 2.12 - Figure 2.15. The system trajectory in the $Y_L Z_L$-plane, the picture plane, represents an arc. So the E2DPDGL very quickly straightens the system's trajectory as shown in Figure 2.12, Figure 2.16, and Figure 2.19. Figure 2.19 also shows that there is a smooth transition to the CPDGL mode of the E2DPDGL when entering the predetermined ε_r area around the origin of picture plane origin in contrast to the previous case shown in Figure 2.11.

2.3.3 Does the E2DPDGL cope with the persisting phase coupling between the channels

The simulation results show that the specially designed for the system (1.1) E2DPDGL copes in an excellent manner with the effect of spiraling into the origin of the picture plane caused by the non-proportionality of the initial conditions while the transition process of putting the ATGM onto the LOS. The effect of spiral type trajectory in the $Y_L Z_L$-plane, the picture plane, is also seen in case of spatial guidance loop with CPDGL and persisting phase coupling between the channels as shown in Section 1.3.2 "Case with phase coupling between two channels" (page 25). So a perfect CLOS guidance law based on the CPDGL should also cope with spiraling into the picture plane origin caused by a persisting phase coupling between both ATGM channels. Therefore applying the E2DPDGL (2.2) in the guidance loop with the system (1.30) - (1.31) is a necessary experimental phase of the development of a globally effective CLOS guidance law based on the E2DPDGL.

Figure 2.20 - Figure 2.23 show some picture plane missile trajectories of the closed loop (1.30) - (1.31) with the E2DPDGL (2.2) compared with the performance of the classical guidance loop (1.30) - (1.31) with the CPDGL (1.3) at four values of the parameter γ_0. In order to eliminate the spiraling caused by the initial conditions the experiments are carried out with proportional to each other initial conditions (1.16). The pair (a_0, a_1) ((1.7), (1.15)) is identical for both CPDGL and E2DPDGL. The other parameters of the E2DPDGL (2.2) represent (2.30) and (2.31).

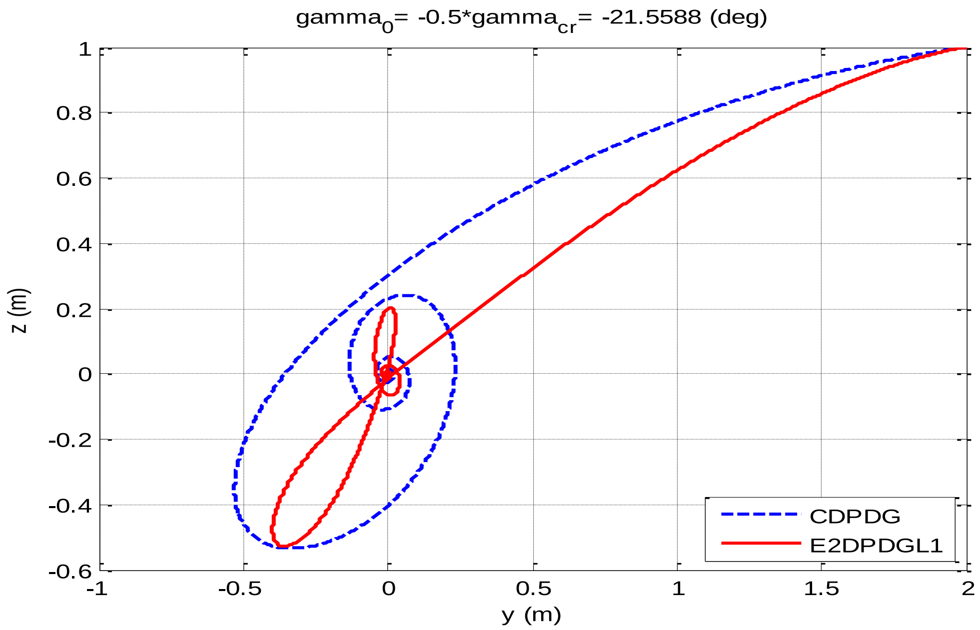

Figure 2.20 Picture plane missile trajectory of the closed loop (1.30) - (1.31) with the E2DPDGL1 (solid line) compared with the performance of the classical guidance loop (1.30) - (1.31) with the CPDGL (dashed line) in case of phase coupling between the channels at $\gamma_0 = -0.5\gamma_{cr} = -21.5588$ deg.

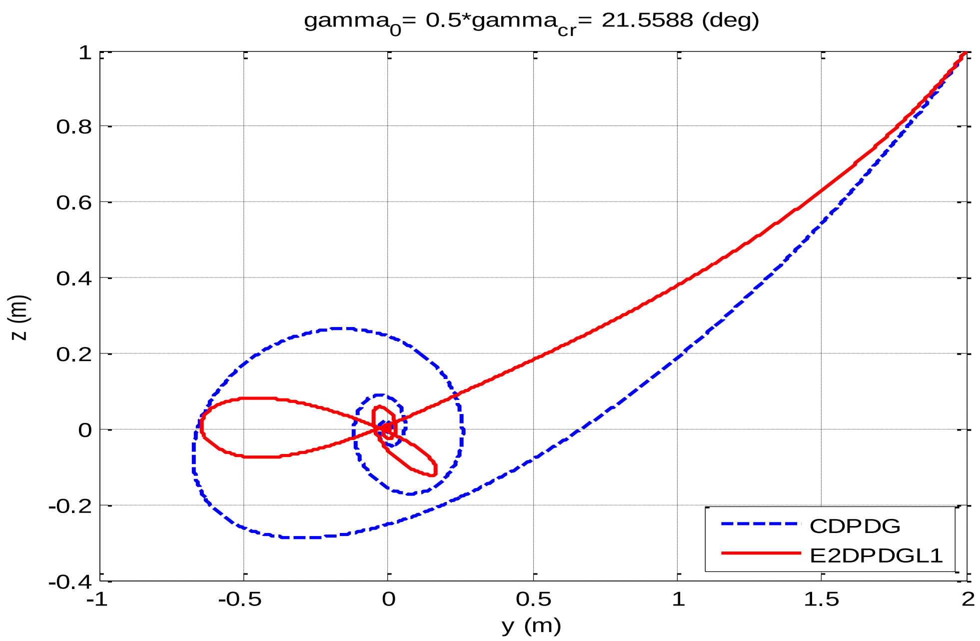

Figure 2.21 Picture plane missile trajectory of the closed loop (1.30) - (1.31) with the E2DPDGL1 (solid line) compared with the performance of the classical guidance loop (1.30) - (1.31) with the CPDGL (dashed line) in case of phase coupling between the channels at $\gamma_0 = 0.5\gamma_{cr} = 21.5588$ deg.

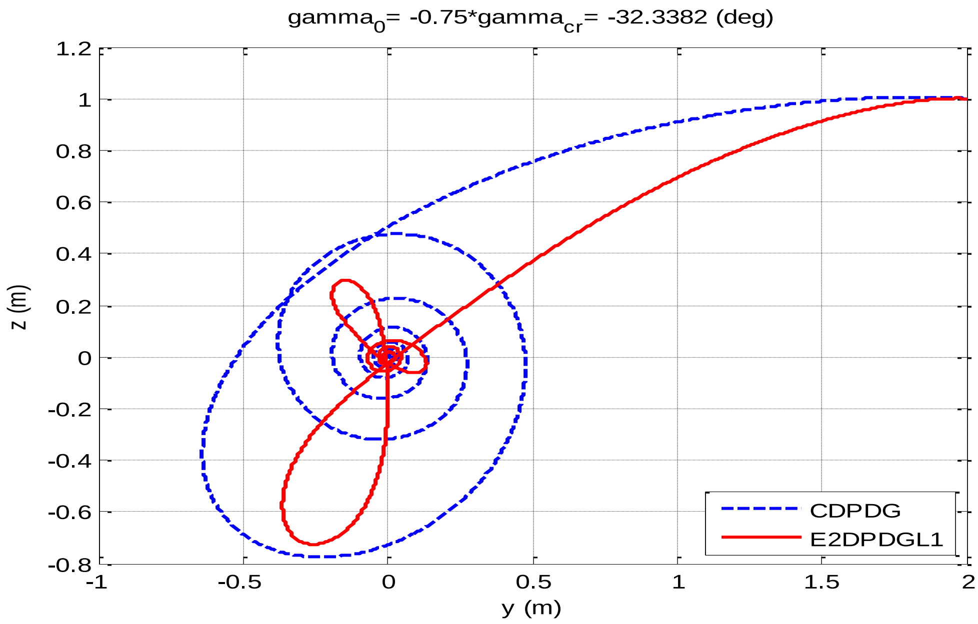

Figure 2.22 Picture plane missile trajectory of the closed loop (1.30) - (1.31) with the E2DPDGL1 (solid line) compared with the performance of the classical guidance loop (1.30) - (1.31) with the CPDGL (dashed line) in case of phase coupling between the channels at $\gamma_0 = -0.75\gamma_{cr} = -32.3382$ deg.

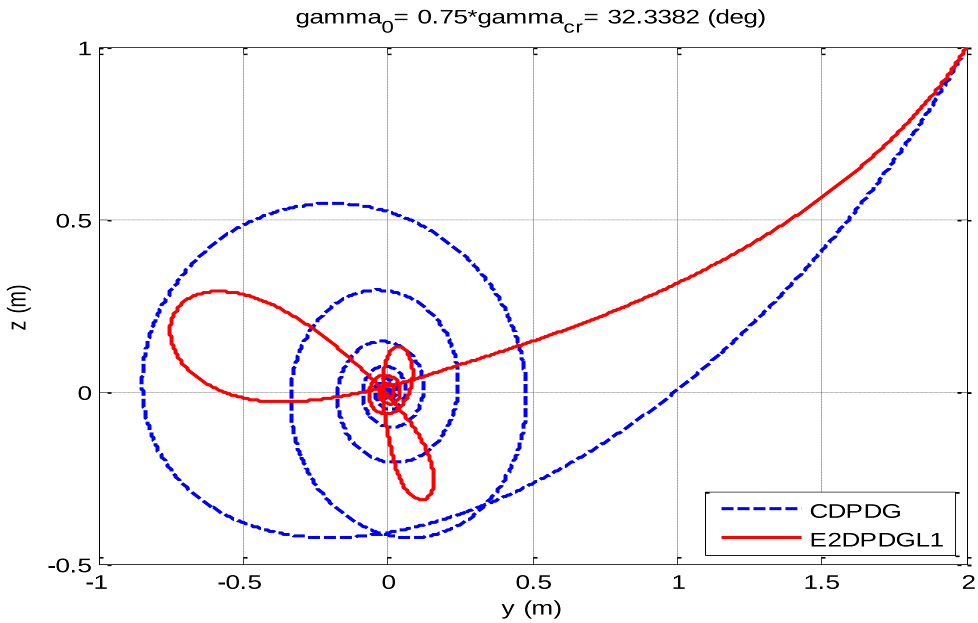

Figure 2.23 Picture plane missile trajectory of the closed loop (1.30) - (1.31) with the E2DPDGL1 (solid line) compared with the performance of the classical guidance loop (1.30) - (1.31) with the CPDGL (dashed line) in case of phase coupling between the channels at $\gamma_0 = 0.75\gamma_{cr} = 32.3382$ deg.

The E2DPDGL improves only in some sections the missile trajectory in the $Y_L Z_L$-plane, the picture plane. There is no trajectory straightening with achievement of symmetry and proportionality between the channels from a general point of view. The decrease of the rotation of the missile pointing vector in the $Y_L Z_L$-plane, the picture plane, in some trajectory sections accompanied with a next „change of the direction" from one section to another suggests the need of additional control of the guidance law vector rotation.

2.4 Conclusion remarks on the E2DPDGL

The E2DPDGL is a continuation of the previous author's studies on ATGM CLOS guidance laws [6], [7], and [8] where the ATGM CLOS control in polar or pseudo-polar coordinates in the $Y_L Z_L$-plane, the picture plane, alongside with a feedback linearization is proposed first. This technique allows splitting the ATGM CLOS closed loop into two new linear looking channels regarding the polar radius and polar angle. Based on this technique a better closed loop performance is achieved with proportionality of the processes in the $Y_L Z_L$-plane, the picture plane. The closed loop comprises also the kinematics in Cartesian coordinates. The rise of obstacles connected with the inverse trigonometric arctangent function for conversion from Cartesian to polar or pseudo-polar coordinates causes the development in the chosen direction get stuck. A rigorous stability proof of the closed loop system is not obtained.

Now the new E2DPDGL is far more sophisticated. The new guidance law is a nonlinear variable structure control law. Outside a predetermined small area in the $Y_L Z_L$-plane, the picture plane, the guidance law includes components based on a feedback linearization and a special pre-coupling between the channels, so that it forms two new linear channels regarding the polar radius and polar angle but without the inverse trigonometric arctangent function in any form. Within the small predetermined area around the picture plane origin – the LOS – the E2DPDGL turns into two CPDGLs with regard to the deviations in both classical horizontal and vertical channels. The E2DPDGL is a nonlinear variable structure control but not a sliding mode control. Its original special design provides straightening the missile trajectory in the $Y_L Z_L$ -plane, the picture plane, and provides an excellent performance while the transition process of putting the ATGM onto the LOS from non-proportional to one another initial deviations in case of no coupling between the channels. The settling time is better as well as the spatial overshooting/falling is improved. These performance benefits enable an improvement of the near-field operational range of the ATGM. Both new and classical proportional-derivative guidance laws use the same input data. Another very important benefit aside from the above advantages is the fact that the global stability of the closed loop with the new E2DPDGL is proven based on a specially designed positive defined Lyapunov function.

The application of the E2DPDGL in a guidance loop with persisting phase coupling between the channels shows definitely the need of a further development and upgrade of the E2DPDGL in order to cope effectively with this case. The idea proposed in Section 2.3.3 “Does the E2DPDGL cope with the persisting phase coupling between the channels” (page 47) outlines an additional control of the guidance law vector rotation.

3 ADAPTIVE EXPANDED TWO-DIMENSIONAL PD CLOS GUIDANCE LAW

3.1 Inclusion of a controlled direction of the E2DPDGL vector

Let us define a controlled variable ψ (rad) in the way (3.1) where u_{ψ} represents the control of the angular velocity $\dot{\psi}$ of the angle ψ. Let also the initial conditions of the angle ψ be (3.2). Rename the controls u_y and u_z of the E2DPDGL (2.2) as controls u_{1y} and u_{1z} and rewrite the E2DPDGL (2.2) as (3.3). Define the E2DPDGL (3.3) in the complex form (3.4) and form the guidance law (3.5) which represents the complex form of the E2DPDGL with controlled vector rotation.

$\frac{d\psi}{dt} = u_{\psi},$	(3.1)
$\psi(0) = 0$	(3.2)
$u_{1y} = \begin{cases} -\dfrac{1}{a_0}(y + a_1\dot{y}) & if\ r \leq \varepsilon_r\ , \\ -\dfrac{1}{a_0}\big(y + a_1(\dot{y} + z\dot{\varphi})\big) - y\dot{\varphi}^2 - 2\dot{r}\dot{\varphi}\sin\varphi + \dfrac{1}{T_{\varphi}}z\dot{\varphi} & if\ r > \varepsilon_r\ , \end{cases}$ $u_{1z} = \begin{cases} -\dfrac{1}{a_0}(z + a_1\dot{z}) & if\ r \leq \varepsilon_r\ , \\ -\dfrac{1}{a_0}\big(z + a_1(\dot{z} - y\dot{\varphi})\big) - z\dot{\varphi}^2 + 2\dot{r}\dot{\varphi}\cos\varphi - \dfrac{1}{T_{\varphi}}y\dot{\varphi} & if\ r > \varepsilon_r\ , \end{cases}$	(3.3)
$u_{1p} = u_{1y} + iu_{1z}$	(3.4)
$u_p = \ e^{i\psi}u_{1p}$	(3.5)

3.2 Problem formulation

The system (1.30) - (1.31) with phase coupling between the channels in terms of the complex variables (8.1) - (8.3) is presented as (8.6). Let us apply in (8.6) the E2DPDGL with controlled vector rotation (3.5):

$\ddot{p} = a_p \,,$ $a_p = e^{i\gamma_0} u_p \,,$ $u_p = e^{i\psi} u_{1p} \,,$ $\dfrac{d\psi}{dt} = u_\psi \,.$	(3.6)

So the problem is to synthesize a control u_ψ of the angular velocity $\dot{\psi}$ of the angle ψ of the controlled direction of the E2DPDGL vector for the system (3.6) with initial conditions according to (1.2) and (3.2) so that the stability of the closed loop system is provided alongside with straightening the missile trajectory in the $Y_L Z_L$-plane, the picture plane.

3.3 Analysis of the system (3.6) and control synthesis of the E2DPDGL vector rotation

The E2DPDGL (3.3) or (2.2) is a nonlinear variable structure control. The effect of straightening the missile trajectory in the $Y_L Z_L$-plane, the picture plane, is achieved outside the predetermined ε_r area around the picture plane origin as shown at consideration of Case 2 (2.6) of Section 2.1 “Guidance law formulation” (page 28) for the case with no coupling between the channels. In order to develop this convention in case with phase coupling between the channels let us consider the case outside the predetermined ε_r area around the picture plane origin but with regard to the system (3.6).

Let us represent the E2DPDGL (3.3) - (3.4) in Case 2 (3.7) in the way (3.8) analogically with the presentation (2.10) of the closed loop system (1.1), (2.2) with the E2DPDGL (2.2) where u_p with components u_r and u_φ represents the E2DPDGL (2.2) in (2.10).

Case 2	$r = \sqrt{y^2 + z^2} > \varepsilon_r$	(3.7)

$$u_{1p} = e^{i\varphi}\left(u_r + iu_\varphi\right), \quad where \quad u_r = -\frac{1}{a_0}(r + a_1\dot{r}) - r\dot{\varphi}^2, \quad u_\varphi = 2\dot{r}\dot{\varphi} - \frac{1}{T_\varphi}r\dot{\varphi}$$	(3.8)

Now the system (3.6) by expression of u_{1p} according to (3.8) and elimination of the inner variables a_p, u_p and u_{1p} represents:

$$\ddot{p} = e^{i\gamma_0}e^{i\psi}e^{i\varphi}\left(\left(-\frac{1}{a_0}(r + a_1\dot{r}) - r\dot{\varphi}^2\right) + i\left(2\dot{r}\dot{\varphi} - \frac{1}{T_\varphi}r\dot{\varphi}\right)\right), \quad \frac{d\psi}{dt} = u_\psi .$$	(3.9)

On the other hand the comparison of the second derivative of p (2.11) with (3.9) results into (3.10) and (3.11) obtained after division of $e^{i\varphi}$ in the first equation of (3.10). The system (3.11) represents the system (3.12) which results into the system (3.13).

$$e^{i\varphi}\left((\ddot{r} - r\dot{\varphi}^2) + i(2\dot{r}\dot{\varphi} + r\ddot{\varphi})\right) = e^{i\gamma_0}e^{i\psi}e^{i\varphi}\left(\left(-\frac{1}{a_0}(r + a_1\dot{r}) - r\dot{\varphi}^2\right) + i\left(2\dot{r}\dot{\varphi} - \frac{1}{T_\varphi}r\dot{\varphi}\right)\right), \quad \frac{d\psi}{dt} = u_\psi .$$	(3.10)
$$\left((\ddot{r} - r\dot{\varphi}^2) + i(2\dot{r}\dot{\varphi} + r\ddot{\varphi})\right) = e^{i(\gamma_0+\psi)}\left(\left(-\frac{1}{a_0}(r + a_1\dot{r}) - r\dot{\varphi}^2\right) + i\left(2\dot{r}\dot{\varphi} - \frac{1}{T_\varphi}r\dot{\varphi}\right)\right), \quad \frac{d\psi}{dt} = u_\psi .$$	(3.11)
$$\ddot{r} - r\dot{\varphi}^2 = u_r\cos(\gamma_0 + \psi) - u_\varphi\sin(\gamma_0 + \psi), \quad 2\dot{r}\dot{\varphi} + r\ddot{\varphi} = u_\varphi\cos(\gamma_0 + \psi) + u_r\sin(\gamma_0 + \psi), \quad \frac{d\psi}{dt} = u_\psi$$	(3.12)

$\ddot{r} - r\dot{\varphi}^2 = \left(-\frac{1}{a_0}(r + a_1\dot{r}) - r\dot{\varphi}^2\right)\cos(\gamma_0 + \psi) -$ $-\left(2\dot{r}\dot{\varphi} - \frac{1}{T_\varphi}r\dot{\varphi}\right)\sin(\gamma_0 + \psi)$ $2\dot{r}\dot{\varphi} + r\ddot{\varphi} = \left(2\dot{r}\dot{\varphi} - \frac{1}{T_\varphi}r\dot{\varphi}\right)\cos(\gamma_0 + \psi) +$ $+\left(-\frac{1}{a_0}(r + a_1\dot{r}) - r\dot{\varphi}^2\right)\sin(\gamma_0 + \psi)$ $\frac{d\psi}{dt} = u_\psi$	(3.13)

Let r^* be the solution of the differential equation (3.14) with initial conditions $r(0)$ and $\dot{r}(0)$ calculated according (2.1) and (2.16) which means (3.15) is valid. Let φ^*, ψ^* and ${u_\psi}^*$ be (3.16). It follows also from (3.16) the respective derivatives of φ^* and ψ^* are (3.17).

$a_0\ddot{r} + a_1\dot{r} + r = 0$	(3.14)
$a_0\ddot{r}^* + a_1\dot{r}^* + r^* = 0$	(3.15)
$\varphi^* = const$ $\psi^* = -\gamma_0 = const\ ,$ ${u_\psi}^* = 0$	(3.16)
$\dot{\varphi}^* = 0\ , \quad \ddot{\varphi}^* = 0\ ,$ $\dot{\psi}^* = 0$	(3.17)

The substitution of all $r^*, \dot{r}^*, \ddot{r}^*, \dot{\varphi}^*, \ddot{\varphi}^*, \psi^*, \dot{\psi}^*$, and ${u_\psi}^*$ from (3.15) - (3.17) into the equations of the system (3.11) results into (3.18) and (3.19). The expression of $\ddot{r}^*$ by r^* and $\dot{r}^*$ from (3.15) and next substitution into (3.19) results into (3.20). The last represents practically three identities.

$\left((\ddot{r}^* - r^*.0^2) + i(2\,\dot{r}^*.0 + r^*.0)\right) =$ $= e^{i(\gamma_0 + (-\gamma_0))}\left(\left(-\frac{1}{a_0}(\,r^* + a_1\dot{r}^*) - r^*.0^2\right) + i\left(2\,\dot{r}^*.0 - \frac{1}{T_\varphi}r^*.0\right)\right)\ ,$ $0 = 0\ .$	(3.18)

$(\ddot{r}^* + i.0) = e^{i.0}\left(\left(-\frac{1}{a_0}(\, r^* + a_1\dot{r}^*)\right) + i.0\right)$ $0 = 0\,.$	(3.19)
$\left(\left(-\frac{1}{a_0}(\, r^* + a_1\dot{r}^*)\right) + i.0\right) = 1.\left(\left(-\frac{1}{a_0}(\, r^* + a_1\dot{r}^*)\right) + i.0\right)$ $0 = 0\,.$	(3.20)

We could conclude that the process (3.15) - (3.17) marked with "*" exists in Case 2 (3.7) outside the predetermined ε_r area around the picture plane origin of the system (3.6) or the system (3.11) or (3.12), or the system (3.13).

Let us linearize the system (3.13) around the process "*" (3.15) - (3.17). Name for convenience the left parts of the first and second differential equations of (3.13) F_{11} and F_{21} while the opposite right parts of the equations – F_{12} and F_{22} respectively. The variables r, φ, ψ, u_ψ and their respective derivatives according to (3.13) are represented in (3.21) - (3.24).

$r = r^* + \Delta r$ $\dot{r} = \dot{r}^* + \Delta\dot{r}$ $\ddot{r} = \ddot{r}^* + \Delta\ddot{r}$	(3.21)
$\varphi = \varphi^* + \Delta\varphi$ $\dot{\varphi} = \dot{\varphi}^* + \Delta\dot{\varphi}$ $\ddot{\varphi} = \ddot{\varphi}^* + \Delta\ddot{\varphi}$	(3.22)
$\psi = \psi^* + \Delta\psi$ $\dot{\psi} = \dot{\psi}^* + \Delta\dot{\psi}$	(3.23)
$u_\psi = {u_\psi}^* + \Delta u_\psi$	(3.24)

The linearization of F_{11} and F_{12} by the first-order Taylor series expansion represents (3.25) - (3.29) and (3.30) - (3.34). Thus the first equation (3.35) of (3.13) represented by the linearized forms (3.29) and (3.34) results into (3.36) and next (3.37) having in mind (3.15).

$F_{11} = F_{11}(r, \ddot{r}, \dot{\varphi}\,) = \ddot{r} - r\dot{\varphi}^2$	(3.25)

$F_{11}(r^*,\ddot{r}^*,\dot{\varphi}^*) = \ddot{r}^*$	(3.26)
$\left.\frac{\partial F_{11}}{\partial r}\right\|_* = 0 \quad \left.\frac{\partial F_{11}}{\partial \ddot{r}}\right\|_* = 1 \quad \left.\frac{\partial F_{11}}{\partial \dot{\varphi}}\right\|_* = 0$	(3.27)
$F_{11} = F_{11}(r,\ddot{r},\dot{\varphi}) \approx F_{11}(r^*,\ddot{r}^*,\dot{\varphi}^*) + + \left.\frac{\partial F_{11}}{\partial r}\right\|_* \Delta r + \left.\frac{\partial F_{11}}{\partial \ddot{r}}\right\|_* \Delta\ddot{r} + \left.\frac{\partial F_{11}}{\partial \dot{\varphi}}\right\|_* \Delta\dot{\varphi}$	(3.28)
$F_{11} \approx \ddot{r}^* + \Delta\ddot{r}$	(3.29)
$F_{12} = F_{12}(r,\dot{r},\dot{\varphi},\psi) = \left(-\frac{1}{a_0}(r + a_1\dot{r}) - r\dot{\varphi}^2\right)\cos(\gamma_0 + \psi) - -\left(2\dot{r}\dot{\varphi} - \frac{1}{T_\varphi} r\dot{\varphi}\right)\sin(\gamma_0 + \psi)$	(3.30)
$F_{12}(r^*,\dot{r}^*,\dot{\varphi}^*,\psi^*) = -\frac{1}{a_0}(r^* + a_1\dot{r}^*)$	(3.31)
$\left.\frac{\partial F_{12}}{\partial r}\right\|_* = -\frac{1}{a_0} \quad \left.\frac{\partial F_{12}}{\partial \dot{r}}\right\|_* = -\frac{a_1}{a_0}$ $\left.\frac{\partial F_{12}}{\partial \dot{\varphi}}\right\|_* = 0 \quad \left.\frac{\partial F_{12}}{\partial \psi}\right\|_* = 0$	(3.32)
$F_{12} = F_{12}(r,\dot{r},\dot{\varphi},\psi) \approx F_{12}(r^*,\dot{r}^*,\dot{\varphi}^*,\psi^*) + + \left.\frac{\partial F_{12}}{\partial r}\right\|_* \Delta r + \left.\frac{\partial F_{12}}{\partial \dot{r}}\right\|_* \Delta\dot{r} + \left.\frac{\partial F_{12}}{\partial \dot{\varphi}}\right\|_* \Delta\dot{\varphi} + \left.\frac{\partial F_{12}}{\partial \psi}\right\|_* \Delta\psi$	(3.33)
$F_{12} \approx -\frac{1}{a_0}(r^* + a_1\dot{r}^*) - \frac{1}{a_0}\Delta r - \frac{a_1}{a_0}\Delta\dot{r}$	(3.34)
$F_{11} = F_{12}$	(3.35)
$\ddot{r}^* + \Delta\ddot{r} = -\frac{1}{a_0}(r^* + a_1\dot{r}^*) - \frac{1}{a_0}\Delta r - \frac{a_1}{a_0}\Delta\dot{r}$	(3.36)
$a_0\Delta\ddot{r} + a_1\Delta\dot{r} + \Delta r = 0$	(3.37)

Analogically the linearization of F_{21} and F_{22} by the first-order Taylor series expansion represents (3.38) - (3.42) and (3.43) - (3.47). The second equation (3.48) of (3.13) represented by the linearized forms (3.42) and (3.47) results into (3.49) and next (3.50). The linearized third equation of (3.13) represents (3.51).

$F_{21} = F_{21}(r, \dot{r}, \dot{\varphi}, \ddot{\varphi}) = 2\dot{r}\dot{\varphi} + r\ddot{\varphi}$	(3.38)
$F_{21}(r^*, \dot{r}^*, \dot{\varphi}^*, \ddot{\varphi}^*) = 0$	(3.39)
$\left.\frac{\partial F_{21}}{\partial r}\right\|_* = 0 \quad \left.\frac{\partial F_{21}}{\partial \dot{r}}\right\|_* = 0$ $\left.\frac{\partial F_{21}}{\partial \dot{\varphi}}\right\|_* = 2\dot{r}^* \quad \left.\frac{\partial F_{21}}{\partial \ddot{\varphi}}\right\|_* = r^*$	(3.40)
$F_{21} = F_{21}(r, \dot{r}, \dot{\varphi}, \ddot{\varphi}) \approx F_{21}(r^*, \dot{r}^*, \dot{\varphi}^*, \ddot{\varphi}^*) + + \left.\frac{\partial F_{21}}{\partial r}\right\|_* \Delta r + \left.\frac{\partial F_{21}}{\partial \dot{r}}\right\|_* \Delta \dot{r} + \left.\frac{\partial F_{21}}{\partial \dot{\varphi}}\right\|_* \Delta \dot{\varphi} + \left.\frac{\partial F_{21}}{\partial \ddot{\varphi}}\right\|_* \Delta \ddot{\varphi}$	(3.41)
$F_{21} \approx 2\dot{r}^* \Delta\dot{\varphi} + r^* \Delta\ddot{\varphi}$	(3.42)
$F_{22} = F_{22}(r, \dot{r}, \dot{\varphi}, \psi) = \left(2\dot{r}\dot{\varphi} - \frac{1}{T_\varphi} r\dot{\varphi}\right)\cos(\gamma_0 + \psi) + + \left(-\frac{1}{a_0}(r + a_1\dot{r}) - r\dot{\varphi}^2\right)\sin(\gamma_0 + \psi)$	(3.43)
$F_{22}(r^*, \dot{r}^*, \dot{\varphi}^*, \psi^*) = 0$	(3.44)
$\left.\frac{\partial F_{22}}{\partial r}\right\|_* = 0 \quad \left.\frac{\partial F_{22}}{\partial \dot{r}}\right\|_* = 0$ $\left.\frac{\partial F_{22}}{\partial \dot{\varphi}}\right\|_* = \left(2\dot{r}^* - \frac{1}{T_\varphi} r^*\right) \quad \left.\frac{\partial F_{22}}{\partial \psi}\right\|_* = \left(-\frac{1}{a_0}(r^* + a_1\dot{r}^*)\right)$	(3.45)
$F_{22} = F_{22}(r, \dot{r}, \dot{\varphi}, \psi) \approx F_{22}(r^*, \dot{r}^*, \dot{\varphi}^*, \psi^*) + + \left.\frac{\partial F_{22}}{\partial r}\right\|_* \Delta r + \left.\frac{\partial F_{22}}{\partial \dot{r}}\right\|_* \Delta \dot{r} + \left.\frac{\partial F_{22}}{\partial \dot{\varphi}}\right\|_* \Delta \dot{\varphi} + \left.\frac{\partial F_{22}}{\partial \psi}\right\|_* \Delta \psi$	(3.46)
$F_{22} \approx \left(2\dot{r}^* - \frac{1}{T_\varphi} r^*\right)\Delta\dot{\varphi} + \left(-\frac{1}{a_0}(r^* + a_1\dot{r}^*)\right)\Delta\psi$	(3.47)
$F_{21} = F_{22}$	(3.48)
$2\dot{r}^*\Delta\dot{\varphi} + r^*\Delta\ddot{\varphi} = \left(2\dot{r}^* - \frac{1}{T_\varphi} r^*\right)\Delta\dot{\varphi} + \left(-\frac{1}{a_0}(r^* + a_1\dot{r}^*)\right)\Delta\psi$	(3.49)
$r^*\Delta\ddot{\varphi} = \left(-\frac{1}{T_\varphi} r^*\right)\Delta\dot{\varphi} + \left(-\frac{1}{a_0}(r^* + a_1\dot{r}^*)\right)\Delta\psi$	(3.50)

$\frac{d\Delta\psi}{dt} = \Delta\dot{\psi} = \Delta u_{\psi}$	(3.51)

The linearization of the system (3.13) consists of the equations (3.37), (3.50), and (3.51) and represents the system:

$a_0\Delta\ddot{r} + a_1\Delta\dot{r} + \Delta r = 0\,,$ $r^*\Delta\ddot{\varphi} = \left(-\frac{1}{T_\varphi}r^*\right)\Delta\dot{\varphi} + \left(-\frac{1}{a_0}(r^* + a_1\dot{r}^*)\right)\Delta\psi\,,$ $\Delta\dot{\psi} = \Delta u_{\psi}\,.$	(3.52)

In order to achieve a more convenient form for the synthesis the linearization of the second equation of (3.13) is done in the form (3.53) - (3.65) which results into the linearized system (3.66) of (3.13).

$F_{21} = F_{21}(r,\dot{r},\dot{\varphi},\ddot{\varphi}) = 2\dot{r}\dot{\varphi} + r\ddot{\varphi}$	(3.53)
$F_{21}(r,\dot{r},\dot{\varphi}^*,\ddot{\varphi}^*) = 0$	(3.54)
$\left.\frac{\partial F_{21}}{\partial\dot{\varphi}}\right\|_{\varphi^*} = 2\dot{r} \quad \left.\frac{\partial F_{21}}{\partial\ddot{\varphi}}\right\|_{\varphi^*} = r$	(3.55)
$F_{21} = F_{21}(r,\dot{r},\dot{\varphi},\ddot{\varphi}\,) \approx\ F_{21}(r,\dot{r},\dot{\varphi}^*,\ddot{\varphi}^*) +\ \left.\frac{\partial F_{21}}{\partial\dot{\varphi}}\right\|_{\varphi^*}\Delta\dot{\varphi} + \left.\frac{\partial F_{21}}{\partial\ddot{\varphi}}\right\|_{\varphi^*}\Delta\ddot{\varphi}$	(3.56)
$F_{21} \approx 2\dot{r}\Delta\dot{\varphi} + r\Delta\ddot{\varphi}$	(3.57)
$F_{22} = F_{22}(r,\dot{r},\dot{\varphi},\psi\,) = \left(2\dot{r}\dot{\varphi} - \frac{1}{T_\varphi}r\dot{\varphi}\right)\cos(\gamma_0 + \psi) +$ $+\left(-\frac{1}{a_0}(r + a_1\dot{r}) - r\dot{\varphi}^2\right)\sin(\gamma_0 + \psi)$	(3.58)
$F_{22}(r,\dot{r},\dot{\varphi}^*,\psi^*) = 0$	(3.59)
$\left.\frac{\partial F_{22}}{\partial\dot{\varphi}}\right\|_{\varphi^*,\psi^*} = \left(2\dot{r} - \frac{1}{T_\varphi}r\right) \quad \left.\frac{\partial F_{22}}{\partial\psi}\right\|_{\varphi^*,\psi^*} = \left(-\frac{1}{a_0}(r + a_1\dot{r})\right)$	(3.60)
$F_{22} = F_{22}(r,\dot{r},\dot{\varphi},\psi\,) \approx\ F_{22}(r,\dot{r},\dot{\varphi}^*,\psi^*) + \left.\frac{\partial F_{22}}{\partial\dot{\varphi}}\right\|_{\varphi^*,\psi^*}\Delta\dot{\varphi} + \left.\frac{\partial F_{22}}{\partial\psi}\right\|_{\varphi^*,\psi^*}\Delta\psi$	(3.61)

$F_{22} \approx \left(2\dot{r} - \frac{1}{T_\varphi} r\right)\Delta\dot{\varphi} + \left(-\frac{1}{a_0}(r + a_1\dot{r})\right)\Delta\psi$	(3.62)
$F_{21} = F_{22}$	(3.63)
$2\dot{r}\Delta\dot{\varphi} + r\Delta\ddot{\varphi} = \left(2\dot{r} - \frac{1}{T_\varphi} r\right)\Delta\dot{\varphi} + \left(-\frac{1}{a_0}(r + a_1\dot{r})\right)\Delta\psi$	(3.64)
$r\Delta\ddot{\varphi} = \left(-\frac{1}{T_\varphi} r\right)\Delta\dot{\varphi} + \left(-\frac{1}{a_0}(r + a_1\dot{r})\right)\Delta\psi$	(3.65)
$a_0\Delta\ddot{r} + a_1\Delta\dot{r} + \Delta r = 0\,,$ $r\Delta\ddot{\varphi} = \left(-\frac{1}{T_\varphi} r\right)\Delta\dot{\varphi} + \left(-\frac{1}{a_0}(r + a_1\dot{r})\right)\Delta\psi\,,$ $\frac{d\Delta\psi}{dt} = \Delta\dot{\psi} = \Delta u_\psi\,.$	(3.66)

Define $\Delta\varphi_1$ as (3.67). Then the system (3.66) is presented in the form (3.68). Let us choose the control Δu_ψ as (3.69) which results with regard to the system (3.68) into the closed loop system (3.70). Note the system (3.70) is decoupled one. The first equation is with regard to Δr only and is asymptotically stable. The rest two equations define a sub-system with regard to $\Delta\varphi_1$ and $\Delta\psi$ only. It is a homogeneous system of differential equations of second order and is presented in a matrix form as (3.71) and as a block-diagram in Figure 3.1. The characteristic polynomial of (3.71) is (3.72) or (3.73). The last refers to an asymptotically stable system except for a limited number of points where the system turns into a neutrally stable one in case when (3.74) occurs which is illustrated in Figure 3.2.

$\Delta\varphi_1 = \Delta\dot{\varphi}$	(3.67)
$a_0\Delta\ddot{r} + a_1\Delta\dot{r} + \Delta r = 0\,,$ $\Delta\dot{\varphi}_1 = \left(-\frac{1}{T_\varphi}\right)\Delta\varphi_1 + \left(-\frac{1}{a_0}\frac{(r + a_1\dot{r})}{r}\right)\Delta\psi\,,$ $\Delta\dot{\psi} = \Delta u_\psi\,.$	(3.68)
$\Delta u_\psi = \left(k_\psi sign(r + a_1\dot{r})\right)\Delta\varphi_1\,, \quad k_\psi = const > 0$	(3.69)

$a_0\Delta\ddot{r} + a_1\Delta\dot{r} + \Delta r = 0\,,$ $\Delta\dot{\varphi}_1 = \left(-\frac{1}{T_\varphi}\right)\Delta\varphi_1 + \left(-\frac{1}{a_0}\frac{(r + a_1\dot{r})}{r}\right)\Delta\psi\,,$ $\Delta\dot{\psi} = \left(k_\psi sign(r + a_1\dot{r})\right)\Delta\varphi_1\,.$	(3.70)
$\begin{pmatrix}\Delta\dot{\varphi}_1\\ \Delta\dot{\psi}\end{pmatrix} = \begin{pmatrix}\left(-\frac{1}{T_\varphi}\right) & \left(-\frac{1}{a_0}\frac{(r + a_1\dot{r})}{r}\right)\\ \left(k_\psi sign(r + a_1\dot{r})\right) & 0\end{pmatrix}\begin{pmatrix}\Delta\varphi_1\\ \Delta\psi\end{pmatrix}$	(3.71)
$f(s) = det\left(\begin{pmatrix}s & 0\\ 0 & s\end{pmatrix} - \begin{pmatrix}\left(-\frac{1}{T_\varphi}\right) & \left(-\frac{1}{a_0}\frac{(r + a_1\dot{r})}{r}\right)\\ \left(k_\psi sign(r + a_1\dot{r})\right) & 0\end{pmatrix}\right)$	(3.72)
$f(s) = s^2 + \left(\frac{1}{T_\varphi}\right)s + \left(\frac{k_\psi}{a_0}\frac{\lvert r + a_1\dot{r}\rvert}{r}\right)$	(3.73)
$r + a_1\dot{r} = 0$	(3.74)

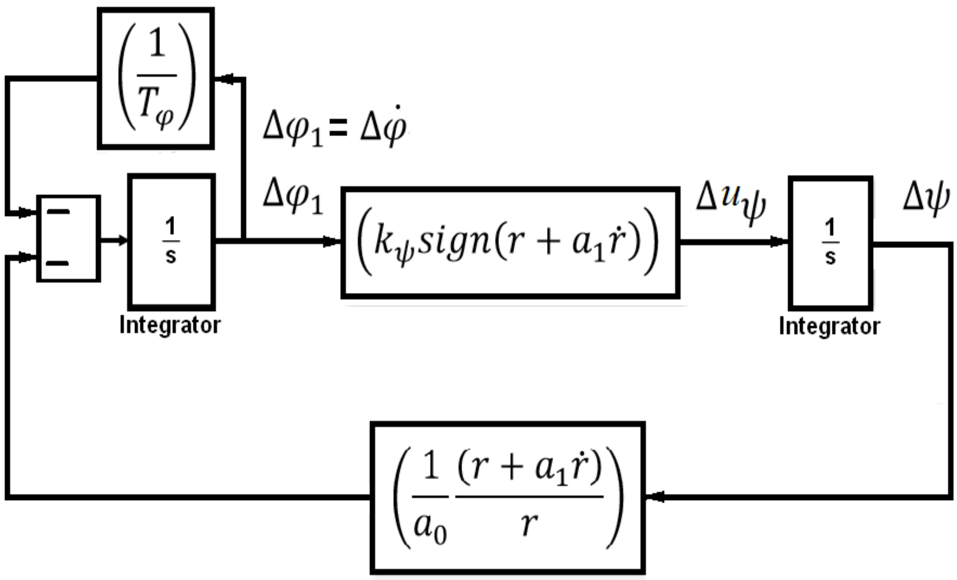

Figure 3.1 Block-diagram of the sub-system (3.71).

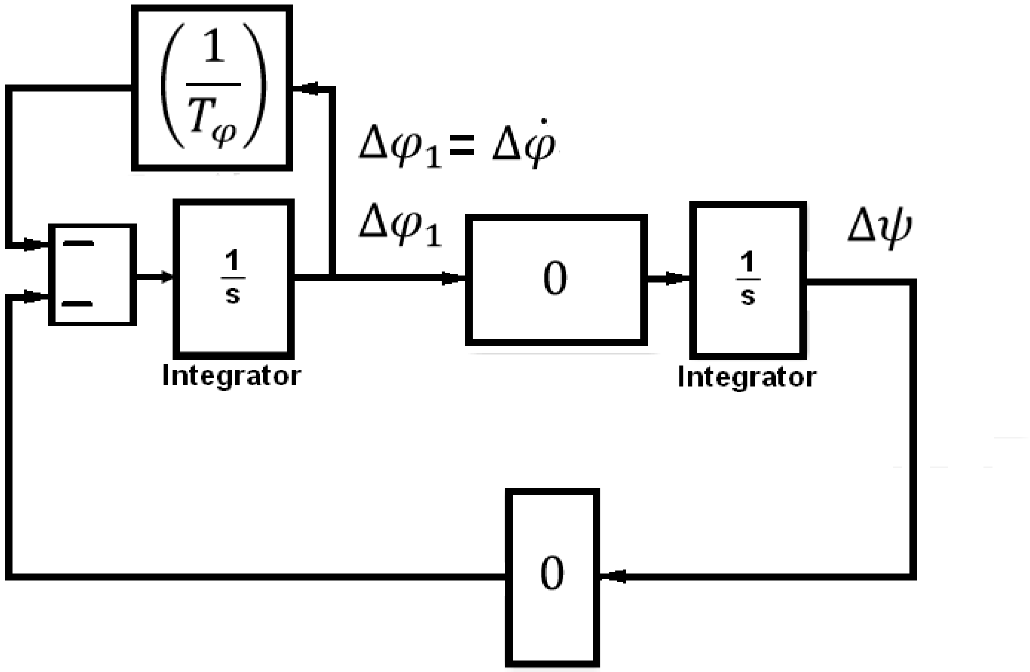

Figure 3.2 Block-diagram of the sub-system (3.71) in case when (3.74) occurs.

The stability of the closed loop system (3.71) leads to (3.75) and consequently to (3.76) and (3.77) having in mind (3.22) and (3.23).

$\lim\limits_{t\to\infty} \Delta\varphi_1 = \lim\limits_{t\to\infty} \Delta\dot{\varphi} = 0$ $\lim\limits_{t\to\infty} \Delta\psi = 0$	(3.75)
$\lim\limits_{t\to\infty} \dot{\varphi} = 0$ $\lim\limits_{t\to\infty} \varphi = const$	(3.76)
$\lim\limits_{t\to\infty} \psi = -\gamma_0$	(3.77)

Thus three main benefits are achieved by the control (3.69):

- The closed loop system (3.66), (3.69) is decoupled by separating into two sub-systems, one with regard to the polar radius only, and the other with regard to the velocity of the polar angle $\dot{\varphi}$ and the angle of rotation ψ of the E2DPDGL vector rotation only. Both sub-systems are stable;

- The control straightens the missile trajectory in the $Y_L Z_L$-plane, the picture plane, outside the predetermined ε_r area around the picture plane origin (3.76);
- The controlled angle of rotation ψ of the E2DPDGL vector rotation strives to the angle $(-\gamma_0)$ (3.77) the opposite of the angle γ_0. This effect of the control (3.69) in the closed loop system (3.71) represents a pre-coupling by the angle $\psi = -\gamma_0$ which cancels the phase coupling between the channels caused by the angle γ_0. This self-adjustment of the control loop in regard to the angle γ_0 is practically implicit. So this control of the angle of rotation of the E2DPDGL vector is an adaptive one. For this reason it could be named an adaptive (A) control of the angle of the E2DPDGL vector rotation. Thus the E2DPDGL with adaptive (A) control of the angle of the E2DPDGL vector rotation is named adaptive (A) E2DPDGL – AE2DPDGL.

Let us form the adaptive control of the angle of the E2DPDGL vector rotation as (3.78) following the convention of the E2DPDGL. Thus the closed loop guidance system of the CLOS ATGM with phase coupling between the channels controlled by the AE2DPDGL represents the group of equations ((1.30) - (1.31), (3.1) - (3.5), and (3.78)) or the system ((3.6), (3.78)) and is illustrated in Figure 3.3.

$$u_\psi = \begin{cases} 0 & if\ r \leq \varepsilon_r \\ \left(k_\psi sign(r + a_1 \dot{r})\right)\dot{\varphi}, \quad k_\psi = const > 0 & if\ r > \varepsilon_r \end{cases} \tag{3.78}$$

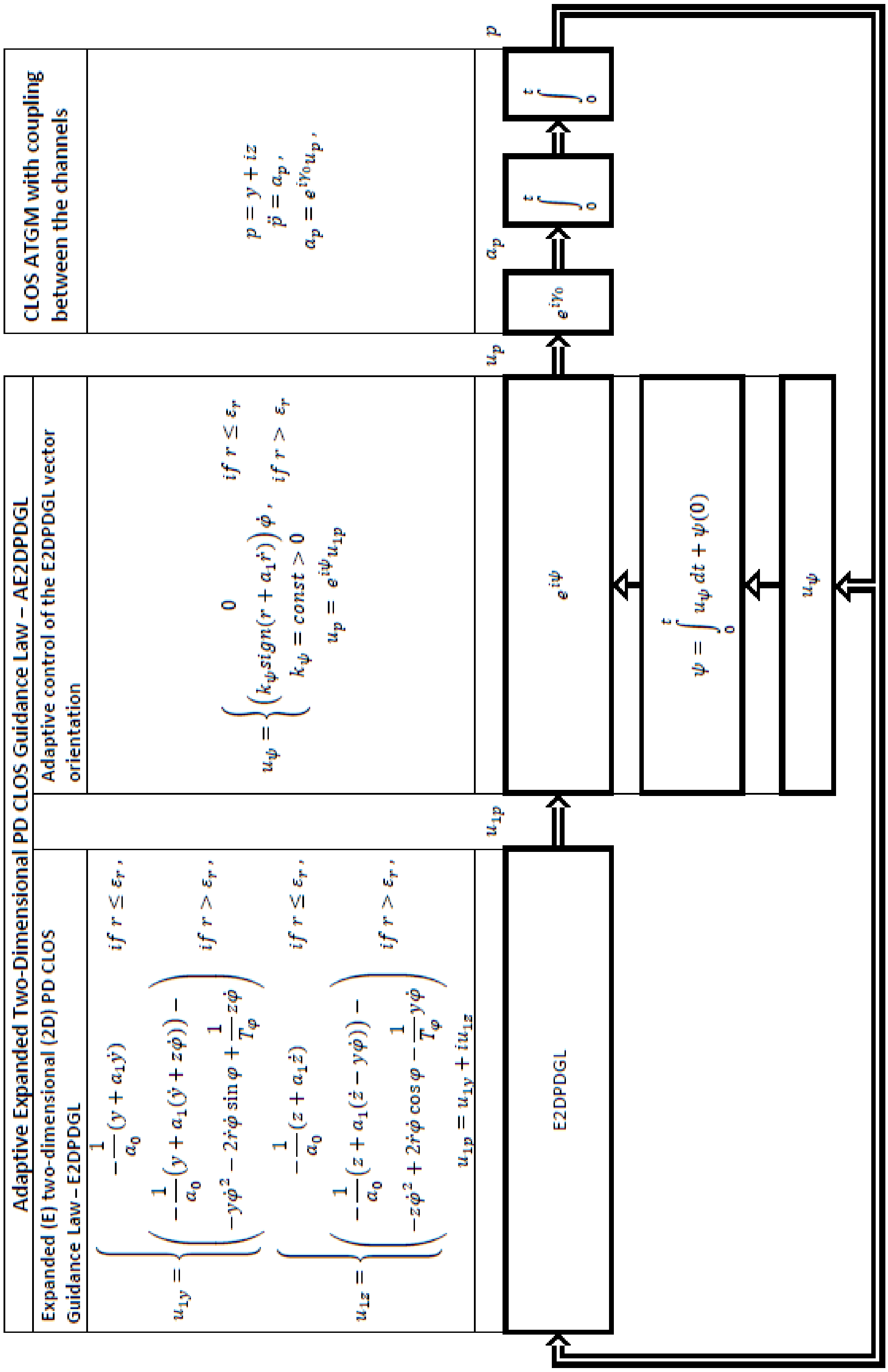

Figure 3.3 The closed loop guidance system of the CLOS ATGM with phase coupling between the channels (1.30) - (1.31) controlled by the AE2DPDGL ((3.1) - (3.5), (3.78)).

3.4 Global stability of the closed loop guidance system with phase coupling between the channels controlled by the AE2DPDGL

Because of the fact that the AE2DPDGL (3.1) - (3.5), (3.78) is a variable structure control according to the switching condition on r the process of the closed loop system in the $Y_L Z_L$-plane, the picture plane, could several times enter or leave the ε_r area around the picture plane origin. Thus, every time the process of the closed loop system in the picture plane enters this ε_r area around the picture plane origin the variable ψ becomes constant for the time the process stays within this ε_r area. Denote the value of this variable ψ for this period of time as ψ_{ε_r} which represents the value of ψ at the boundary of the ε_r area outside it when $r \to \varepsilon_r$. In case the process of the closed loop system starts within the ε_r area the first value of ψ_{ε_r} is zero according to (3.2).

Suppose the system trajectory in the $Y_L Z_L$-plane (the picture plane) starts from a point outside the ε_r area around the picture plane origin or there is a crossing of the border of this ε_r area from inside at some point of this boundary. Name for convenience the area outside the ε_r area around the picture plane origin as area B. Let the time of the process evolution since that moment outside the ε_r area be Δt_j^B where j is a counter which indicates the $j-th$ time when the system stays in the area B – outside the ε_r area. In case there is a following crossing the ε_r area boundary by the system trajectory then define the time interval of stay outside the ε_r area till crossing this boundary as $\Delta t_j^{BC} = \Delta t_j^B$. This occurrence is illustrated in Figure 3.4 with the "Do while loop" with regard to "Inner loop B".

Suppose the system trajectory in the $Y_L Z_L$-plane (the picture plane) starts from a point within the ε_r area around the picture plane origin or there is a crossing of the border of this ε_r area from outside at some point of this boundary. Name for convenience the area within the ε_r area around the picture plane origin as area A. Let the time of the process evolution from that point within the ε_r area be Δt_j^A where j is the counter defined already above with regard to Δt_j^B and Δt_j^{BC}. In case there is a following crossing the ε_r area boundary by the system trajectory then define the time interval of stay within the ε_r area till crossing its boundary as $\Delta t_0^{AC} = \Delta t_0^A$ when the system trajectory starts at $t = 0$ within the ε_r area or as $\Delta t_j^{AC} = \Delta t_j^A$ having in mind j indicates the jth time when the system enters the area A following the jth time of stay in the area B. This occurrence is illustrated in Figure 3.4 with the "Do while loop" with regard to "Inner loop A".

Note with regard to "Inner loop B" that the closed loop system outside the ε_r area as we have shown turns into a system with regard to the variables r , $\dot{\varphi}$ and ψ. This system is a stable one and decoupled. So there is straightening of the system trajectory being outside the ε_r area, the variables $\dot{\varphi}$ and ψ strive to 0 and $(-\gamma_0)$ respectively, and the system enters surely the ε_r area around the picture plane origin crossing the boundary of this area (because of the stability of the decoupled sub-system on r). Thus every stay of the system outside the ε_r area ends with "Inner loop B" termination and obtaining the limited value of Δt_j^{BC} for the current $j-th$ time of stay outside the ε_r area.

Note also that the value of ψ remains constant or "frozen" while the system is not outside the ε_r area.

3.4.1 Global stability analysis of the closed loop guidance system based on the summary time of stays outside the ε_r area

Denote the maximum number of stays outside the ε_r area as j_{max}. Suppose the system evolution has $j_{max} \geq 1$ number of stays outside the ε_r area and denote the summary time of stay there as

$$\Delta t_{sum}^{BC} = \sum_{j=1}^{j_{max}} \Delta t_j^{BC} \,. \tag{3.79}$$

In order to analyze the stability of the closed loop guidance system let us study consequently all cases of the summary time of stays outside the predetermined ε_r area Δt_{sum}^{BC} (3.79) according to the sorting in the following Table 3.1 (page 67).

Table 3.1 Sorting the summary time of stays outside the ε_r area.

Summary time of stays outside the predetermined ε_r area Δt_{sum}^{BC}	**Case**
$\Delta t_{sum}^{BC} \to \infty$	1
$0 < \Delta t_{sum}^{BC} < \infty$	2
No stays outside the ε_r area	3

3.4.1.1 Case of infinite summary time of stays outside the ε_r area

Let us assume (3.80). It implies also that (3.81) is valid. At $t \to \infty$ the variables $\dot{\varphi}$ and ψ become 0 and $(-\gamma_0)$ according to (3.76) and (3.77) respectively. Due to the asymptotic stability with respect to r of the system outside the ε_r area the system trajectory surely intersects the ε_r area boundary in some point. Thus the point on the ε_r area boundary where the switching occurs satisfies the conditions (3.82). It follows from (3.82) that there is a proportionality with regard to the initial conditions for the current system process within the ε_r area. From the other side the closed loop system (3.6) within the ε_r area having in mind (3.77) represents the system (3.83) which results into the system (1.4). So the system trajectory within the ε_r area lies on the same straight line as outside the area. Note that the E2DPDGL u_{1p} (3.3) which is a component of the AE2DPDGL in case of (3.76) and (3.77) turns into (3.84) and next (3.85). The last means that the closed loop system within the ε_r area as well as outside of it represents the asymptotic stable system (1.4) with proportional to one another processes on y and z . The system trajectory subsides to the picture plane origin and since some moment stays wholly within the ε_r area around the picture plane origin. This means that there is no stay of the system since that moment outside the ε_r area and the summary time of stay outside the ε_r area is limited by this moment. The last contradicts the assumption (3.80) with regard to the summary time of stay outside the ε_r area. So the assumption (3.80) is not true. This case is marked as Case 1 of Table 3.2 (page 70).

$\Delta t_{sum}^{BC} \to \infty$	(3.80)

$j_{max} \to \infty$	(3.81)
$r = \varepsilon_r = \sqrt{y^2 + z^2}\,,$ $\dot{\varphi} = \dfrac{\dot{z}y - \dot{y}z}{y^2 + z^2} = 0$	(3.82)
$\ddot{p} = \ddot{y} + i\ddot{z} = a_p\,,$ $a_p = e^{i\gamma_0} u_p\,,$ $u_p = e^{i\psi} u_{1p}\,,$ $u_{1p} = u_{1y} + iu_{1z} = \left(-\dfrac{1}{a_0}(y + a_1\dot{y})\right) + i\left(-\dfrac{1}{a_0}(z + a_1\dot{z})\right)$	(3.83)
$u_{1y} = \begin{cases} -\dfrac{1}{a_0}(y + a_1\dot{y}) & if\ r \le \varepsilon_r\,, \\ -\dfrac{1}{a_0}(y + a_1\dot{y}) & if\ r > \varepsilon_r\,, \end{cases}$ $u_{1z} = \begin{cases} -\dfrac{1}{a_0}(z + a_1\dot{z}) & if\ r \le \varepsilon_r\,, \\ -\dfrac{1}{a_0}(z + a_1\dot{z}) & if\ r > \varepsilon_r \end{cases}$	(3.84)
$u_{1y} = -\dfrac{1}{a_0}(y + a_1\dot{y})\,,$ $u_{1z} = -\dfrac{1}{a_0}(z + a_1\dot{z})$	(3.85)

3.4.1.2 Case of limited but non-zero summary time of stays outside the ε_r area

Let us now assume the summary time of stays outside the ε_r area is limited but non-zero (3.86). There are two alternative possibilities with regard to the maximum number of stays outside the ε_r area: (3.87) or (3.88). Note that every $j - th$ stay outside is preceded by a limited stay within the ε_r area for a time Δt_{j-1}^{AC}. In case $j = 1$ the time of stay Δt_0^{AC} is $\Delta t_0^{AC} > 0$ when the system evolution is from an initial point within the ε_r area at beginning the process at $t = 0$ and represents the time of the system evolution till crossing the switching boundary. When the process starts at $t = 0$ from a point outside the ε_r area formally $\Delta t_0^{AC} = 0$ according to the control-flow block-diagram in Figure 3.4. Thus (3.89) is valid. It follows from (3.86) and (3.89) that after $(\Delta t_{sum}^{BC} + \Delta t_{sum}^{AC})$ the system trajectory is surely within the ε_r area (3.90) and "Inner loop A" in Figure 3.4 becomes an infinite loop. For instance, if we suppose there is a termination of "Inner loop A" at some moment after

$(\Delta t_{sum}^{BC} + \Delta t_{sum}^{AC})$ then j becomes $j = j + 1$ and a next limited stay outside the ε_r area Δt_j^{BC} occurs. Thus $\Delta t_{sum}^{BC} = \Delta t_{sum}^{BC} + \Delta t_j^{BC}$ which contradicts the assumption Δt_{sum}^{BC} is limited (3.86) and is already achieved. Furthermore, in case (3.88) $j = j_{max}$ becomes $j = j_{max} + 1$ which contradicts to the assumption that j_{max} is supposed to be a limited maximum number of stays outside the ε_r area. The consideration in this case under this assumption is marked as Case 2 of Table 3.2 (page 70).

The final value of the controlled angle of the AE2DPDGL vector rotation is (3.91) and next (3.92). It follows (3.93) from the above conclusion with regard to the system trajectory final stay within the ε_r area (3.90) under the assumption (3.86). Thus in case (3.94) the system trajectory subsides to the origin of the picture plane but in case (3.95) limited steady oscillations within the ε_r area around the picture plane origin are possible.

$$0 < \sum_{j=1}^{j_{max}} \Delta t_j^{BC} = \Delta t_{sum}^{BC} < \infty$$	(3.86)
$$j_{max} \to \infty$$	(3.87)
$$0 < j_{max} < \infty$$	(3.88)
$$\sum_{j=1}^{j_{max}} \Delta t_{j-1}^{AC} = \Delta t_{sum}^{AC} < \infty$$	(3.89)
$$r(t) = \sqrt{y(t)^2 + z(t)^2} \leq \varepsilon_r \ \forall t > (\Delta t_{sum}^{BC} + \Delta t_{sum}^{AC})$$	(3.90)
$$\psi(\infty) = \psi(\Delta t_{sum}^{BC} + \Delta t_{sum}^{AC}) = \psi(0) + \sum_{j=1}^{j_{max}} \Delta\psi\left(\Delta t_j^{BC}\right) \neq (-\gamma_0)$$	(3.91)
$$\psi_{\varepsilon_r}(\infty) = \psi_{\varepsilon_r}(\Delta t_{sum}^{BC} + \Delta t_{sum}^{AC}) = \psi(\Delta t_{sum}^{BC} + \Delta t_{sum}^{AC})$$	(3.92)
$$\left|(\psi_{\varepsilon_r}(\infty) + \gamma_0)\right| \leq \gamma_{cr}$$	(3.93)
$$\left|(\psi_{\varepsilon_r}(\infty) + \gamma_0)\right| < \gamma_{cr}$$	(3.94)
$$\left|(\psi_{\varepsilon_r}(\infty) + \gamma_0)\right| = \gamma_{cr}$$	(3.95)

3.4.1.3 Case of no stays outside the ε_r area around the picture plane origin

Let us assume finally that there are no stays outside the ε_r area around the picture plane origin (3.96). It follows according to the control-flow block-diagram in Figure 3.4 that the initial conditions refer to a point within the ε_r area around the picture plane origin and there is no termination of “Inner Loop A” in Figure 3.4. Thus since the very beginning at $t = 0$ the system process stays forever within the ε_r area around the picture plane origin (3.97). The controlled angle of the EA2DPDGL vector rotation stays zero (3.98) and (3.99) is valid. The last results into the cases (3.100) and (3.101). The system trajectory subsides to the picture plane origin when (3.100) while in case (3.101) limited steady oscillations within the ε_r area around the picture plane origin are possible. This consideration is presented shortly as Case 3 of Table 3.2 (page 70).

$j = j_{max} = 0$	(3.96)
$r(t) = \sqrt{y(t)^2 + z(t)^2} \leq \varepsilon_r \ \forall\, t \geq 0$	(3.97)
$\psi(t) = \psi(0) = 0 \ \ \forall\, t \geq 0$	(3.98)
$\lvert(\psi(t) + \gamma_0)\rvert = \lvert(0 + \gamma_0)\rvert = \lvert\gamma_0\rvert \leq \gamma_{cr} \ \ \forall\, t \geq 0$	(3.99)
$\lvert(\psi(t) + \gamma_0)\rvert = \lvert(0 + \gamma_0)\rvert = \lvert\gamma_0\rvert < \gamma_{cr} \ \ \forall\, t \geq 0$	(3.100)
$\lvert(\psi(t) + \gamma_0)\rvert = \lvert(0 + \gamma_0)\rvert = \lvert\gamma_0\rvert = \gamma_{cr} \ \ \forall\, t \geq 0$	(3.101)

Table 3.2 Study summary of the cases with regard to the summary time of stays of the system outside the predetermined ε_r area around the picture plane origin.

Case	**Assumption**		**Possibility and short conclusion with regard to the system trajectory evolution**
1	$\Delta t_{sum}^{BC} \to \infty$	(3.80)	This case is not possible.

2		$0 < \Delta t_{sum}^{BC} < \infty$	(3.86)	The case is possible. At $t \to \infty$ the system trajectory remains within the ε_r area around the picture plane origin, regardless of the value of γ_0.
	Only possible sub-cases of Case 2			
	2.1	$\lvert(\psi_{\varepsilon_r}(\infty) + \gamma_0)\rvert < \gamma_{cr}$	(3.94)	+ The system trajectory subsides to the origin of the picture plane.
	2.2	$\lvert(\psi_{\varepsilon_r}(\infty) + \gamma_0)\rvert = \gamma_{cr}$	(3.95)	+ There exist limited steady oscillations within the ε_r area around the picture plane origin.
3		$j = j_{max} = 0$	(3.96)	The case is possible. At $t \to \infty$ the system trajectory remains within the ε_r area around the picture plane origin.
	Only possible sub-cases of Case 3			
	3.1	$\lvert(\psi(t) + \gamma_0)\rvert =$ $= \lvert(0 + \gamma_0)\rvert =$ $= \lvert\gamma_0\rvert < \gamma_{cr} \;\; \forall\, t \geq 0$	(3.100)	+ The system trajectory subsides to the origin of the picture plane.
	3.2	$\lvert(\psi(t) + \gamma_0)\rvert =$ $= \lvert(0 + \gamma_0)\rvert =$ $= \lvert\gamma_0\rvert = \gamma_{cr} \;\; \forall\, t \geq 0$	(3.101)	+ There exist limited steady oscillations within the ε_r area around the picture plane origin.

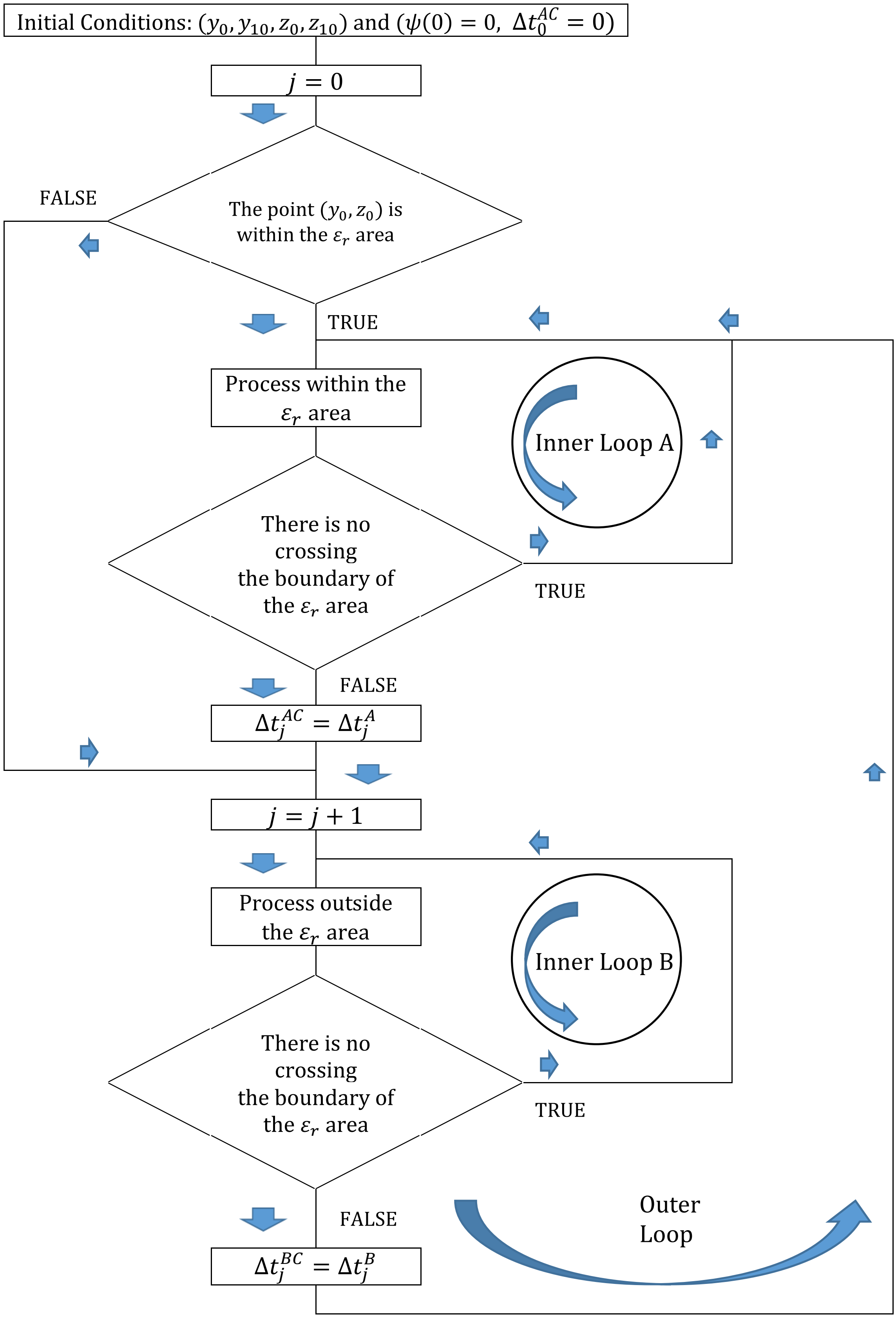

Figure 3.4 Control-flow block-diagram of the closed loop guidance system with phase coupling between the channels controlled by the AE2DPDGL.

3.4.2 General conclusion on the global stability of the closed loop system

The study summary in Table 3.2 (page 70) covers all cases with regard to the summary time of stays outside the predetermined ε_r area around the picture plane origin. Thus the only possible evolution of the closed loop guidance system at $t \to \infty$ represents subsiding to the picture plane origin or a limited process within the predetermined ε_r area around the picture plane origin. So regardless of the initial conditions or the value of the angle γ_0 determining the phase coupling between the channels the AE2DPDGL guarantees straightening the system trajectory outside the ε_r area and the final stay of the system trajectory within the ε_r area. The AE2DPDGL provides surely a final value of the controlled angle of the E2DPDGL vector rotation ψ so that the absolute value of the sum of this final value of ψ and the value of the angle γ_0 is no greater than γ_{cr} (8.55):

$$\left|(\psi_{\varepsilon_r}(\infty) + \gamma_0)\right| \le \gamma_{cr} \tag{3.102}$$

Thus the type of the final stay within the ε_r area could be only a subsiding to the picture plane origin process or represents limited steady oscillations within this ε_r area.

3.5 Simulations

In order to illustrate the global stability of the closed loop guidance system alongside with straightening the missile trajectory in the $Y_L Z_L$ -plane, the picture plane, regardless of the value of the phase coupling angle γ_0 and the initial conditions at starting the controlled ATGM, flight simulations of the closed loop guidance system of the CLOS ATGM with phase coupling between the channels (1.30) - (1.31) controlled by the AE2DPDGL ((3.1) - (3.5), (3.78)) are carried out.

The performance of the closed loop guidance system is illustrated with four cases of initial conditions. The first one is with proportional to each other initial conditions (1.16) with proportionality $k = 0.5$ according to (1.10) and (1.14). The second group is with non-proportional to each other initial conditions (1.17). The third group is with the non-proportional to each other initial conditions (3.103), and the fourth group is with initial conditions (3.104) which are non-proportional to each other but very close to the strictly proportional initial conditions (1.16).

$y_0 = -2, \quad y_{10} = 2,$ $z_0 = 1, \quad z_{10} = -5$	(3.103)
$y_0 = 2, \quad y_{10} = 0 + 0.1,$ $z_0 = 1, \quad z_{10} = 0 - 0.05$	(3.104)

The varying of the phase coupling angle γ_0 is in the range of $[-\pi, \pi]$ according to (3.105) - (3.113). The value of the critical phase coupling angle γ_{cr} is calculated according to (8.55) from Section 8.1.3 “General conclusion on the stability of the closed loop system” (page 195).

$\gamma_0 = 0$	(3.105)
$\gamma_0 = +\gamma_{cr}$	(3.106)
$\gamma_0 = -\gamma_{cr}$	(3.107)
$\gamma_0 = +2\gamma_{cr}$	(3.108)
$\gamma_0 = -2\gamma_{cr}$	(3.109)
$\gamma_0 = +\frac{\pi}{2}$	(3.110)
$\gamma_0 = -\frac{\pi}{2}$	(3.111)
$\gamma_0 = +\pi$	(3.112)
$\gamma_0 = -\pi$	(3.113)

The illustrations are made first for the case with a pair conjugate complex roots of the characteristic polynomial (1.5) and then – for the case with negative roots of the characteristic polynomial (1.5).

3.5.1 Performance of the AE2DPDGL in case the pair (a_0, a_1) defines a pair complex conjugate roots of the characteristic polynomial $f(s)$ (1.5)

Let pair the pair (a_0, a_1) represent ((1.7), (1.15)), the parameter ε_r and the time constant T_φ of the of the AE2DPDGL ((3.1) - (3.5), (3.78)) be the same (2.30) and (2.31) from Section 2.3 (page 35), but the parameter k_ψ of the adaptive control of the angle ψ of the E2DPDGL vector rotation (3.78) be (3.114).

$k_\psi = 10$	(3.114)

The calculated critical value of the phase coupling angle according to (8.55) is $\gamma_{cr} = 43.1176$ deg. from Section 8.1.4 “Example” (page 195).

Let us illustrate first the performance of the closed loop guidance system with no coupling between the channels and initial conditions (1.16) with proportionality $k = 0.5$ according to (1.10) and (1.14). The processes of the closed loop guidance system are presented in Figure 3.5 and show the AE2DPDGL acts as two CPDGL.

Figure 3.6 - Figure 3.9 illustrate the crucial role of the adaptive control of the E2DPDGL vector rotation for providing stability of the closed loop with phase coupling between the channels and simultaneously an excellent performance. The design of the E2DPDGL (2.2) provides straightening the system trajectory in the $Y_L Z_L$ -plane, the picture plane, and an excellent performance when the initial conditions are non-proportional to each other as well as global stability of the closed loop guidance system in case of no coupling between the channels. Regrettably this new guidance law cannot cope with persisting phase coupling between the channels and fails there as shown in Section 2.3.3 “Does the E2DPDGL cope with the persisting phase coupling between the channels” (page 47). Now the upgrade of the E2DPDGL (2.2) into an adaptive E2DPDGL with self-adjusting angle ψ of the E2DPDGL vector rotation copes easily with the phase coupling between the channels except in the critical cases when $\gamma_0 = \gamma_{cr}$ (3.106) or $\gamma_0 = -\gamma_{cr}$ (3.107) also far beyond as shown in Figure 3.8 and Figure 3.9. This angle ψ strives to $(-\gamma_0)$ and the steady value of the sum of ψ and the phase coupling angle γ_0 represents (3.115) when $\gamma_0 = \gamma_{cr}$ (3.106) and (3.116) when $\gamma_0 = -\gamma_{cr}$ (3.107) as shown in Figure 3.6d and Figure 3.7d. It should be noticed that the achievement of this effect with regard to the closed loop guidance system performance is at similar control costs shown in Figure 3.6f and in Figure 3.7f in comparison with the control cost in the ideal simple case in Figure 3.5f.

$\left\|\psi_{\varepsilon_r}(\infty) + \gamma_0\right\| = 1.0022 < \ \gamma_{cr} = 43.1176$ deg.	(3.115)
$\left\|\psi_{\varepsilon_r}(\infty) + \gamma_0\right\| = 1.0195 < \ \gamma_{cr} = 43.1176$ deg.	(3.116)

Figure 3.10 - Figure 3.14 illustrate the performance of the closed loop guidance system at initial conditions (1.17) and cases (3.105) - (3.107), (3.110), and (3.112) when the phase coupling angle $\gamma_0 = 0,\ \pm\gamma_{cr},\ \frac{\pi}{2},\ \pi$ rad respectively. Note that initial conditions (1.17) and the cases (3.106), (3.110), and (3.112) of the phase coupling angle $\gamma_0 = +\gamma_{cr},\ \frac{\pi}{2},\ \pi$ respectively shown in Figure 3.11, Figure 3.13, and Figure 3.14 cause simultaneous clockwise spiraling. Even in the worst case with regard to the phase coupling angle γ_0 when $\gamma_0 = \pi$ rad (3.112) shown in Figure 3.14 the AE2DPDGL except stability of the closed loop system provides straightening the ATGM trajectory in the $Y_L Z_L$-plane, the picture plane. The controlled self-adjusting angle of the AE2DPDGL vector rotation ψ strives to $(-\pi)$ and the steady value of the sum of ψ and γ_0 represents (3.117).

$\left|\psi_{\varepsilon_r}(\infty) + \gamma_0\right| = 0.2530 < \gamma_{cr} = 43.1176$ deg.	(3.117)

Figure 3.15 - Figure 3.19 illustrate the performance of the closed loop guidance system at initial conditions (3.103) and cases of the phase coupling angle (3.105) - (3.109) when $\gamma_0 = 0,\ \pm\gamma_{cr},\ \pm 2\gamma_{cr}$ rad respectively. The self-adjusting angle of the AE2DPDGL vector rotation ψ strives to $(-\gamma_0)$ and the steady values of the sum of ψ and the angle γ_0 are represented in the following Table 3.3.

Table 3.3 Steady values of the sum of the adaptive self-adjusting angle $\boldsymbol{\psi}$ and the phase coupling angle $\boldsymbol{\gamma_0}$.

Case	**Phase coupling angle $\boldsymbol{\gamma_0}$ (deg.)**		**Steady value of the sum $\left|\boldsymbol{\psi_{\varepsilon_r}(\infty) + \gamma_0}\right|$ (deg.)**
1	$\gamma_0 = 0$	(3.105)	$4.7666 < \gamma_{cr} = 43.1176$
2	$\gamma_0 = +\gamma_{cr} = +43.1176$	(3.106)	$4.4477 < \gamma_{cr} = 43.1176$
3	$\gamma_0 = -\gamma_{cr} = -43.1176$	(3.107)	$1.8392 < \gamma_{cr} = 43.1176$
4	$\gamma_0 = +2\gamma_{cr} = +86.2352$	(3.108)	$0.1975 < \gamma_{cr} = 43.1176$
6	$\gamma_0 = -2\gamma_{cr} = -86.2352$	(3.109)	$1.3176 < \gamma_{cr} = 43.1176$

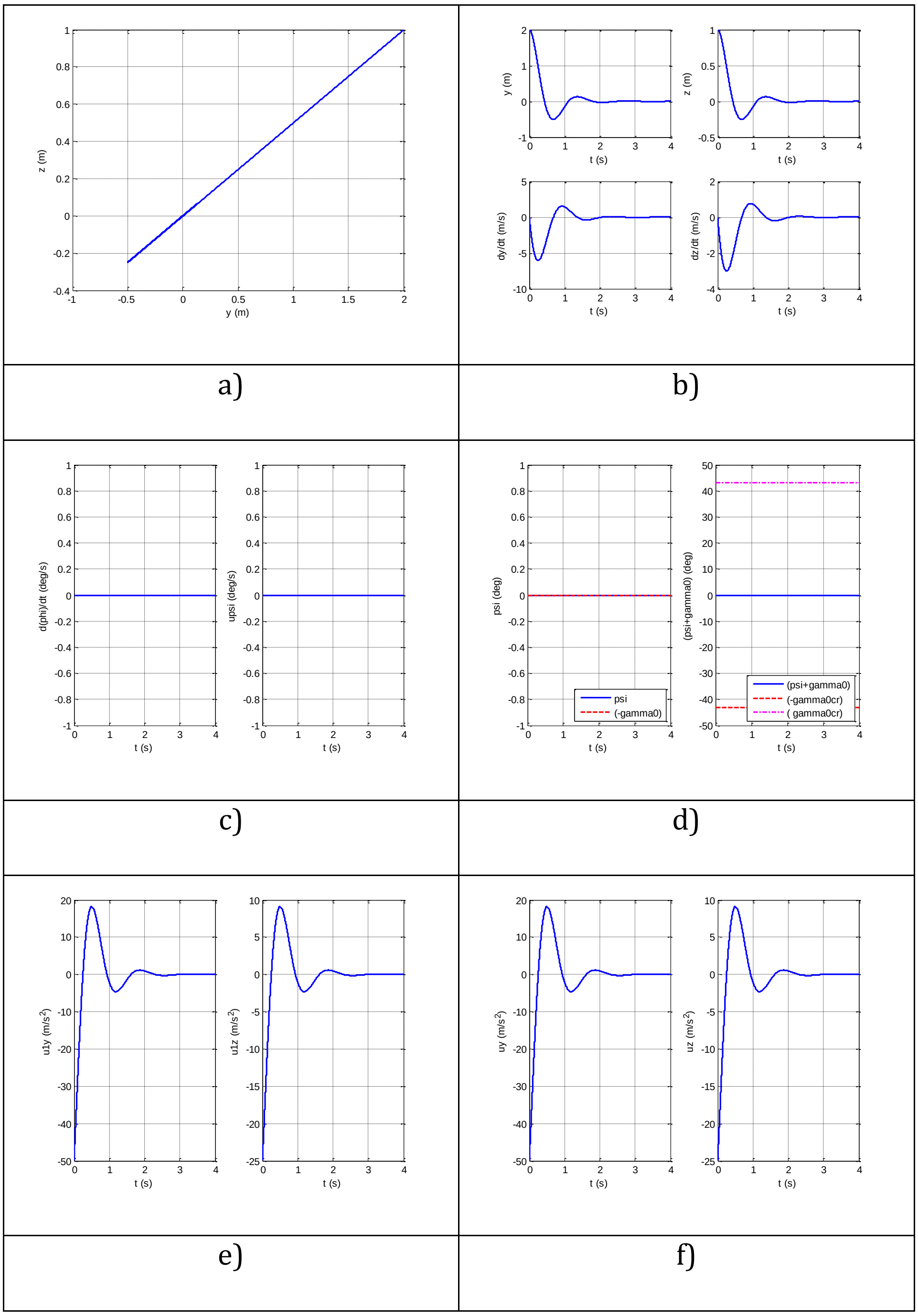

Figure 3.5 Performance of the closed loop guidance system with AE2DPDGL in case of Section 3.5.1 at proportional to each other initial conditions (1.16) and phase coupling angle $\gamma_0 = 0$ (3.105) with regard to: a) ATGM trajectory in the $Y_L Z_L$-plane, the picture plane; b) $y, \dot{y}, z$ and $\dot{z}$; c) $\dot{\varphi}$ and the adaptive control u_ψ (3.78); d) the self-adjusting angle ψ of the E2DPDGL vector rotation and the sum of ψ and γ_0; e) the components of the E2DPDGL (3.3) - (3.4) as a part of the AE2DPDGL; f) the components of the AE2DPDGL (3.5).

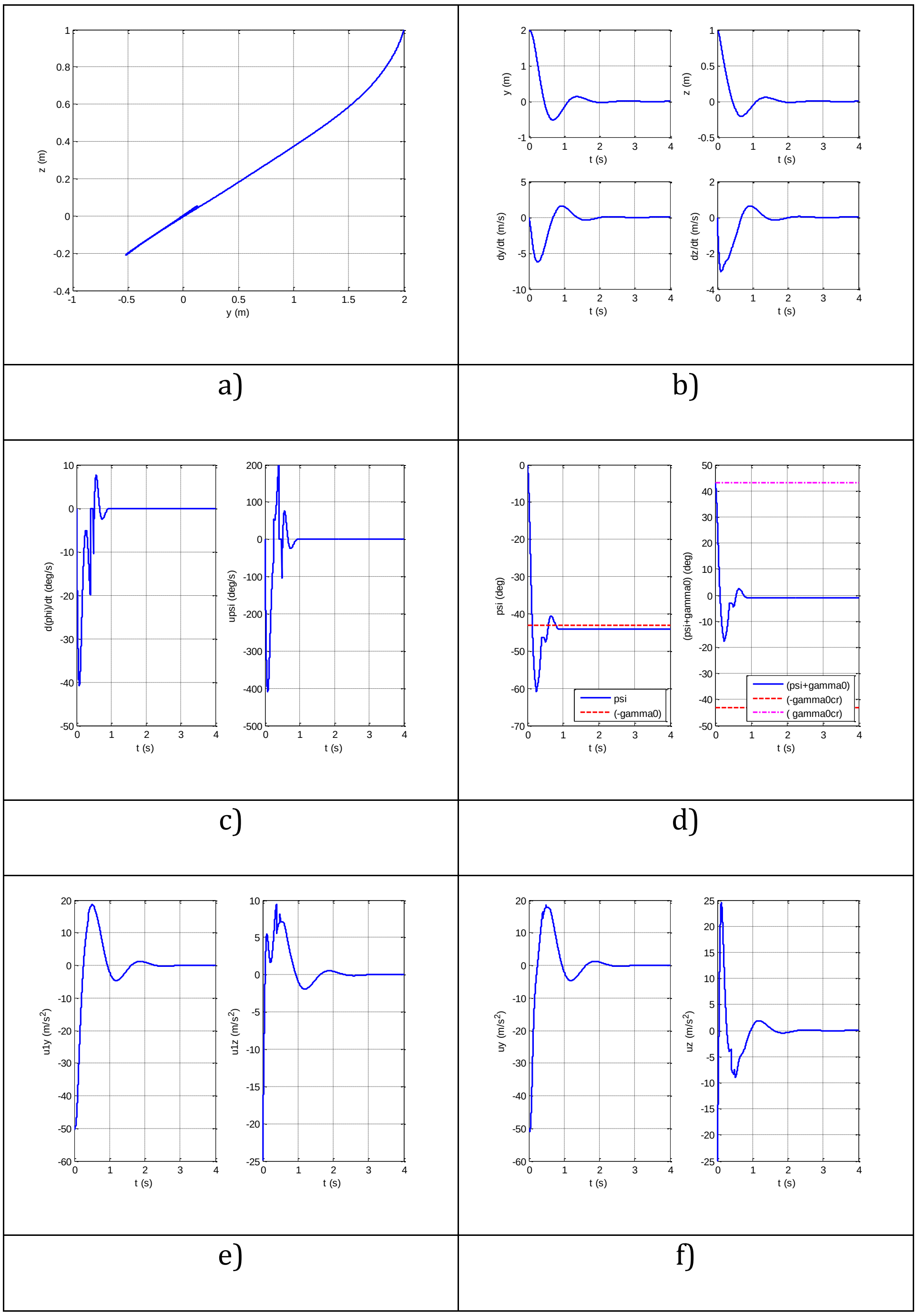

Figure 3.6 Performance of the closed loop guidance system with AE2DPDGL in case of Section 3.5.1 at proportional to each other initial conditions (1.16) and phase coupling angle $\gamma_0 = \gamma_{cr}$ (3.106) where $\gamma_{cr} = 43.1176$ deg. with regard to: a) ATGM trajectory in the $Y_L Z_L$-plane, the picture plane; b) $y, \dot{y}, z$ and $\dot{z}$; c) $\dot{\varphi}$ and the adaptive control u_ψ (3.78); d) the self-adjusting angle ψ of the AE2DPDGL and the sum of ψ and γ_0; e) the components of the E2DPDGL (3.3) - (3.4) as a part of the AE2DPDGL; f) the components of the AE2DPDGL (3.5).

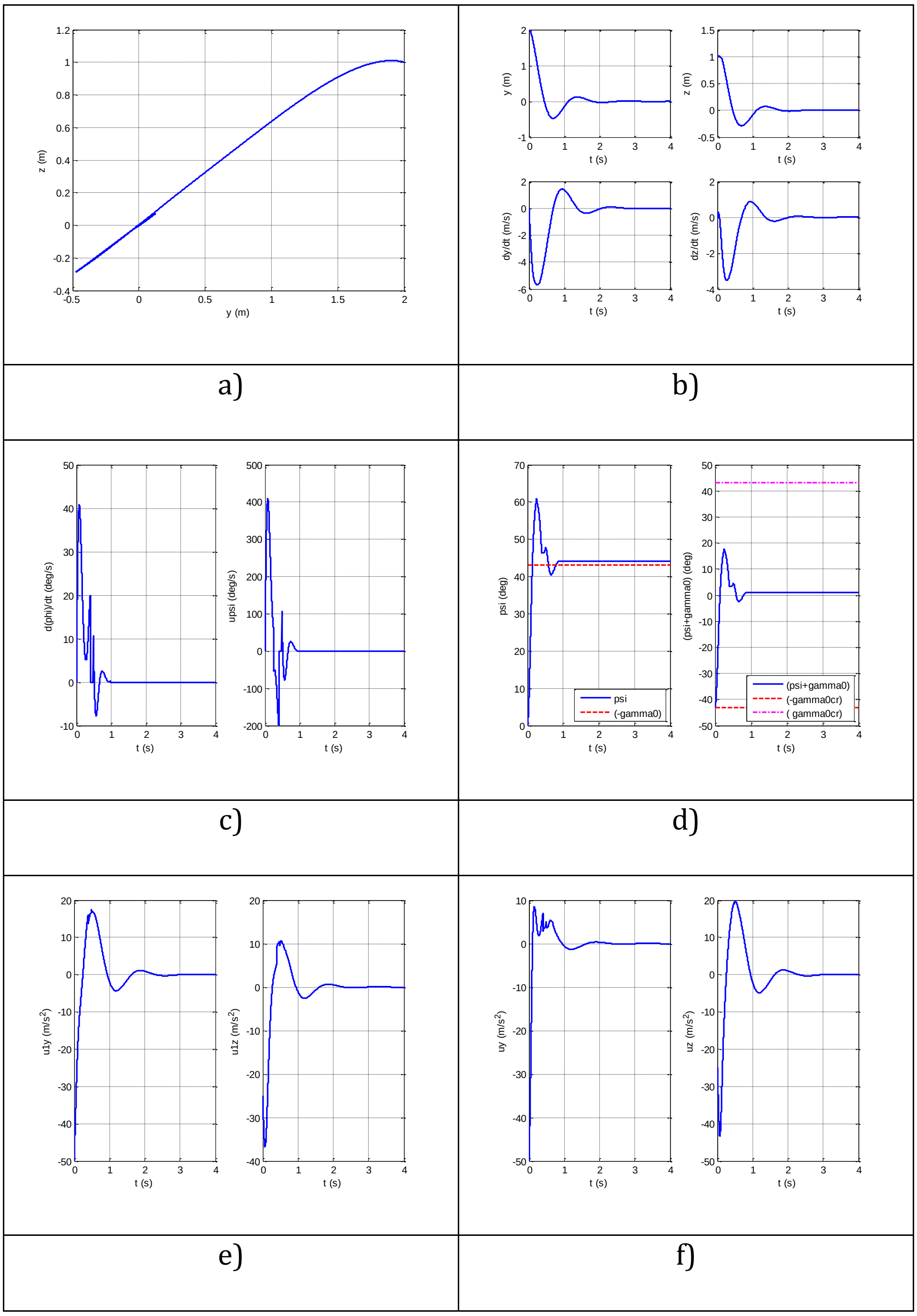

Figure 3.7 Performance of the closed loop guidance system with AE2DPDGL in case of Section 3.5.1 at proportional to each other initial conditions (1.16) and phase coupling angle $\gamma_0 = -\gamma_{cr}$ (3.107) where $\gamma_{cr} = 43.1176$ deg. with regard to: a) ATGM trajectory in the $Y_L Z_L$-plane, the picture plane; b) $y, \dot{y}, z$ and $\dot{z}$; c) $\dot{\varphi}$ and the adaptive control u_ψ (3.78); d) the self-adjusting angle ψ of the AE2DPDGL and the sum of ψ and γ_0; e) the components of the E2DPDGL (3.3) - (3.4) as a part of the AE2DPDGL; f) the components of the AE2DPDGL (3.5).

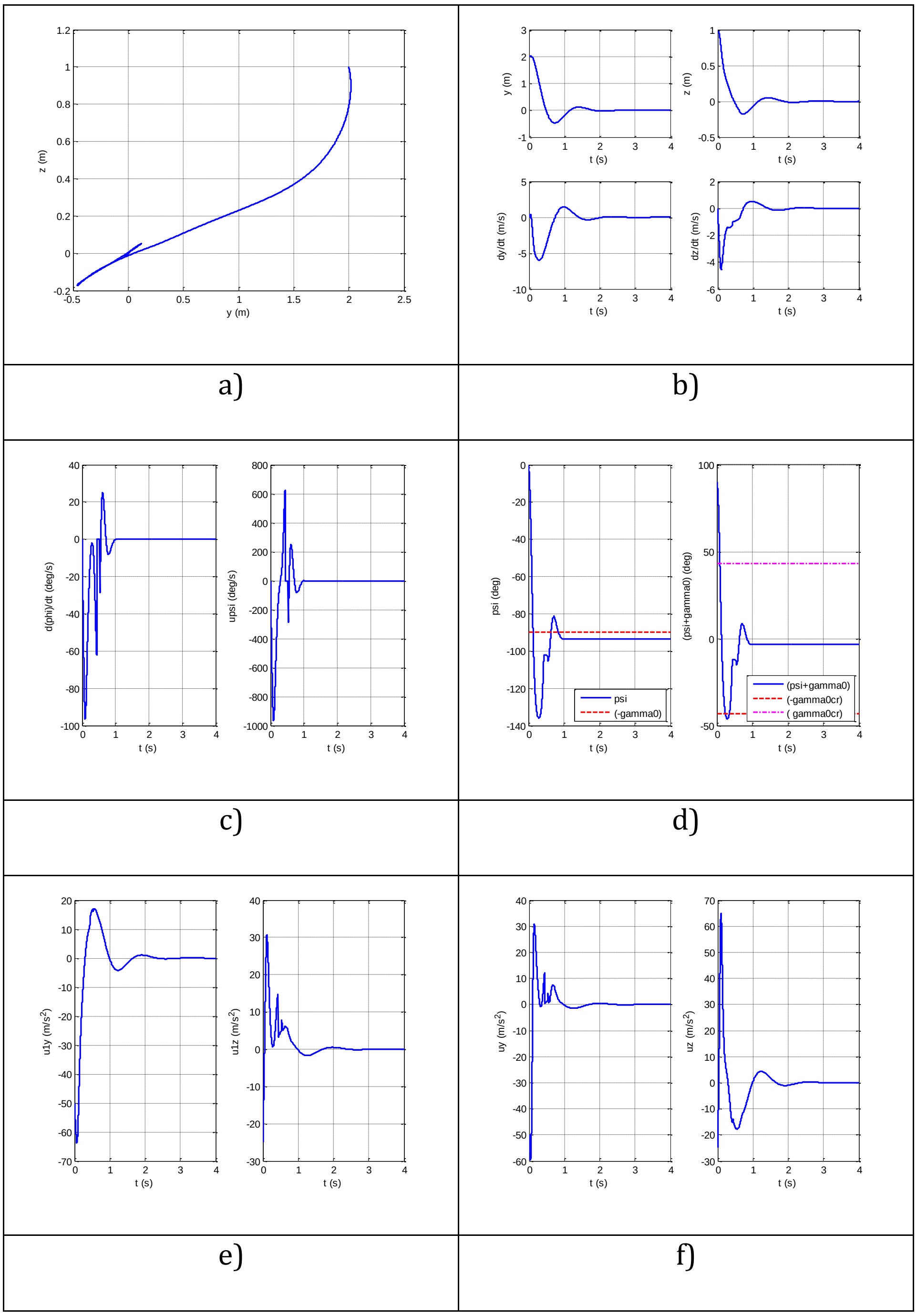

Figure 3.8 Performance of the closed loop guidance system with AE2DPDGL in case of Section 3.5.1 at proportional to each other initial conditions (1.16) and phase coupling angle $\gamma_0 = +\frac{\pi}{2}$ rad (3.110) with regard to: a) ATGM trajectory in the $Y_L Z_L$-plane, the picture plane; b) $y, \dot{y}, z$ and $\dot{z}$; c) $\dot{\varphi}$ and the adaptive control u_ψ (3.78); d) the self-adjusting angle ψ of the AE2DPDGL and the sum of ψ and γ_0; e) the components of the E2DPDGL (3.3) - (3.4) as a part of the AE2DPDGL; f) the components of the AE2DPDGL (3.5).

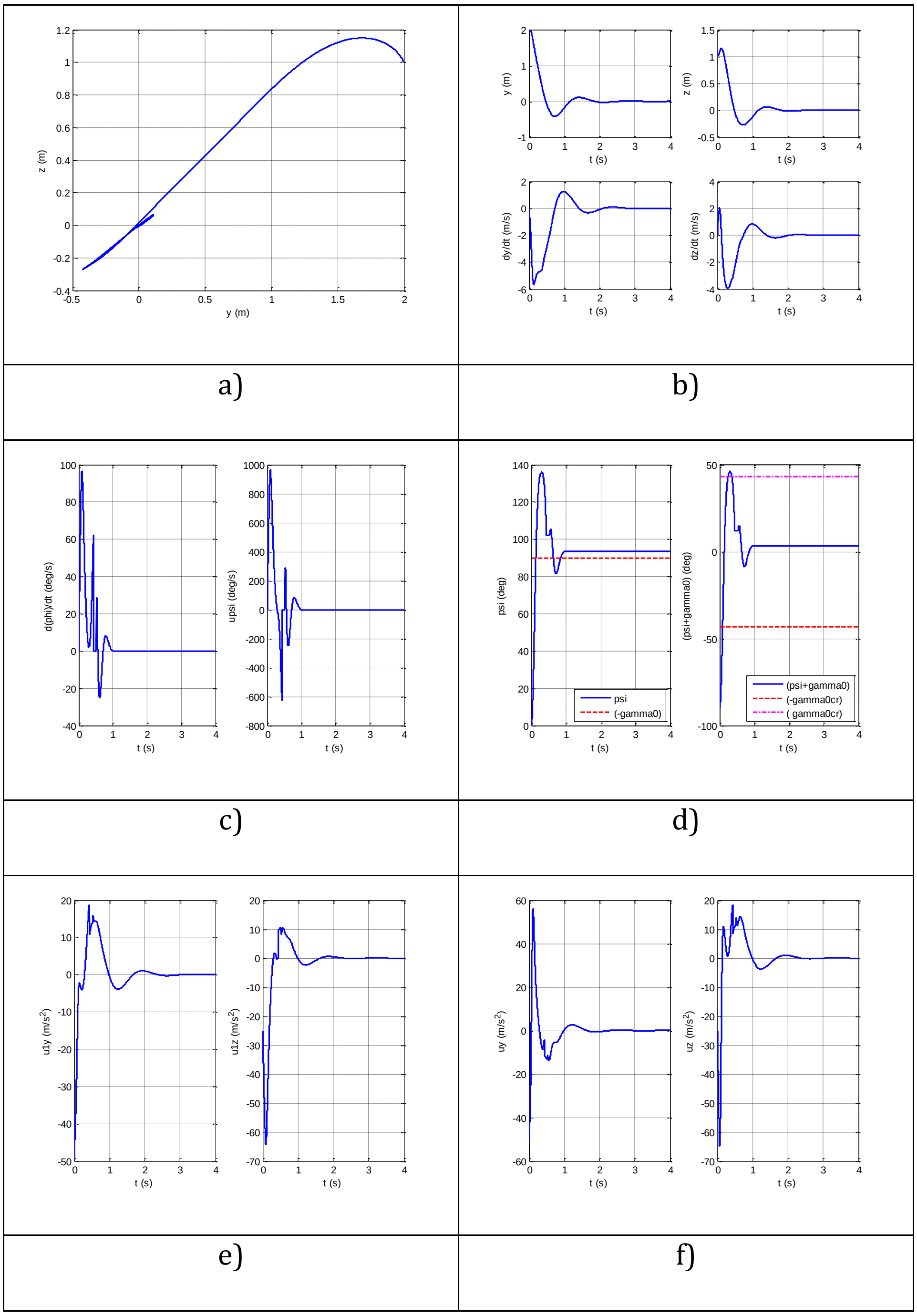

Figure 3.9 Performance of the closed loop guidance system with AE2DPDGL in case of Section 3.5.1 at proportional to each other initial conditions (1.16) and phase coupling angle $\gamma_0 = -\frac{\pi}{2}$ rad (3.111) with regard to: a) ATGM trajectory in the $Y_L Z_L$-plane, the picture plane; b) $y, \dot{y}, z$ and $\dot{z}$; c) $\dot{\varphi}$ and the adaptive control u_ψ (3.78); d) the self-adjusting angle ψ of the AE2DPDGL and the sum of ψ and γ_0; e) the components of the E2DPDGL (3.3) - (3.4) as a part of the AE2DPDGL; f) the components of the AE2DPDGL (3.5).

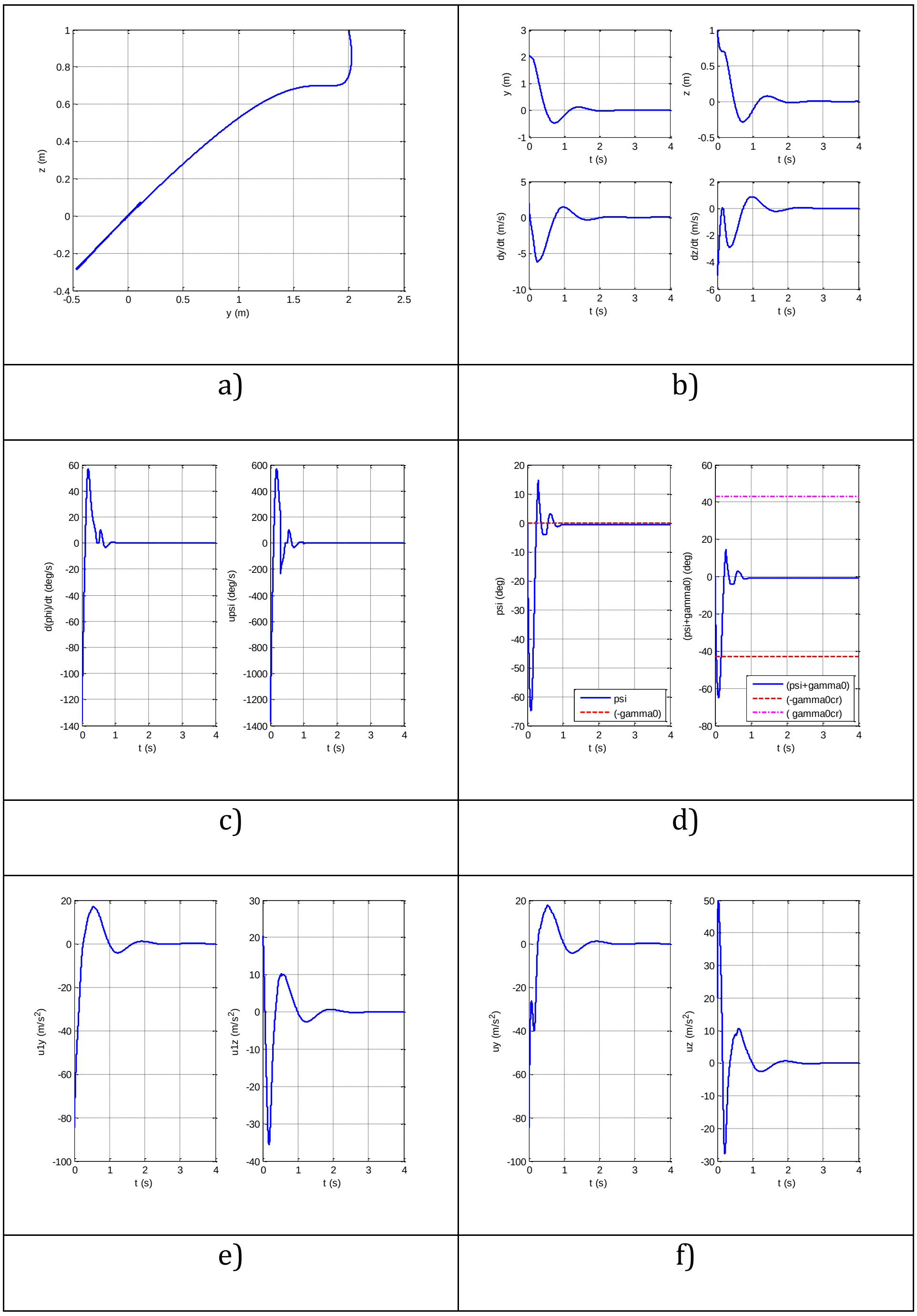

Figure 3.10 Performance of the closed loop guidance system with AE2DPDGL in case of Section 3.5.1 at non-proportional to each other initial conditions (1.17) and phase coupling angle $\gamma_0 = 0$ (3.105) with regard to: a) ATGM trajectory in the $Y_L Z_L$-plane, the picture plane; b) $y, \dot{y}, z$ and $\dot{z}$; c) $\dot{\varphi}$ and the adaptive control u_ψ (3.78); d) the self-adjusting angle ψ of the AE2DPDGL and the sum of ψ and γ_0; e) the components of the E2DPDGL (3.3) - (3.4) as a part of the AE2DPDGL; f) the components of the AE2DPDGL (3.5).

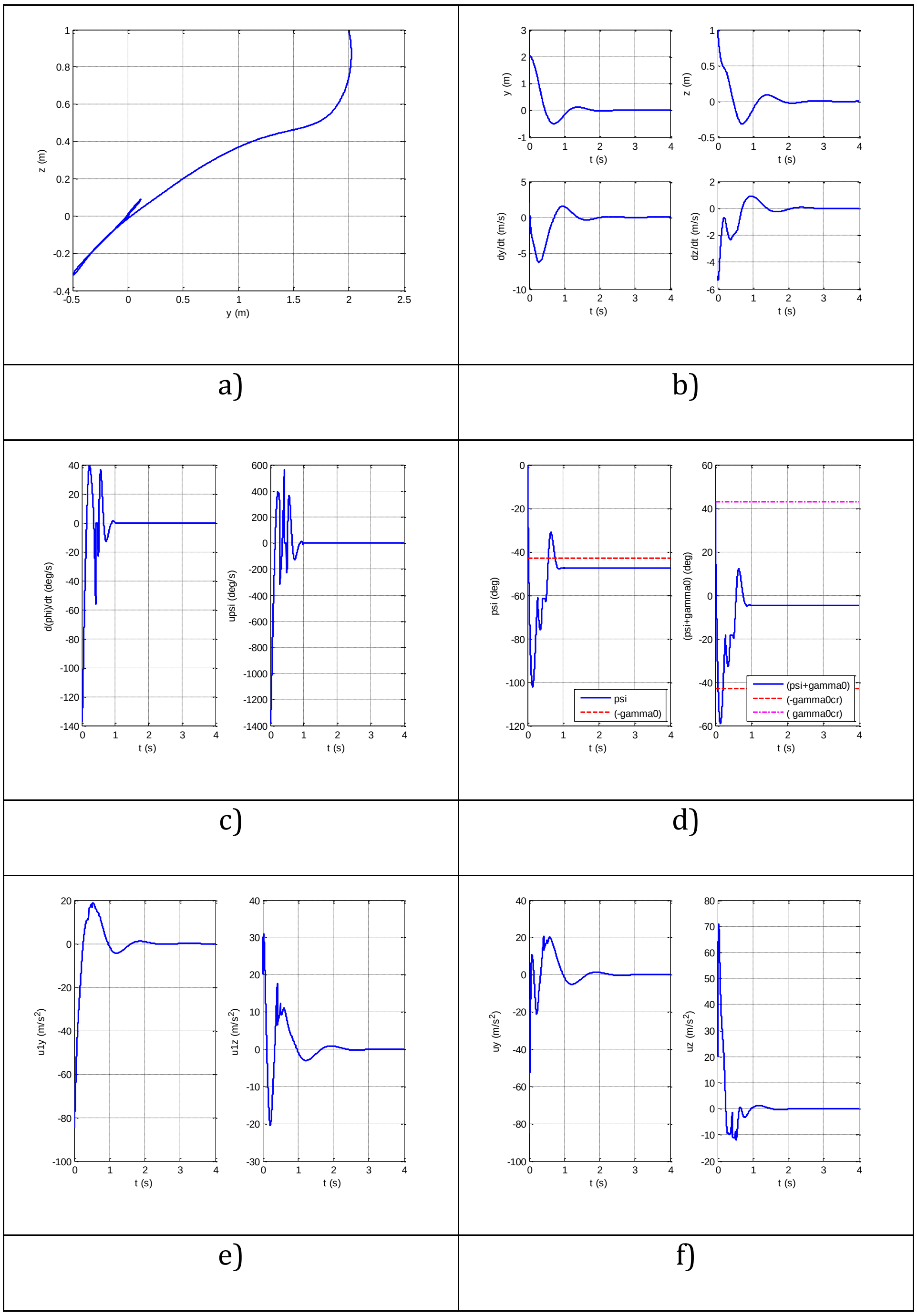

Figure 3.11 Performance of the closed loop guidance system with AE2DPDGL in case of Section 3.5.1 at non-proportional to each other initial conditions (1.17) and phase coupling angle $\gamma_0 = \gamma_{cr}$ (3.106) where $\gamma_{cr} = 43.1176$ deg. with regard to: a) ATGM trajectory in the $Y_L Z_L$-plane, the picture plane; b) $y, \dot{y}, z$ and $\dot{z}$; c) $\dot{\varphi}$ and the adaptive control u_ψ (3.78); d) the self-adjusting angle ψ of the AE2DPDGL and the sum of ψ and γ_0; e) the components of the E2DPDGL (3.3) - (3.4) as a part of the AE2DPDGL; f) the components of the AE2DPDGL (3.5).

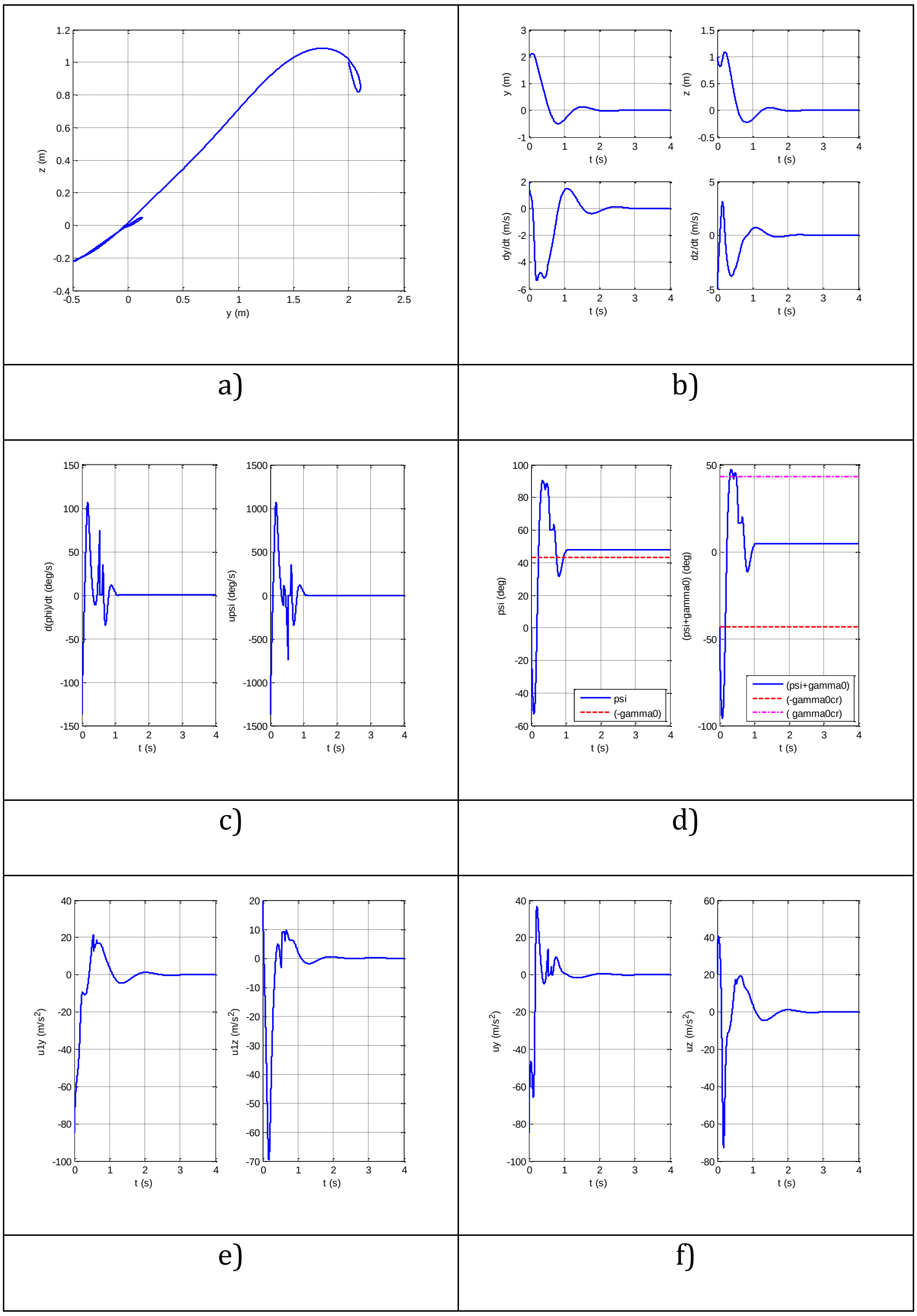

Figure 3.12 Performance of the closed loop guidance system with AE2DPDGL in case of Section 3.5.1 at non-proportional to each other initial conditions (1.17) and phase coupling angle $\gamma_0 = -\gamma_{cr}$ (3.107) where $\gamma_{cr} = 43.1176$ deg. with regard to: a) ATGM trajectory in the $Y_L Z_L$-plane, the picture plane; b) $y, \dot{y}, z$ and $\dot{z}$; c) $\dot{\varphi}$ and the adaptive control u_ψ (3.78); d) the self-adjusting angle ψ of the AE2DPDGL and the sum of ψ and γ_0; e) the components of the E2DPDGL (3.3) - (3.4) as a part of the AE2DPDGL; f) the components of the AE2DPDGL (3.5).

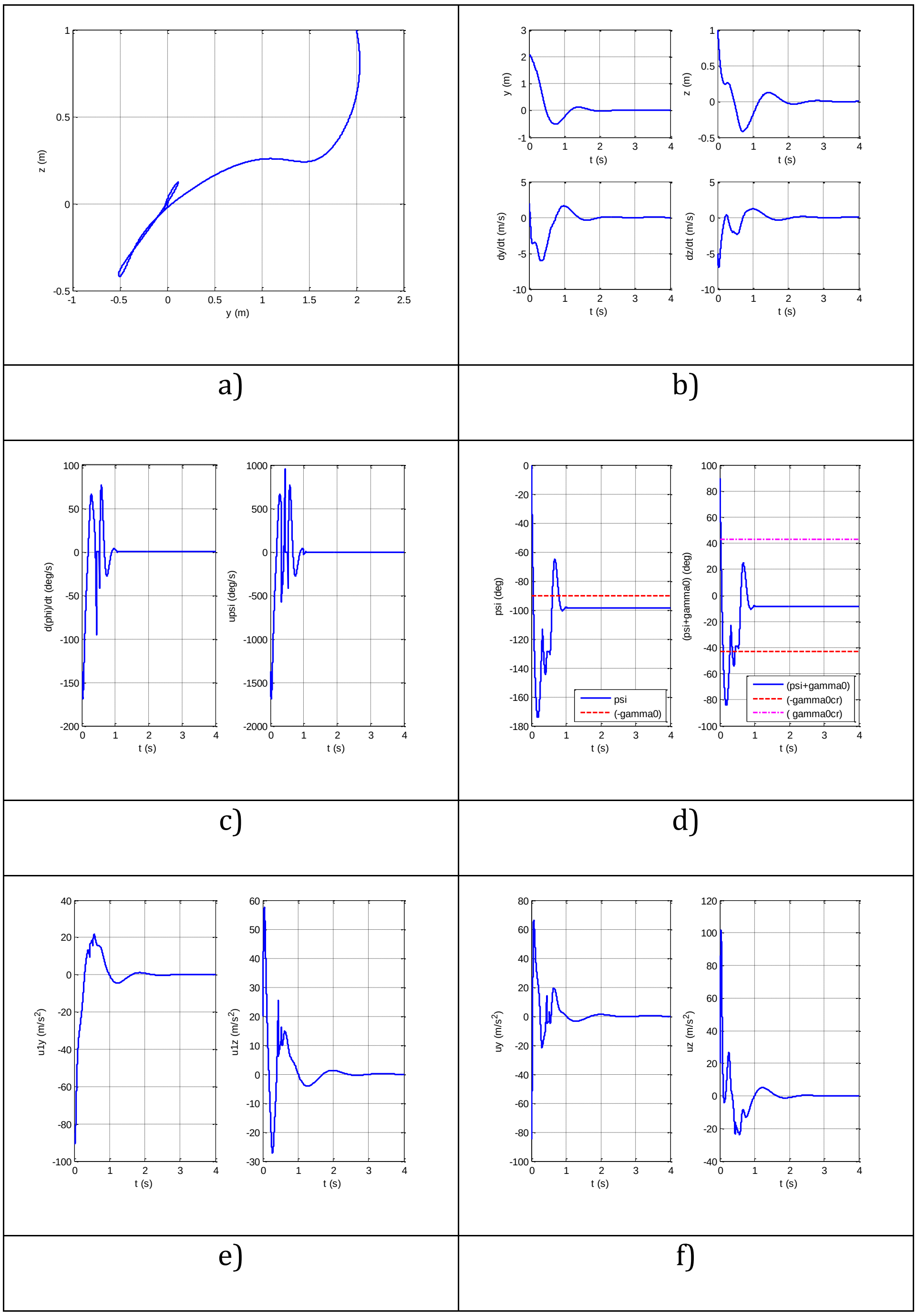

Figure 3.13 Performance of the closed loop guidance system with AE2DPDGL in case of Section 3.5.1 at non-proportional to each other initial conditions (1.17) and phase coupling angle $\gamma_0 = +\frac{\pi}{2}$ rad (3.110) with regard to: a) ATGM trajectory in the $Y_L Z_L$-plane, the picture plane; b) $y, \dot{y}, z$ and $\dot{z}$; c) $\dot{\varphi}$ and the adaptive control u_ψ (3.78); d) the self-adjusting angle ψ of the AE2DPDGL and the sum of ψ and γ_0; e) the components of the E2DPDGL (3.3) - (3.4) as a part of the AE2DPDGL; f) the components of the AE2DPDGL (3.5).

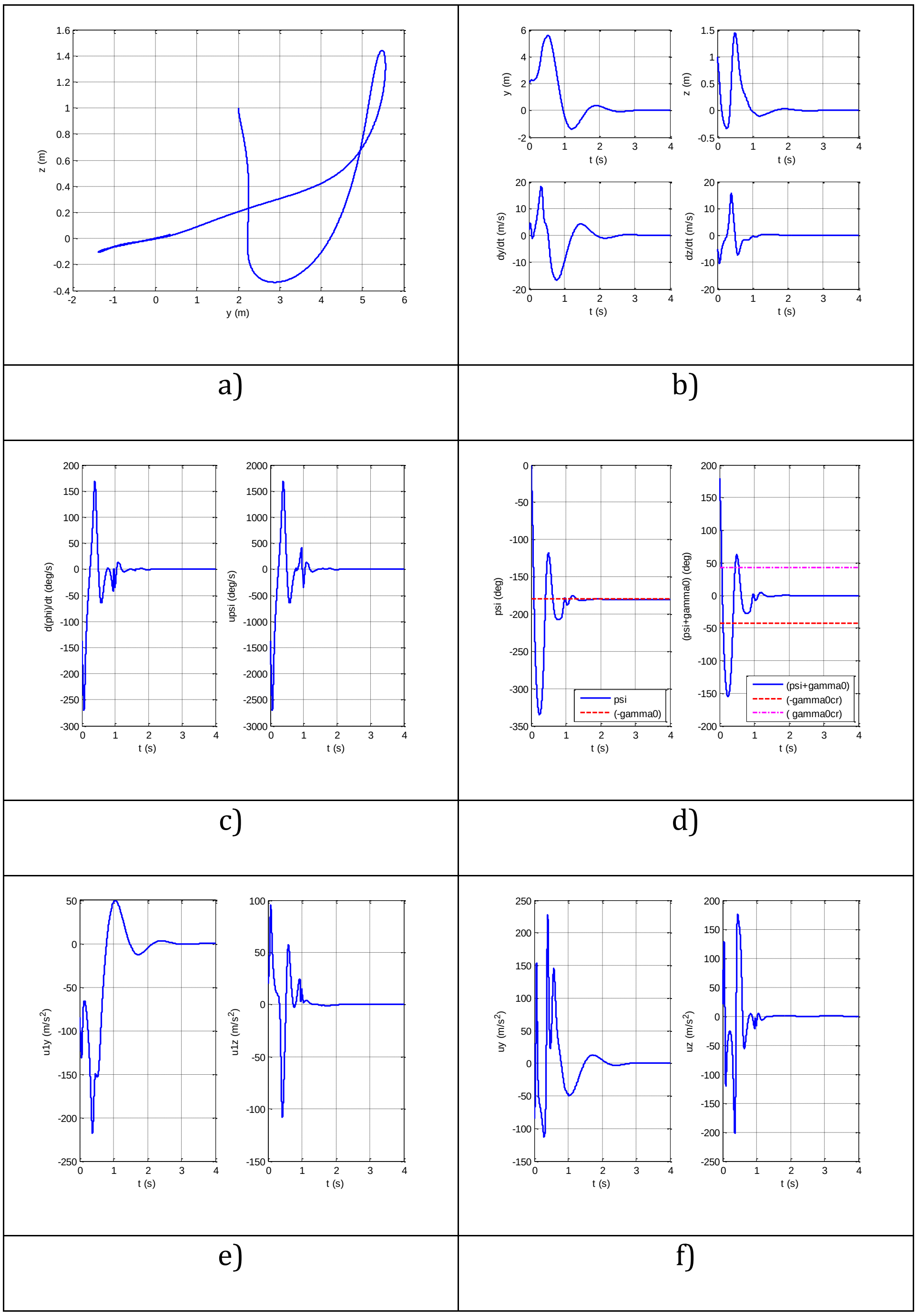

Figure 3.14 Performance of the closed loop guidance system with AE2DPDGL in case of Section 3.5.1 at non-proportional to each other initial conditions (1.17) and phase coupling angle $\gamma_0 = \pi$ rad (3.111) with regard to: a) ATGM trajectory in the $Y_L Z_L$-plane, the picture plane; b) $y, \dot{y}, z$ and $\dot{z}$; c) $\dot{\varphi}$ and the adaptive control u_ψ (3.78); d) the self-adjusting angle ψ of the AE2DPDGL and the sum of ψ and γ_0; e) the components of the E2DPDGL (3.3) - (3.4) as a part of the AE2DPDGL; f) the components of the AE2DPDGL (3.5).

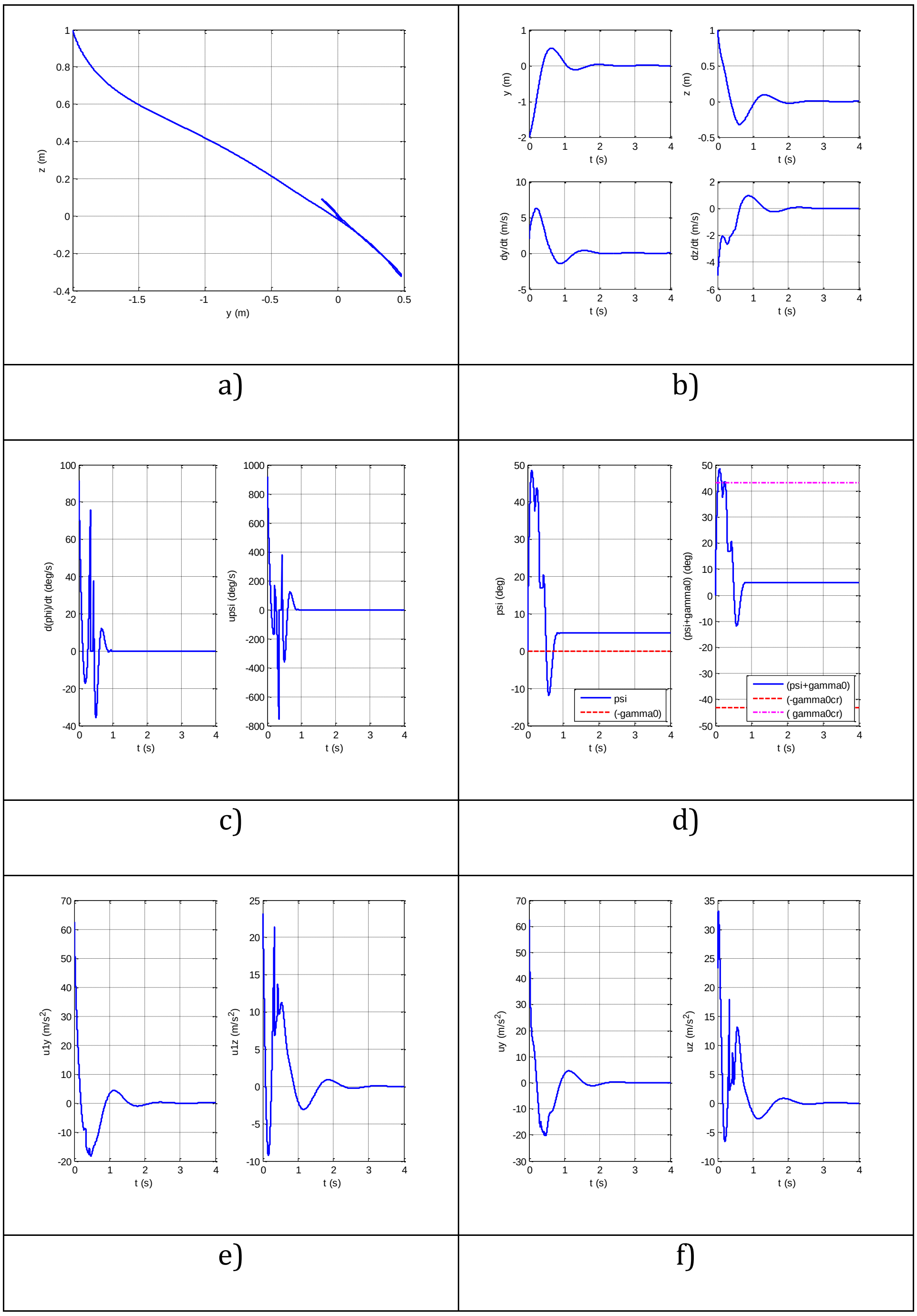

Figure 3.15 Performance of the closed loop guidance system with AE2DPDGL in case of Section 3.5.1 at non-proportional to each other initial conditions (3.103) and phase coupling angle $\gamma_0 = 0$ (3.105) with regard to: a) ATGM trajectory in the $Y_L Z_L$-plane, the picture plane; b) $y, \dot{y}, z$ and $\dot{z}$; c) $\dot{\varphi}$ and the adaptive control u_ψ (3.78); d) the self-adjusting angle ψ of the AE2DPDGL and the sum of ψ and γ_0; e) the components of the E2DPDGL (3.3) - (3.4) as a part of the AE2DPDGL; f) the components of the AE2DPDGL (3.5).

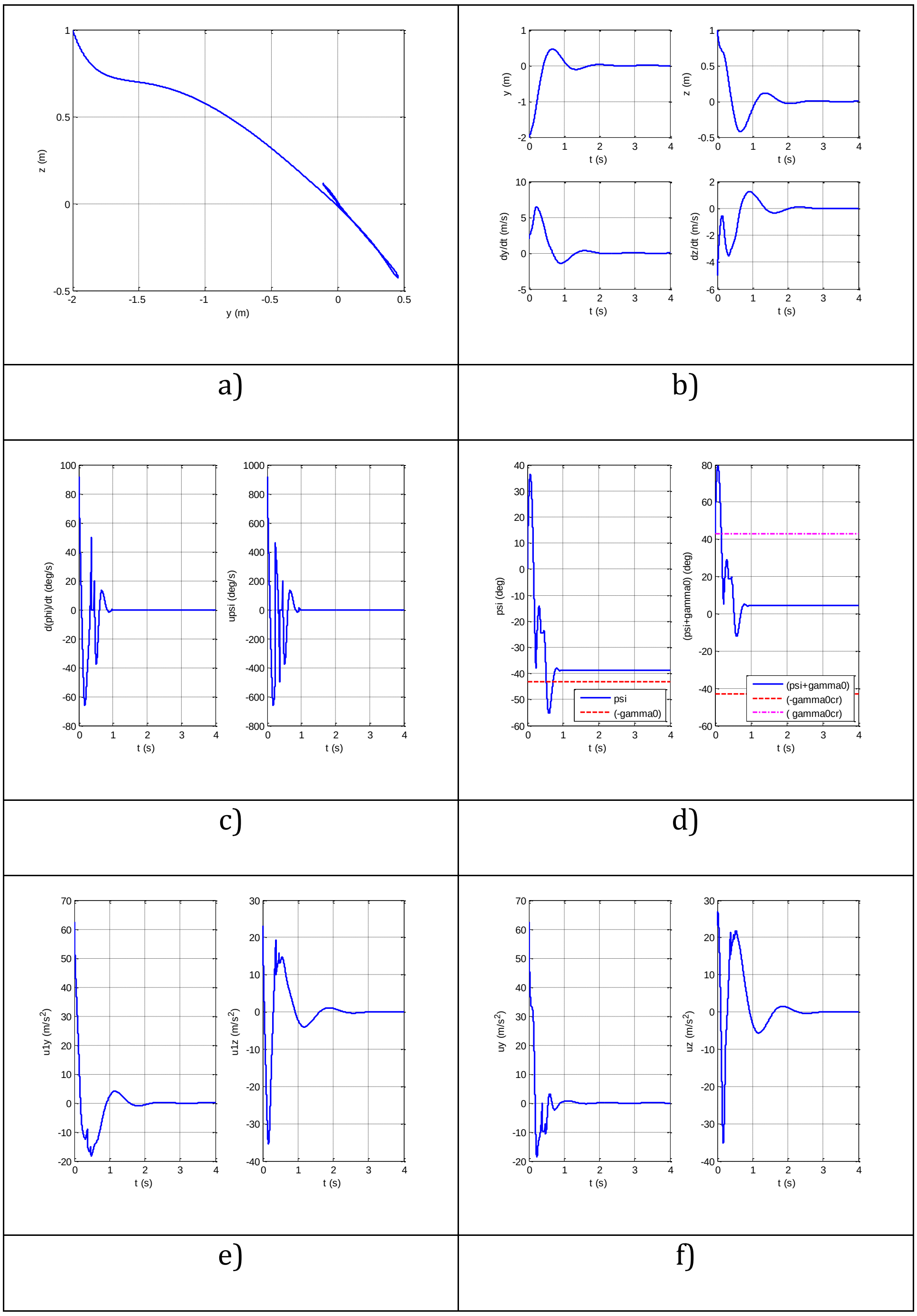

Figure 3.16 Performance of the closed loop guidance system with AE2DPDGL in case of Section 3.5.1 at non-proportional to each other initial conditions (3.103) and phase coupling angle $\gamma_0 = \gamma_{cr}$ (3.106) where $\gamma_{cr} = 43.1176$ deg. with regard to: a) ATGM trajectory in the $Y_L Z_L$-plane, the picture plane; b) $y, \dot{y}, z$ and $\dot{z}$; c) $\dot{\varphi}$ and the adaptive control u_{ψ} (3.78); d) the self-adjusting angle ψ of the AE2DPDGL and the sum of ψ and γ_0; e) the components of the E2DPDGL (3.3) - (3.4) as a part of the AE2DPDGL; f) the components of the AE2DPDGL (3.5).

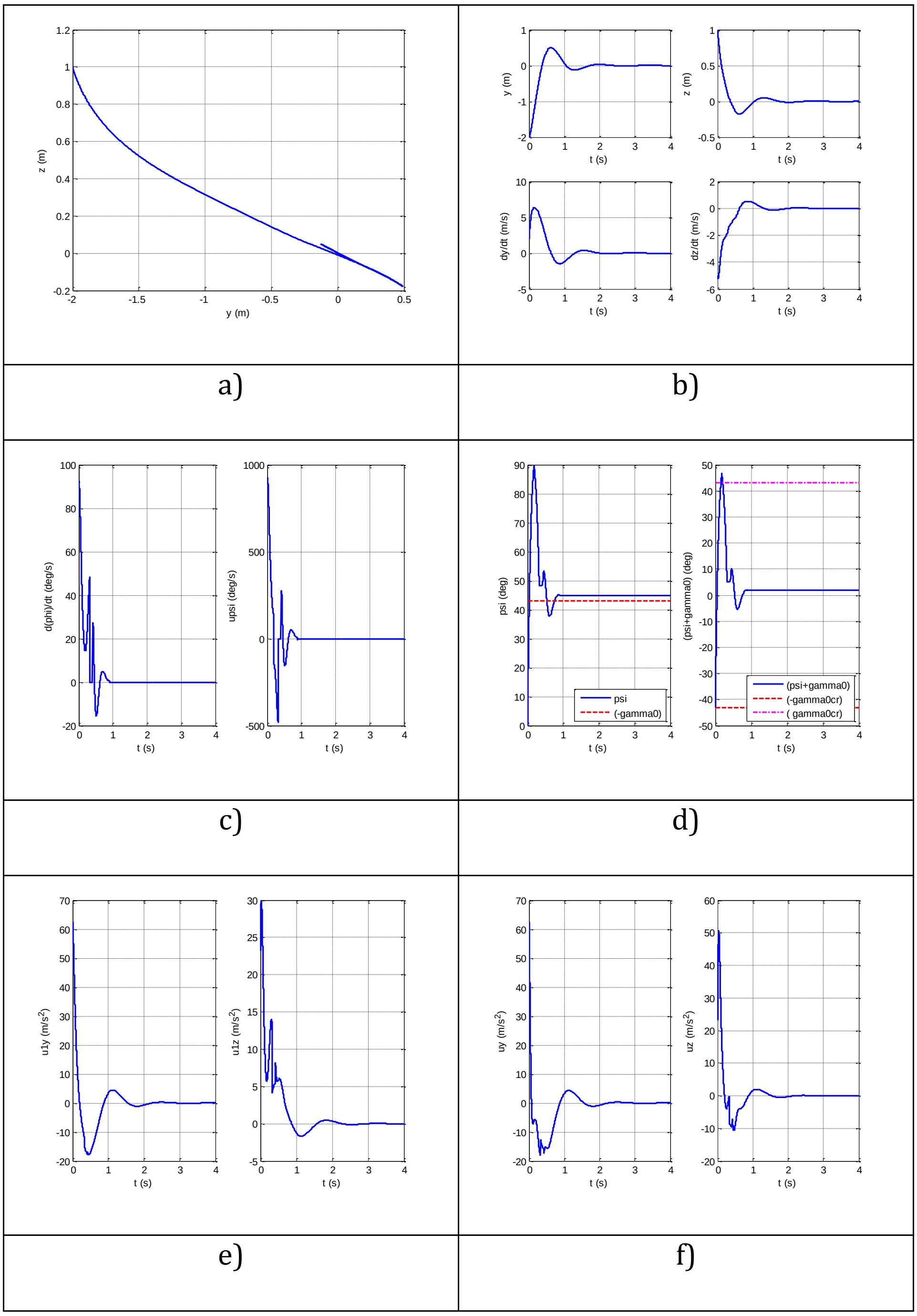

Figure 3.17 Performance of the closed loop guidance system with AE2DPDGL in case of Section 3.5.1 at non-proportional to each other initial conditions (3.103) and phase coupling angle $\gamma_0 = -\gamma_{cr}$ (3.107) where $\gamma_{cr} = 43.1176$ deg. with regard to: a) ATGM trajectory in the $Y_L Z_L$-plane, the picture plane; b) $y, \dot{y}, z$ and $\dot{z}$; c) $\dot{\varphi}$ and the adaptive control u_ψ (3.78); d) the self-adjusting angle ψ of the AE2DPDGL and the sum of ψ and γ_0; e) the components of the E2DPDGL (3.3) - (3.4) as a part of the AE2DPDGL; f) the components of the AE2DPDGL (3.5).

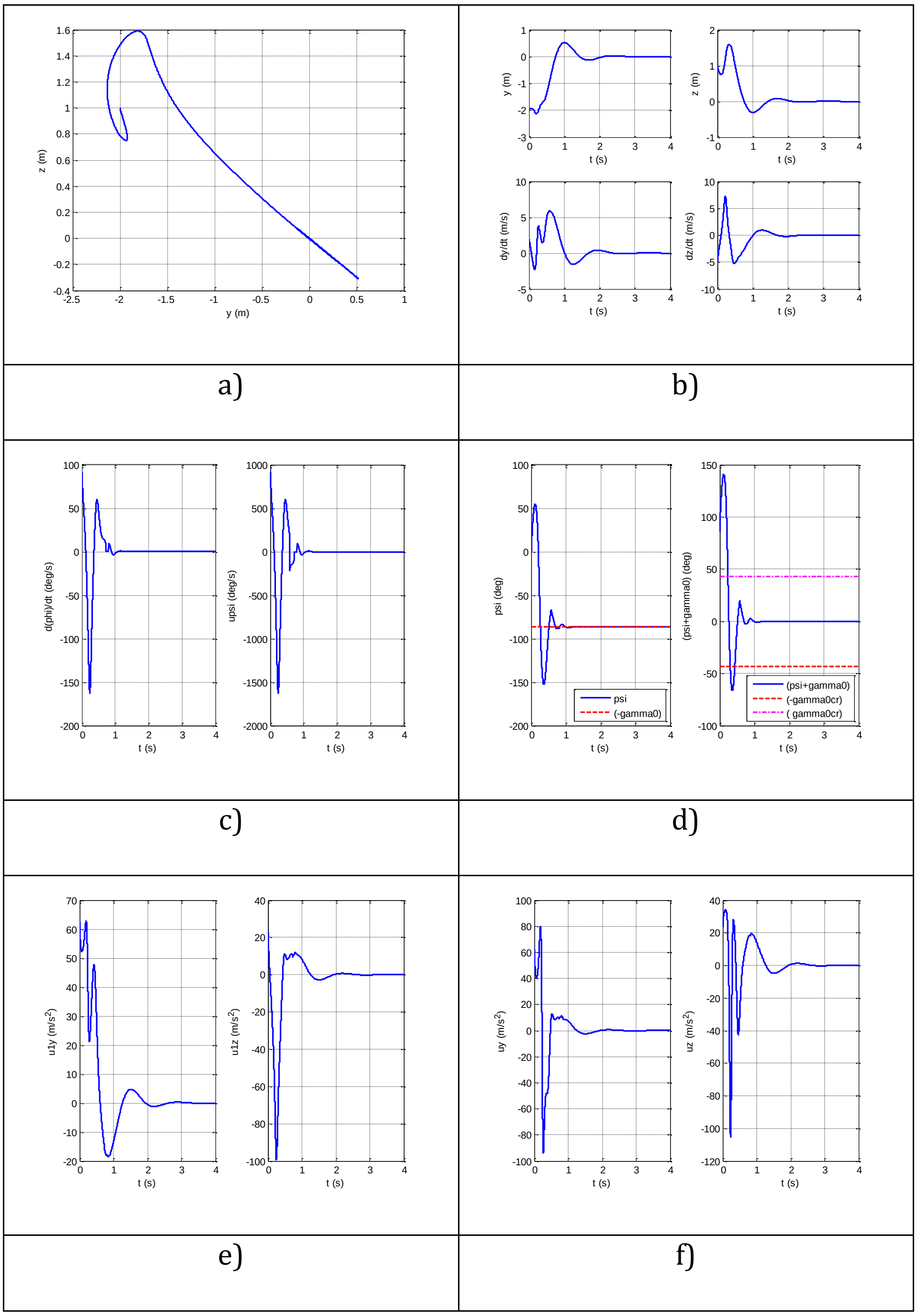

Figure 3.18 Performance of the closed loop guidance system with AE2DPDGL in case of Section 3.5.1 at non-proportional to each other initial conditions (3.103) and phase coupling angle $\gamma_0 = 2\gamma_{cr} = 86.2352$ (3.108) where $\gamma_{cr} =$ 43.1176 deg. with regard to: a) ATGM trajectory in the $Y_L Z_L$-plane, the picture plane; b) $y, \dot{y}, z$ and $\dot{z}$; c) $\dot{\varphi}$ and the adaptive control u_ψ (3.78); d) the self-adjusting angle ψ of the AE2DPDGL and the sum of ψ and γ_0; e) the components of the E2DPDGL (3.3) - (3.4) as a part of the AE2DPDGL; f) the components of the AE2DPDGL (3.5).

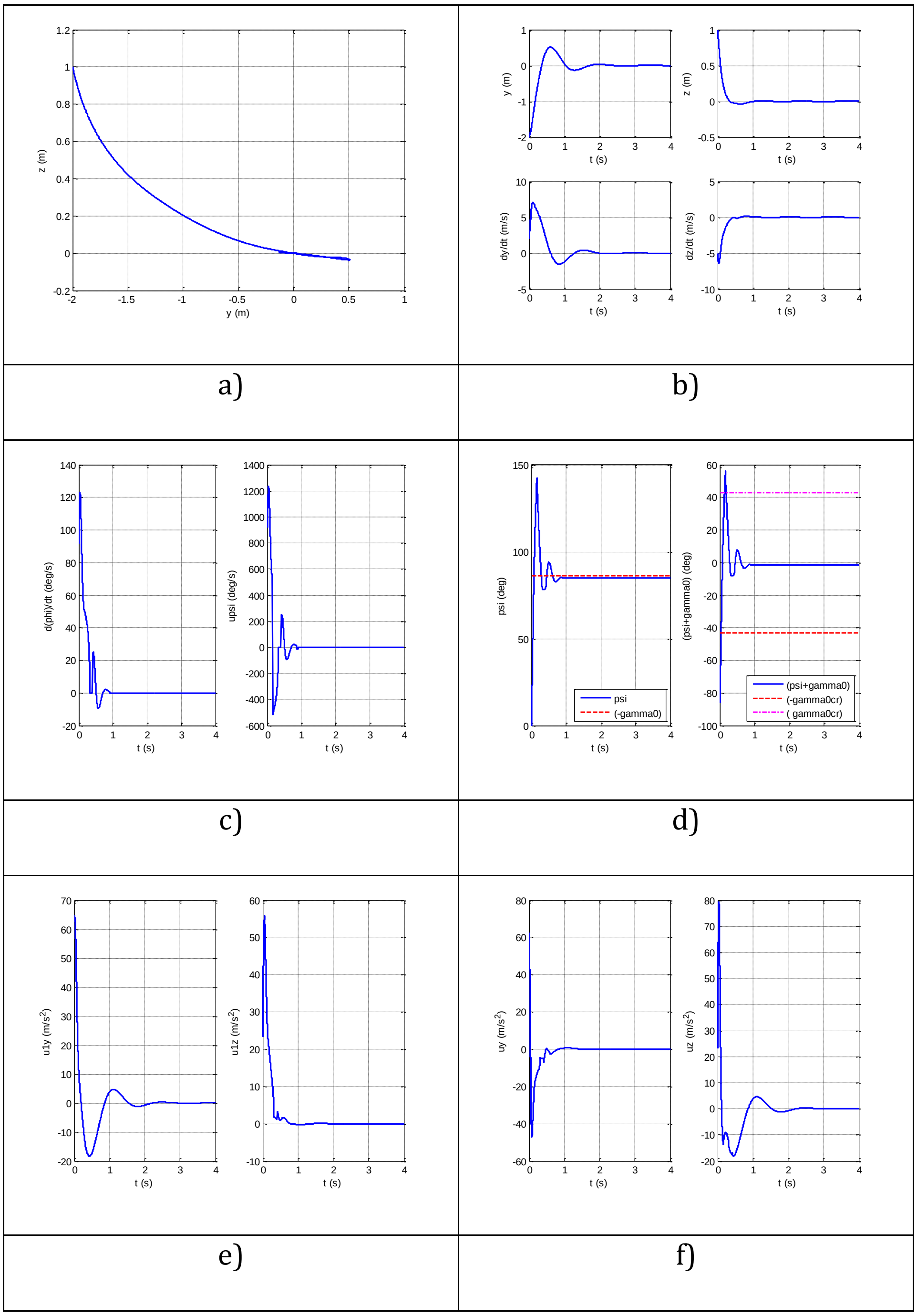

Figure 3.19 Performance of the closed loop guidance system with AE2DPDGL in case of Section 3.5.1 at non-proportional to each other initial conditions (3.103) and phase coupling angle $\gamma_0 = -2\gamma_{cr} = -86.2352$ deg. (3.109) where $\gamma_{cr} = 43.1176$ deg. with regard to: a) ATGM trajectory in the $Y_L Z_L$-plane, the picture plane; b) $y, \dot{y}, z$ and $\dot{z}$; c) $\dot{\varphi}$ and the adaptive control u_ψ (3.78); d) the self-adjusting angle ψ of the AE2DPDGL and the sum of ψ and γ_0; e) the components of the E2DPDGL (3.3) - (3.4) as a part of the AE2DPDGL; f) the components of the AE2DPDGL (3.5).

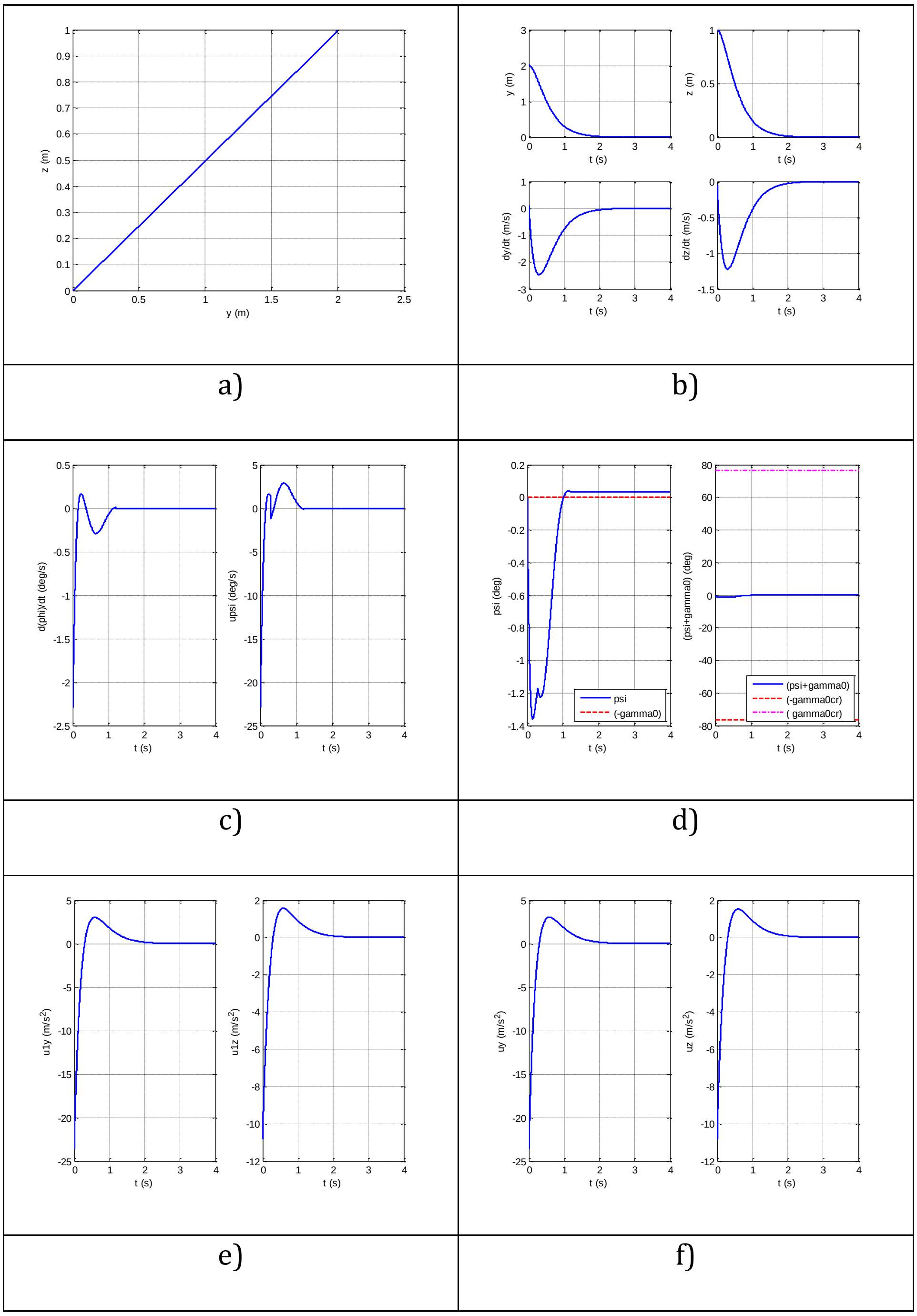

Figure 3.20 Performance of the closed loop guidance system with AE2DPDGL in case of Section 3.5.2 at non-proportional to each other initial conditions (3.104) and phase coupling angle $\gamma_0 = 0$ (3.105) with regard to: a) ATGM trajectory in the $Y_L Z_L$-plane, the picture plane; b) $y, \dot{y}, z$ and $\dot{z}$; c) $\dot{\varphi}$ and the adaptive control u_ψ (3.78); d) the self-adjusting angle ψ of the AE2DPDGL and the sum of ψ and γ_0; e) the components of the E2DPDGL (3.3) - (3.4) as a part of the AE2DPDGL; f) the components of the AE2DPDGL (3.5).

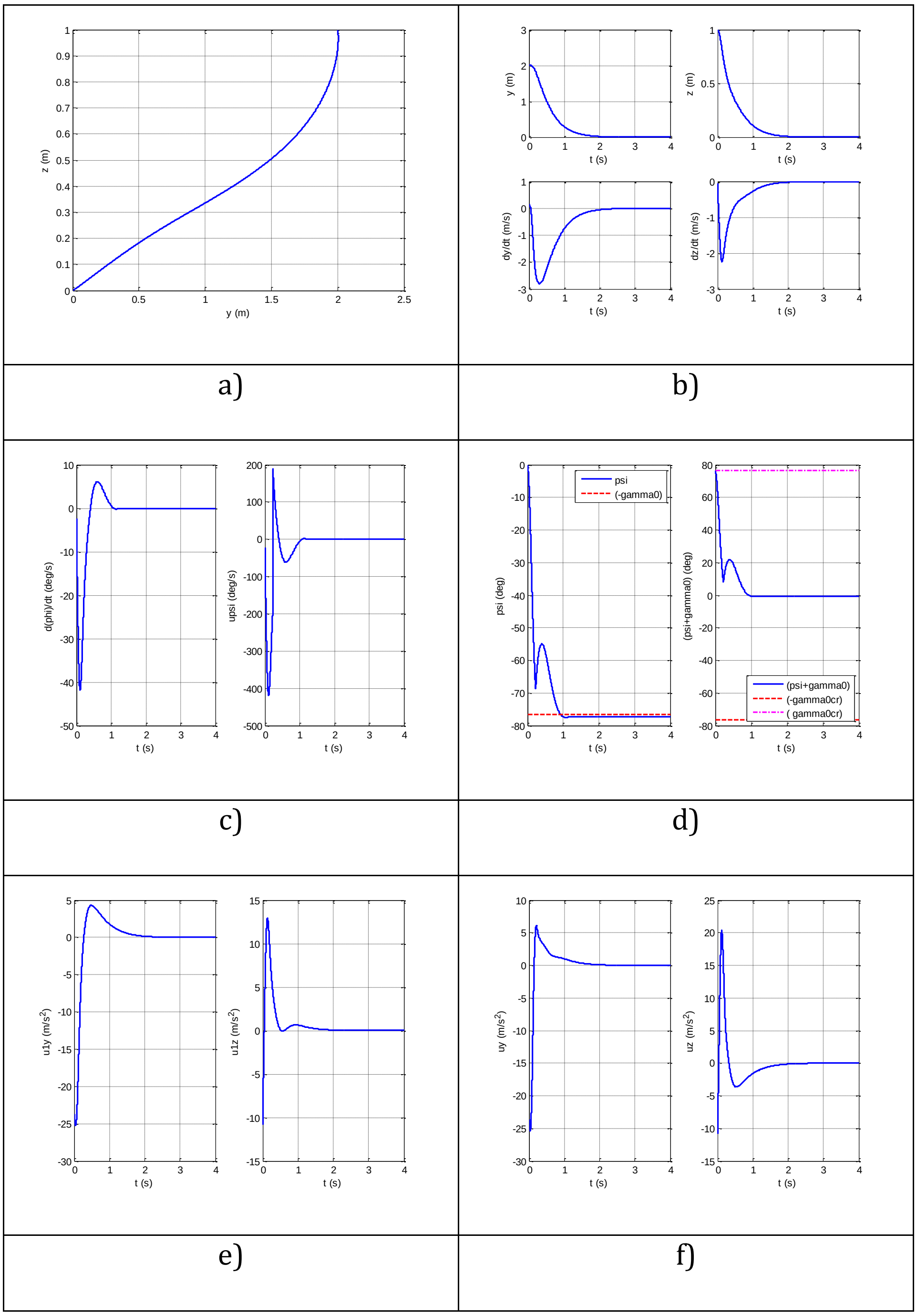

Figure 3.21 Performance of the closed loop guidance system with AE2DPDGL in case of Section 3.5.2 at non-proportional to each other initial conditions (3.104) and phase coupling angle $\gamma_0 = \gamma_{cr}$ (3.106) where $\gamma_{cr} = 76.6924$ deg. with regard to: a) ATGM trajectory in the $Y_L Z_L$-plane, the picture plane; b) $y, \dot{y}, z$ and $\dot{z}$; c) $\dot{\varphi}$ and the adaptive control u_ψ (3.78); d) the self-adjusting angle ψ of the AE2DPDGL and the sum of ψ and γ_0; e) the components of the E2DPDGL (3.3) - (3.4) as a part of the AE2DPDGL; f) the components of the AE2DPDGL (3.5).

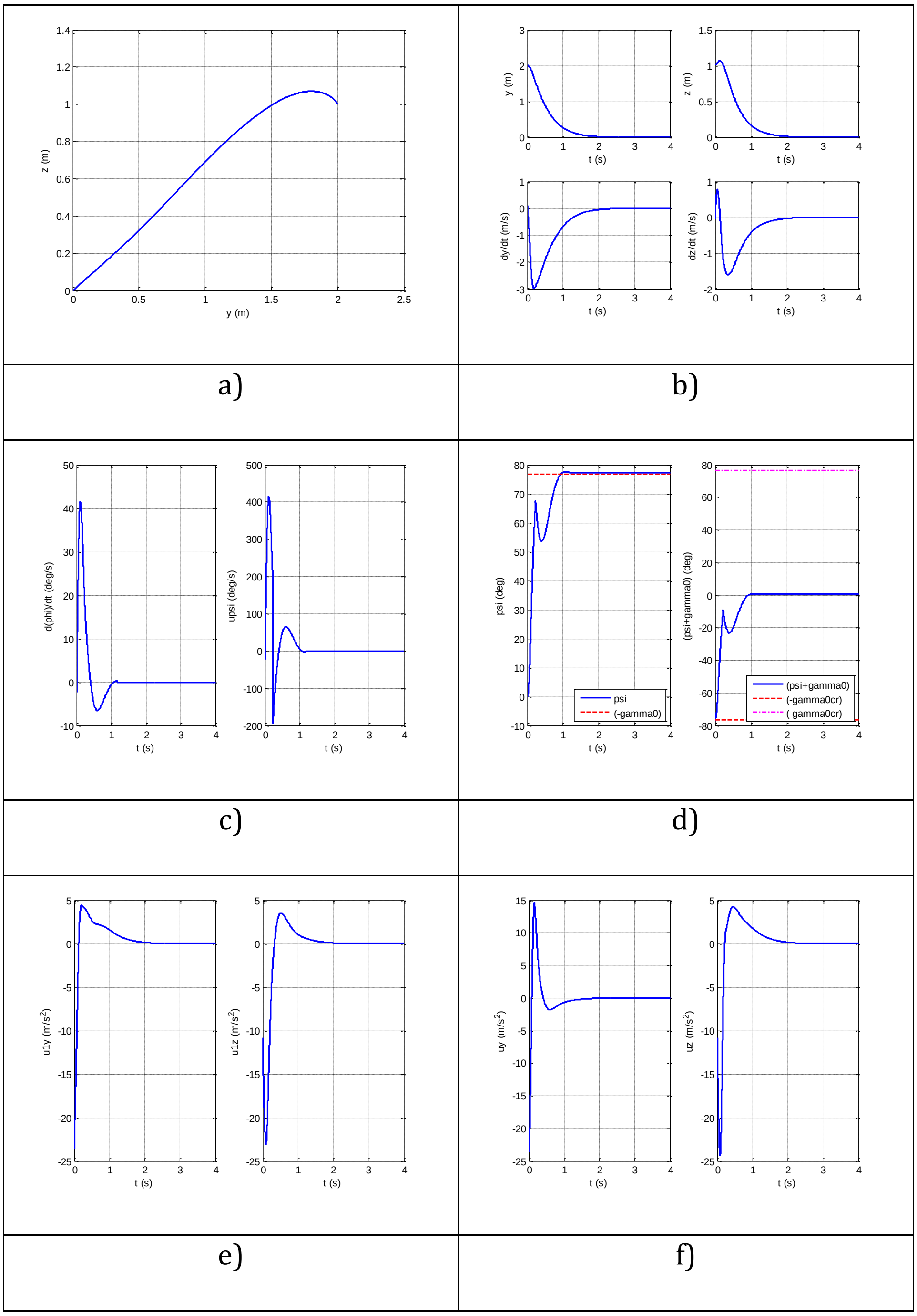

Figure 3.22 Performance of the closed loop guidance system with AE2DPDGL in case of Section 3.5.2 at non-proportional to each other initial conditions (3.104) and phase coupling angle $\gamma_0 = -\gamma_{cr}$ (3.107) where $\gamma_{cr} = 76.6924$ deg. with regard to: a) ATGM trajectory in the $Y_L Z_L$-plane, the picture plane; b) $y, \dot{y}, z$ and $\dot{z}$; c) $\dot{\varphi}$ and the adaptive control u_ψ (3.78); d) the self-adjusting angle ψ of the AE2DPDGL and the sum of ψ and γ_0; e) the components of the E2DPDGL (3.3) - (3.4) as a part of the AE2DPDGL; f) the components of the AE2DPDGL (3.5).

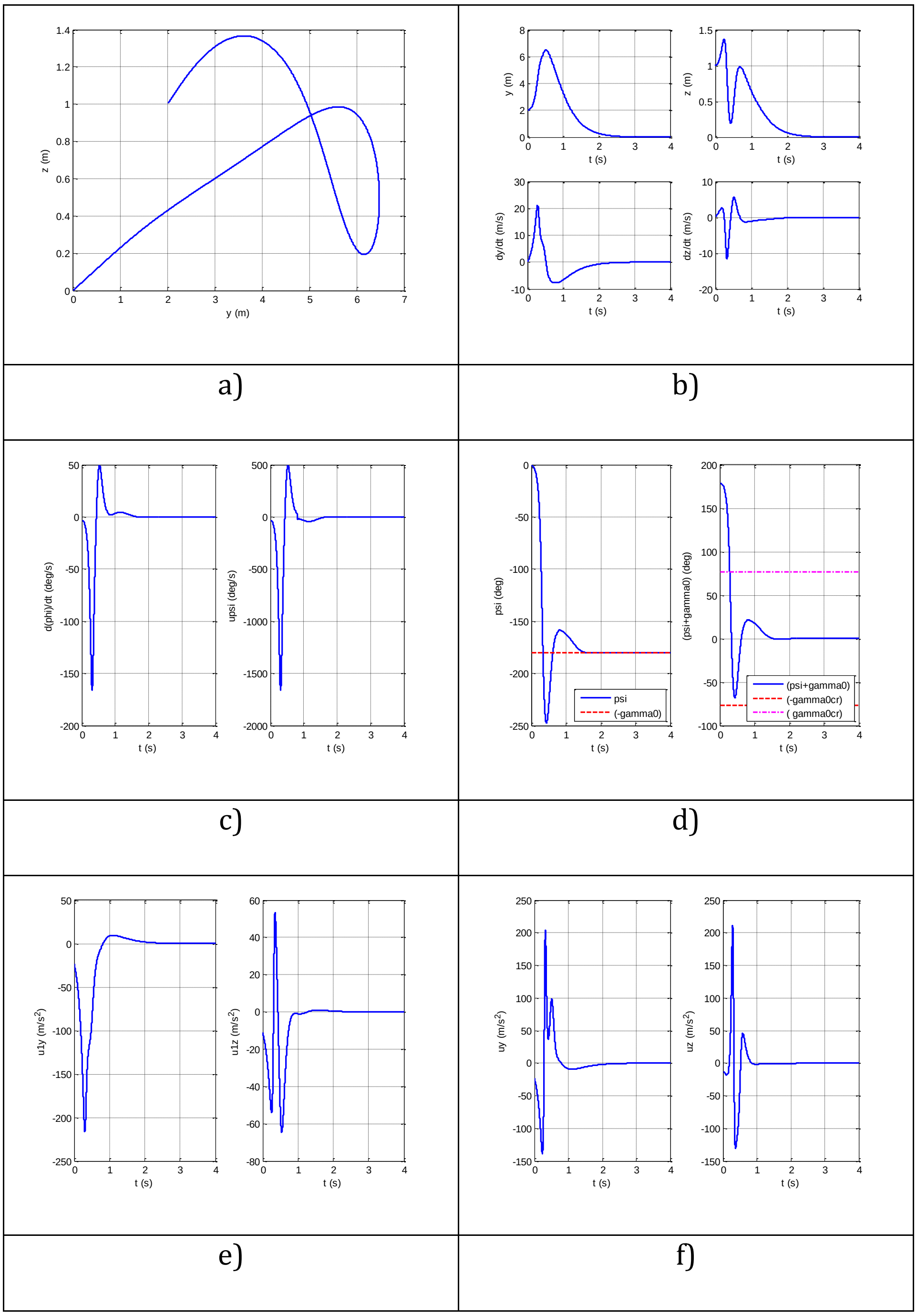

Figure 3.23 Performance of the closed loop guidance system with AE2DPDGL in case of Section 3.5.2 at non-proportional to each other initial conditions (3.104) and phase coupling angle $\gamma_0 = \pi$ (3.112) with regard to: a) ATGM trajectory in the $Y_L Z_L$-plane, the picture plane; b) $y, \dot{y}, z$ and $\dot{z}$; c) $\dot{\varphi}$ and the adaptive control u_ψ (3.78); d) the self-adjusting angle ψ of the AE2DPDGL and the sum of ψ and γ_0; e) the components of the E2DPDGL (3.3) - (3.4) as a part of the AE2DPDGL; f) the components of the AE2DPDGL (3.5).

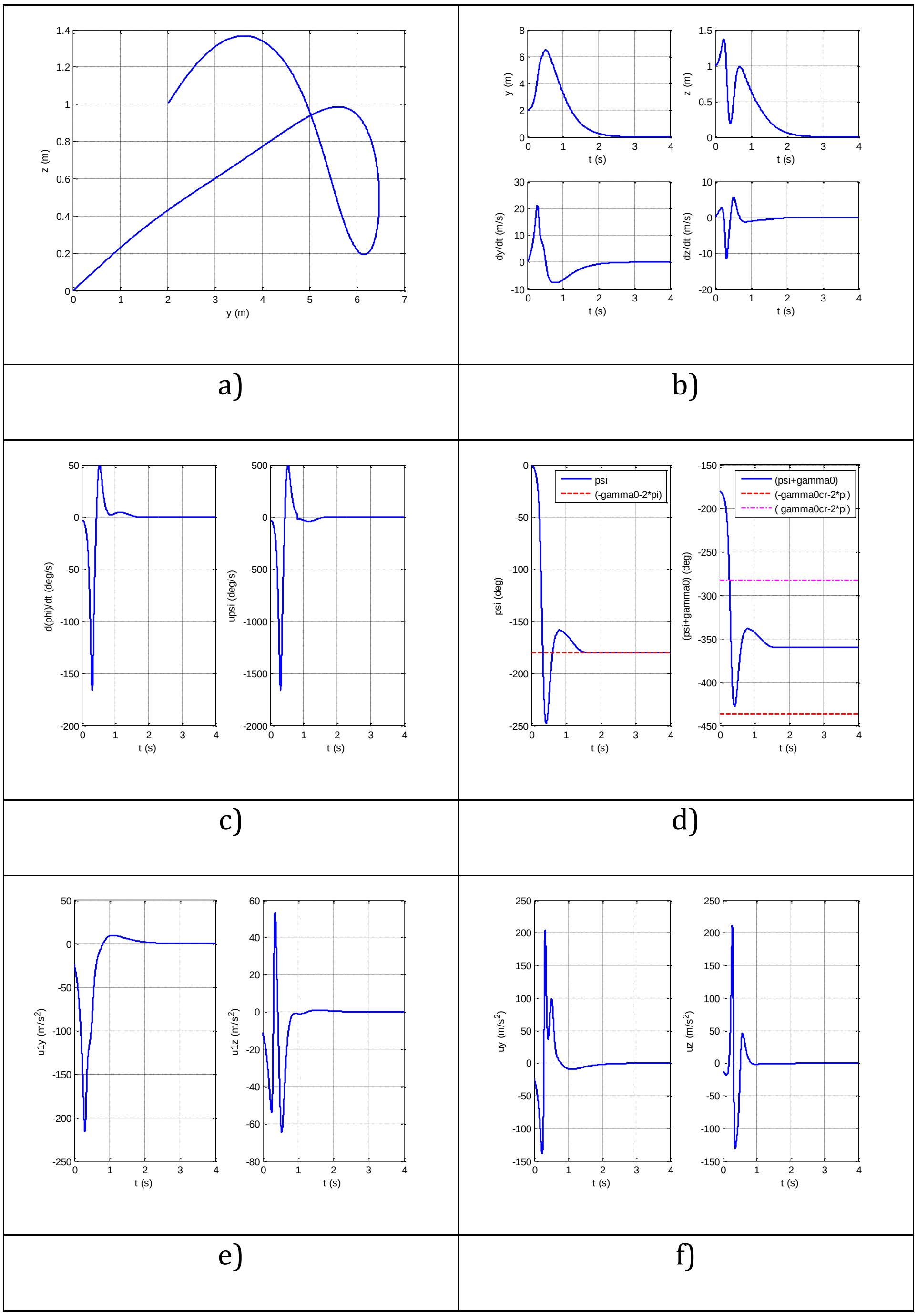

Figure 3.24 Performance of the closed loop guidance system with AE2DPDGL in case of Section 3.5.2 at non-proportional to each other initial conditions (3.104) and phase coupling angle $\gamma_0 = -\pi$ (3.113) with regard to: a) ATGM trajectory in the $Y_L Z_L$-plane, the picture plane; b) $y, \dot{y}, z$ and $\dot{z}$; c) $\dot{\varphi}$ and the adaptive control u_ψ (3.78); d) the self-adjusting angle ψ of the AE2DPDGL and the sum of ψ and γ_0; e) the components of the E2DPDGL (3.3) - (3.4) as a part of the AE2DPDGL; f) the components of the AE2DPDGL (3.5).

3.5.2 Performance of the AE2DPDGL in case the pair (a_0, a_1) defines negative roots of the characteristic polynomial $f(s)$ (1.5)

Let us complete the illustrations of the performance of the closed loop guidance system in this case choosing the same pair (a_0, a_1) ((1.19), (1.23)) as in Section 2.3.2 "Performance of the guidance loop with E2DPDGL in case the pair (a_0, a_1) defines negative roots of the characteristic polynomial $f(s)$ (1.5)" (page 39). Let also the initial conditions be non-proportional to each other (3.104) but very close to the strictly proportional initial conditions (1.16). The calculated critical value of the phase coupling angle γ_0 for this pair (a_0, a_1) ((1.19), (1.23)) is $\gamma_{cr} = 76.6924$ deg. according to (8.55) from Section 8.1.4 "Example" (page 195).

Figure 3.20 - Figure 3.24 illustrate the performance of the closed loop guidance system with AE2DPDGL in cases (3.105) - (3.107), (3.112), and (3.113) when the phase coupling angle $\gamma_0 = 0, \pm\gamma_{cr}, \pm\pi$ respectively. The global stability of the closed loop guidance system alongside with the effect of straightening the system trajectory in the picture plane is provided in the whole range of $[-\pi, \pi]$ of the phase coupling angle γ_0. The results in Figure 3.23 when $\gamma_0 = \pi$ and Figure 3.24 when $\gamma_0 = \pi - 2\pi = -\pi$ are identical as expected.

3.5.3 Summary

All simulations of the closed loop guidance system with phase coupling between the channels controlled by the AE2DPDGL confirm the already theoretically proven system's global stability.

The parameters of the AE2DPDGL are the ε_r area radius, the pair (a_0, a_1), the time constant T_φ, and the coefficient k_ψ. There are the following recommendations for their adjustment.

- The first step is choosing the pair (a_0, a_1) in accordance with the desired performance of both identical one-dimensional closed loop systems with one and the same characteristic polynomial (1.5) of the spatial closed loop system (1.1) - (1.4).
- The second step comprises choosing the ε_r area radius and the time constant T_φ. Both are parameters of the E2DPDGL. The time constant T_φ determines how fast we desire to straighten the system trajectory in the

$Y_L Z_L$-plane, the picture plane, according to the second equation of (2.15) in case of a closed loop guidance system with no coupling between the channels and controlled by the E2DPDGL.

- The third step is choosing the coefficient k_ψ of the adaptive control (3.78) of the angle ψ of the E2DPDGL vector rotation as a part of the AE2DPDGL.

The proper adjustment of the AE2DPDGL parameters results in achieving a performance of the CLOS ATGM closed loop guidance system which is impossible for the classical scheme as shown at the simulation illustrations. Besides this, the performance of the spatial closed loop system is kept similar and at similar control costs for a broad variety of initial conditions and values of the phase coupling angle.

3.6 Conclusions

The classical spatial closed loop guidance system with phase coupling between the channels caused by the angle γ_0 has acceptable performance at values of $|\gamma_0|$ close to $|\gamma_0| = 0$ and far away from the critical value γ_{cr} of the phase coupling angle γ_0. The increase of $|\gamma_0|$ worsens the performance of the guidance loop till losing stability at $|\gamma_0| \geq \gamma_{cr}$ which is seen as spiraling of the system trajectory in the $Y_L Z_L$-plane, the picture plane, with increasing amplitude of oscillations.

Now the AE2DPDGL provides global stability of the closed loop guidance system with phase coupling between the channels regardless of the values of the phase coupling angle γ_0 from the whole range of $[-\pi, \pi]$. The AE2DPDGL effectively fights also the system trajectory's spiraling in the $Y_L Z_L$-plane, the picture plane, not only when it is caused by the phase coupling angle but in cases when the spiraling is due to the non-proportional initial conditions.

The effectiveness of the AE2DPDGL is attributed to the simultaneous action of the following two factors.

- The first factor represents the adaptive control of the angle of the expanded two-dimensional proportional-derivative guidance law (E2DPDGL) vector rotation which angle is self-adjusted to the opposite angle $(-\gamma_0)$ of the phase coupling angle γ_0 so that the summary phase coupling between the channels strives to zero.

- The second factor represents the expanded two-dimensional proportional-derivative guidance law (E2DPDGL) of itself which straightens the system trajectory in the $Y_L Z_L$-plane, the picture plane, in case of no-coupling between the channels providing proportionality between them with a determined dynamics of each one based on one and the same characteristic polynomial.

Thus the problem with the intertwining between the channels and non-proportionality of the initial condition is solved finally by the new and complex AE2DPDGL.

4 SIMPLIFIED ADAPTIVE TWO-DIMENSIONAL PD CLOS GUIDANCE LAW

The core idea of the AE2DPDGL developed in the previous Chapter 3 is to introduce an additional variable vector rotation of the E2DPDGL and respective control synthesis of this additional variable vector rotation aimed at providing stability of the closed loop system with phase coupling between the channels alongside with straightening the system trajectory in the picture plane. As a result of the synthesis a global stability of the closed loop system is achieved. The synthesized AE2DPDGL features a compensation of the phase coupling angle by an adaptive control of the variable vector rotation of the E2DPDGL and straightening the missile trajectory in the $Y_L Z_L$-plane, the picture plane, outside the predetermined ε_r area around the picture plane origin though the existence of non-proportional initial conditions and phase coupling between the channels. The proposed idea of controlling the direction of the already synthesized guidance law vector in the complex plane is very attractive. It makes sense to try to apply this idea not to control only the vector rotation of the E2DPDGL but to control the vector rotation in the complex plane of the guidance law based on two classical PD guidance laws.

4.1 Problem formulation

Let us formulate the variable direction in the complex plane of the summary vector of the identical classical PD guidance laws of y and z-channels in the same way as for the variable direction of the E2DPDGL from Sections 3.1 and 3.2. Thus let the controlled variable ψ (rad) defined in the way (3.1) be (4.1) here where u_ψ represents the control of the angular velocity of the angle ψ. Let also the initial conditions ((3.2) from Section 3.1) of the angle ψ be (4.2) here. Rename the controls u_y and u_z of the CPDGL (1.3) as controls u_{1y} and u_{1z} and rewrite the CPDGL (1.3) as

(4.3). Define the summary vector of the two CPDGLs (4.3) in the complex form (4.4) and form the guidance law (4.5) which represents the complex form of the spatial CPDGL with controlled vector rotation.

$\frac{d\psi}{dt} = u_{\psi},$	(4.1)
$\psi(0) = 0$	(4.2)
$u_{1y} = -\frac{1}{a_0}(y + a_1\dot{y}),$ $u_{1z} = -\frac{1}{a_0}(z + a_1\dot{z})$	(4.3)
$u_{1p} = u_{1y} + iu_{1z}$	(4.4)
$u_p = e^{i\psi}u_{1p}$	(4.5)

Analogically with the problem formulation in Section 3.2 (page 53) the spatial system (1.30) - (1.31) with phase coupling between the channels and controlled by two CPDGLs but with controlled vector rotation (4.5) in terms of the complex variables represents (4.6).

$\ddot{p} = a_p\ ,$ $a_p = e^{i\gamma_0}u_p\ ,$ $u_p = e^{i\psi}u_{1p}\ ,$ $\frac{d\psi}{dt} = u_{\psi}$	(4.6)

Our aim is to synthesize a control u_{ψ} of the angular velocity of the angle ψ of the controlled direction of the spatial CPDGL vector for the system (4.6) with initial conditions according to (1.2) and (4.2) so that the phase coupling between the channels caused by the angle γ_0 is compensated alongside with providing stability of the closed loop system. Note that we omit here the requirement to straighten the missile trajectory in the $Y_L Z_L$-plane, the picture plane, which exists at the problem formulation of the E2DPDGL with controlled vector rotation in Section 3.2 (page 53).

4.2 Analysis of the system (4.6)

Let us consider the first three equations (4.7) of the system (4.6). Define the angle γ_1 as (4.8). The system (4.6) represents (4.9) where γ_1 is practically the summary phase coupling angle of the system (4.6). The system (4.9) corresponds to the system (8.8) where γ_0 is replaced here with γ_1. According to the general conclusion on the stability of the closed loop system from Section 8.1.3 (page 195) in Appendix 8.1 "Analysis of the stability of the closed loop system (1.30) - (1.31) with control (1.3) in function of the parameter γ" (page 185) the closed loop system (4.9) is asymptotically stable when the summary phase coupling angle γ_1 (4.8) is within the interval of stability $(-\gamma_{cr},\ \gamma_{cr})$ (4.10) where the critical value of the phase coupling angle γ_{cr} is calculated according to (8.55).

$\ddot{p} = a_p,$ $a_p = e^{i\gamma_0} u_p,$ $u_p = e^{i\psi} u_{1p}$	(4.7)
$\gamma_1 = \gamma_0 + \psi$	(4.8)
$\ddot{p} = a_p\ ,$ $a_p = e^{i\gamma_1} u_{1p}\ ,$ $u_{1p} = \left(\frac{-1}{a_0} (p + a_1 \dot{p}) \right)$	(4.9)
$\gamma_1 \in (-\gamma_{cr}, \gamma_{cr})$	(4.10)

Let us consider the system (4.9) in terms of the variables r and φ which represent respectively the magnitude and the argument of the complex representation of the variable p (2.1). We obtain (4.11) for the first derivative of p having in mind (2.8). Then the control u_{1p} in (4.9) represents (4.12). Thus the system (4.9) represents (4.13) or (4.14) in terms of the variables r and φ. The comparison of $\ddot{p}$ (4.14) with $\ddot{p}$ (2.11) ((2.11) represents the second derivative of $p(t) = r(t)e^{i\varphi(t)}$ (2.1)) results into (4.15). The last equation leads to the system (4.16). Thus the system (4.9) in terms of the variables r and φ and γ_1 represents the system (4.16).

$$\begin{aligned}\dot{p} &= \dot{y} + i\dot{z} = \\ &= (\dot{r}\cos\varphi - r\sin\varphi\,\dot{\varphi}) + i(\dot{r}\sin\varphi + r\cos\varphi\,\dot{\varphi}) = \\ &= e^{i\varphi}(\dot{r} + ir\dot{\varphi})\end{aligned}$$	(4.11)
$$\begin{aligned}u_{1p} &= \left(\frac{-1}{a_0}(p + a_1\dot{p})\right) = \\ &= \left(\frac{-1}{a_0}\left(re^{i\varphi} + a_1 e^{i\varphi}(\dot{r} + ir\dot{\varphi})\right)\right) = \\ &= e^{i\varphi}\left(\frac{-1}{a_0}\left(r + a_1(\dot{r} + ir\dot{\varphi})\right)\right)\end{aligned}$$	(4.12)
$$\begin{aligned}&\ddot{p} = a_p\,, \\ &a_p = e^{i\gamma_1}u_{1p}\,, \\ &u_{1p} = e^{i\varphi}\left(\frac{-1}{a_0}\left(r + a_1(\dot{r} + ir\dot{\varphi})\right)\right)\end{aligned}$$	(4.13)
$$\ddot{p} = e^{i\gamma_1}e^{i\varphi}\left(\frac{-1}{a_0}\left(r + a_1(\dot{r} + ir\dot{\varphi})\right)\right)$$	(4.14)
$$\begin{aligned}\ddot{p} &= e^{i\gamma_1}e^{i\varphi}\left(\frac{-1}{a_0}\left(r + a_1(\dot{r} + ir\dot{\varphi})\right)\right) = \\ &= e^{i\varphi}\left((\ddot{r} - r\dot{\varphi}^2) + i(2\dot{r}\dot{\varphi} + r\ddot{\varphi})\right)\end{aligned}$$	(4.15)
$$\begin{aligned}\ddot{r} - r\dot{\varphi}^2 &= -\frac{1}{a_0}(r + a_1\dot{r})\cos\gamma_1 + \frac{a_1}{a_0}r\dot{\varphi}\sin\gamma_1\,, \\ 2\dot{r}\dot{\varphi} + r\ddot{\varphi} &= -\frac{a_1}{a_0}r\dot{\varphi}\cos\gamma_1 - \frac{1}{a_0}(r + a_1\dot{r})\sin\gamma_1\end{aligned}$$	(4.16)

Let us define the first derivative of φ as φ_1 (4.17). The system (4.16) represents (4.18) or the system (4.19) in terms of r and φ_1 considering γ_1 as an input variable.

$$\frac{d\varphi}{dt} = \varphi_1$$	(4.17)
$$\begin{aligned}\ddot{r} - r{\varphi_1}^2 &= -\frac{1}{a_0}(r + a_1\dot{r})\cos\gamma_1 + \frac{a_1}{a_0}r\varphi_1\sin\gamma_1\,, \\ 2\dot{r}\varphi_1 + r\dot{\varphi}_1 &= -\frac{a_1}{a_0}r\varphi_1\cos\gamma_1 - \frac{1}{a_0}(r + a_1\dot{r})\sin\gamma_1\end{aligned}$$	(4.18)

$$\begin{aligned} \ddot{r} &= -\frac{1}{a_0}(r + a_1\dot{r})\cos\gamma_1 + \frac{a_1}{a_0}r\varphi_1\sin\gamma_1 + r{\varphi_1}^2, \\ r\dot{\varphi}_1 &= -\frac{a_1}{a_0}r\varphi_1\cos\gamma_1 - \frac{1}{a_0}(r + a_1\dot{r})\sin\gamma_1 - 2\dot{r}\varphi_1 \end{aligned}$$	(4.19)

In order to obtain a presentation of the dependence of φ_1 (4.17) from the summary phase coupling angle γ_1 (4.8) for the needs of the synthesis let us make some simplifying assumptions.

Let us suppose the summary phase coupling angle γ_1 (4.8) is a constant angle within the interval of stability $(-\gamma_{cr},\ \gamma_{cr})$ (4.10) according to (4.20) i.e. suppose the system (4.9) is asymptotically stable. Because of the asymptotic stability of the system (4.9) it is easily seen that the process on r descents to zero too (4.21).

Let us suppose also the initial conditions of the system (4.9) defined as (1.2) satisfy also (4.22). This means the initial conditions are proportional to one another according to (1.10) and (1.14) which also means taking into account the relations (2.16) that the initial conditions of the systems (4.18) and (4.19) with respect to r and φ_1 satisfy (4.23). Figure 8.4 - Figure 8.8 in Section 8.1.4 “Example” (page 195) illustrate the processes on y and z as well as the processes in the yz-plane of system (4.9) in such a case. It can be seen there that the vector pointing the missile position in the picture plane starts rotating always in an opposite direction to the value of the phase coupling angle. Considering the second equation of the system (4.19) with initial conditions according to (4.23) we obtain (4.24) for the first derivative of φ_1 at the initial moment, which answers the question regarding the direction of rotation.

$$\begin{gathered} \gamma_1 \in (-\gamma_{cr}, \gamma_{cr}), \\ \gamma_1 = \gamma_{10} = const. \end{gathered}$$	(4.20)
$$\lim_{t\to\infty} r(t) = \lim_{t\to\infty}\sqrt{y(t)^2 + z(t)^2} = 0$$	(4.21)
$$\begin{gathered} y_0 \neq 0, \\ y_{10} = z_{10} = 0 \end{gathered}$$	(4.22)

$r(0) = \sqrt{{y_0}^2 + {z_0}^2} > 0,$ $\dot{r}(0) = \dfrac{y_0 y_{10} + z_0 z_{10}}{\sqrt{{y_0}^2 + {z_0}^2}} = 0,$ $\varphi_1(0) = \dot{\varphi}(0) = \dfrac{z_{10} y_0 - y_{10} z_0}{{y_0}^2 + {z_0}^2} = 0$	(4.23)
$\dot{\varphi}_1(0) = -\dfrac{1}{a_0} \sin \gamma_{10}$	(4.24)

Let us try to find out the parameters of the steady state of the system (4.19) in function of the parameter γ_{10}. We suppose (4.25).

$\lim_{t\to\infty} r(t) = r_{ss} = 0,$ $\lim_{t\to\infty} \dot{r}(t) = \dot{r}_{ss} = 0,$ $\lim_{t\to\infty} \varphi_1(t) = \varphi_{1ss} = const.$	(4.25)

Let us consider first the case (4.26) with no coupling between the channels. Taking into account that the initial conditions of the system (4.19) satisfy (4.23) the system (4.19) represents (4.27). It is easily seen the steady state in this case represents (4.28). The processes in Figure 1.3, Figure 1.4, and Figure 1.5 marked with solid (red) line as well as Figure 8.4 illustrate this case where there is no rotation of the vector pointing the missile position in the picture plane while the transition process to the picture plane origin.

$\gamma_1 = \gamma_{10} = 0$	(4.26)
$\ddot{r} = -\dfrac{1}{a_0}(r + a_1 \dot{r}),$ $r\dot{\varphi}_1 = 0$	(4.27)
$\lim_{t\to\infty} r(t) = r_{ss} = 0,$ $\lim_{t\to\infty} \dot{r}(t) = \dot{r}_{ss} = 0,$ $\varphi_1(t) = 0 \; \forall t \geq 0, \;\; \varphi_{1ss} = 0$	(4.28)

Let us now consider the case (4.29). We obtain by substitution of the steady state parameters (4.25) into the equations of the system (4.19) the system (4.30). The last transforms into (4.31) from which we cannot determine the value of the parameter φ_{1ss}. For this reason let us try another way. Let the right parts of the equations of the system (4.19) be F_{12} and F_{22} (4.32). Define r_1 as (4.33). Suppose in our case of initial conditions (4.23) and summary phase coupling angle (4.29) there exists the boundary (4.34). Then we can represent F_{22} from (4.32) in the steady state as (4.35), (4.36). Let us suppose the steady state solution satisfies also (4.37). Thus from (4.37) we obtain φ_{1ss} (4.38).

$\gamma_1 \in (-\gamma_{cr}, \gamma_{cr}),$ $\gamma_1 = \gamma_{10} = const \ \neq 0.$	(4.29)
$0 = -\frac{1}{a_0}(0 + a_1 0)\cos\gamma_{10} + \frac{a_1}{a_0} 0\varphi_{1ss}\sin\gamma_{10} + 0{\varphi_{1ss}}^2,$ $0 = -\frac{a_1}{a_0} 0\varphi_{1ss}\cos\gamma_{10} - \frac{1}{a_0}(0 + a_1 0)\sin\gamma_{10} - 20\varphi_{1ss}$	(4.30)
$0 = 0,$ $0 = 0$	(4.31)
$F_{12} = -\frac{1}{a_0}(r + a_1\dot{r})\cos\gamma_1 + \frac{a_1}{a_0} r\varphi_1 \sin\gamma_1 + r{\varphi_1}^2,$ $F_{22} = -\frac{a_1}{a_0} r\varphi_1 \cos\gamma_1 - \frac{1}{a_0}(r + a_1\dot{r})\sin\gamma_1 - 2\dot{r}\varphi_1$	(4.32)
$r_1 = \frac{\dot{r}}{r}$	(4.33)
$-\infty < \lim_{t\to\infty}\frac{\dot{r}(t)}{r(t)} = r_{1ss} < \infty$	(4.34)
$F_{22}(r_{ss}, \dot{r}_{ss}, \varphi_{1ss}, \gamma_{10}) = r_{ss}F_{23}(r_{1ss}, \varphi_{1ss}, \gamma_{10})$	(4.35)
$F_{23}(r_{1ss}, \varphi_{1ss}, \gamma_{10}) =$ $= -\frac{a_1}{a_0}\varphi_{1ss}\cos\gamma_{10} - \frac{1}{a_0}(1 + a_1 r_{1ss})\sin\gamma_{10} - 2r_{1ss}\varphi_{1ss}$	(4.36)
$F_{23}(r_{1ss}, \varphi_{1ss}, \gamma_{10}) = 0$	(4.37)
$\varphi_{1ss} = \frac{-(1 + a_1 r_{1ss})}{a_1\cos\gamma_{10} + 2a_0 r_{1ss}}\sin\gamma_{10}$	(4.38)

It is interesting to see what happens with the second equation of the system (4.19) when $r = 0$ (4.39). In this case this equation transforms into (4.40) from which it follows (4.41). Given $r = 0$ (4.39) but this is not yet the steady state i.e. $\dot{r} \neq 0$ (4.42) we obtain (4.43).

$r = 0$	(4.39)
$0 = -\frac{a_1 \dot{r}}{a_0} \sin \gamma_1 - 2\dot{r}\varphi_1$	(4.40)
$\dot{r}\left(\frac{a_1}{a_0} \sin \gamma_1 + 2\varphi_1\right) = 0$	(4.41)
$\dot{r} \neq 0$	(4.42)
$\varphi_1 = -\frac{a_1}{2a_0} \sin \gamma_1$	(4.43)

Having in mind the cases at the initial moment (4.24) and at the transition through the picture plane origin (4.43) we can definitely conclude that the dependence of the direction of rotation of the vector pointing to the missile position in the picture plane from the summary phase coupling angle could be described as nearly proportional with a negative coefficient. Regarding the steady state there is seen also a proportionality between the value of the summary phase coupling angle and the steady angular velocity of rotation of the above vector (4.38).

As an illustration of the above conclusion in Figure 4.1 are shown some results of the simulations of the closed loop system from Section 8.1.4 “Example” (page 195) in function of the phase coupling angle with regard to the trajectories in the picture plane as well as the processes on r_1 and φ_1. The processes on r_1 and φ_1 are obtained by the transformation of the simulation data in terms of the system (4.9). It is seen the boundary r_{1ss} (4.34) exists as well as the steady state φ_{1ss} (4.38). A short summary is presented in Table 4.1 below. Note that for the example $\gamma_{cr} = 0.7525$ rad or $\gamma_{cr} = 43.1176$ deg.

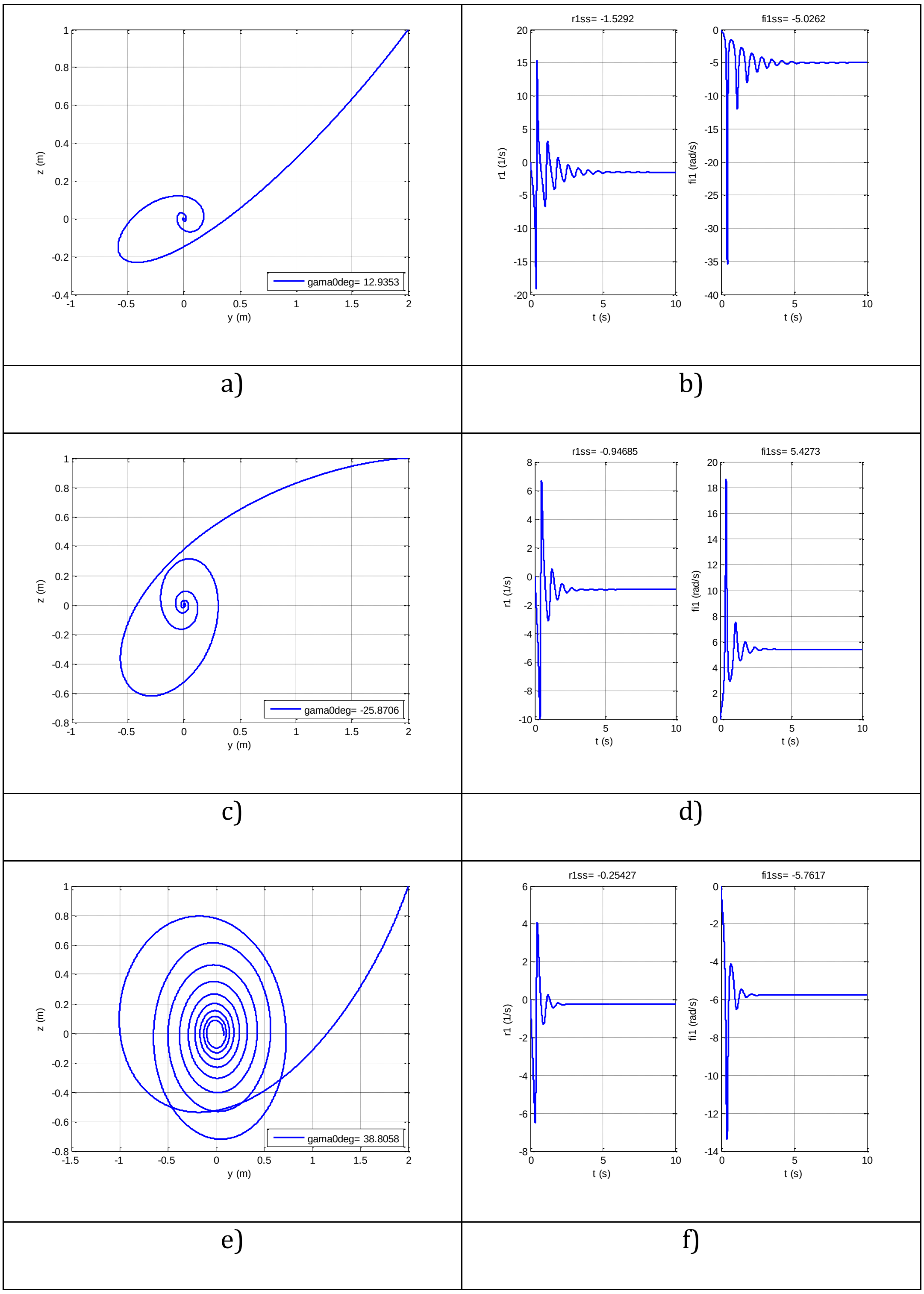

Figure 4.1 Trajectories in the picture plane and processes on r_1 and φ_1 in function of the summary phase coupling angle γ_{10} for the classical spatial closed loop system with identical PD guidance laws in the y and z-channels: a) and b) when $\gamma_{10} = 0.3\gamma_{cr} = 12.94 \approx 13$ deg.; c) and d) when $\gamma_{10} = -0.6\gamma_{cr} = -25.87 \approx -26$ deg.; e) and f) when $\gamma_{10} = 0.9\gamma_{cr} = 38.81 \approx 39$ deg.

Table 4.1 Short summary of the processes on r_1 and φ_1 in function of the summary phase coupling angle γ_{10} for the classical spatial closed loop system with identical PD guidance laws in the y and z-channels.

$\frac{\gamma_{10}}{\gamma_{cr}}$	$\mathbf{0.3}$	$\mathbf{-0.6}$	$\mathbf{0.9}$
γ_{10} **(rad)**	0.23	-0.45	0.68
γ_{10} **(deg.)**	$12.94 \approx 13$	$-25.87 \approx -26$	$38.81 \approx 39$
r_{1ss} **(1/s)**	-1.53	-0.95	-0.25
φ_{1ss} **(rad/s)** **(Simulation Data)**	-5.03	5.43	-5.76
φ_{1ss} **(rad/s)** **(According to (4.38))**	-5.03	5.43	-5.76
$\varphi_{1ss}/\sin\gamma_{10}$ **(rad/s)**	-22.45	-12.44	-9.19
$\varphi_{1ss}/\gamma_{10}$ **(1/s)**	-22.26	-12.02	-8.51

Let us suppose also the steady state regarding r and $\dot{r}$ is achieved. Then having in mind (4.34) the second equation of the system (4.19) around the steady state on r and $\dot{r}$ represents (4.44). Let us define the time constant $T_{\varphi 1}$ and the coefficient $k_{\varphi 1}$ according to (4.46) assuming (4.45). Assume also (4.47). Thus we can represent (4.44) by the transfer function $W_{\varphi 1\gamma 1}(s)$ (4.48). When (4.49) occurs the transfer function $W_{\varphi 1\gamma 1}(s)$ transforms into (4.51) where the coefficient $k_{\varphi 1}$ is according to (4.50). A short summary of the values of the time constant $T_{\varphi 1}$ and the coefficient $k_{\varphi 1}$ at different values of γ_{10} is presented in Table 4.2.

$\dot{\varphi}_1 = -\left(\frac{a_1}{a_0}\cos\gamma_{10} + 2r_{1ss}\right)\varphi_1 - \frac{1}{a_0}(1 + a_1 r_{1ss})\sin\gamma_{10}$	(4.44)
$\left(\frac{a_1}{a_0}\cos\gamma_{10} + 2r_{1ss}\right) \neq 0$	(4.45)

$T_{\varphi 1} = \dfrac{1}{\left(\dfrac{a_1}{a_0}\cos\gamma_{10} + 2r_{1ss}\right)}$ $k_{\varphi 1} = \dfrac{-\dfrac{1}{a_0}(1 + a_1 r_{1ss})}{\left(\dfrac{a_1}{a_0}\cos\gamma_{10} + 2r_{1ss}\right)}$	(4.46)
$\sin\gamma_{10} \approx \gamma_{10}$	(4.47)
$W_{\varphi 1\gamma 1}(s) = \dfrac{k_{\varphi 1}}{T_{\varphi 1}s + 1}$	(4.48)
$\left(\dfrac{a_1}{a_0}\cos\gamma_{10} + 2r_{1ss}\right) = 0$	(4.49)
$k_{\varphi 1} = -\dfrac{1}{a_0}(1 + a_1 r_{1ss})$	(4.50)
$W_{\varphi 1\gamma 1}(s) = k_{\varphi 1}$	(4.51)

Table 4.2 Short summary of the values of the time constant $T_{\varphi 1}$ and the coefficient $k_{\varphi 1}$ at different values of γ_{10}.

$\dfrac{\gamma_{10}}{\gamma_{cr}}$	$\mathbf{0.3}$	$\mathbf{-0.6}$	$\mathbf{0.9}$
γ_{10} **(rad)**	0.23	−0.45	0.68
γ_{10} **(deg.)**	$12.94 \approx 13$	$-25.87 \approx -26$	$38.81 \approx 39$
$T_{\varphi 1}$ **(s)**	1.2	0.6	0.4
$k_{\varphi 1} = \varphi_{1ss}/\gamma_{10}$ **(1/s)**	−22.3	−12.0	−8.5

4.3 Synthesis of the guidance law

4.3.1 Synthesis of the control of the vector rotation of the spatial CPDGL

Based on the transfer function $W_{\varphi 1\gamma 1}(s)$ (4.48) we propose the control (4.52) of the vector rotation of the spatial CPDGL. Thus employing only the second equation of the system (4.19) we synthesize the closed loop (4.53) which is represented also in Figure 4.2.

$u_{\psi} = k_{\psi}\varphi_1,\ k_{\psi} > 0$	(4.52)
$\varphi_1(s) = \dfrac{k_{\varphi 1}}{T_{\varphi 1}s + 1}\gamma_1(s),$ $\gamma_1(s) = \gamma_0(s) + \psi(s),$ $\psi(s) = \dfrac{1}{s}u_{\psi}(s),$ $u_{\psi}(s) = k_{\psi}\varphi_1(s)$	(4.53)

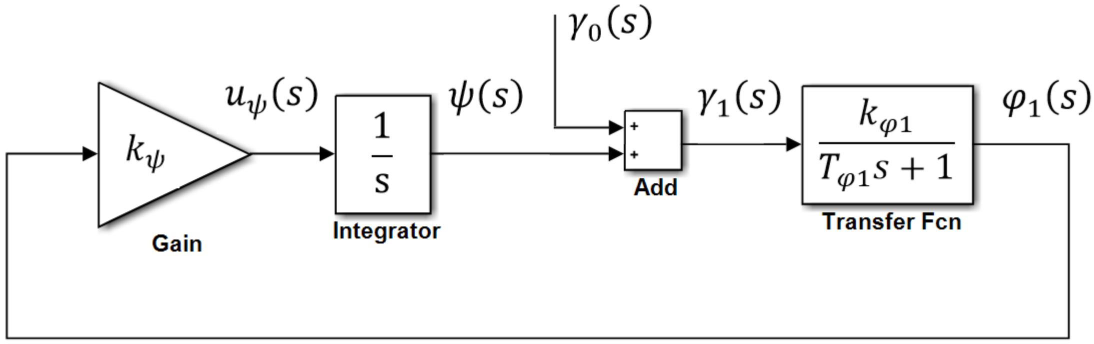

Figure 4.2 The synthesized closed loop for controlling the vector rotation of the spatial CPDGL.

Note that we could employ also the above presentation in case of (4.49) substituting $T_{\varphi 1} = 0$ having in mind that $k_{\varphi 1}$ becomes (4.50). The characteristic polynomial of the above closed loop system (4.53) represents (4.54). In case of (4.49) the characteristic polynomial becomes (4.55). We could conclude that though varying the coefficients $T_{\varphi 1}$ and $k_{\varphi 1}$ (see Table 4.2) the asymptotic stability of the closed loop is provided based on the proposed control (4.52) of the variable direction ψ of the spatial vector of the CPDGL in the complex plane.

$H(s) = T_{\varphi 1}s^2 + s - k_{\varphi 1}k_{\psi}$	(4.54)
$H(s) = s - k_{\varphi 1}k_{\psi}$	(4.55)

Because of the simplicity of the synthesized closed loop it is easily seen that in the steady state the introduced variable direction ψ of the summary vector of the two CPDGLs in the complex plane becomes $(-\gamma_0)$ (4.56), the summary phase coupling between the channels γ_1 becomes zero (4.57), the angular velocity $\varphi_1 = \dot{\varphi}$ of the polar angle of the vector pointing to the missile position in the picture plane becomes zero too (4.58). Thus the asymptotic stability of the above adaptive mechanism leads to decoupling of the spatial closed loop system with phase coupling between the channels with a zero steady state of the summary phase coupling between the channels γ_1 (4.57) which provides the asymptotic stability of the whole spatial closed loop system.

$\psi_{ss} = -\gamma_0$	(4.56)
$\gamma_{1ss} = \psi_{ss} + \gamma_0 = 0$	(4.57)
$\varphi_{1ss} = 0$	(4.58)

4.3.2 Further simplification of the guidance law

Let us consider the proposed control (4.52). It is based on the angular velocity $\varphi_1 = \dot{\varphi}$. The last is obtained according to the second equation of (2.16) - (4.59). In order to avoid division by zero when $r = 0$ and the uncertainty let us introduce φ_{1r} as (4.60) and name it an index of disproportionality. Based on the relation (4.61) we modify the control (4.52) into (4.62). Thus we implement practically the principle of feedback but reinforced here with regard to the distance to the plane origin. The closed loop remains stable because the forms of the characteristic polynomial (4.54) or (4.55) turn respectively into (4.63) and (4.64) when $r \neq 0$. The occurrence $r = 0$ in some number of points before achieving the steady state breaks the loop (u_ψ (4.62) becomes zero when $r = 0$), but the compensation of the phase coupling angle γ_0 via the controlled angle ψ remains intact since ψ is the output of the integrator whose input is the control u_ψ (4.62). So these occurrences do not destroy the stability of the synthesized closed loop system. The benefits of this modification consist in the avoidance of the employment of variable structure control (there is no division by zero) as well as reinforcing the implemented here feedback principle by taking into account the distance from the plane origin.

$\varphi_1 = \dot{\varphi} = \dfrac{\dot{z}\cos\varphi - \dot{y}\sin\varphi}{r} = \dfrac{\dot{z}y - \dot{y}z}{y^2 + z^2}$	(4.59)
$\varphi_{1r} = \dot{z}y - \dot{y}z$	(4.60)
$\varphi_{1r} = r^2\dot{\varphi}$	(4.61)
$u_\psi = k_\psi \varphi_{1r}$	(4.62)
$H(s) = T_{\varphi 1}s^2 + s - k_{\varphi 1}k_\psi r^2 \; when \; r \neq 0$	(4.63)
$H(s) = s - k_{\varphi 1}k_\psi r^2 \; when \; r \neq 0$	(4.64)

Finally the control u_ψ of the introduced variable direction of the summary vector of the two CPDGLs of y and z-channels in the complex plane in terms of Cartesian coordinates represents (4.65).

$u_\psi = k_\psi(\dot{z}y - \dot{y}z)$	(4.65)

Let us name the two identical classical PD guidance laws of y and z-channels alongside with the proposed control (4.65) of the direction of their summary vector in the complex plane by the variable angle ψ simplified (S) adaptive (A) two-dimensional (2D) proportional-derivative (PD) guidance (G) law (L) – SA2DPDGL.

4.3.3 Final representation of the SA2DPDGL in terms of Cartesian coordinates

The representation of (4.5) in Cartesian coordinates is (4.66). Having in mind the representation (4.67) of u_p from (2.3) we obtain the output of the guidance law (4.68).

$\begin{aligned} u_p &= e^{i\psi}u_{1p} = \\ &= (\cos\psi + i\sin\psi)\left(u_{1y} + iu_{1z}\right) = \\ &= \left(u_{1y}\cos\psi - u_{1z}\sin\psi\right) + i\left(u_{1z}\cos\psi + u_{1y}\sin\psi\right) \end{aligned}$	(4.66)
$u_p = u_y + iu_z$	(4.67)
$u_y = u_{1y}\cos\psi - u_{1z}\sin\psi\,, \quad u_z = u_{1z}\cos\psi + u_{1y}\sin\psi$	(4.68)

Thus the whole SA2DPDGL in terms of Cartesian coordinates represents the system consisting of (4.1), (4.2), (4.3), (4.65), and (4.68), whose summary is the following system (4.69).

$u_{1y} = -\dfrac{1}{a_0}(y + a_1\dot{y}),$ $u_{1z} = -\dfrac{1}{a_0}(z + a_1\dot{z}),$ $u_{\psi} = k_{\psi}(\dot{z}y - \dot{y}z),$ $\dfrac{d\psi}{dt} = u_{\psi}, \quad \psi(0) = 0,$ $u_y = u_{1y}\cos\psi - u_{1z}\sin\psi\,,$ $u_z = u_{1z}\cos\psi + u_{1y}\sin\psi$	(4.69)

4.4 Simulations

Let us continue studying the closed loop guidance system from Section 8.1.4 “Example” (page 195) and replace the two identical classical PD guidance laws of y and z-channels by the developed SA2DPDGL. The only adjustment regarding the new SA2DPDGL consists in a proper choice of the coefficient k_{ψ} while the parameters a_0 and a_1 are kept the same as in the classical case. Thus the closed loop guidance system represents the equations (1.30) - (1.31) with the guidance law (4.69). The pair (a_0, a_1) represents (8.26) ((8.26) corresponds to (1.7), (1.15)) while the coefficient k_{ψ} is chosen (4.70).

$k_{\psi} = 0.5$	(4.70)

Figure 4.3 shows the trajectories in the picture plane from initial conditions (1.16) as well as the adaptive control u_{ψ} (4.65) of the SA2DPDGL and the summary phase coupling angle $\gamma_1 = \gamma_0 + \psi$ (4.8) for some cases of the phase coupling angle γ_0 when it is within the interval of stability $\gamma_0 \in (-\gamma_{cr}, \gamma_{cr})$. Here the trajectories in the picture plane are compared with the respective trajectories in the picture plane but obtained in the classical application by two CPDGLs. A short summary of the results is represented in Table 4.3. It is clearly seen that the summary phase coupling angle γ_1 shows an improvement and the steady state γ_{1ss} being within the interval

of stability is closer to zero than its initial value γ_0. The settling time t_s in comparison with the settling time in the classical case with no coupling between the channels ($\gamma_0 = 0$) named t_s^*, where $t_s^* = 1.52\ s$, remains almost the same in case of the SA2DPDGL while in the classical case of two identical PD guidance laws it increases when the absolute value of the phase coupling γ_0 approaches its critical value γ_{cr} (here $\gamma_{cr} = 0.7525$ rad or $\gamma_{cr} = 43.1176$ deg.). The maximum overload $\max(n_y, n_z)$ remains practically the same as when there is no coupling between the channels. The last is easily to explain by the fact that the new SA2DPDGL guidance law rotates only the summary vector of the two CPDGLs but does not change its magnitude. It is seen also that there is no substantial straightening of the trajectory in the picture plane as the SA2DPDGL is not aimed at achieving this effect but only compensating for the phase coupling angle γ_0. Thus, the observed partial straightening is due to the improvement of the summary phase coupling angle between the channels and hence the much less pronounced spiral type of trajectory in the picture plane.

Table 4.3 Short summary of the effectiveness of the new SA2DPDGL when the initial value of the phase coupling angle is within the interval of stability.

$\boldsymbol{\frac{\gamma_0}{\gamma_{cr}}}$	$\mathbf{0}$	$\mathbf{0.3}$	$\mathbf{-0.6}$	$\mathbf{0.9}$
$\boldsymbol{\gamma_0}$ **(rad)**	0	0.23	−0.45	0.68
$\boldsymbol{\gamma_0}$ **(deg.)**	0	13	−26	39
$\boldsymbol{\gamma_{1ss}}$ **(deg.)**	0	−4	9	−15
$\frac{t_s}{t_s^*}$ (%) at CPDGL	100	105	158	576
$\frac{t_s}{t_s^*}$ (%) at SA2DPDGL	100	100	101	101
$\max(n_y, n_z)$ at SA2DPDGL	5	4	6	5
$\frac{\max(n_y,n_z)}{\max(n_y^*,n_z^*)}$ (%) at SA2DPDGL	100	80	120	100

Figure 4.4 shows the trajectories in the picture plane from initial conditions (1.16) as well as the adaptive control u_ψ (4.65) of the SA2DPDGL and the summary phase coupling angle $\gamma_1 = \gamma_0 + \psi$ (4.8) for some cases of the phase coupling angle γ_0 when it is outside the interval of stability $\gamma_0 \notin (-\gamma_{cr}, \gamma_{cr})$. A short summary of the results is represented in Table 4.4. Note that the classical closed loop guidance systems when $\gamma_0 \notin (-\gamma_{cr}, \gamma_{cr})$ are not asymptotically stable while the SA2DPDGL provides stability in a very wide range from $\gamma_0 = -90\,deg$ to $\gamma_0 = 90\,deg$ accompanied with an acceptable performance too. The maximum overload $\max(n_y, n_z)$ remains practically the same as in the classical case when there is no coupling between the channels. Analogically with the trajectories in the picture plane from Figure 4.3 here in Figure 4.4 there is no straightening of the trajectories too. The spiral type of the trajectories here is more pronounced versus the trajectories of the closed loop guidance system with the SA2DPDFL from Figure 4.3.

Table 4.4 Short summary of the effectiveness of the new SA2DPDGL when the initial value of the phase coupling angle is outside the interval of stability.

$\boldsymbol{\frac{\gamma_0}{\gamma_{cr}}}$	$\mathbf{0}$	$\mathbf{1.39}$	$\mathbf{2.0873}$	$\mathbf{-2.0873}$
$\boldsymbol{\gamma_0}$ **(rad)**	0	1.0472	1.5708	−1.5708
$\boldsymbol{\gamma_0}$ **(deg.)**	0	60	90	−90
$\boldsymbol{\gamma_{1ss}}$ **(deg.)**	0	−28	−22	22
$\frac{t_s}{t_s^*}$ (%) at CPDGL	100	∞ – unstable system	∞ – unstable system	∞ – unstable system
$\frac{t_s}{t_s^*}$ (%) at SA2DPDGL	100	106	222	222
$\max(n_y, n_z)$ at SA2DPDGL	5	6	6	5
$\frac{\max(n_y, n_z)}{\max(n_y^*, n_z^*)}$ (%) at SA2DPDGL	100	120	120	100

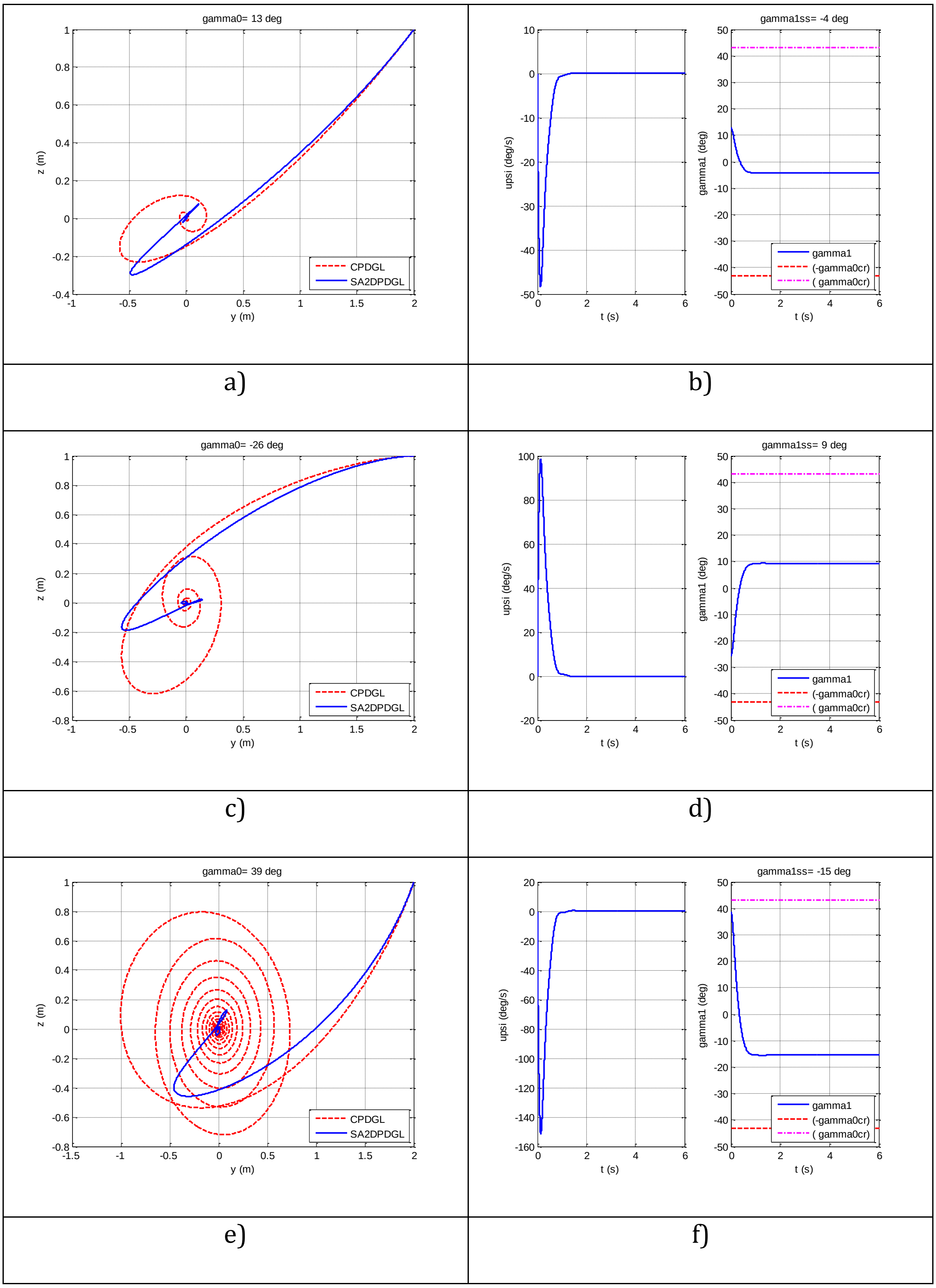

Figure 4.3 Trajectories in the picture plane from initial conditions (1.16), the adaptive control u_ψ (4.65) of the SA2DPDGL and the summary phase coupling angle $\gamma_1 = \gamma_0 + \psi$ (4.8) for some cases of the phase coupling angle γ_0 when it is within the interval of stability $\gamma_0 \in (-\gamma_{cr}, \gamma_{cr})$: a) and b) when $\gamma_0 = 0.3\gamma_{cr} = 12.94 \approx 13$ deg.; c) and d) when $\gamma_0 = -0.6\gamma_{cr} = -25.87 \approx -26$ deg. ; e) and f) when $\gamma_0 = 0.9\gamma_{cr} = 38.81 \approx 39$ deg.

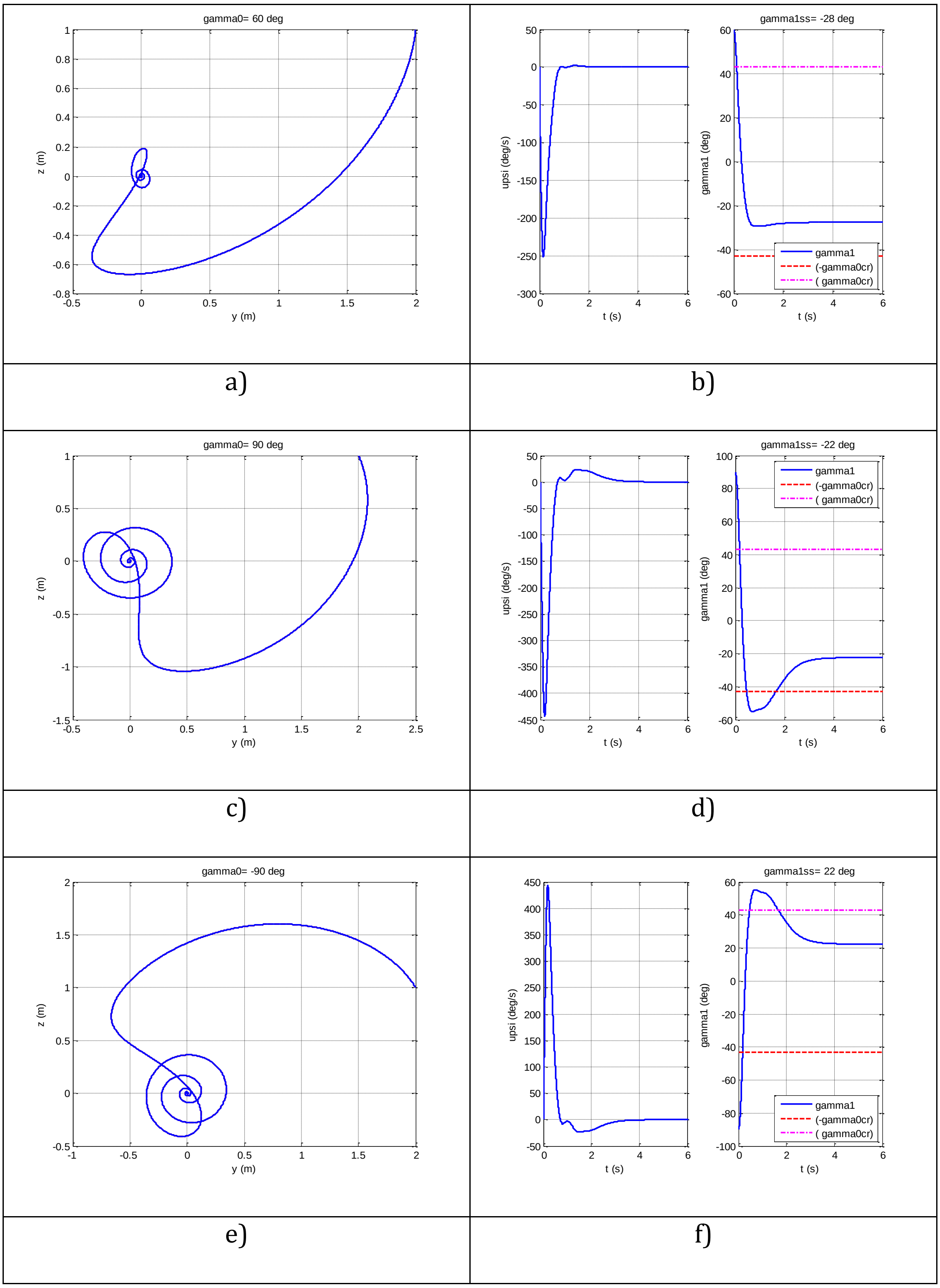

Figure 4.4 **Trajectories in the picture plane from initial conditions (1.16), the adaptive control u_{ψ} (4.65) of the SA2DPDGL and the summary phase coupling angle $\gamma_1 = \gamma_0 + \psi$ (4.8) for some cases of the phase coupling angle γ_0 when it is outside the interval of stability $\gamma_0 \notin (-\gamma_{cr}, \gamma_{cr})$: a) and b) when $\gamma_{10} = 1.39\gamma_{cr} = 60$ deg.; c) and d) when $\gamma_1 = 2.0873\gamma_{cr} = 90$ deg. ; e) and f) when $\gamma_{10} = -2.0873\gamma_{cr} = -90$ deg.**

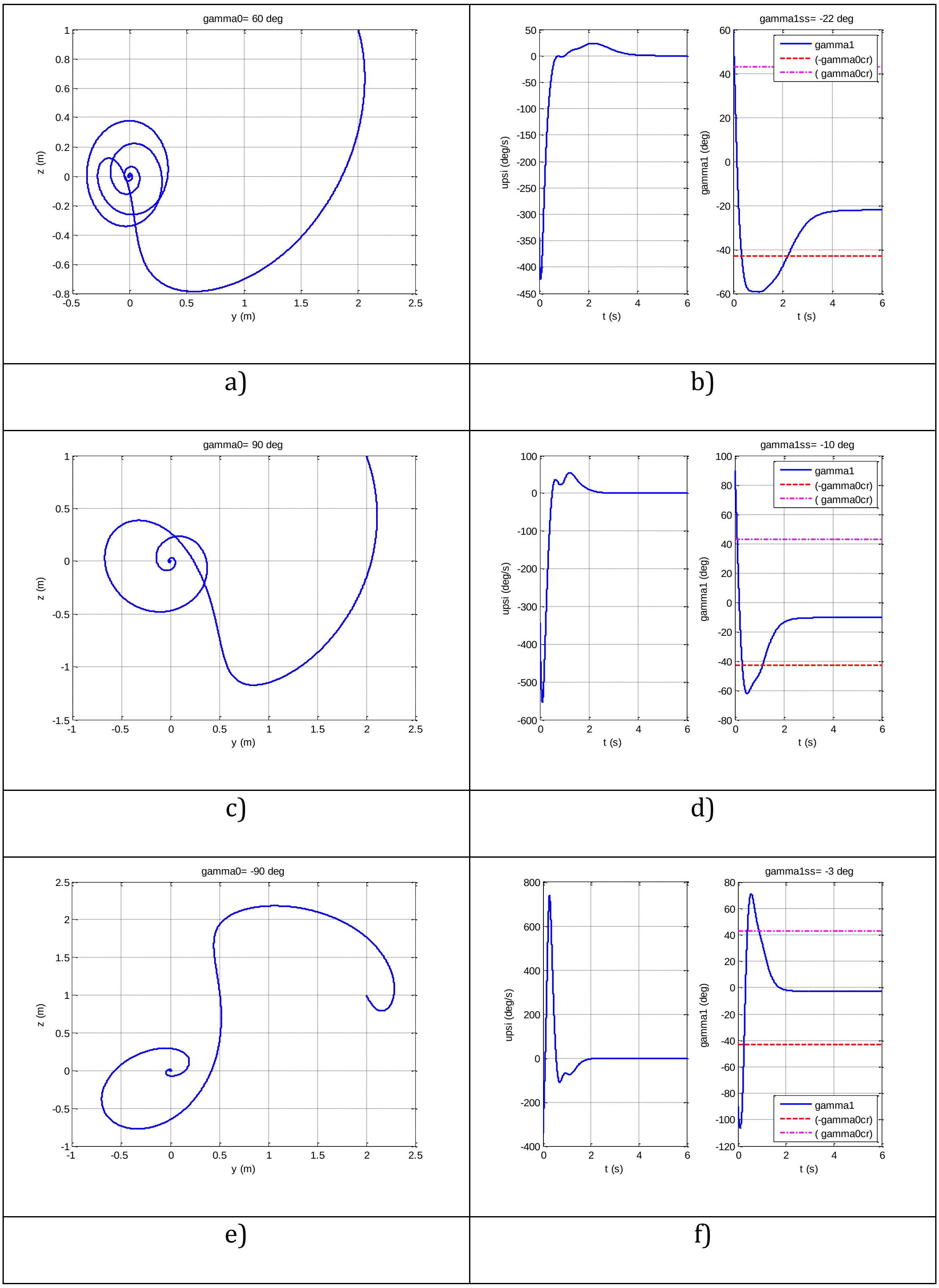

Figure 4.5 Trajectories in the picture plane from initial conditions (1.17), the adaptive control u_ψ (4.65) of the SA2DPDGL and the summary phase coupling angle $\gamma_1 = \gamma_0 + \psi$ (4.8) for some cases of the phase coupling angle γ_0 when it is outside the interval of stability $\gamma_0 \notin (-\gamma_{cr}, \gamma_{cr})$: a) and b) when $\gamma_{10} = 1.39\gamma_{cr} = 60$ deg.; c) and d) when $\gamma_1 = 2.0873\gamma_{cr} = 90$ deg. ; e) and f) when $\gamma_{10} = -2.0873\gamma_{cr} = -90$ deg.

Figure 4.5 shows the trajectories in the picture plane as well as the adaptive control u_ψ (4.65) of the SA2DPDGL and the summary phase coupling angle $\gamma_1 = \gamma_0 + \psi$ (4.8) for the same cases of the phase coupling angle γ_0 as in Figure 4.4 when γ_0 is outside the interval of stability $\gamma_0 \notin (-\gamma_{cr}, \gamma_{cr})$ but obtained at non-proportional to each other initial conditions (1.17). The results show the SA2DPDGL manages well and keeps its effectiveness though the existence of initial conditions causing an additional angular velocity of rotation at the initial moment.

4.5 Conclusions

The synthesized SA2DPDGL boasts the following:

- The SA2DPDGL is really very simple. It does only rotate the summary vector of the two CPDGLs of y and z -channels in the complex plane by the angle ψ whose angular velocity $\dot{\psi}$ is directly proportional to the index of disproportionality $\varphi_{1r} = \dot{z}y - \dot{y}z$ in m^2/s with a coefficient of proportionality k_ψ. The SA2DPDGL does not change the magnitude of the summary vector of the two CPDGLs of y and z -channels in the complex plane. The introduced and controlled angle ψ of rotation of the summary vector of the two CPDGLs of y and z -channels is aimed at the compensation of the unknown phase coupling angle γ_0 so that the steady state of the summary phase coupling angle $\gamma_1 = \gamma_0 + \psi$ is within the stability interval tending theoretically to zero. Thus the asymptotic stability of the adaptive mechanism leads to decoupling of the spatial closed loop system with phase coupling between the channels with a zero steady state of the summary phase coupling between the channels γ_1 which provides the asymptotic stability of the whole spatial closed loop guidance system.

- The SA2DPDGL manages well even with cases outside the interval of stability for the phase coupling between the channels in the classical application where the spatial CPDGL does not provide stability at all, for example – in a very wide range from $\gamma_0 = -90\ deg$ to $\gamma_0 = 90\ deg$;

- The closed loop guidance system with the SA2DPDGL is not a variable structure system;

- The input data for the new guidance law are the same as in the classical case;

- The only parameter for adjustment is the coefficient k_ψ of the adaptive control (4.65).

All above benefits are gained by a synthesis based on the idea of compensation only for the phase coupling between the channels omitting the requirement to straighten the trajectory in the picture plane.

5 SOPHISTICATED ADAPTIVE EXPANDED TWO-DIMENSIONAL PD CLOS GUIDANCE LAW

The synthesized in Chapter 3 (page 52) adaptive control (3.78) of the introduced variable angle of the vector rotation in the complex plane of the expanded two-dimensional PD CLOS guidance law (E2DPDGL) features variable structure control. According to (3.78) (see also Figure 3.3) the adaptive control (3.78) acts practically only when the current trajectory point in the picture plane is outside the predetermined ε_r area around the picture plane origin. While the current trajectory point in the picture plane is within the predetermined ε_r area the adaptive control (3.78) produces zero. Thus taking into account also the variable structure of the expanded two-dimensional PD CLOS guidance law (E2DPDGL) the closed loop guidance system within the predetermined ε_r area around the picture plane origin turns into a classical two-dimensional closed loop guidance system with two identical classical PD guidance laws for y and z-channels. As it is shown, the adaptive expanded two-dimensional PD CLOS guidance law (AE2DPDGL) provides global stability of the closed loop guidance system and features an excellent performance and straightens the missile trajectory when the initial trajectory point in the picture plane is outside the predetermined ε_r area around the picture plane origin.

Let us consider the following case when the initial point of the process is within the predetermined ε_r area around the picture plane origin and the phase coupling angle is outside the interval of stability. It is easy to be explained by the control-flow block-diagram in Figure 3.4 (page 72) how the AE2DPDGL acts in this case. The system trajectory starting within the ε_r area crosses surely the ε_r area boundary and enters the area outside it. Thus being outside the area the adaptive control of the variable angle of the vector rotation of the E2DPDGL provides stability of the closed loop and self-adjustment to the opposite value of the phase coupling angle so that the summary phase coupling of the system strives to zero and the system trajectory surely enters the ε_r area from outside. While staying within the ε_r area the achieved value of the variable angle direction remains constant. The number of such transitions is limited and the final stay of the system is within the ε_r area. So in order to reduce the number of these transitions through the ε_r area let us employ the simplified adaptive two-dimensional proportional-derivative CLOS guidance law (SA2DPDGL) when the current point of the system trajectory is within the ε_r area. Thus we replace the absence of adaptive control within the ε_r area with an adaptive control of the vector rotation of the guidance law there by the simplified adaptive two-dimensional proportional-derivative guidance law. As a result the partial control of the vector rotation of the E2DPDGL by the adaptive control (3.78) transforms into a full control of the vector rotation of the E2DPDGL (5.1) where the coefficient $k_{\psi 2}$ represents the coefficient k_{ψ} of the adaptive control (3.78) while the coefficient $k_{\psi 1}$ represents the coefficient k_{ψ} of the adaptive control (4.65) or (4.69). So we obtain a new CLOS guidance law representing the E2DPDGL but with a variable vector rotation (3.1) - (3.5) by the adaptive control (5.1) of this direction. Let us name it sophisticated (S) adaptive (A) expanded (E) two-dimensional (2D) proportional-derivative (PD) guidance (G) law (L) – SAE2DPDGL.

$$u_{\psi} = \begin{cases} k_{\psi 1}(\dot{z}y - \dot{y}z), & k_{\psi 1} = const > 0 \quad if\ r \leq \varepsilon_r \\ k_{\psi 2} sign(r + a_1\dot{r})\dot{\varphi}, & k_{\psi 2} = const > 0 \quad if\ r > \varepsilon_r \end{cases} \tag{5.1}$$

The whole representation of the SAE2DPDGL is the following system (5.2). Note that $\dot{r}$ and $\dot{\varphi}$ in (5.2) are calculated according to the relations (2.16) and they are calculated only when $r > \varepsilon_r$. The closed loop guidance system represented in a complex form including the SAE2DPDGL and the CLOS ATGM with phase coupling between the channels is shown in Figure 5.1 (the CLOS ATGM is represented here at an ideal case consisting only of the phase coupling between the channels and the kinematic relations).

$$u_{1y} = \begin{cases} -\frac{1}{a_0}(y + a_1\dot{y}) & if\ r \le \varepsilon_r\,, \\ -\frac{1}{a_0}\big(y + a_1(\dot{y} + z\dot{\varphi})\big) - y\dot{\varphi}^2 - 2\dot{r}\dot{\varphi}\sin\varphi + \frac{1}{T_\varphi}z\dot{\varphi} & if\ r > \varepsilon_r\,, \end{cases}$$

$$u_{1z} = \begin{cases} -\frac{1}{a_0}(z + a_1\dot{z}) & if\ r \le \varepsilon_r\,, \\ -\frac{1}{a_0}\big(z + a_1(\dot{z} - y\dot{\varphi})\big) - z\dot{\varphi}^2 + 2\dot{r}\dot{\varphi}\cos\varphi - \frac{1}{T_\varphi}y\dot{\varphi} & if\ r > \varepsilon_r\,, \end{cases}$$

$$u_\psi = \begin{cases} k_{\psi 1}(\dot{z}y - \dot{y}z), \quad k_{\psi 1} = const > 0 & if\ r \le \varepsilon_r\,, \\ k_{\psi 2}sign(r + a_1\dot{r})\dot{\varphi}, \quad k_{\psi 2} = const > 0 & if\ r > \varepsilon_r\,, \end{cases}$$

$$\frac{d\psi}{dt} = u_\psi, \quad \psi(0) = 0,$$

$$u_y = u_{1y}\cos\psi - u_{1z}\sin\psi\,,$$
$$u_z = u_{1z}\cos\psi + u_{1y}\sin\psi \tag{5.2}$$

5.1 Global stability analysis of the closed loop guidance system

Let us deal with the stability analysis of the closed loop guidance system consisting of the new SAE2DPDGL, the phase coupling between the channels and the kinematic relations as shown in Figure 5.1 applying the same approach from Section 3.4 “Global stability of the closed loop guidance system with phase coupling between the channels controlled by the AE2DPDGL” (page 65). This consideration leads to the only difference here consisting of the exclusion of Case 2.2 and Case 3.2 of the summary Table 3.2 because of the asymptotic stability of the closed loop when $r \le \varepsilon_r$ due to the adaptive control of the variable vector rotation in the complex plane of the spatial CPDGL within the ε_r area. Thus the new SAE2DPDGL provides global asymptotic stability of the considered closed loop guidance system.

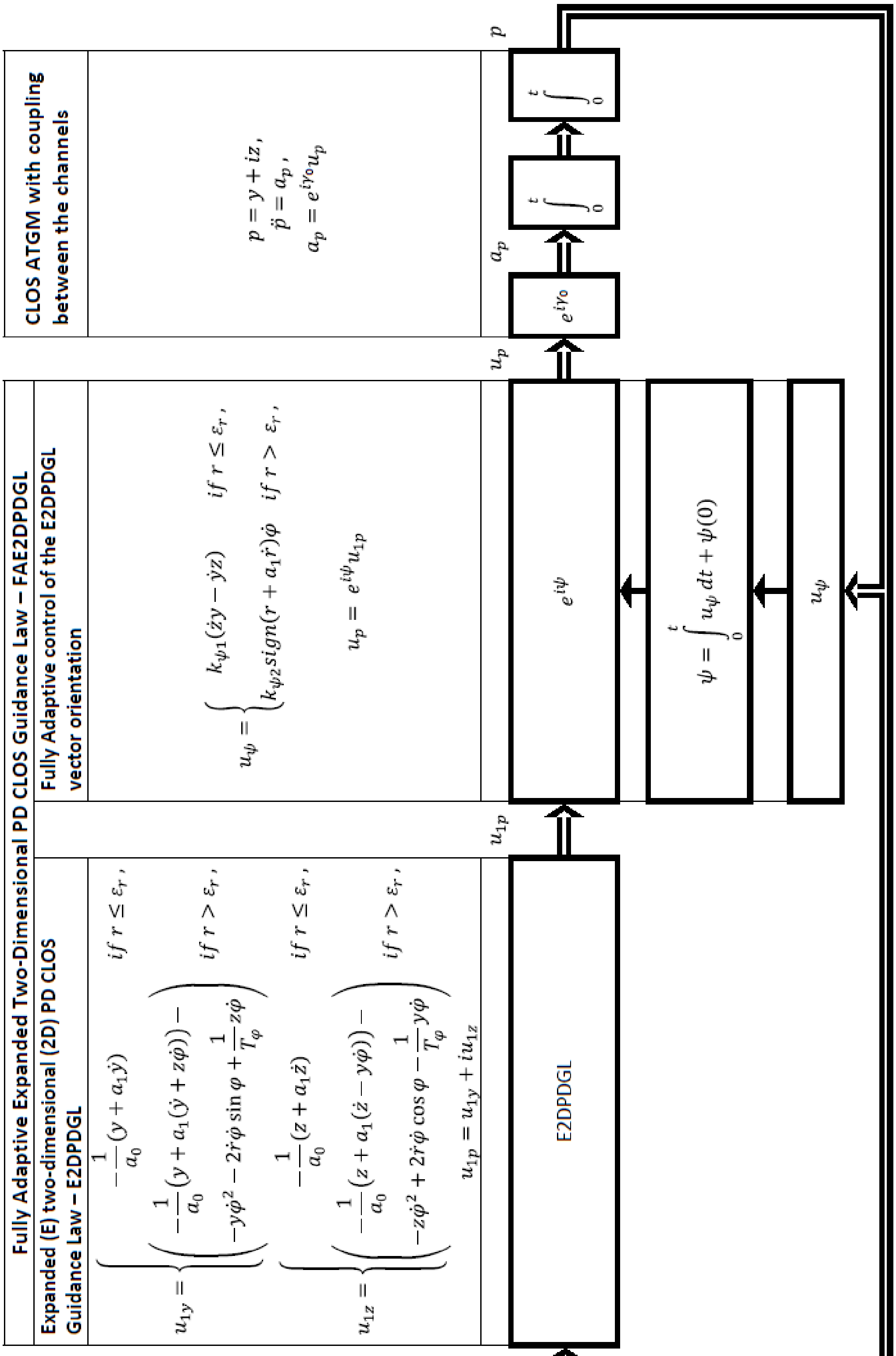

Figure 5.1 The closed loop guidance system of the CLOS ATGM with phase coupling between the channels (1.30) - (1.31) controlled by the SAE2DPDGL (5.2).

6 A MORE REALISTIC HYPOTHETICAL EXAMPLE

The detailed information on the ATGM control systems is classified. Because of that let us consider a more realistic hypothetical example which includes not only the kinematic relations but also a hypothetic dynamics of the missile fin control actuation system and aerodynamics.

Let us suppose the velocity of a roll stabilized CLOS ATGM is $V_M = 300$ m/s. Let us suppose also the transfer function of each pitch and yaw channels (the vertical and horizontal channels respectively), including the missile fin control actuation system, aerodynamics, missile velocity, and CLOS kinematic relations, presented in form (6.1) is (6.2).

6.1 Classical closed loop guidance and control system

6.1.1 One-dimensional closed loop system with classical PD guidance law

Let us suppose first there is no coupling between the channels. Let the synthesized classical PD guidance law (compensator) in each of both identical one-dimensional closed loop systems be (6.3). The open loop transfer function $L_0(s)$ represents (6.4) and both identical one-dimensional closed loop systems are asymptotically stable according to Figure 6.1. The critical value of the phase coupling angle is (6.6). The transition processes of the spatial closed loop system with no coupling between the channels (6.1) - (6.3) from the proportional to each other initial conditions (1.16) are presented in Figure 6.2.

$W_{yu_y}(s) = W_{zu_z}(s) = \dfrac{N(s)}{s^2 D(s)},$ $where\ N(0) \neq 0\ and\ D(0) \neq 0$	(6.1)

$W_{yu_y}(s) = W_{zu_z}(s) = \dfrac{N(s)}{s^2 D(s)} =$ $= \dfrac{-0.0027s^2 - 0.072s + 301}{s^2[(2.7e-06)s^3 + (1.62e-04)s^2 + 0.03s + 1]}$	(6.2)
$W_c(s) = k_c(T_c s + 1)$, $k_c = 0.11 > 0,\ T_c = 0.27 > 0$	(6.3)
$L(s)\vert_{\gamma_0=0} = L_0(s) = \dfrac{k_c(T_c s + 1)N(s)}{s^2 D(s)}$	(6.4)
$(-\gamma_{cr}, \gamma_{cr})$	(6.5)
$\gamma_{cr} = PM_0 = 52.516 \approx 52.5$ deg.	(6.6)

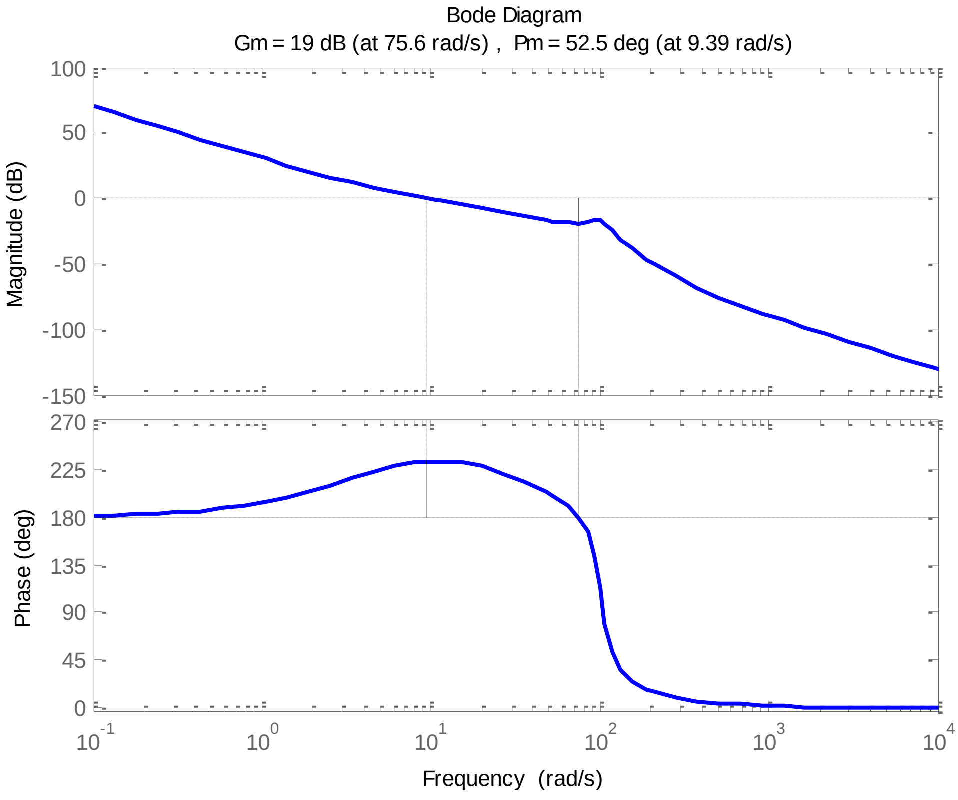

Figure 6.1 **Bode diagram of the open loop system with stability margins.**

6.1.2 Analysis of the synthesized classical spatial closed loop system with phase coupling between the channels

6.1.2.1 Stability of the classical spatial closed loop system with phase coupling between the channels

Let us suppose now there is a phase coupling between the channels determined by the phase coupling angle γ_0. Figure 6.3 illustrates the bad performance of the spatial closed loop system when the phase coupling angle $\gamma_0 = 0.9\gamma_{cr}$. Figure 6.4 illustrates the following stability loss of the spatial closed loop system when the phase coupling angle $\gamma_0 = 1.02\gamma_{cr}$. In general, the spatial closed loop system has an acceptable performance at values of the phase coupling angle around zero and far from the boundaries of the interval of stability $(-\gamma_{cr}, \gamma_{cr})$ (6.5) where the critical value of the phase coupling angle γ_{cr} represents (6.6).

6.1.2.2 Analysis of the influence of the external disturbances

Let the external disturbances in the horizontal and the vertical channels be presented as accelerations a_{dy} and a_{dz} respectively. Let also their common representation in complex form be (6.7) and their inclusion into the system be (6.8). Taking into account the PD compensator's presentation (6.9), the spatial closed loop system represents (6.8) - (6.9). It follows from (6.8) - (6.9) that the transfer function regarding the complex variables p (the missile position in the picture plane in complex form) and a_{dp} (the external disturbances in complex form) represents (6.10).

$a_{dp} = a_{dy} + ia_{dz}$	(6.7)
$s^2 p(s) = a_p(s),$ $a_p(s) = e^{i\gamma_0}\dfrac{N(s)}{D(s)}u(s) + a_{dp}(s)$	(6.8)
$u(s) = \big(-k_c(T_c s + 1)\big)p(s)$	(6.9)
$W_{pa_{dp}}(s) = \dfrac{p(s)}{a_{dp}(s)} = \dfrac{D(s)}{s^2 D(s) + e^{i\gamma_0}N(s)\big(k_c(T_c s + 1)\big)}$	(6.10)

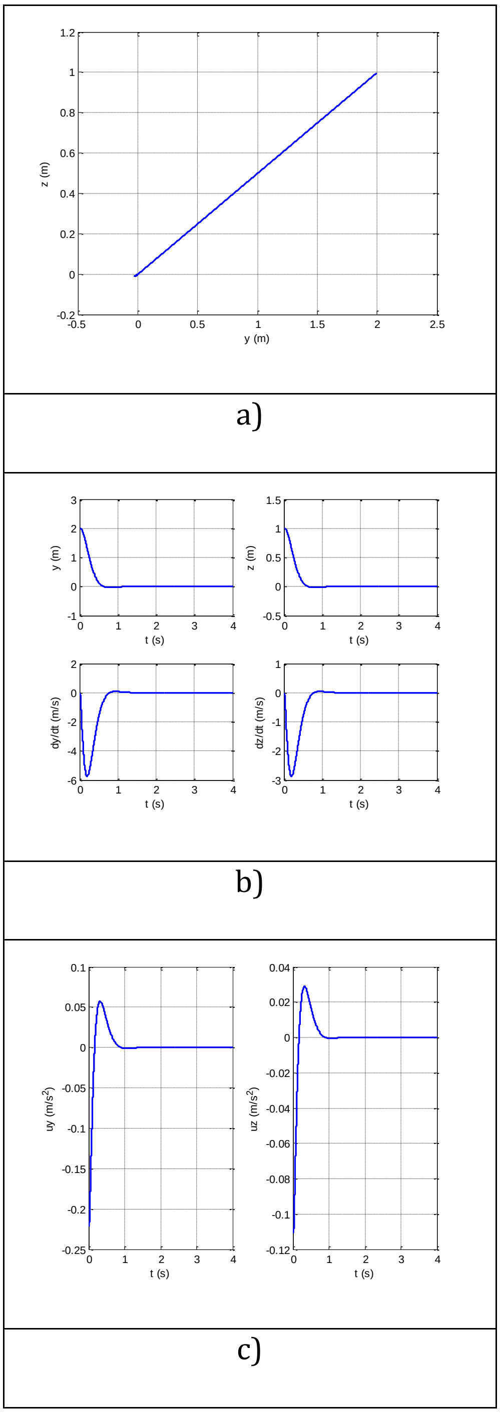

Figure 6.2 Performance of the spatial closed loop guidance system with no coupling between the channels comprising two identical one-dimensional closed loop systems controlled by identical PD compensators in each channel in case of proportional to each other initial conditions (1.16): a) ATGM trajectory in the $Y_L Z_L$-plane, the picture plane; b) $y, \dot{y}, z$ and $\dot{z}$; c) the components of the PD control in each channel.

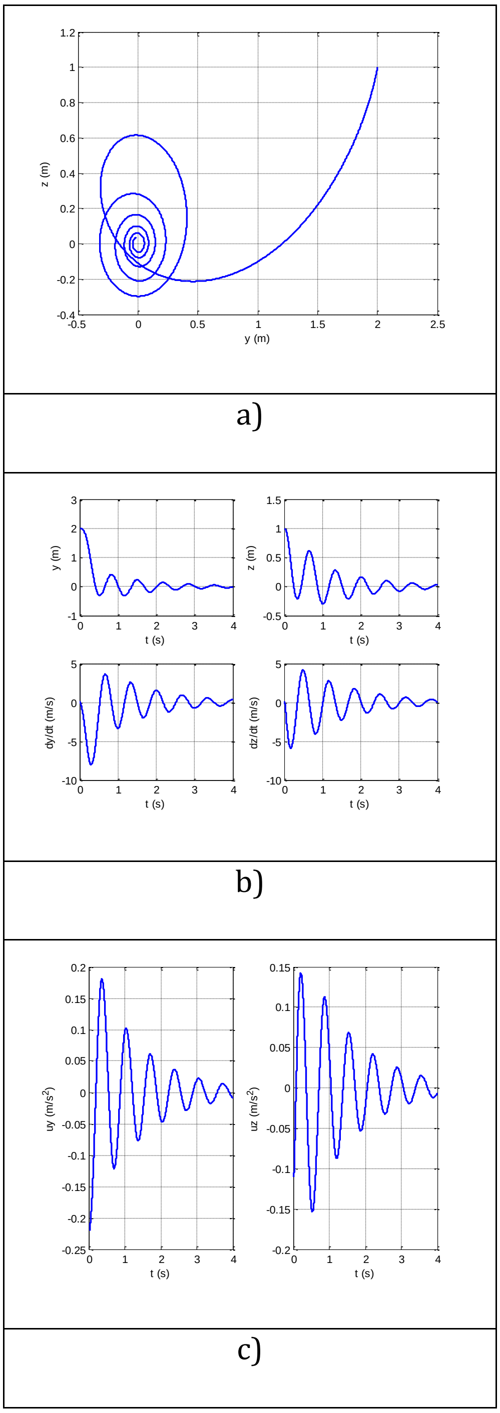

Figure 6.3 Performance of the spatial closed loop guidance system controlled by identical classical PD compensators in each channel in case of phase coupling between the channels when $\gamma_0 = 0.9\gamma_{cr} = 47.264$ deg. and proportional to each other initial conditions (1.16) : a) ATGM trajectory in the $Y_L Z_L$-plane, the picture plane; b) $y, \dot{y}, z$ and $\dot{z}$; c) the components of the PD control in each channel.

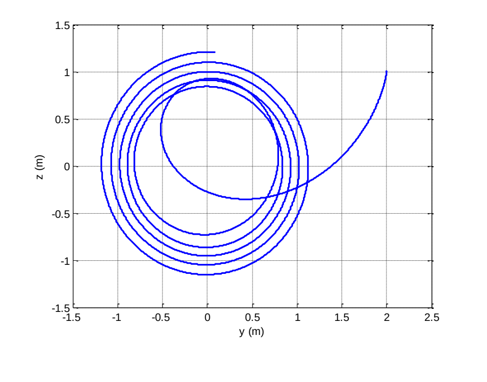

a)

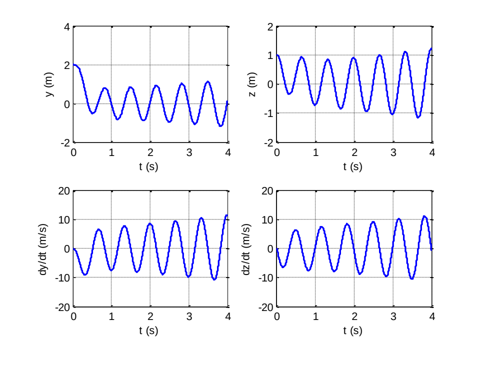

b)

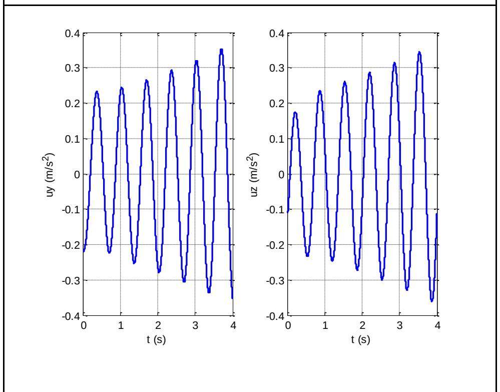

c)

Figure 6.4 Performance of the spatial closed loop guidance system controlled by identical classical PD compensators in each channel in case of phase coupling between the channels when $\gamma_0 = 1.02\gamma_{cr} = 53.566$ deg. and proportional to each other initial conditions (1.16) : a) ATGM trajectory in the $Y_L Z_L$-plane, the picture plane; b) $y, \dot{y}, z$ and $\dot{z}$; c) the components of the PD control in each channel.

6.1.2.2.1 Steady state responses to various type of external disturbances

Let us consider the steady state responses to various type of external disturbances having in mind the phase coupling angle γ_0 is within the interval of stability (6.11). Let us first suppose (6.12). For this case we obtain (6.13).

$\gamma \in (-\gamma_{cr}, \gamma_{cr}), \qquad 0 < \gamma_{cr} < \dfrac{\pi}{2}$	(6.11)
$a_{dp} = a_{dy0}1(t) + ia_{dz0}1(t),$ $where\ a_{dy0} = const. and\ a_{dz0} = const.$	(6.12)
$p(\infty) = \dfrac{(a_{dy0} + ia_{dz0})(\cos\gamma_0 - i\sin\gamma_0)}{k_c(N(0)/D(0))} = y(\infty) + iz(\infty),$ $y(\infty) = \dfrac{1}{k_c(N(0)/D(0))}(a_{dy0}\cos\gamma_0 + a_{dz0}\sin\gamma_0),$ $z(\infty) = \dfrac{1}{k_c(N(0)/D(0))}(a_{dz0}\cos\gamma_0 - a_{dy0}\sin\gamma_0),$	(6.13)

Let us now suppose the external disturbance represents a short impulse (6.14) with length $(t_2 - t_1)$ seconds acting during the flight to the target before collision. In this case we obtain (6.15).

$a_{dp} = \quad (a_{dy0} + ia_{dz0})(1(t - t_1) - 1(t - t_2)),\ \ where$ $a_{dy0} = const.,\ \ a_{dz0} = const.,\ \ 0 \le t_1 < t_2 \ll \infty$	(6.14)
$p(\infty) = 0 + i0 = y(\infty) + iz(\infty),$ $y(\infty) = 0,$ $z(\infty) = 0$	(6.15)

6.1.2.2.2 Influence of the missile weight

This external disturbance is represented by the gravity acceleration “g”, which in form (6.12) is expressed as (6.16). According to (6.13) the steady response to this input becomes (6.17). The estimation of (6.17) taking into account (6.11) is (6.18) which calculated according to the data (6.2) - (6.6) represents (6.19). Figure 6.5 illustrates the transition processes in the picture plane of the spatial closed loop system at different values of the phase coupling angle γ_0 within the interval of stability (6.11) taking into account the gravity acceleration. Besides the spiraling caused by the phase coupling angle γ_0 it is also seen a variety of steady states according to (6.17) but complying with the estimation (6.19).

$\begin{gathered} a_{dy0} = 0, \\ a_{dz0} = -g = -9.8\, m/s^2 \end{gathered}$	(6.16)
$\begin{gathered} p(\infty) = y(\infty) + iz(\infty), \\ y(\infty) = \frac{-g \sin \gamma_0}{k_c(N(0)/D(0))}, \\ z(\infty) = \frac{-g \cos \gamma_0}{k_c(N(0)/D(0))}, \end{gathered}$	(6.17)
$\begin{gathered} \lvert y(\infty) \rvert < \frac{g \sin \gamma_{cr}}{k_c(N(0)/D(0))}, \\ 0 > z(\infty) \geq \frac{-g}{k_c(N(0)/D(0))} \end{gathered}$	(6.18)
$\begin{gathered} \lvert y(\infty) \rvert < \frac{g \sin \gamma_{cr}}{k_c(N(0)/D(0))} = 0.2349 \approx 0.24\, m, \\ 0 > z(\infty) \geq \frac{-g}{k_c(N(0)/D(0))} = -0.2959 \approx -0.3\, m \end{gathered}$	(6.19)

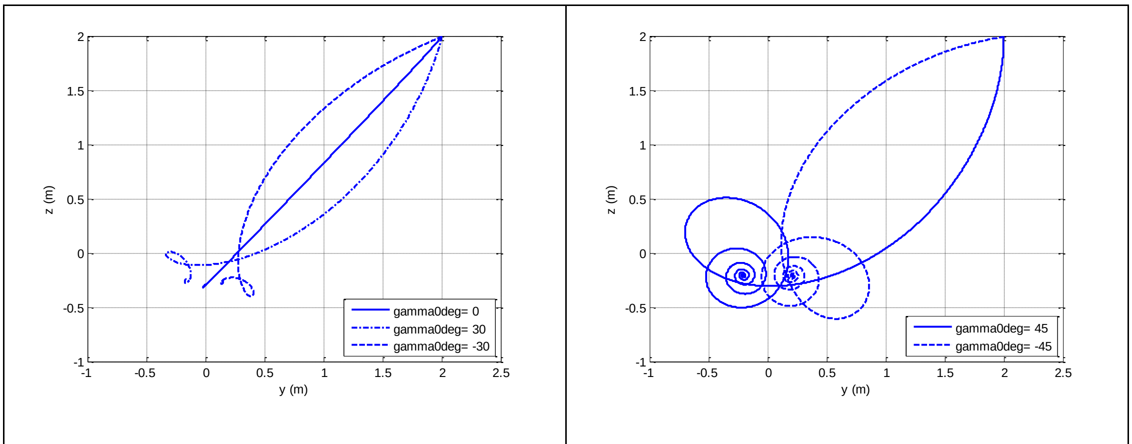

a) b)

Figure 6.5 Trajectories of the transition process of the classical ATGM spatial closed loop guidance system with coupling between the channels in the picture plane taking into account the missile weight at different values of the phase coupling angle γ_0 : a) $\gamma_0 = 0, 30, -30$ deg.; b) $\gamma_0 = 45, -45$ deg.

6.1.2.2.3 Influence of the target's movement

Let us consider the target's movement in the horizontal plane which is a typical external disturbance of a CLOS ATGM system. In this case the external disturbance as acceleration in complex form a_{dp} (6.7) represents (6.20). Suppose also (6.21), i.e.

there is no angular acceleration $\ddot{\beta}_{LOS}$ of the LOS in the horizontal plane and the LOS moves with a constant angular velocity $\dot{\beta}_{LOS}$. Thus the presentation of a_{dp} (6.7) in form (6.12) is (6.22). For the steady state response in this case we obtain (6.23) based on (6.13). An estimation of (6.23) is (6.24) having in mind the phase coupling angle γ_0 is within the interval of stability (6.11).

For example, let the component $\left(2\dot{\beta}_{LOS}V_M\right)$ in (6.23) and (6.24) be (6.25) which corresponds to the case of missile velocity $V_M = 300\ m/s$ and a movement of the target at a distance of 1000 (m) in front of the Ground tracker with a velocity of 10 m/s. Thus we obtain the following numerical values (6.26) for the steady state response to this exemplary movement of the target. Figure 6.6 illustrates the trajectories of the spatial closed loop system in the picture plane taking into account only the influence of this exemplary movement of the target at different values of the phase coupling angle γ_0 within the interval of stability (6.11).

$a_{dy} = 2\dot{\beta}_{LOS}V_M + D_{GTT}\ddot{\beta}_{LOS}\,,$ $a_{dz} = 0$	(6.20)
$\dot{\beta}_{LOS} = const., \quad \ddot{\beta}_{LOS} = 0$	(6.21)
$a_{dp} = a_{dy0}1(t) + ia_{dz0}1(t),$ $where\ a_{dy0} = 2\dot{\beta}_{LOS}V_M = const.,$ $a_{dz0} = 0$	(6.22)
$p(\infty) = y(\infty) + iz(\infty),$ $y(\infty) = \dfrac{2\dot{\beta}_{LOS}V_M \cos\gamma_0}{k_c(N(0)/D(0))},$ $z(\infty) = \dfrac{-2\dot{\beta}_{LOS}V_M \sin\gamma_0}{k_c(N(0)/D(0))}$	(6.23)
$\lvert y(\infty)\rvert \le \dfrac{2\lvert\dot{\beta}_{LOS}\rvert V_M}{k_c(N(0)/D(0))},$ $\lvert z(\infty)\rvert < \dfrac{2\lvert\dot{\beta}_{LOS}\rvert V_M \sin\lvert\gamma_{cr}\rvert}{k_c(N(0)/D(0))}$	(6.24)
$2\dot{\beta}_{LOS}V_M = 6\ (\mathrm{m}/s^2)$	(6.25)

$$
\begin{aligned}
|y(\infty)| &\leq \frac{2|\dot{\beta}_{LOS}|V_M}{k_c(N(0)/D(0))} = 0.1812 \approx 0.19\, m, \\
|z(\infty)| &< \frac{2|\dot{\beta}_{LOS}|V_M \sin|\gamma_{cr}|}{k_c(N(0)/D(0))} = 0.1438 \approx 0.15\, m
\end{aligned} \qquad (6.26)
$$

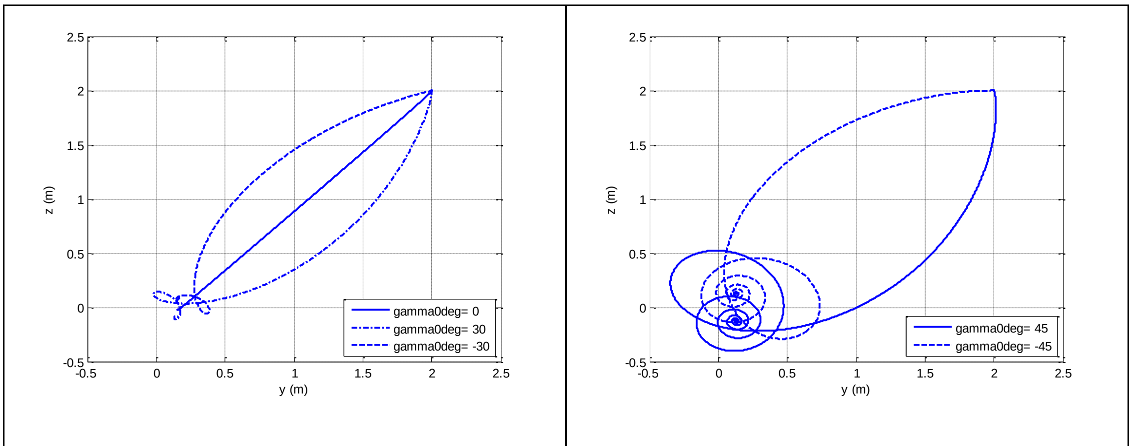

a)	b)

Figure 6.6 Trajectories in the in the $Y_L Z_L$-plane, the picture plane, of the classical ATGM spatial closed loop guidance system with coupling between the channels taking into account only the influence of the target's movement (6.22), (6.25) at different values of the phase coupling angle γ_0 : a) $\gamma_0 = 0, 30, -30$ deg.; b) $\gamma_0 = 45, -45$ deg.

6.1.2.2.4 Influence of the wind gust

The consideration of such type of external disturbance means applying of an external acceleration in form of a short lasting impulse according to (6.14). As we have shown (6.15) the steady state response to such type of external disturbance does not affect the zero steady state of the system. The influence concerns only the initial conditions of the kinematic relations at the moment t_2 – the finish of the impulse (6.14). Thus, after this moment the spatial closed loop system has been evolving from the following initial conditions of the kinematic relations $y(t_2), \dot{y}(t_2), z(t_2), \dot{z}(t_2)$ and without external disturbance. Since all considerations of the study are made taking into account that the initial conditions of the system are non-zero it could be concluded that there is no need of a special consideration of another transition process from non-zero initial conditions.

6.1.2.2.5 Summary effect of all considered external disturbances

According to (6.16) and (6.22) we obtain for the summary external disturbances (6.27). Let us suppose (6.28). Having also in mind (6.11) we obtain the estimation (6.29) for the component $y(\infty)$ of (6.13). Dealing with the estimation of the component $z(\infty)$ of (6.13) in the same way we obtain the summary estimation (6.30) for the summary external disturbances (6.27).

The estimation (6.30) calculated according to the data (6.2) - (6.6) represents (6.31). Figure 6.7 illustrates the summary effect of the considered external disturbances on the transition processes in the picture plane at various values of the phase coupling angle γ_0 within the interval of stability (6.11).

$a_{dp} = a_{dy0}1(t) + ia_{dz0}1(t),$ $a_{dy0} = 2\dot{\beta}_{LOS}V_M = const.$ $a_{dz0} = -g = const.$	(6.27)
$0 \le \lvert a_{dy0}\rvert = \lvert 2\dot{\beta}_{LOS}V_M\rvert \le \lvert a_{dz0}\rvert = g$	(6.28)
$\lvert y(\infty)\rvert \le \frac{1}{k_c(N(0)/D(0))}\left(\lvert a_{dy0}\rvert \cos\lvert\gamma_0\rvert + \lvert a_{dz0}\rvert \sin\lvert\gamma_0\rvert\right) =$ $= \frac{\sqrt{\lvert a_{dy0}\rvert^2 + \lvert a_{dz0}\rvert^2}}{k_c(N(0)/D(0))}\left(\begin{array}{l} \frac{\lvert a_{dy0}\rvert}{\sqrt{\lvert a_{dy0}\rvert^2 + \lvert a_{dz0}\rvert^2}}\cos\lvert\gamma_0\rvert + \\ + \frac{\lvert a_{dz0}\rvert}{\sqrt{\lvert a_{dy0}\rvert^2 + \lvert a_{dz0}\rvert^2}}\sin\lvert\gamma_0\rvert \end{array}\right) \le$ $\le \frac{g\sqrt{2}}{k_c(N(0)/D(0))}\cos(\varphi_1 - \lvert\gamma_0\rvert) \le \frac{g\sqrt{2}}{k_c(N(0)/D(0))},$ $0 \le \cos\varphi_1 = \frac{\lvert a_{dy0}\rvert}{\sqrt{\lvert a_{dy0}\rvert^2 + \lvert a_{dz0}\rvert^2}} \le \frac{1}{\sqrt{2}}, \qquad \pi/2 \ge \varphi_1 \ge \pi/4$	(6.29)
$p(\infty) = y(\infty) + iz(\infty),$ $\lvert y(\infty)\rvert \le \frac{g\sqrt{2}}{k_c(N(0)/D(0))},$ $\lvert z(\infty)\rvert \le \frac{g\sqrt{2}}{k_c(N(0)/D(0))}$	(6.30)
$\lvert y(\infty)\rvert \le 0.42\ m,$ $\lvert z(\infty)\rvert \le 0.42\ m$	(6.31)

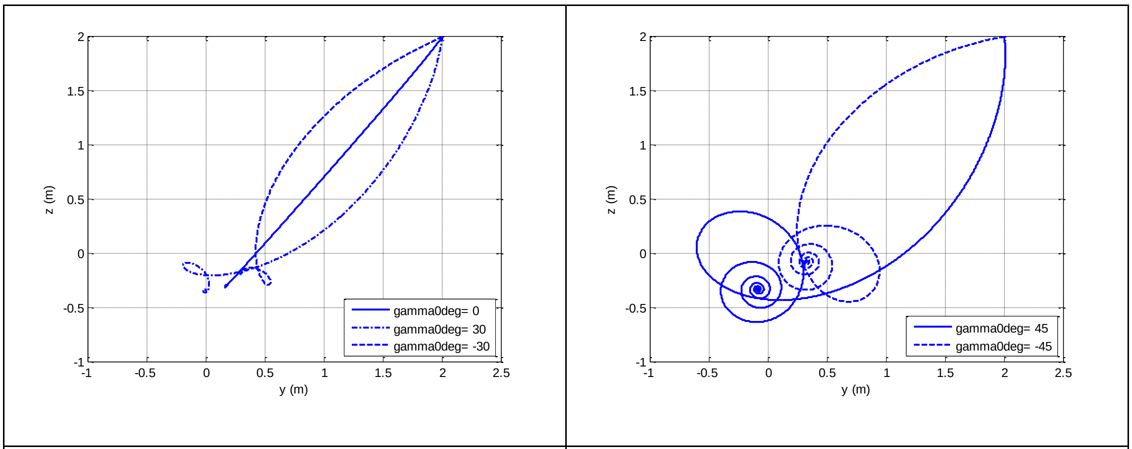

a)	b)

Figure 6.7 Trajectories in the in the $Y_L Z_L$-plane, the picture plane, of the classical ATGM spatial closed loop guidance system with coupling between the channels taking into account the missile weight as well as the influence of the target's movement (6.22), (6.25) at different values of the phase coupling angle γ_0 : a) $\gamma_0 = 0, 30, -30$ deg.; b) $\gamma_0 = 45, -45$ deg.

6.1.2.3 Inclusion of a feedforward control for the missile weight compensation

Let us consider the classical spatial closed loop guidance system with existence of external disturbances in the form (6.27). Let us modify the guidance law in the way (6.32). The Laplace transform of (6.32) is (6.33). The Laplace transform of the external disturbances (6.27) represents (6.34). Thus the spatial closed loop system with the modified CPDGL consists of the equations (6.8), (6.33) and (6.34). We obtain for the steady state of the considered system (6.35). The components of (6.35) concerning the target's movement are the same as in (6.23). The comparison with (6.17) regarding the steady state response to the missile weight shows that the component $y(\infty)$ remains the same while $z(\infty)$ here becomes zero when $\gamma_0 = 0$ in contrast to the non-zero steady state on z in (6.17). So in order to take the advantage of this compensation technique representing a combination of a feedforward and feedback control we do need only to replace the variable z at forming the guidance laws with the variable z_m where z_m represents (6.36). All other variables $y, \dot{y}$ and $\dot{z}$ are kept the same. For example, according to the data (6.2), (6.3) the compensation component in (6.36) represents (6.37).

$$u_p = -k_c(T_c\dot{p} + p) + i(-k_c)\left(\frac{-g}{k_c(N(0)/D(0))}\right)1(t)$$	(6.32)
$$u_p(s) = -k_c(T_c s + 1)p(s) + i(-k_c)\left(\frac{-g}{k_c(N(0)/D(0))}\right)\frac{1}{s}$$	(6.33)
$$a_{dp}(s) = \frac{1}{s}(a_{dy0} + ia_{dz0}),$$ $$a_{dy0} = 2\dot{\beta}_{LOS}V_M = const.$$ $$a_{dz0} = -g = const.$$	(6.34)
$$p(\infty) = y(\infty) + iz(\infty),$$ $$y(\infty) = -\sin\gamma_0\frac{g}{k_c(N(0)/D(0))} + \cos\gamma_0\frac{2\dot{\beta}_{LOS}V_M}{k_c(N(0)/D(0))},$$ $$z(\infty) = (1-\cos\gamma_0)\frac{g}{k_c(N(0)/D(0))} - \sin\gamma_0\frac{2\dot{\beta}_{LOS}V_M}{k_c(N(0)/D(0))}$$	(6.35)
$$z_m = z + \left(\frac{-g}{k_c(N(0)/D(0))}\right)$$	(6.36)
$$\left(\frac{-g}{k_c(N(0)/D(0))}\right) \approx -0.3\ (m)$$	(6.37)

The effectiveness of this compensation technique is shown in Figure 6.8 where the trajectories in the picture plane without and with compensation of the missile weight according to (6.36) and (6.37) at different values of the phase coupling angle within the interval of stability are compared: Figure 6.8-a versus Figure 6.8-b and Figure 6.8-c versus Figure 6.8-d.

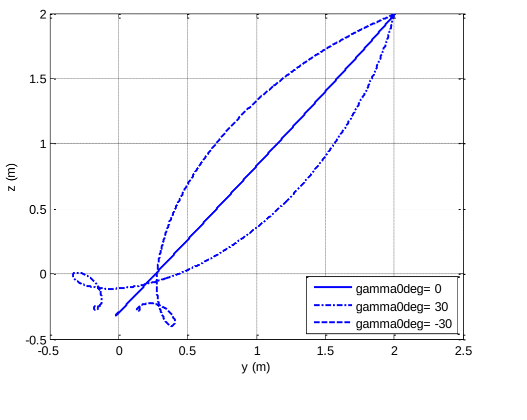

a)

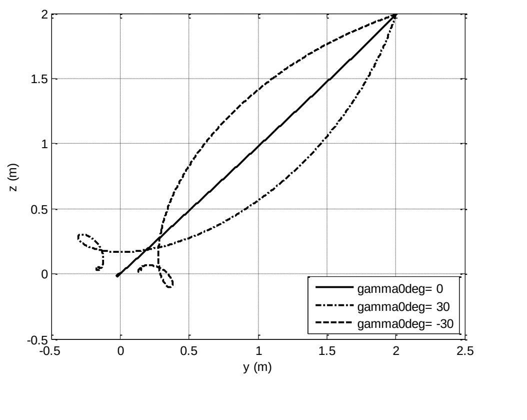

b)

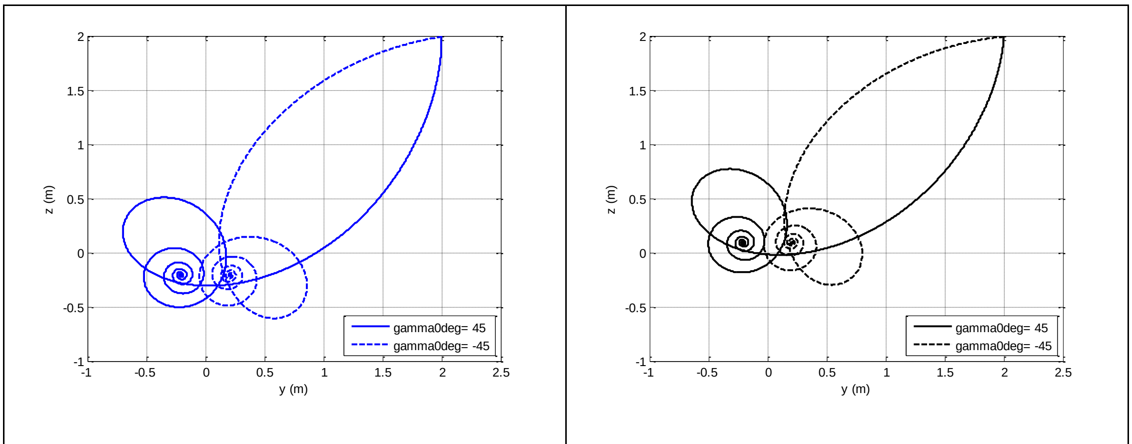

c)	d)

Figure 6.8 Comparison of the trajectories in the picture plane without and with compensation of the missile weight at different values of the phase coupling angle γ_0 within the interval of stability $(-\gamma_{cr}, \gamma_{cr})$ (6.5): Figure 6.8-a versus Figure 6.8-b and Figure 6.8-c versus Figure 6.8-d.

6.2 New spatial closed loop guidance and control system based on the AE2DPDGL

Let us now deal with the spatial closed loop guidance system based on the new AE2DPDGL. The parameters of the guidance law are presented in (6.38) and (6.39). The pair (a_0, a_1) (6.38) is based on the parameters of the synthesized closed loop system (6.1) - (6.3) with the classical PD control law (6.3) while the other three parameters of the new guidance law ε_r, T_φ and the coefficient k_ψ represent (6.39).

$a_0 = 0.03 \approx \dfrac{1}{k_c(N(0)/D(0))} = 0.0302\ s^2,$ $a_1 = T_c = 0.27\ s$	(6.38)
$\varepsilon_r = 0.5\ m,$ $T_\varphi = 0.025\ s,$ $k_\psi = 10$	(6.39)

6.2.1 Performance of the new spatial closed loop system with the AE2DPDGL

A performance comparison between the classical spatial closed loop guidance system based on two identical PD guidance laws and the new closed loop guidance system based on the AE2DPDGL is shown in Figure 6.9. It presents a case where the phase coupling between the channels kills the stability of the classical guidance loop. The AE2DPDGL provides not only stability of the closed loop guidance system but also straightens the ATGM trajectory in the picture plane with even a small improvement of the settling time $t_s = 0.49\ s$ in comparison with the settling time in the classical case with no coupling between the channels which represents the settling time of the nominal case $t_s^* = 0.53\ s$.

The simulations of the spatial closed loop guidance system with the AE2DPDGL are aimed at studying first the performance of the new spatial closed loop guidance system regarding a variety of initial trajectory points in the picture plane as well as values of the phase coupling angle γ_0.

When the initial trajectory point is outside the predetermined ε_r area around the picture plane origin the spatial closed loop guidance system shows an excellent performance within a very wide interval of stability (6.40) regarding the phase coupling angle γ_0. This interval of stability is wider more than twice as wide as the classical interval of stability (6.5), (6.6). Some results are presented in Figure 6.10 and Figure 6.11, and summarized in Table 6.1, Table 6.2, and Table 6.3 for the cases when the initial trajectory point (y_0, z_0) in the picture plane represents respectively the points $(2,2), (1,1)$ and $(0.5,0.5)$. The results show that the performance of the spatial closed loop guidance system with the AE2DPDGL is kept acceptable within the whole range of the interval of stability (6.40) which is not possible in the classical case with CPDGL.

$$\gamma_0 \in [-2.2\gamma_{cr}, 2.2\gamma_{cr}] \tag{6.40}$$

When the initial trajectory point is within the predetermined ε_r area around the picture plane origin the spatial closed loop guidance system keeps its stability but worsens its performance indices. The summary in Table 6.4 for the initial point (0.25,0.25) and the illustrations in Figure 6.12 and Figure 6.13 show that the transition processes when the phase coupling angle γ_0 is outside the classical interval of stability $(-\gamma_{cr}, \gamma_{cr})$ include always an initial leaving the predetermined ε_r area with a next return and final descent in form of an almost straight line to the picture plane origin but with an intermediate period of stay outside the area.

Although the interval of stability of the closed loop guidance system represents two times wider range (6.40) than the classical case, these effects when the phase coupling angle is outside the classical interval $(-\gamma_{cr}, \gamma_{cr})$ lead to an increase in the settling time and the normal overloads and finally an unfavorable system trajectory.

6.3 Improving the performance of the new spatial closed loop guidance and control system by the SAE2DPDGL

In order to improve the performance of the new spatial closed loop guidance system within the ε_r area let us employ the SAE2DPDGL (5.2) which has been synthesized in Chapter 5 (page 121) just for this purpose. Thus the absence of an adaptive control of the vector rotation of the E2DPDGL within the ε_r area by the AE2DPDGL according to (3.78) is replaced with a sophisticated adaptive one by the SAE2DPDGL according to (5.1) which provides an adaptive control of the vector rotation of the E2DPDGL not only outside the ε_r area but also within it. For the studied example the parameters of the adaptive control (5.1) of the vector rotation of the E2DPDGL represent (6.41) where the coefficient $k_{\psi 2}$ represents k_ψ from (6.39).

$k_{\psi 1} = 3$, $k_{\psi 2} = 10$	(6.41)

The other parameters of the SAE2DPDGL (5.2) are the same from (6.38) and (6.39). Thus the whole set of parameters of the SAE2DPDGL (5.2) represents (6.42).

$a_0 = 0.03\ s^2, a_1 = 0.27\ s,$ $\varepsilon_r = 0.5\ m,$ $T_\varphi = 0.025\ s,$ $k_{\psi 1} = 3\ m^{-2},$ $k_{\psi 2} = 10$	(6.42)

A performance comparison of the guidance system with the AE2DPDGL and the system with the SAE2DPDGL when the initial trajectory point in the picture plane $(y_0, z_0) = (0.25{,}0.25)$ is within the ε_r area regarding the phase coupling angle γ_0 is shown in Table 6.5 and illustrated in Figure 6.14 and Figure 6.15. The results show clearly the improvement in the transition processes. There is no leaving the ε_r area by the system trajectory with an intermediate stay for a while outside it and next final return to the plane origin for the range of $[-1.9\gamma_{cr}, 1.9\gamma_{cr}]$. The settling times are far better as well as the normal overloads decrease drastically. The established interval of stability remains the same (6.40) but the acceptable range regarding γ_0 is shrunk slightly (6.43).

$$\gamma_0 \in [-1.9\gamma_{cr}, 1.9\gamma_{cr}] \tag{6.43}$$

The repetition of the simulation experiments regarding the performance of the new spatial closed loop guidance system with the SAE2DPDGL instead of the AE2DPDGL with the same initial trajectory points outside the ε_r area shows practically the same results with negligible differences compared with the performance of the guidance system with the AE2DPDGL. Thus a smoothness in the performance of the closed loop guidance system regarding the initial conditions is achieved by the SAE2DPDGL for the very broad range of γ_0 (6.43) within the interval of stability (6.40).

6.3.1 Response to the external disturbances

Some simulation results regarding the influence of the considered external disturbances representing the missile weight and the target's movement are summarized in Table 6.6 and Table 6.7 and shown in Figure 6.16 and Figure 6.17. The results in Table 6.6 with respect to the steady state response $z(\infty)$ show clearly the effectiveness of the missile weight compensation technique presented in Section 6.1.2.3 (page 136). The accuracy is very high and almost constant within the range of the phase coupling angle (6.43). This effect is due to the adaptive control of the vector rotation ψ of the E2DPDGL by the SAE2DPDGL not only outside the ε_r area but also within it. Thus the steady state of the summary phase coupling angle $\gamma_1 = (\psi + \gamma_0)$ is not only within the interval $(-\gamma_{cr}, \gamma_{cr})$ but also could theoretically strive to zero which results practically to a full compensation for the missile weight according to (6.35).

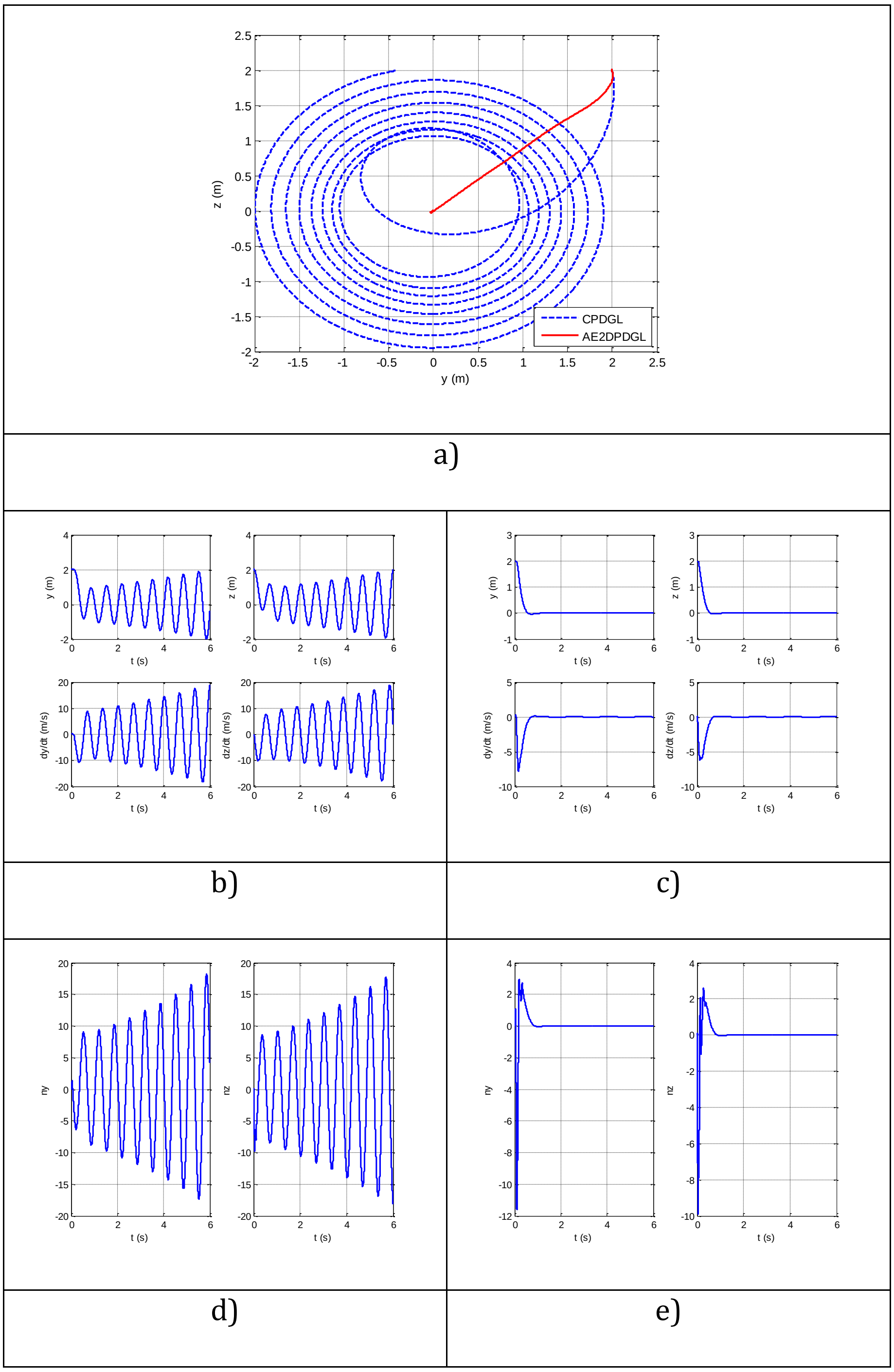

Figure 6.9 Performance comparison between the spatial closed loop guidance system with the CPDGL and the closed loop guidance system with the AE2DPDGL in case of phase coupling between the channels when $\gamma_0 = 1.02\gamma_{cr} = 53.566$ deg. and proportional to each other initial conditions (1.16): a) ATGM trajectory in the $Y_L Z_L$-plane, the picture plane; b) $y, \dot{y}, z$ and $\dot{z}$ in the case of the CPDGL; c) $y, \dot{y}, z$ and $\dot{z}$ in the case of the AE2DPDGL; d) the normal overloads in the case of the CPDGL; e) the normal overloads in the case of the AE2DPDGL.

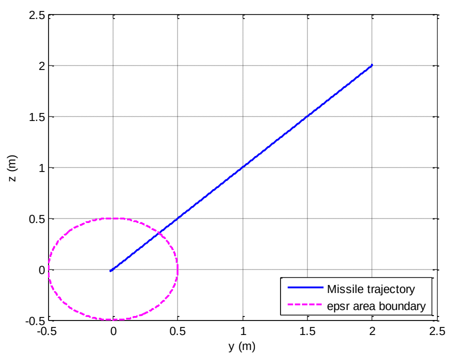

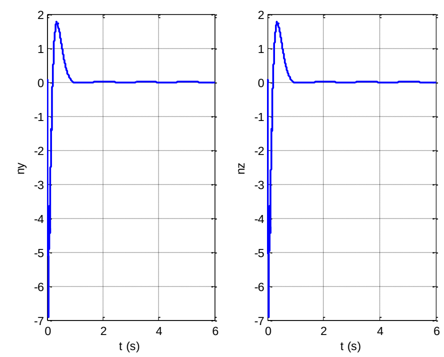

a) $\gamma_0 = 0$ deg.

b) $\gamma_0 = 0$ deg.

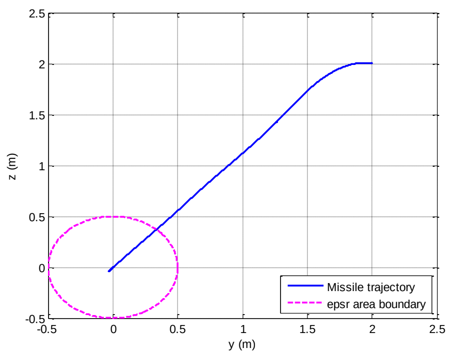

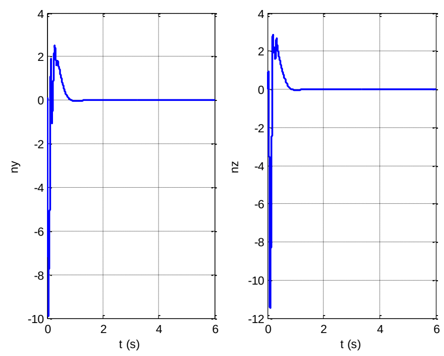

c) $\gamma_0 = -\gamma_{cr} = -52.516$ deg.

d) $\gamma_0 = -\gamma_{cr} = -52.516$ deg.

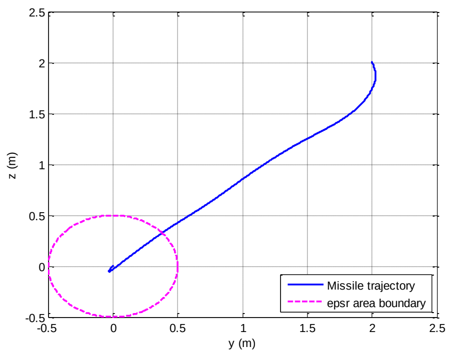

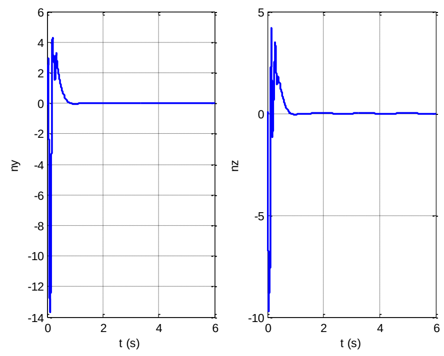

e) $\gamma_0 = 1.25\gamma_{cr} = 65.645$ deg.

f) $\gamma_0 = 1.25\gamma_{cr} = 65.645$ deg.

Figure 6.10 Performance of the spatial closed loop guidance system with AE2DPDGL in the picture plane with respective normal overloads in each channel at different values of the phase coupling angle γ_0 within the interval of stability (6.40) $\gamma_0 \in [-2.2\gamma_{cr}, 2.2\gamma_{cr}]$ where $\gamma_{cr} = 52.516$ deg.: a) and b) $\gamma_0 = 0$ deg.; c) and d) $\gamma_0 = -\gamma_{cr} = -52.516$ deg.; e) and f) $\gamma_0 = 1.25\gamma_{cr} = 65.645$ deg.

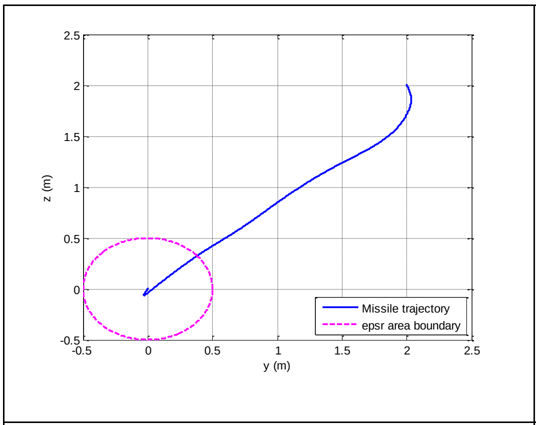

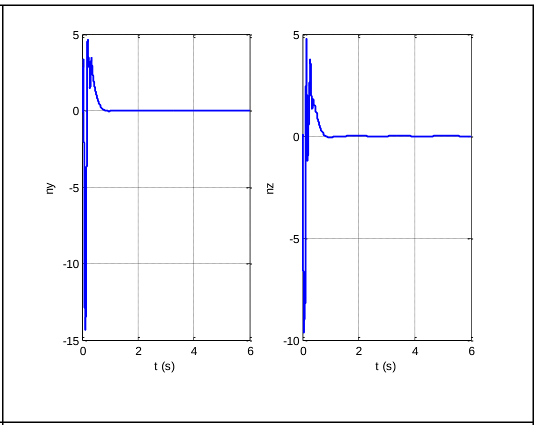

a) $\gamma_0 = 1.3\gamma_{cr} = 68.3$ deg.

b) $\gamma_0 = 1.3\gamma_{cr} = 68.3$ deg.

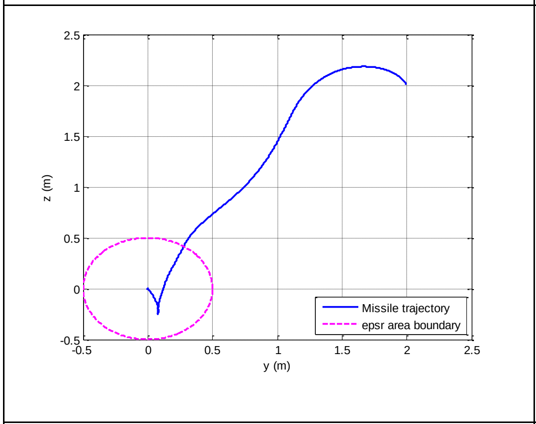

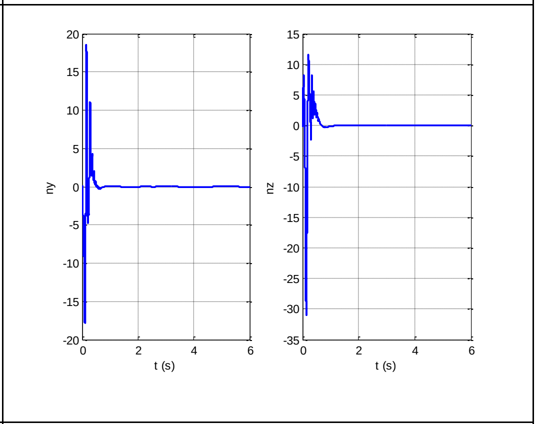

c) $\gamma_0 = -2\gamma_{cr} = -105$ deg.

d) $\gamma_0 = -2\gamma_{cr} = -105$ deg.

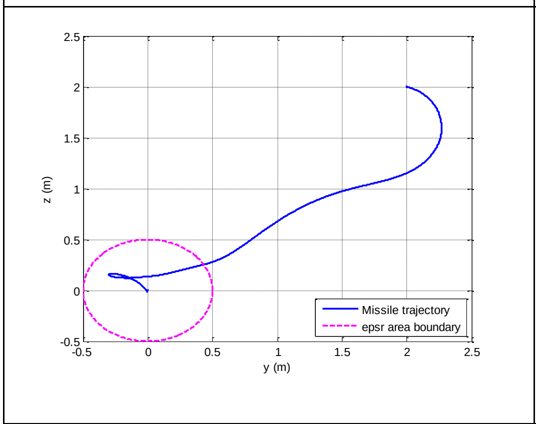

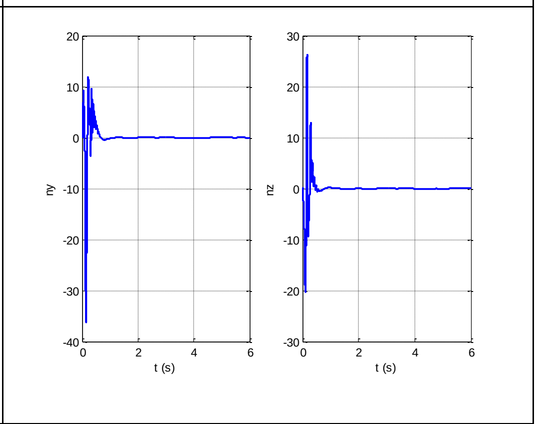

e) $\gamma_0 = 2.2\gamma_{cr} = 115.5$ deg.

f) $\gamma_0 = 2.2\gamma_{cr} = 115.5$ deg.

Figure 6.11 Performance of the spatial closed loop guidance system with AE2DPDGL in the picture plane with respective normal overloads in each channel at different values of the phase coupling angle γ_0 within the interval of stability (6.40) $\gamma_0 \in [-2.2\gamma_{cr}, 2.2\gamma_{cr}]$ where $\gamma_{cr} = 52.516$ deg.: a) and b) $\gamma_0 = 1.3\gamma_{cr} = 68.3$ deg.; c) and d) $\gamma_0 = -2\gamma_{cr} = -105$ deg.; e) and f) $\gamma_0 = 2.2\gamma_{cr} = 115.5$ deg.

Table 6.1 Summary of the simulation studies of the spatial closed loop guidance system with AE2DPDGL when the initial trajectory point in the picture plane represents $(\boldsymbol{y_0}, \boldsymbol{z_0}) = (\mathbf{2}, \mathbf{2})$ regarding the phase coupling angle $\boldsymbol{\gamma_0}$.

$\boldsymbol{\gamma_0}$	$\mathbf{0}$	$-\boldsymbol{\gamma_{cr}}$	$\mathbf{1.2}\boldsymbol{\gamma_{cr}}$	$\mathbf{1.25}\boldsymbol{\gamma_{cr}}$	$\mathbf{1.3}\boldsymbol{\gamma_{cr}}$	$-\mathbf{2}\boldsymbol{\gamma_{cr}}$	$\mathbf{2.2}\boldsymbol{\gamma_{cr}}$
$\gamma_0\ (deg)$	0	−52.5	63.0	65.6	68.3	−105.0	115.5
$\frac{t_s}{t_s^*}$ (%)	100	92	88	87	86	142	149
$\max(n_y, n_z)$	7	11	13.1	13.7	14.4	30.9	36.2
$\frac{\max(n_y, n_z)}{\max(n_y^*, n_z^*)}$ (%)	100	158	187	196	206	441	517

Table 6.2 Summary of the simulation studies of the spatial closed loop guidance system with AE2DPDGL when the initial trajectory point in the picture plane represents $(\boldsymbol{y_0}, \boldsymbol{z_0}) = (\mathbf{1}, \mathbf{1})$ regarding the phase coupling angle $\boldsymbol{\gamma_0}$.

$\boldsymbol{\gamma_0}$	$\mathbf{0}$	$-\boldsymbol{\gamma_{cr}}$	$\mathbf{1.2}\boldsymbol{\gamma_{cr}}$	$\mathbf{1.25}\boldsymbol{\gamma_{cr}}$	$\mathbf{1.3}\boldsymbol{\gamma_{cr}}$	$-\mathbf{2}\boldsymbol{\gamma_{cr}}$	$\mathbf{2.2}\boldsymbol{\gamma_{cr}}$
$\gamma_0\ (deg)$	0	−52.5	63.0	65.6	68.3	−105.0	115.5
$\frac{t_s}{t_s^*}$ (%)	100	92	89	88	87	129	135
$\max(n_y, n_z)$	3.5	5.7	6.6	6.8	7.2	15.5	18.1
$\frac{\max(n_y, n_z)}{\max(n_y^*, n_z^*)}$ (%)	100	163	186	194	206	443	517

Table 6.3 Summary of the simulation studies of the spatial closed loop guidance system with AE2DPDGL when the initial trajectory point in the picture plane represents $(y_0, z_0) = (0.5, 0.5)$ regarding the phase coupling angle γ_0.

$\boldsymbol{\gamma_0}$	**0**	$-\gamma_{cr}$	$1.2\gamma_{cr}$	$1.25\gamma_{cr}$	$1.3\gamma_{cr}$	$-2\gamma_{cr}$	$2.2\gamma_{cr}$
$\gamma_0\ (deg)$	0	−52.5	63.0	65.6	68.3	−105.0	115.5
$\frac{t_s}{t_s^*}$ (%)	100	95	98	107	120	148	140
$\max(n_y, n_z)$	1.7	2.9	3.3	3.4	3.6	7.7	9
$\frac{\max(n_y, n_z)}{\max(n_y^*, n_z^*)}$ (%)	100	171	194	200	212	453	529

Table 6.4 Summary of the simulation studies of the spatial closed loop guidance system with AE2DPDGL when the initial trajectory point in the picture plane represents $(y_0, z_0) = (0.25, 0.25)$ regarding the phase coupling angle γ_0.

$\boldsymbol{\gamma_0}$	**0**	$-\gamma_{cr}$	$1.2\gamma_{cr}$	$1.25\gamma_{cr}$	$1.3\gamma_{cr}$	$-2\gamma_{cr}$	$2.2\gamma_{cr}$
$\gamma_0\ (deg)$	0	−52.5	63.0	65.6	68.3	−105.0	115.5
$\frac{t_s}{t_s^*}$ (%)	100	Steady (undamped) oscillations within the ε_r area	439	405	370	282	270
$\max(n_y, n_z)$	0.9	1.3	16.6	20	16.6	19.6	18.2
$\frac{\max(n_y, n_z)}{\max(n_y^*, n_z^*)}$ (%)	100	144	1844	2222	1844	2178	2022

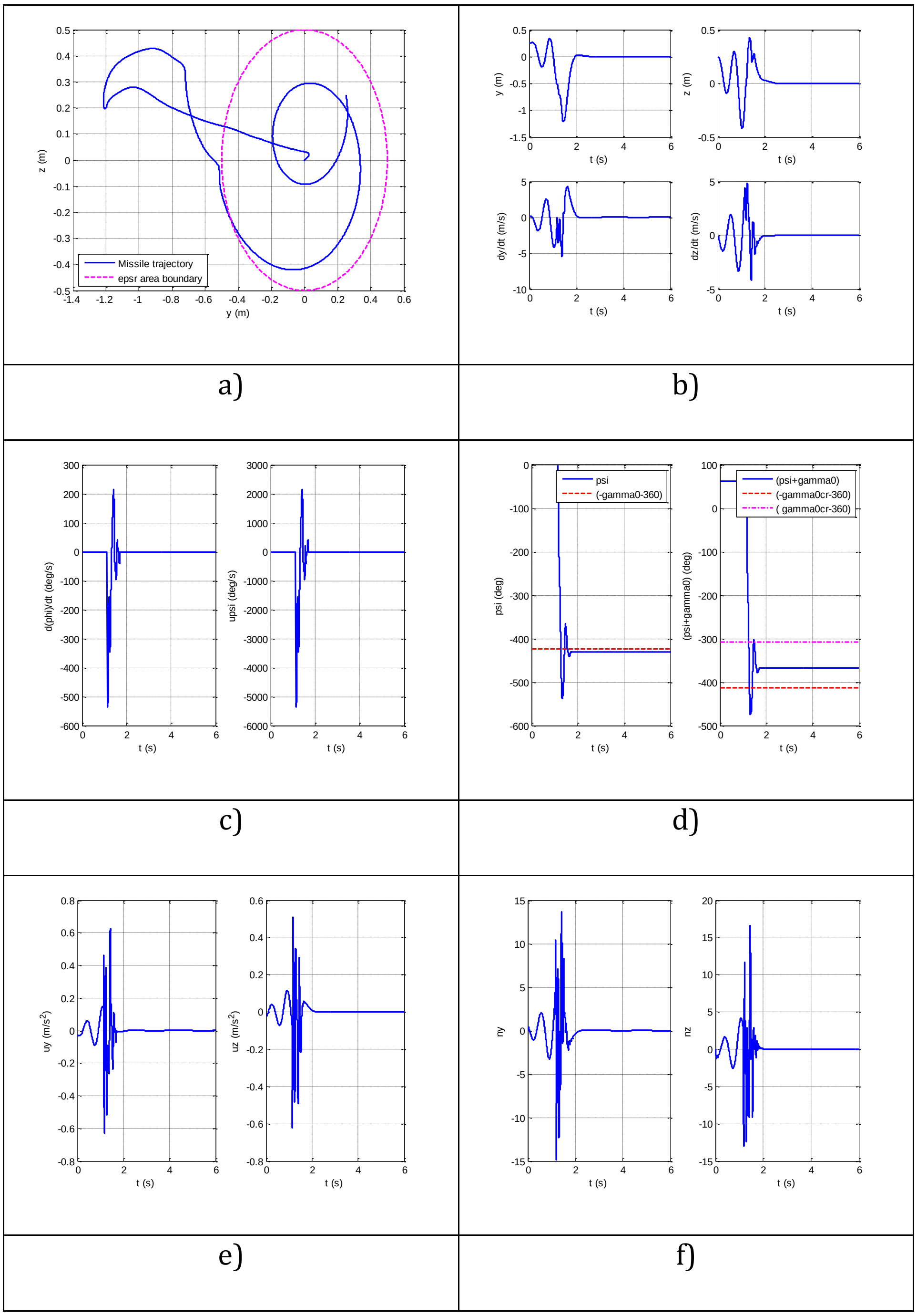

Figure 6.12 Performance of the closed loop guidance system with AE2DPDGL in case the initial trajectory point in the picture plane represents $(y_0, z_0) = (0.25, 0.25)$ and the phase coupling angle $\gamma_0 = 1.2\gamma_{cr} = 63$ deg. where $\gamma_{cr} = 52.516$ deg. with regard to: a) ATGM trajectory in the $Y_L Z_L$-plane, the picture plane; b) $y, \dot{y}, z$ and $\dot{z}$; c) $\dot{\varphi}$ and the adaptive control u_ψ (3.78); d) the self-adjusting angle ψ of the AE2DPDGL vector rotation and the sum of ψ and γ_0; e) the components u_y and u_z of the AE2DPDGL (3.5); f) the normal overloads n_y and n_z.

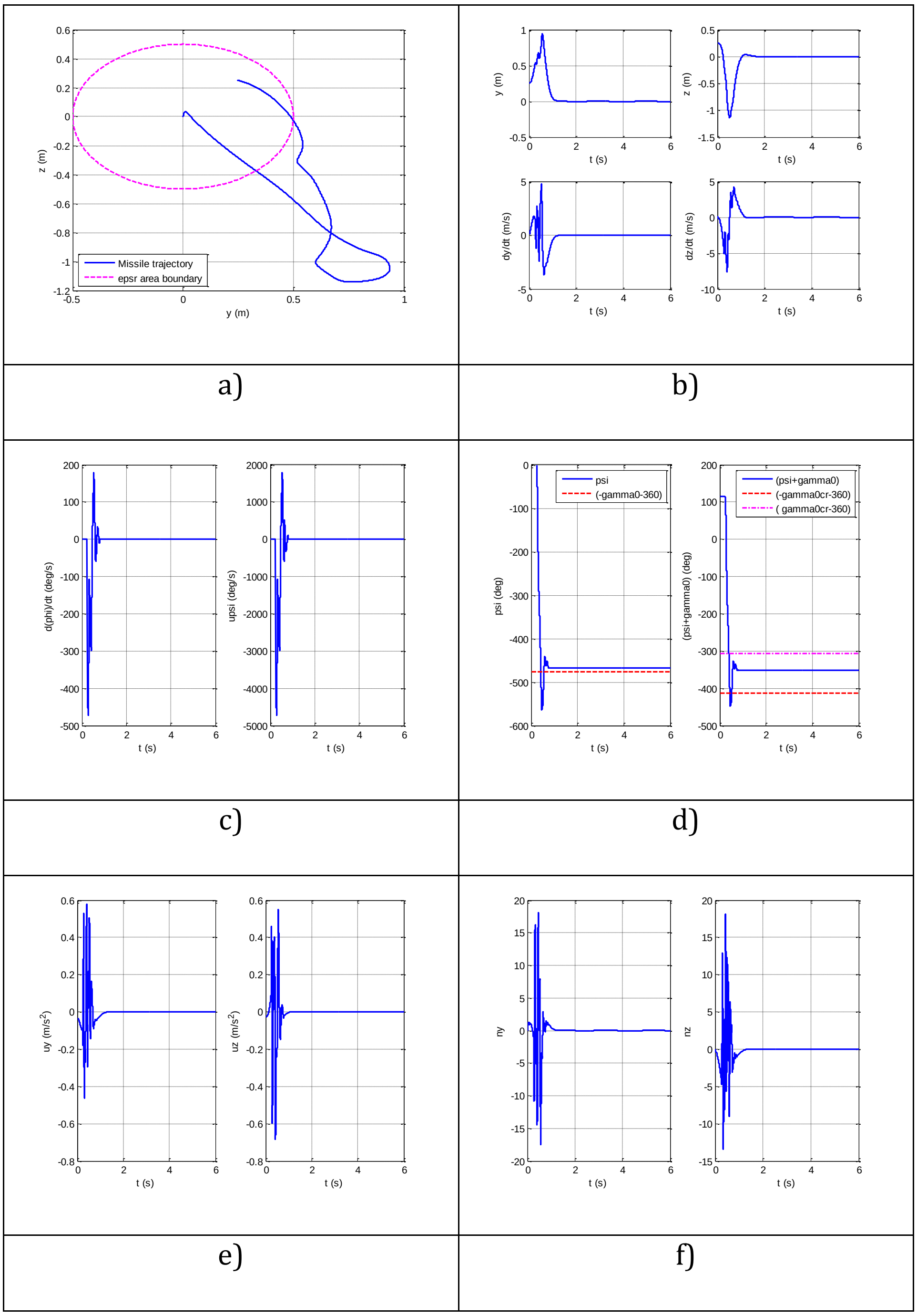

Figure 6.13 Performance of the closed loop guidance system with AE2DPDGL in case the initial trajectory point in the picture plane represents $(y_0, z_0) = (0.25, 0.25)$ and the phase coupling angle $\gamma_0 = 2.2\gamma_{cr} = 115.5$ deg. where $\gamma_{cr} = 52.516$ deg. with regard to: a) ATGM trajectory in the $Y_L Z_L$-plane, the picture plane; b) $y, \dot{y}, z$ and $\dot{z}$; c) $\dot{\varphi}$ and the adaptive control u_ψ (3.78); d) the self-adjusting angle ψ of the AE2DPDGL vector rotation and the sum of ψ and γ_0; e) the components u_y and u_z of the AE2DPDGL (3.5); f) the normal overloads n_y and n_z.

Table 6.5 Performance comparison of the closed loop guidance system with the AE2DPDGL and the system with the SAE2DPDGL when the initial trajectory point in the picture plane represents $(y_0, z_0) = (0.25, 0.25)$ regarding the phase coupling angle γ_0.

γ_0	$\mathbf{0}$	γ_{cr}	$1.2\gamma_{cr}$	$1.25\gamma_{cr}$	$1.3\gamma_{cr}$	$1.9\gamma_{cr}$	$2\gamma_{cr}$
$\gamma_0\ (deg)$	0	52.5	63.0	65.6	68.3	99.8	105.0
$\frac{t_s}{t_s^*}$ (%) by the AE2DPDGL	100	Steady (undamped) oscillations within the ε_r area.	439	405	370	282	282
$\frac{t_s}{t_s^*}$ (%) by the SAE2DPDGL	100	273	313	304	294	242	265
$\max(n_y, n_z)$ by the AE2DPDGL	0.9	1.3	16.6	20	16.6	19.6	19.6
$\max(n_y, n_z)$ by the SAE2DPDGL	0.9	1.2	1.3	1.4	1.5	4	15.5
$\frac{\max(n_y, n_z)}{\max(n_y^*, n_z^*)}$ (%) by the AE2DPDGL	100	144	1844	2222	1844	2178	2178
$\frac{\max(n_y, n_z)}{\max(n_y^*, n_z^*)}$ (%) at the SAE2DPDGL	100	133	144	156	167	444	1722

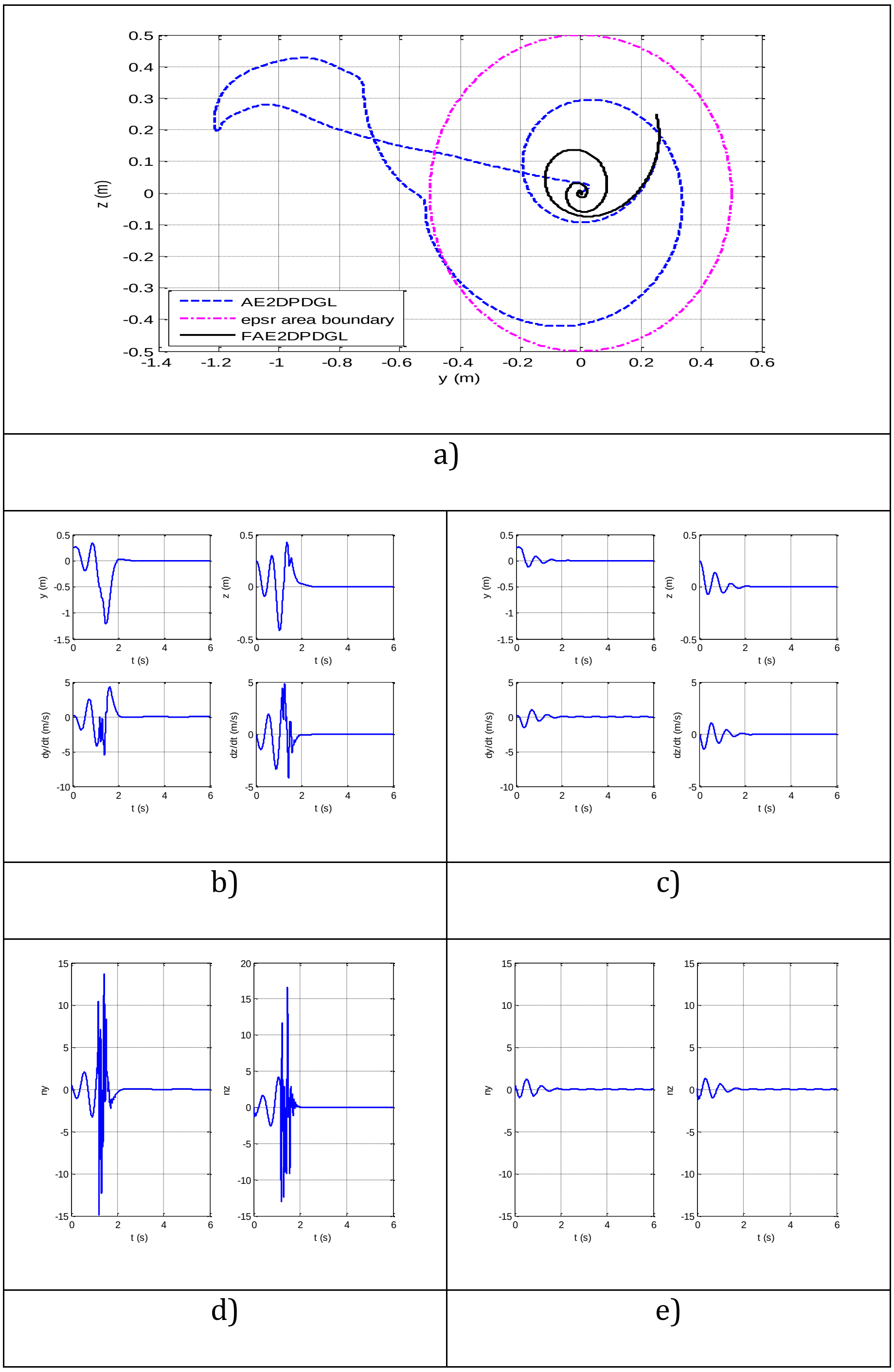

Figure 6.14 Performance comparison between the spatial closed loop guidance system with the AE2DPDGL and the spatial closed loop guidance system with the SAE2DPDGL in case the initial trajectory point in the picture plane represents $(y_0, z_0) = (0.25, 0.25)$ and the phase coupling angle $\gamma_0 = 1.2\gamma_{cr} = 63$ deg. where $\gamma_{cr} = 52.516$ deg. with regard to: a) ATGM trajectory in the $Y_L Z_L$-plane, the picture plane; b) $y, \dot{y}, z$ and $\dot{z}$ in case of AE2DPDGL; c) $y, \dot{y}, z$ and $\dot{z}$ in case of SAE2DPDGL; d) the normal overloads by the AE2DPDGL; e) the normal overloads by the SAE2DPDGL.

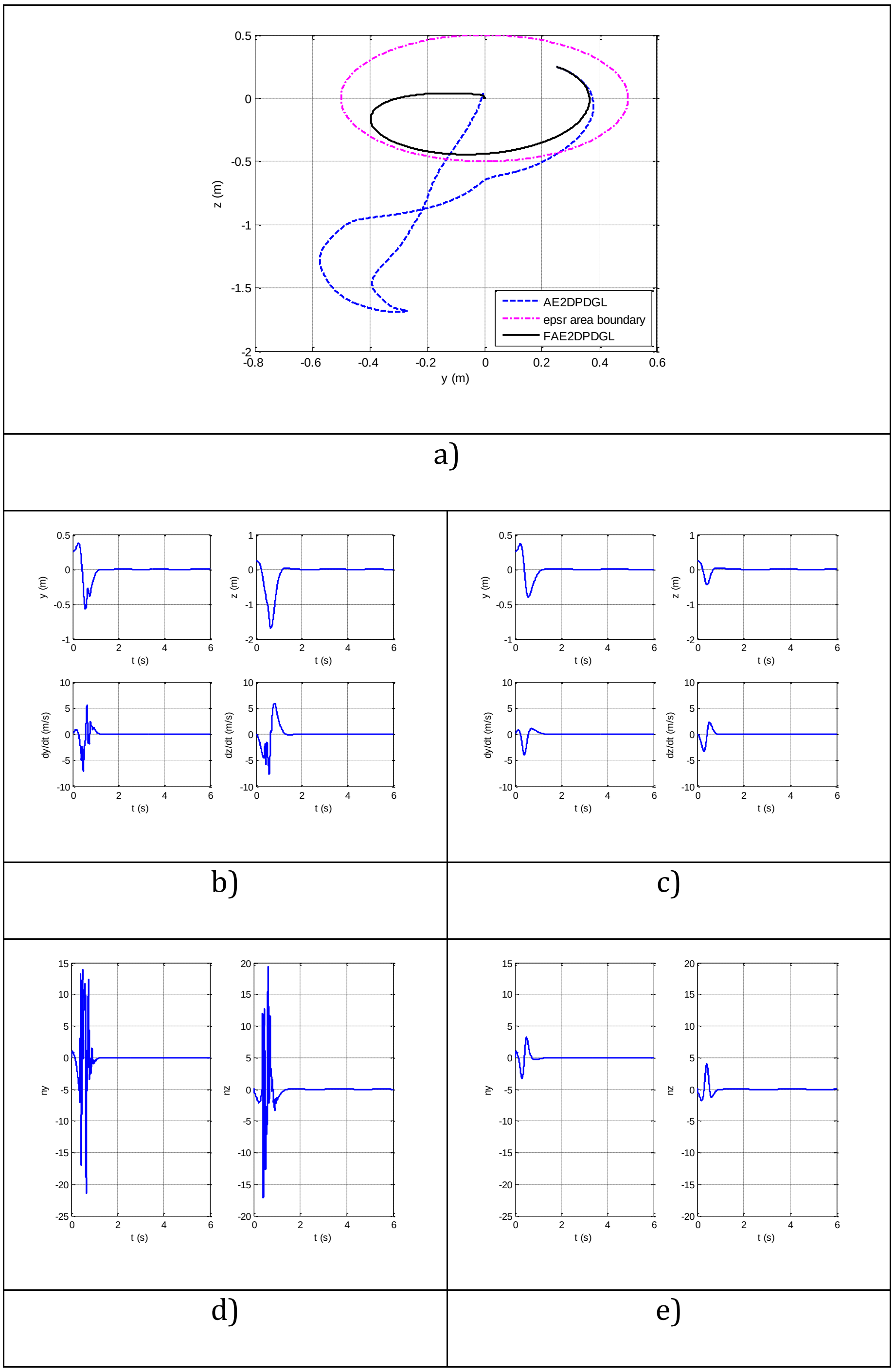

Figure 6.15 Performance comparison between the spatial closed loop guidance system with the AE2DPDGL and the spatial closed loop guidance system with the SAE2DPDGL in case the initial trajectory point in the picture plane represents $(y_0, z_0) = (0.25, 0.25)$ and the phase coupling angle $\gamma_0 = 1.9\gamma_{cr} = 99.8$ deg. where $\gamma_{cr} = 52.516$ deg. with regard to: a) ATGM trajectory in the $Y_L Z_L$-plane, the picture plane; b) $y, \dot{y}, z$ and $\dot{z}$ in case of AE2DPDGL; c) $y, \dot{y}, z$ and $\dot{z}$ in case of SAE2DPDGL; d) the normal overloads by the AE2DPDGL; e) the normal overloads by the SAE2DPDGL.

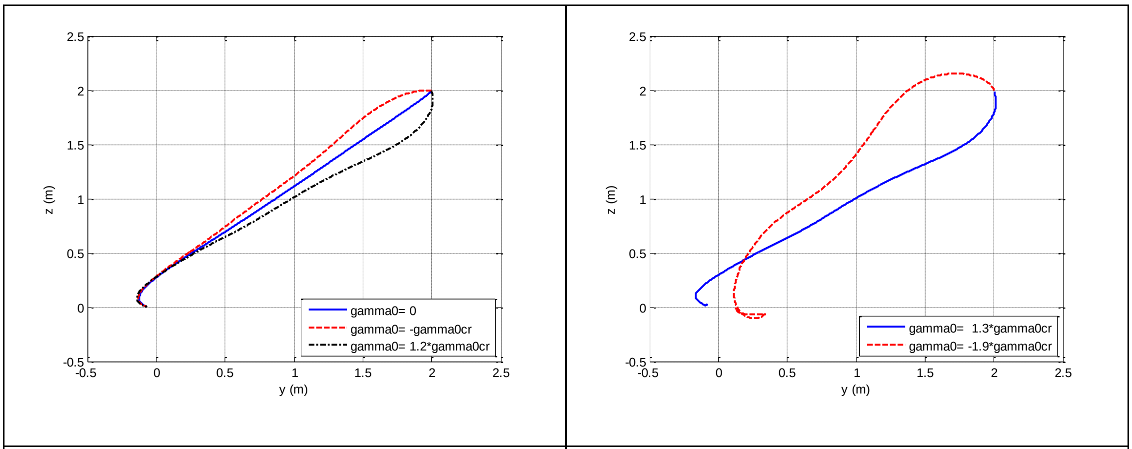

a) b)

Figure 6.16 Picture plane trajectories of the response of the spatial closed loop guidance system with the SAE2DPDGL and weight compensation to the missile weight regarding the phase coupling angle γ_0 within the interval of stability (6.40).

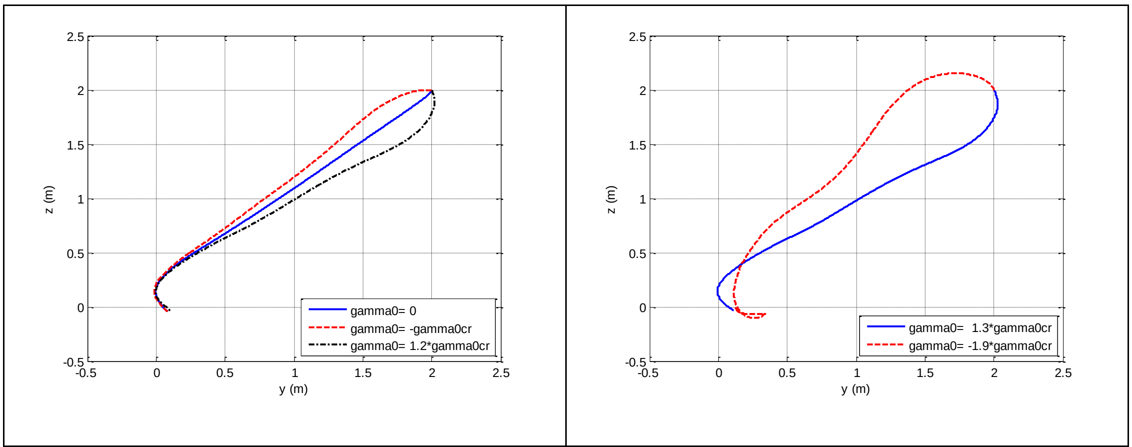

a) b)

Figure 6.17 Picture plane trajectories of the response of the spatial closed loop guidance system with SAE2DPDGL and weight compensation to the simultaneous influence of the missile weight and the target's movement (6.27), (6.25) regarding the phase coupling angle γ_0 within the interval of stability (6.40).

Table 6.6 Summary of the steady state response of the spatial closed loop guidance system with the SAE2DPDGL and weight compensation to the missile weight regarding the phase coupling angle $\boldsymbol{\gamma_0}$ within the interval of stability (6.40).

$\boldsymbol{\gamma_0}$	**0**	$-\boldsymbol{\gamma_{cr}}$	$\mathbf{1.2}\boldsymbol{\gamma_{cr}}$	$\mathbf{1.25}\boldsymbol{\gamma_{cr}}$	$\mathbf{1.3}\boldsymbol{\gamma_{cr}}$	$-\mathbf{1.9}\boldsymbol{\gamma_{cr}}$	$\mathbf{1.9}\boldsymbol{\gamma_{cr}}$
$\gamma_0\ (deg)$	0	-52.5	63.0	65.6	68.3	-99.8	99.8
$y(\infty)\ (m)$	-0.07	-0.07	-0.07	-0.08	-0.09	0.14	-0.11
$z(\infty)\ (m)$	0.01	0.01	0.01	0.02	0.02	-0.02	0.03

Table 6.7 Summary of the steady state response of the spatial closed loop guidance system with the SAE2DPDGL and weight compensation to the simultaneous influence of the missile weight and the target's movement (6.27), (6.25) regarding the phase coupling angle $\boldsymbol{\gamma_0}$ within the interval of stability (6.40).

$\boldsymbol{\gamma_0}$	**0**	$-\boldsymbol{\gamma_{cr}}$	$\mathbf{1.2}\boldsymbol{\gamma_{cr}}$	$\mathbf{1.25}\boldsymbol{\gamma_{cr}}$	$\mathbf{1.3}\boldsymbol{\gamma_{cr}}$	$-\mathbf{1.9}\boldsymbol{\gamma_{cr}}$	$\mathbf{1.9}\boldsymbol{\gamma_{cr}}$
$\gamma_0\ (deg)$	0	-52.5	63.0	65.6	68.3	-99.8	99.8
$y(\infty)\ (m)$	0.08	0.08	0.11	0.11	0.11	0.14	0.02
$z(\infty)\ (m)$	-0.03	-0.03	-0.03	-0.03	-0.03	-0.02	-0.04

6.4 Robustness of the closed loop system

6.4.1 Robust asymptotic stability of the one-dimensional closed loop system

Let us deal first with the one-dimensional closed loop system. Let us suppose the parameters of the transfer function (6.1), (6.2) as well as the parameters of the PD compensator (6.3) vary. Let each one of the coefficients of the polynomials $N(s)$ and $D(s)$ of the transfer function (6.1), (6.2) vary within a closed interval. Let the common form of the polynomials $N(s)$ and $D(s)$ of (6.1) be presented as (6.44) but the polynomials $N(s)$ and $D(s)$ in (6.2) be named nominal polynomials $N^*(s)$ and $D^*(s)$ with nominal coefficients $b^*_{M0,1,2}$ and $a^*_{M0,1,2,3}$ according to (6.45). Let everyone coefficient of (6.44) could vary independently within its own interval according to (6.46). Dealing in the same way with the parameters of the PD compensator (6.3) we obtain (6.47) where the nominal coefficients k^*_c and T^*_c represent these from (6.3).

$N(s) = -b_{M0}s^2 - b_{M1}s + b_{M2}, \qquad b_{M0,1,2} > 0$ $D(s) = a_{M0}s^3 + a_{M1}s^2 + a_{M2}s + a_{M3}, \qquad a_{M0,1,2,3} > 0$	(6.44)
$N^*(s) = -b^*_{M0}s^2 - b^*_{M1}s + b^*_{M2},$ $D^*(s) = a^*_{M0}s^3 + a^*_{M1}s^2 + a^*_{M2}s + a^*_{M3}$	(6.45)
$\underline{b}_{M0} = b^*_{M0}(1-\Delta_M) \le b_{M0} \le b^*_{M0}(1+\Delta_M) = \overline{b}_{M0},$ $\underline{b}_{M1} = b^*_{M1}(1-\Delta_M) \le b_{M1} \le b^*_{M1}(1+\Delta_M) = \overline{b}_{M1},$ $\underline{b}_{M2} = b^*_{M2}(1-\Delta_M) \le b_{M2} \le b^*_{M2}(1+\Delta_M) = \overline{b}_{M2},$ $\underline{a}_{M0} = a^*_{M0}(1-\Delta_M) \le a_{M0} \le a^*_{M0}(1+\Delta_M) = \overline{a}_{M0},$ $\underline{a}_{M1} = a^*_{M1}(1-\Delta_M) \le a_{M1} \le a^*_{M1}(1+\Delta_M) = \overline{a}_{M1},$ $\underline{a}_{M2} = a^*_{M2}(1-\Delta_M) \le a_{M2} \le a^*_{M2}(1+\Delta_M) = \overline{a}_{M2},$ $\underline{a}_{M3} = a^*_{M3}(1-\Delta_M) \le a_{M3} \le a^*_{M3}(1+\Delta_M) = \overline{a}_{M3},$ $where\ 0 < \Delta_M < 1$	(6.46)
$\underline{k}_c = k^*_c(1-\Delta_c) \le k_c \le k^*_c(1+\Delta_c) = \overline{k}_c\ ,$ $\underline{T}_c = T^*_c(1-\Delta_c) \le T_c \le T^*_c(1+\Delta_c) = \overline{T}_c\ ,$ $where\ 0 < \Delta_c < 1$	(6.47)

Let us consider now the characteristic polynomial $f(s)$ (6.48) of the one-dimensional closed loop system with open loop transfer function $L_0(s)$ (6.4). The polynomial $f(s)$ represented in descending order of power of s is (6.49) where the coefficients $c_{0,1,2,3,4,5}$ represent (6.50). Their lower and upper limits are (6.51). Let us name $f(s)$ (6.49) $f^*(s)$ (6.52) when the coefficients $c_{0,1,2,3,4,5}$ are calculated by the nominal coefficients of the PD compensator k^*_c and T^*_c , and the nominal coefficients of the polynomials $N(s)$ and $D(s)$ $b^*_{M0,1,2}$ and $a^*_{M0,1,2,3}$. The numerical data for (6.52) represent (6.53). $f^*(s)$ (6.52) with coefficients $c^*_{0,1,2,3,4,5}$ (6.53) is a Hurwitz polynomial (6.54).

$f(s) = s^2 D(s) + N(s)\big(k_c(T_c s + 1)\big)$	(6.48)
$f(s) = c_0 s^5 + c_1 s^4 + c_2 s^3 + c_3 s^2 + c_4 s + c_5$	(6.49)
$c_0 = a_{M0}$ $c_1 = a_{M1}$ $c_2 = a_{M2} - k_c T_c b_{M0}$ $c_3 = a_{M3} - k_c T_c b_{M1} - k_c b_{M0}$ $c_4 = k_c T_c b_{M2} - k_c b_{M1}$ $c_5 = k_c b_{M2}$	(6.50)
$\underline{c}_0 = \underline{a}_{M0}\,, \quad \overline{c}_0 = \overline{a}_{M0}\,,$ $\underline{c}_1 = \underline{a}_{M1}\,, \quad \overline{c}_1 = \overline{a}_{M1}\,,$ $\underline{c}_2 = \underline{a}_{M2} - \overline{k}_c \overline{T}_c \overline{b}_{M0}\,, \quad \overline{c}_2 = \overline{a}_{M2} - \underline{k}_c \underline{T}_c \underline{b}_{M0}\,,$ $\underline{c}_3 = \underline{a}_{M3} - \overline{k}_c \overline{T}_c \overline{b}_{M1} - \overline{k}_c \overline{b}_{M0}\,, \quad \overline{c}_3 = \overline{a}_{M3} - \underline{k}_c \underline{T}_c \underline{b}_{M1} - \underline{k}_c \underline{b}_{M0}\,,$ $\underline{c}_4 = \underline{k}_c \underline{T}_c \underline{b}_{M2} - \overline{k}_c \overline{b}_{M1}\,, \quad \overline{c}_4 = \overline{k}_c \overline{T}_c \overline{b}_{M2} - \underline{k}_c \underline{b}_{M1}\,,$ $\underline{c}_5 = \underline{k}_c \underline{b}_{M2}\,, \quad \overline{c}_5 = \overline{k}_c \overline{b}_{M2}$	(6.51)
$f^*(s) = c_0^* s^5 + c_1^* s^4 + c_2^* s^3 + c_3^* s^2 + c_4^* s + c_5^*$	(6.52)
$c_0^* = 2.7e-06 \quad c_1^* = 0.000162 \quad c_2^* = 0.02992$ $c_3^* = 0.99756 \quad c_4^* = 8.9318 \quad c_5^* = 33.11$	(6.53)
$f^*(s) \in H$	(6.54)

Let us suppose: $\Delta_M = 0.1$ and $\Delta_c = 0$ (6.55). The numerical values of the lower and upper limits of the coefficients of the interval polynomials $N(s)$ and $D(s)$ in this case are (6.56) while the parameters of the PD compensator are (6.57) where the lower and upper limits coincide with the nominal parameters (6.3). According to (6.51) and the data (6.56), (6.57) we obtain (6.58) for the numerical values of the lower and upper limits of the coefficients $c_{0,1,2,3,4,5}$ of the characteristic polynomial $f(s)$ (6.49).

$\Delta_M = 0.1\,, \quad \Delta_c = 0$	(6.55)

$\underline{b}_{M0} = 0.00243 \leq b_{M0} \leq 0.00297 = \overline{b}_{M0},$ $\underline{b}_{M1} = 0.0648 \leq b_{M1} \leq 0.0792 = \overline{b}_{M1},$ $\underline{b}_{M2} = 270.9 \leq b_{M2} \leq 331.1 = \overline{b}_{M2},$ $\underline{a}_{M0} = 2.43e-06 \leq a_{M0} \leq 2.97e-06 = \overline{a}_{M0},$ $\underline{a}_{M1} = 0.0001458 \leq a_{M1} \leq 0.0001782 = \overline{a}_{M1},$ $\underline{a}_{M2} = 0.027 \leq a_{M2} \leq 0.033 = \overline{a}_{M2},$ $\underline{a}_{M3} = 0.9 \leq a_{M3} \leq 1.1 = \overline{a}_{M3},$	(6.56)
$\underline{k}_c = 0.11 = k_c^* = k_c = \overline{k}_c\,,$ $\underline{T}_c = 0.27 = T_c^* = T_c = \overline{T}_c$	(6.57)
$\underline{c}_0 = 2.43e-06 \leq c_0 \leq 2.97e-06 = \overline{c}_0,$ $\underline{c}_1 = 0.0001458 \leq c_1 \leq 0.0001782 = \overline{c}_1,$ $\underline{c}_2 = 0.026912 \leq c_2 \leq 0.032928 = \overline{c}_2,$ $\underline{c}_3 = 0.89732 \leq c_3 \leq 1.0978 = \overline{c}_3,$ $\underline{c}_4 = 8.037 \leq c_4 \leq 9.8265 = \overline{c}_4,$ $\underline{c}_5 = 29.799 \leq c_5 \leq 36.421 = \overline{c}_5,$	(6.58)

Let us now consider the group of interval polynomials G_+ (6.59) where the lower and upper limits of the coefficients c_j represent (6.58). The four Kharitonov's (Харитонов) polynomials [45] for this group of interval polynomials G_+ represent (6.60). It is easily to check that every one of these four polynomials is a Hurwitz polynomial $f_j(s) \in H, j = 1,2,3,4$. Let us employ the Kharitonov theorem "$G_+ \in H$ *if and only if* $f_j(s) \in H, j = 1,2,3,4$" [45]. Thus the conclusion is that $G_+ \in H$ or all polynomials (6.59) in this case are Hurwitz polynomials.

So the one-dimensional closed loop system with open loop transfer function $L_0(s)$ (6.4) where the polynomials $N(s)$ and $D(s)$ are interval polynomials with limits of their coefficients (6.56) but the parameters of the PD compensator (6.3) are fixed is robust asymptotically stable.

$G_+ = \begin{Bmatrix} f(s) = c_0s^5 + c_1s^4 + c_2s^3 + c_3s^2 + c_4s + c_5 \\ \underline{c}_j \leq c_j \leq \overline{c}_j,\ \ j = 0,1,\dots,5 \end{Bmatrix}$	(6.59)
$f_1(s) = \overline{c}_0s^5 + \underline{c}_1s^4 + \underline{c}_2s^3 + \overline{c}_3s^2 + \overline{c}_4s + \underline{c}_5$ $f_2(s) = \underline{c}_0s^5 + \underline{c}_1s^4 + \overline{c}_2s^3 + \overline{c}_3s^2 + \underline{c}_4s + \underline{c}_5$ $f_3(s) = \underline{c}_0s^5 + \overline{c}_1s^4 + \overline{c}_2s^3 + \underline{c}_3s^2 + \underline{c}_4s + \overline{c}_5$ $f_4(s) = \overline{c}_0s^5 + \overline{c}_1s^4 + \underline{c}_2s^3 + \underline{c}_3s^2 + \overline{c}_4s + \overline{c}_5$	(6.60)

The repetition of the above consideration but for the cases (6.61) and (6.62) leads to the same conclusion regarding the robust asymptotic stability of the one one-dimensional closed loop system.

$\Delta_M = 0.1\,, \quad \Delta_c = 0.05$	(6.61)
$\Delta_M = 0.1\,, \quad \Delta_c = 0.1$	(6.62)

6.4.2 Robust asymptotic stability of the classical spatial closed loop system with phase coupling between the channels

According to the consideration in Section 6.1.2.1 "Stability of the classical spatial closed loop system with phase coupling between the channels" the spatial closed loop system with phase coupling between the channels is asymptotically stable when the phase coupling angle γ_0 is within the interval of stability $(-\gamma_{cr}, \gamma_{cr})$. The critical value of the phase coupling angle γ_{cr} represents (6.6) which is the phase margin PM_0 for the closed loop system with the open loop frequency response function $L_0(i\omega)$ (at $\gamma_0 = 0$) i.e. the open loop frequency response function of the one-dimensional system. So in order to guarantee now the robust asymptotic stability of spatial closed loop system with phase coupling between the channels it is necessary to obtain the minimum of the phase margin PM_0 for the closed loop system with the open loop frequency response function $L_0(i\omega)$ in case when the coefficients of the polynomials of the open loop transfer function $L_0(s)$ (6.4) vary.

6.4.2.1 Case of varying coefficients $\Delta_M = 0.1$ and $\Delta_c = 0$

Let us deal first with the case (6.55) ($\Delta_M = 0.1$ and $\Delta_c = 0$). The polynomial $N(s)$ has 3 varying coefficients $b_{M0,1,2,3}$ with respective lower and upper limits for each of them, the polynomial $D(s)$ – 4 varying coefficients $a_{M0,1,2,3,4}$ but the parameters of the PD compensator (6.3) are fixed. Thus the number of the extremal representations of the open loop transfer function $L_0(s)$ (6.4) and their respective frequency response function $L_0(i\omega)$ is $2^{(3+4)} = 128$. The summary representation of all extremal Bode diagrams of $L_0(i\omega)$ alongside with the nominal Bode diagram of $L_0(i\omega)$ is in Figure 6.18. The analysis of the stability margins by all extremal open loop frequency response functions $L_0(i\omega)$ is represented in Table 6.8. We obtain (6.63) for the minimum value of the critical phase coupling angle $\underline{\gamma}_{cr} = 48.985\ deg$.

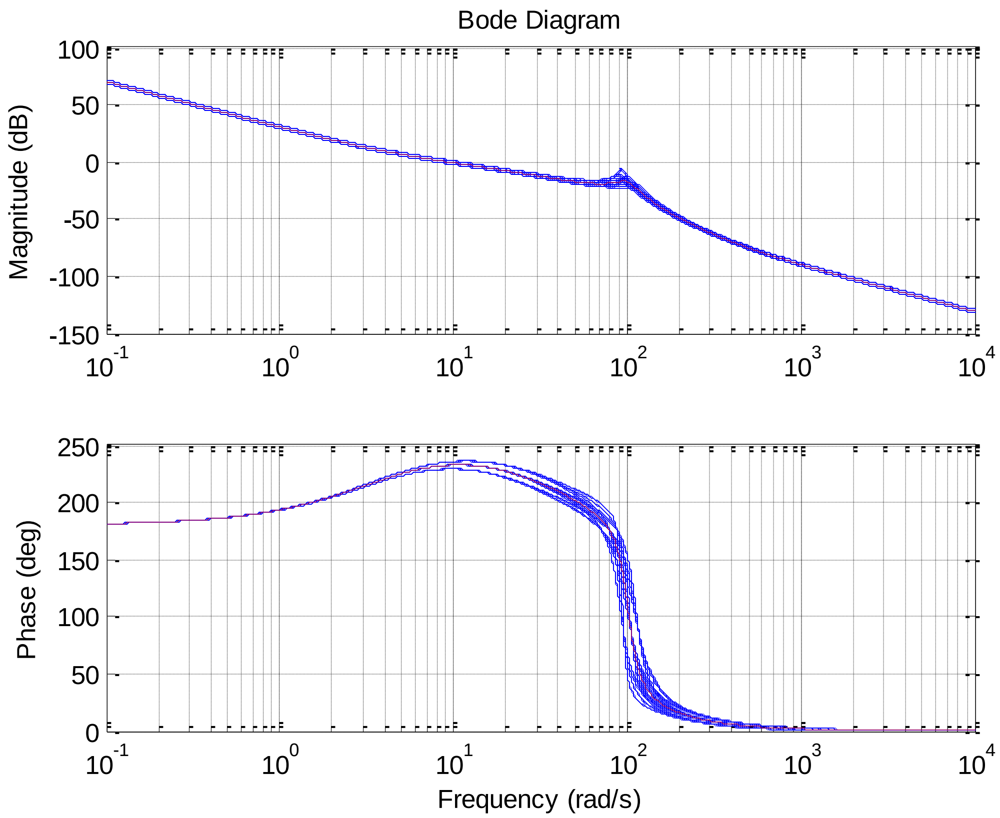

Figure 6.18 Summary representation of all extremal Bode diagrams of $L_0(i\omega)$ in case (6.55) ($\Delta_M = 0.1$ and $\Delta_c = 0$) alongside with the nominal Bode diagram of $L_0(i\omega)$.

Table 6.8 Summary of the stability margins by all extremal open loop frequency response functions $L_0(i\omega)$ in case (6.55) ($\Delta_M = 0.1$ and $\Delta_c = 0$).

	Minimum value	Nominal value	Maximum value
$PM_0\ (deg)$	48.985	52.516	55.423
$\omega_{cg0}\ (rad/s)$	7.9242	9.3881	11.189
$GM_0\ (dB)$	11.13	18.955	22.359
$\omega_{-\pi}\ (rad/s)$	66.574	75.642	85.827

So in case (6.55) regarding the limits of varying coefficients of the open loop transfer function $L_0(s)$ (6.4) the spatial closed loop with phase coupling between the channels is robust asymptotically stable when the phase coupling angle γ_0 is within the interval of stability $\left(-\underline{\gamma_{cr}}, \underline{\gamma_{cr}}\right)$ (6.64) where $\underline{\gamma_{cr}}$ represents (6.63) $\underline{\gamma_{cr}} = 48.985\ (deg)$.

$\underline{\gamma_{cr}} = \min(\gamma_{cr}) = \min(PM_0) = 48.985\ deg$	(6.63)
$\gamma_0 \in \left(-\underline{\gamma_{cr}}, \underline{\gamma_{cr}}\right)$	(6.64)

6.4.2.2 Case of varying coefficients $\Delta_M = 0.1$ and $\Delta_c = 0.05$

When in the second case the limits regarding the varying coefficients of the open loop transfer function $L_0(s)$ (6.4) are according to (6.61) ($\Delta_M = 0.1$ and $\Delta_c = 0.05$) the polynomial $N(s)$ has 3 varying coefficients $b_{M0,1,2,3}$ with respective lower and upper limits for each of them, the polynomial $D(s)$ – 4 varying coefficients $a_{M0,1,2,3,4}$, and the parameters of the PD compensator – 2 varying parameters with respective lower and upper limits for each of them: the coefficient k_c and the time constant T_c. Thus the number of the extremal representations of the open loop transfer function $L_0(s)$ (6.4) and their respective frequency response function $L_0(i\omega)$ becomes $2^{(3+4+2)} = 512$. The obtained summary representation in this case of all extremal Bode diagrams of $L_0(i\omega)$ alongside with the nominal Bode diagram of $L_0(i\omega)$ is in Figure 6.19. The analysis of the stability margins for the closed loop system by all extremal open loop frequency response functions $L_0(i\omega)$ is represented in Table 6.9. Thus we obtain (6.65) for the minimum value of the critical phase coupling angle $\underline{\gamma_{cr}} = 47.803\ deg$.

So in this second case (6.61) ($\Delta_M = 0.1$ and $\Delta_c = 0.05$) the spatial closed loop with phase coupling between the channels is robust asymptotically stable when the phase coupling angle γ_0 is within the interval of stability $\left(-\underline{\gamma_{cr}}, \underline{\gamma_{cr}}\right)$ (6.64) where $\underline{\gamma_{cr}}$ represents now (6.65) $\underline{\gamma_{cr}} = 47.803\ deg$.

$\underline{\gamma_{cr}} = \min(\gamma_{cr}) = \min(PM_0) = 47.803\ deg$	(6.65)

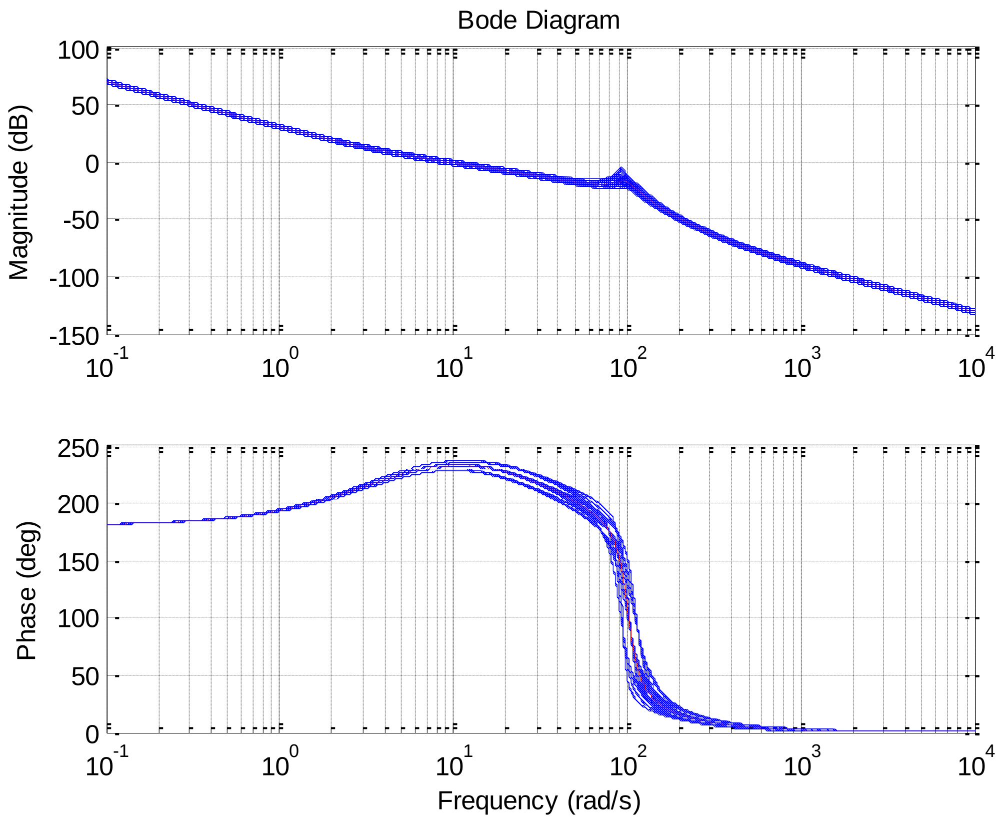

Figure 6.19 Summary representation of all extremal Bode diagrams of $L_0(i\omega)$ in case (6.61) ($\Delta_M = 0.1$ and $\Delta_c = 0.05$) alongside with the Bode diagram of $L_0(i\omega)$ in the nominal case.

Table 6.9 Summary of the stability margins by all extremal open loop frequency response functions $L_0(i\omega)$ in case (6.61) ($\Delta_M = 0.1$ and $\Delta_c = 0.05$).

	Minimum value	Nominal value	Maximum value
$PM_0\ (deg)$	47.803	52.516	56.745
$\omega_{cg0}\ (rad/s)$	7.3521	9.3881	12.139
$GM_0\ (dB)$	10.256	18.955	23.253
$\omega_{-\pi}\ (rad/s)$	66.384	75.642	85.866

6.4.2.3 Case of varying coefficients $\Delta_M = 0.1$ and $\Delta_c = 0.1$

Studying the case (6.62) ($\Delta_M = 0.1$ and $\Delta_c = 0.1$) in the same way we obtain for the all $2^{(3+4+2)} = 512$ extremal cases of the open loop transfer function $L_0(s)$ and their respective frequency response function the summary representation of their Bode diagrams in Figure 6.20 and summary analysis of the respective stability margins in Table 6.10. Thus the minimum value of the critical phase coupling angle here is $\underline{\gamma}_{cr} = 46.108\ deg$ (6.66).

Analogically with the consideration in the previous Section 6.4.2.2 the conclusion is that in this third case (6.62) (Δ_M= 0.1 and Δ_c= 0.1) of varying coefficients of the open loop transfer function $L_0(s)$ (6.4) the spatial closed loop with phase coupling between the channels is robust asymptotically stable when the phase coupling angle γ_0 is within the interval of stability $\left(-\underline{\gamma}_{cr}, \underline{\gamma}_{cr}\right)$ (6.64) where $\underline{\gamma}_{cr}$ represents now (6.66) $\underline{\gamma}_{cr} = 46.108\ deg$.

$$\underline{\gamma}_{cr} = \min(\gamma_{cr}) = \min(PM_0) = 46.108\ deg \qquad (6.66)$$

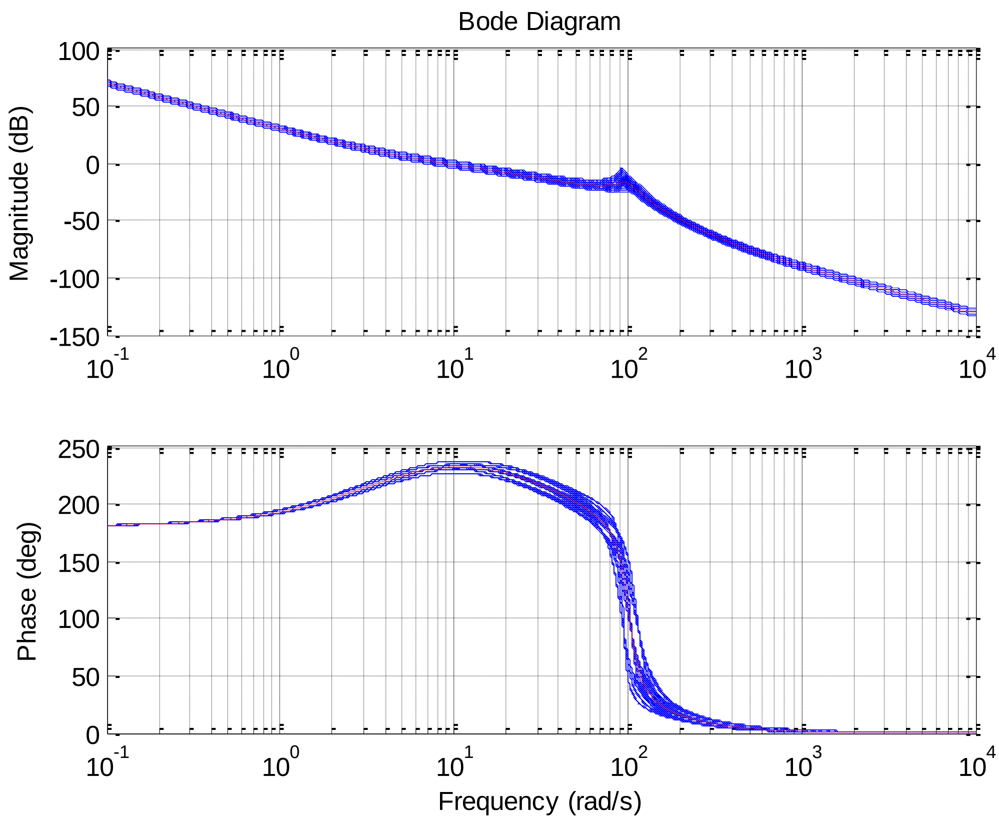

Figure 6.20 Summary representation of all extremal Bode diagrams of $L_0(i\omega)$ in case (6.62) (Δ_M= 0.1 and Δ_c= 0.1) alongside with the nominal Bode diagram of $L_0(i\omega)$.

Table 6.10 Summary of the stability margins by all extremal open loop frequency response functions $L_0(i\omega)$ in case (6.62) ($\Delta_M = 0.1$ and $\Delta_c = 0.1$).

	Minimum value	**Nominal value**	**Maximum value**
$PM_0\ (deg)$	46.108	52.516	57.72
$\omega_{cg0}\ (rad/s)$	6.8229	9.3881	13.139
$GM_0\ (dB)$	9.4228	18.955	24.196
$\omega_{-\pi}\ (rad/s)$	66.171	75.642	85.902

6.4.3 Performance of the robust asymptotically stable classical spatial closed loop system with phase coupling between the channels

In order to study the performance of the spatial closed loop system with phase coupling between the channels and with varying parameters there have been carried out many experiments which simulate varying the coefficients of the open loop transfer function within their lower and upper limits and taking its extremal representations as well as varying the phase coupling angle within its already determined interval of stability guaranteeing the robustness of the closed loop system. The existence of the external disturbances is excluded.

Figure 6.21 shows a summary of all extremal trajectories in the picture plane of the spatial closed loop system with phase coupling between the channels at different values of the phase coupling angle γ_0 within the interval of robust stability $\left(-\underline{\gamma}_{cr}, \underline{\gamma}_{cr}\right)$ for the case (6.55) ($\Delta_M = 0.1$ and $\Delta_c = 0$) whose robust stability is studied in Section 6.4.2.1 “Case of varying coefficients $\Delta_M = 0.1$ and $\Delta_c = 0$”. A summary of the maximum settling times $\bar{t}_s$ of all extremal representations of the system at each one case of the angle γ_0 within the interval of robust stability $\left(-\underline{\gamma}_{cr}, \underline{\gamma}_{cr}\right)$ is shown in Table 6.11 where the settling time of the nominal case $t_s^* = 0.53\ s$ (t_s^* represents the settling time of the one-dimensional closed loop system with nominal parameters which is identical with the settling time of the classical spatial closed loop system at phase coupling angle $\gamma_0 = 0$).

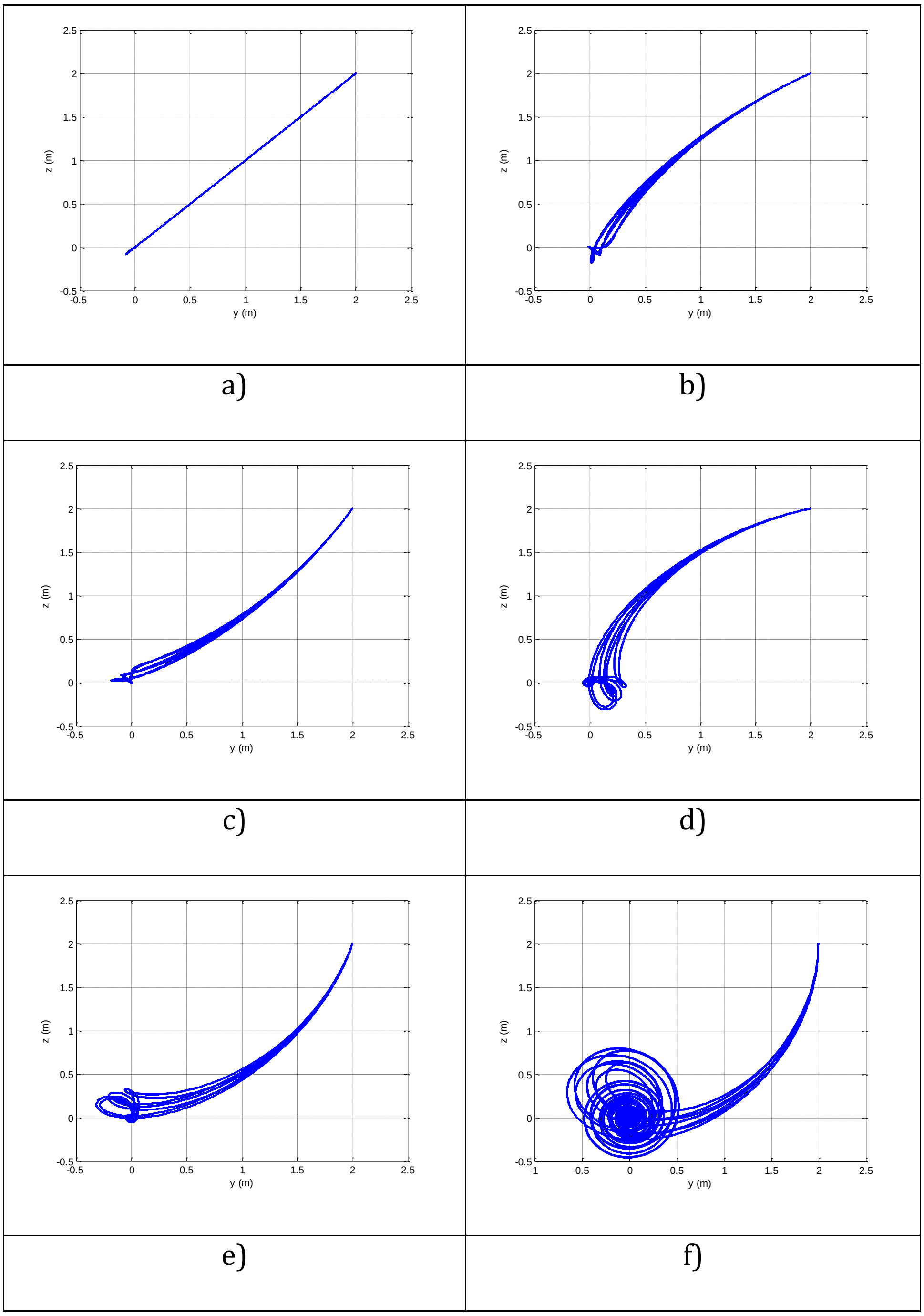

Figure 6.21 Summary of all extremal trajectories in the picture plane of the classical spatial closed loop system with phase coupling between the channels at different values of the phase coupling angle γ_0 within the interval of robust stability $\left(-\underline{\gamma}_{cr}, \underline{\gamma}_{cr}\right)$, $\underline{\gamma}_{cr} = 48.985$ deg. (6.63), guaranteeing robust asymptotic stability of the system: a) $\gamma_0 = 0$; b) $\gamma_0 = -15$ deg.; c) $\gamma_0 = 15$ deg.; d) $\gamma_0 = -30$ deg.; e) $\gamma_0 = 30$ deg.; f) $\gamma_0 = 45$ deg.

Table 6.11 Summary of the maximum values of the settling times $\bar{t}_s$ of all extremal transition processes of the spatial closed loop system with phase coupling between the channels at different values of the phase coupling angle γ_0 within the interval of robust stability $\left(-\underline{\gamma}_{cr}, \underline{\gamma}_{cr}\right)$, $\underline{\gamma}_{cr} = 48.985$ deg. (6.63) guaranteeing robust asymptotic stability of the system.

$\gamma_0\ (deg)$	$\gamma_0 = 0$	$\gamma_0 = -15$	$\gamma_0 = 15$	$\gamma_0 = -30$	$\gamma_0 = 30$	$\gamma_0 = 45$
$\frac{\bar{t}_s}{t_s^*}$ (%)	106.88	167.03	167.03	188.96	188.96	626.69

The presented results illustrate once again the fact that the performance of the classical closed loop spatial guidance system is acceptable at values of the phase coupling angle around zero and far away from the determined boundaries of its interval of stability. Except the increasing oscillations and spiraling alongside with an increase of the overshooting/falling the settling time increases drastically too when there is an increase of the phase coupling between the channels. For the presented example a phase coupling within $[-15, 15]$ deg. could be considered as acceptable. At $|\gamma_0| = 15$ deg. the maximum settling time $\bar{t}_s$ of all extremal representations of the open loop transfer function becomes 167.03 (%) versus the settling time in the nominal case. The further increase of $|\gamma_0|$ (but still keeping $|\gamma_0| < \underline{\gamma}_{cr}$) worsens the performance of the spatial closed loop guidance system in an unacceptable way though this closed loop system stays robust asymptotically stable.

6.4.3.1 Summary effect of all considered external disturbances in case of varying coefficients of the open loop transfer function $L_0(s)$ and applying the missile weight compensation technique

Let us employ the technique of compensation of the missile weight from Section 6.1.2.3 "Inclusion of a feedforward control for the missile weight compensation" for the case of varying coefficients of the open loop transfer function $L_0(s)$ and phase coupling between the channels. Thus the variable z_m (6.36) is formed by the respective nominal parameters and becomes (3.64). The complex form of the guidance law (6.32) becomes (6.68) whose Laplace transform is (6.69). The spatial closed loop guidance system with the external disturbances (6.34) and modified guidance law (6.69) represents the equations (6.8), (6.34) and (6.69). We obtain for the steady state of this system (6.70).

$z_m = z + \left(\dfrac{-g}{k_c^* \dfrac{N^*(0)}{D^*(0)}}\right)$	(6.67)
$u_p = -k_c(T_c\dot{p} + p) + i(-k_c)\left(\dfrac{-g}{k_c^* \dfrac{N^*(0)}{D^*(0)}}\right)1(t)$	(6.68)
$u_p(s) = -k_c(T_c s + 1)p(s) + i(-k_c)\left(\dfrac{-g}{k_c^* \dfrac{N^*(0)}{D^*(0)}}\right)\dfrac{1}{s}$	(6.69)
$p(\infty) = y(\infty) + iz(\infty)$, $y(\infty) = -\sin\gamma_0 \dfrac{g}{k_c\left(\dfrac{N(0)}{D(0)}\right)} + \cos\gamma_0 \dfrac{2\dot{\beta}_{LOS}V_M}{k_c\left(\dfrac{N(0)}{D(0)}\right)}$, $z(\infty) = g\left(\dfrac{1}{k_c^*\left(\dfrac{N^*(0)}{D^*(0)}\right)} - \dfrac{\cos\gamma_0}{k_c\left(\dfrac{N(0)}{D(0)}\right)}\right) - \sin\gamma_0 \dfrac{2\dot{\beta}_{LOS}V_M}{k_c\left(\dfrac{N(0)}{D(0)}\right)}$	(6.70)

Let us suppose the target in non-maneuvering. The steady states $y(\infty)$ and $z(\infty)$ from (6.70) become (6.71). Their estimations are (6.72) - (6.75). For the case of varying coefficients (6.55) (Δ_M= 0.1 and Δ_c= 0) with the respective data (6.56), (6.57) and the data from Table 6.8 having in mind $\overline{\gamma}_{cr} = \overline{PM}_0$ the numerical values of the estimations (6.72) - (6.75) represent (6.76).

$y(\infty) = -\sin\gamma_0 \dfrac{g}{k_c\left(\dfrac{N(0)}{D(0)}\right)}$, $z(\infty) = g\left(\dfrac{1}{k_c^*\left(\dfrac{N^*(0)}{D^*(0)}\right)} - \dfrac{\cos\gamma_0}{k_c\left(\dfrac{N(0)}{D(0)}\right)}\right)$	(6.71)

$\min y(\infty) > -\sin\overline{\gamma}_{cr}\dfrac{g}{\underline{k}_c\left(\dfrac{\underline{b}_{M2}}{\overline{\overline{a}}_{M3}}\right)} = -\sin\overline{\gamma}_{cr}\dfrac{g}{k_c^*(1-\Delta_c)\left(\dfrac{b_{M2}^*(1-\Delta_M)}{a_{M3}^*(1+\Delta_M)}\right)},$ $\min y(\infty) > -\sin\overline{\gamma}_{cr}\dfrac{g}{k_c^*\left(\dfrac{b_{M2}^*}{a_{M3}^*}\right)}\left(\dfrac{(1+\Delta_M)}{(1-\Delta_c)(1-\Delta_M)}\right)$	(6.72)
$\max y(\infty) < \sin\overline{\gamma}_{cr}\dfrac{g}{k_c^*\left(\dfrac{b_{M2}^*}{a_{M3}^*}\right)}\left(\dfrac{(1+\Delta_M)}{(1-\Delta_c)(1-\Delta_M)}\right)$	(6.73)
$\min z(\infty) \geq g\left(\dfrac{1}{k_c^*\left(\dfrac{N^*(0)}{D^*(0)}\right)} - \dfrac{\cos 0}{\underline{k}_c\left(\dfrac{\underline{b}_{M2}}{\overline{\overline{a}}_{M3}}\right)}\right),$ $\min z(\infty) \geq \dfrac{g}{k_c^*\left(\dfrac{N^*(0)}{D^*(0)}\right)}\left(1-\dfrac{(1+\Delta_M)}{(1-\Delta_c)(1-\Delta_M)}\right)$	(6.74)
$\max z(\infty) < \dfrac{g}{k_c^*\left(\dfrac{N^*(0)}{D^*(0)}\right)}\left(1-\cos\overline{\gamma}_{cr}\dfrac{(1-\Delta_M)}{(1+\Delta_c)(1+\Delta_M)}\right)$	(6.75)
$-0.28 < y(\infty) < 0.28\ (m)$ $-0.06 < z(\infty) < 0.15\ (m)$	(6.76)

6.4.4 Robustness of the spatial closed loop system with the SAE2DPDGL and the feedforward control for the missile weight compensation

In order to study the robustness of the synthesized spatial closed loop system with the SAE2DPDGL we suppose the varying coefficients of the open loop transfer function $L_0(s)$ (6.4) are according to the case (6.55) ($\Delta_M = 0.1$ and $\Delta_c = 0$) with the respective data (6.56), (6.57). The simulation studies of the nominal case presented in Section 6.3 (page 140) show that the interval of stability with acceptable performance indices of the new guidance system with the SAE2DPDGL is shrunk to (6.43). Thus in order to guarantee an acceptable system performance in case of varying coefficients according to the case (6.55) ($\Delta_M = 0.1$ and $\Delta_c = 0$) the study here is focused on a further proper determination of the width of the above interval (6.43) in the considered case of varying coefficients.

In order to obtain more realistic results the simulations are carried out taking into account the missile gravity acceleration as an external disturbance. The guidance law represents the SAE2DPDGL but with inclusion of the considered feedforward control for the missile weight compensation which guidance law is named SAE2DPDGL with (w) missile (M) weight (W) compensation (C) – SAE2DPDGLwMWC.

The performance of the closed loop guidance system with the SAE2DPDGLwMWC regarding the phase coupling angle γ_0 in case of varying coefficients of the open loop transfer function is illustrated by four cases of initial trajectory point (y_0, z_0) in the picture plane supposing the target is non-maneuvering: Figure 6.22 with Table 6.12 when the initial trajectory point $(y_0, z_0) = (2{,}2)$; Figure 6.23 with Table 6.13 when $(y_0, z_0) = (1{,}1)$; Figure 6.24 with Table 6.14 when $(y_0, z_0) = (0.5{,}0.5)$; Figure 6.25 with Table 6.15 when $(y_0, z_0) = (0.25{,}0.25)$.

Note that the center of the ε_r area due to the inclusion of the proposed feedforward control is shifted from the plane origin to the point (0, 0.3) in the picture plane according to (6.36), (6.37) and (6.67). The first three initial trajectory points above $(y_0, z_0) = (2{,}2), (1{,}1), (0.5{,}0.5)$ are outside the ε_r area of the SAE2DPDGLwMWC while $(y_0, z_0) = (0.25{,}0.25)$ is within the ε_r area. The rectangles within the ε_r areas in the above figures marked with a solid red line represent the steady state areas of all extremal system trajectories in the picture plane and correspond to the data with respect to $\min y(\infty)$, $\max y(\infty)$, $\min z(\infty)$ and $\max z(\infty)$ from the respective tables above. Note that all considered above cases regarding the phase coupling angle are outside the classical interval of robust stability $\left(-\underline{\gamma}_{cr}, \underline{\gamma}_{cr}\right)$. The established here interval of robust stability of the closed loop guidance system with the SAE2DPDGLwMWC for the case of varying coefficients (6.55) (Δ_M= 0.1 and Δ_c= 0) is wider than $\left[-1.8\underline{\gamma}_{cr}, 1.8\underline{\gamma}_{cr}\right]$. The spatial closed loop guidance system shows an excellent performance within the range of γ_0 (6.78). This interval is more than four times wider than the width of the interval with acceptable performance of the classical spatial closed loop guidance system.

$\gamma_0 \in \left[-1.8\underline{\gamma}_{cr}, 1.8\underline{\gamma}_{cr}\right]$	(6.77)
$\gamma_0 \in \left[-1.4\underline{\gamma}_{cr}, 1.4\underline{\gamma}_{cr}\right] \approx [-69, 69]$ deg.	(6.78)

6.5 Conclusions

In order to validate the far better effectiveness of the spatial closed loop guidance system based on the synthesized new guidance laws versus the classical spatial closed loop guidance system with phase coupling between the channels based on the classical PD guidance laws a thorough analysis and synthesis along with a great number simulation experiments have been carried out with a hypothetical but more realistic model of an ATGM. The model takes into consideration the transfer functions of the yaw and pitch channels (the horizontal and vertical channels) and the phase coupling between them. The transfer functions of both channels take into account the missile fin control actuation system, aerodynamics, missile velocity, the CLOS kinematic relations and existence of some external disturbances as the missile weight, a target's movement and a wind gust. The robustness of the new spatial closed loop guidance system has been studied. The stages of the study represent practically a methodology for upgrading the classical spatial closed loop guidance system with a new one based on the new guidance laws.

6.5.1 Short description of the methodology for upgrading the classical spatial guidance and control closed loop system to a new one based on the new guidance laws

6.5.1.1 Stage 1

The first stage includes an analysis and synthesis of the classical one-dimensional closed loop guidance and control system with classical PD law.

6.5.1.2 Stage 2

The second stage represents an analysis and synthesis of the classical spatial closed loop guidance and control system with phase coupling between the channels. This stage includes:

- Stability analysis of the spatial closed loop guidance system with phase coupling between the channels;
- Analysis of the influence of the external disturbances such as the missile weight, the target's movement, the wind gust, et cetera not only separately but also their summary effect on the performance of the spatial closed loop guidance system;
- Inclusion of a feedforward control for the missile weight compensation.

6.5.1.3 Stage 3

The aim of this stage is the design of the new spatial closed loop guidance system with phase coupling between the channels on the basis of the AE2DPDGL. An initial determination of the new parameters of the new guidance law is done: the ε_r area radius; the time constant T_φ; the coefficient k_ψ of the adaptive control of the angle ψ of the AE2DPDGL vector rotation. By a study of the performance of the closed loop guidance and control system with the AE2DPDGL it is determined: the width of the new extended interval of stability regarding the angle of the phase coupling between the channels; the width of the interval with acceptable performance with respect to the phase coupling angle for a variety of initial trajectory points in the picture plane and system states not only outside the ε_r area but also within it.

A conclusion is made regarding the need of an additional improvement of the spatial closed loop guidance and control system's performance by the SAE2DPDGL in order to cope even in a better way with the system cases when the initial trajectory points are outside but close to the boundary of the ε_r area and within the ε_r area around the picture plane origin.

6.5.1.4 Stage 4

An initial determination of the coefficient k_ψ of the SA2DPDGL as a part of the SAE2DPDGL is done regarding the initial trajectory points within the ε_r area around the picture plane origin. Then the performance of the spatial closed loop guidance and control system with the SAE2DPDGL is studied for the variety of initial trajectory points not only outside but also within the ε_r area around the picture plane origin with respect to the phase coupling angle.

As a result the new parameters of the SAE2DPDGL are determined: the ε_r area radius; the time constant T_φ; the coefficient $k_{\psi 2}$ of the adaptive control of the angle ψ of the AE2DPDGL vector rotation; the coefficient $k_{\psi1}$ of the SA2DPDGL. It is established the range of the phase coupling angle where the spatial closed loop guidance system with phase coupling between the channels and controlled by the SAE2DPDGL has acceptable performance indices.

6.5.1.5 Stage 5

The studies here are aimed at a final tuning of the parameters of the SAE2DPDGL by carrying out the full set of simulations of the spatial closed loop guidance and control system with phase coupling between the channels and controlled by the SAE2DPDGL but with the included feedforward control for the missile weight compensation named SAE2DPDGLwMWC. This set of experiments consists of all extremal cases of varying coefficients, a full variety of initial conditions and a full variety of phase coupling angles. In order to achieve an excellent performance in all extremal cases of varying coefficients and variety of exemplary initial conditions within a maximum possible range of the phase coupling angle the emphasis here is on the proper adjustment of the coefficients of the adaptive control of the angle ψ of the guidance law vector rotation: the coefficient $k_{\psi2}$ of the AE2DPDGL and the coefficient $k_{\psi1}$ of the SA2DPDGL.

The expected results are: the final values of the nominal parameters of the SAE2DPDGLwMWC; the established new range of the phase coupling angle where the new spatial closed loop guidance and control system with phase coupling between the channels has a guaranteed acceptable performance within the predetermined range of varying coefficients and regardless of the phase coupling angle and initial conditions.

6.5.2 Benefits of the system upgrading with the SAE2DPDGLwMWC

If we have to describe the new spatial closed loop guidance and control system with phase coupling between the channels and controlled by the SAE2DPDGLwMWC in one word this is excellence. The system possesses:

- Robust asymptotic stability within a very broad range of phase coupling angles compared to the classical closed loop guidance system.

The established here interval of robust stability of the closed loop guidance and control system with the SAE2DPDGLwMWC for the case of varying coefficients

(6.55) (Δ_M= 0.1 and Δ_c= 0) is $\left[-1.8\underline{\gamma}_{cr}, 1.8\underline{\gamma}_{cr}\right]$ (6.77). This interval is 1.8 times wider than the classical interval of robust stability $\left(-\underline{\gamma}_{cr}, \underline{\gamma}_{cr}\right)$ (6.64) where $\underline{\gamma}_{cr}$ represents (6.63) $\underline{\gamma}_{cr} = 48.985$ deg.

- Excellent performance indices within a very broad range of the phase coupling angle compared to the classical closed loop guidance system.

The classical system provides acceptable performance when the phase coupling between the channels is around $\gamma_0 = 0$ and far from the boundaries of its stability interval $(-\gamma_{cr}, \gamma_{cr})$ while the new guidance and control system possesses an excellent performance even beyond the boundaries of the classical interval $(-\gamma_{cr}, \gamma_{cr})$. The established interval with excellent performance for the case of varying coefficients (6.55) (Δ_M= 0.1 and Δ_c= 0) with respect to the considered example represents $\left[-1.4\underline{\gamma}_{cr}, 1.4\underline{\gamma}_{cr}\right] \approx [-69, 69]$ deg. (6.78). This interval is more than four times wider than the classical interval with acceptable performance.

These advantages are due to the special design of the SAE2DPDGL. The SAE2DPDGL straightens the system trajectory in the picture plane outside the ε_r area around the picture plane origin. It fights the spiraling outside the ε_r area caused by the existence of phase coupling between the channels and by the existence of non-proportional to each other initial conditions by compensating for the phase coupling between the channels and straightening the system trajectory. When the trajectory point is within the ε_r area the SAE2DPDGL compensates only for the phase coupling angle between the channels so that the summary phase coupling between the channels strives to zero.

- High steady state accuracy.

The inclusion of a feedforward control for the missile weight compensation into the guidance law so that the SAE2DPDGL becomes SAE2DPDGLwMWC provides a high steady state accuracy for the above broad range of the phase coupling angle in the considered case of varying coefficients. The simulation experiments for the full set of extremal varying coefficients, initial trajectory points and phase coupling angles fully comply with the estimations: $-0.28 < y(\infty) < 0.28\ (m), -0.06 < z(\infty) < 0.15\ (m)$ (6.67).

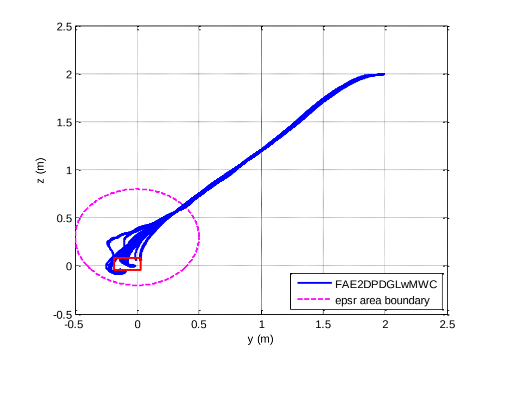

a) $\gamma_0 = -\underline{\gamma}_{cr} = -48.99$ deg.;

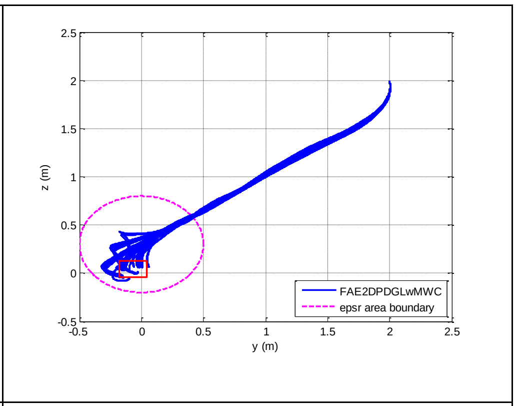

b) $\gamma_0 = 1.2\underline{\gamma}_{cr} = 58.78$ deg.;

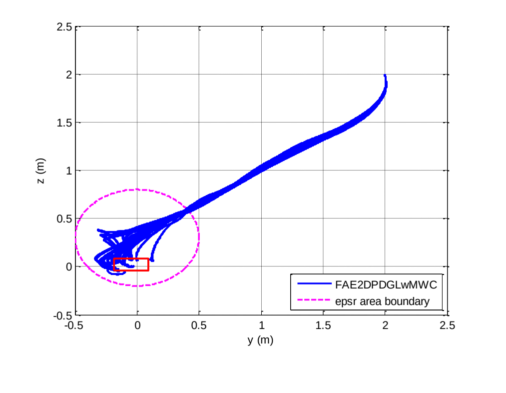

c) $\gamma_0 = 1.3\underline{\gamma}_{cr} = 63.68$ deg.;

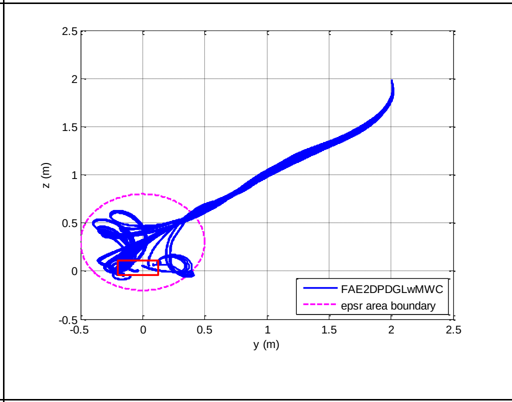

d) $\gamma_0 = 1.4\underline{\gamma}_{cr} = 68.58$ deg.;

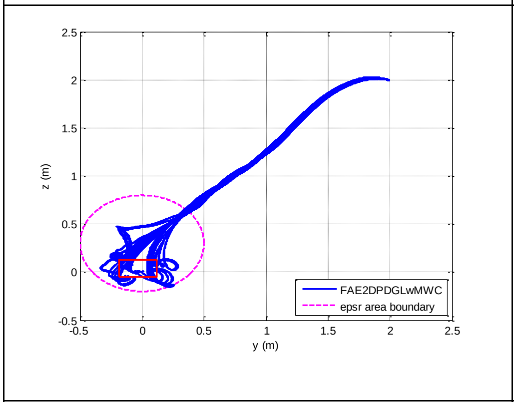

e) $\gamma_0 = -1.4\underline{\gamma}_{cr} = -68.58$ deg.;

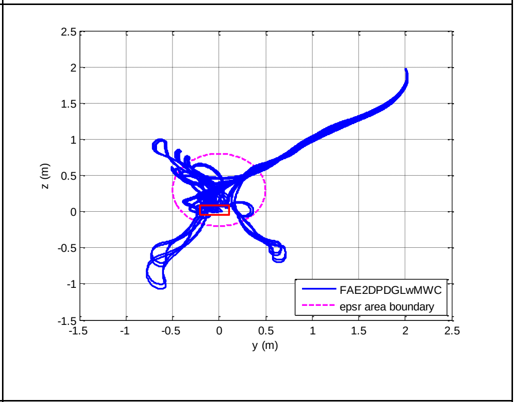

f) $\gamma_0 = 1.5\underline{\gamma}_{cr} = 73.48$ deg.

Figure 6.22 Summary of all extremal trajectories in the picture plane of the spatial closed loop system with the SAE2DPDGLwMWC with initial point $(y_0, z_0) = (2, 2)$ at different values of the phase coupling angle γ_0 : a) $\gamma_0 = -\underline{\gamma}_{cr} = -48.99$ deg.; b) $\gamma_0 = 1.2\underline{\gamma}_{cr} = 58.78$ deg.; c) $\gamma_0 = 1.3\underline{\gamma}_{cr} = 63.68$ deg.; d) $\gamma_0 = 1.4\underline{\gamma}_{cr} = 68.58$ deg.; e) $\gamma_0 = -1.4\underline{\gamma}_{cr} = -68.58$ deg.; f) $\gamma_0 = 1.5\underline{\gamma}_{cr} = 73.48$ deg.

Table 6.12 Summary of some performance indicators of the spatial closed loop guidance system with the SAE2DPDGLwMWC when the initial trajectory point in the picture plane $(y_0, z_0) = (2, 2)$ regarding the phase coupling angle γ_0.

$\boldsymbol{\gamma_0}$	$\mathbf{0}$	$-\underline{\gamma}_{cr}$	$\mathbf{1.2}\underline{\gamma}_{cr}$	$\mathbf{1.3}\underline{\gamma}_{cr}$	$\mathbf{1.4}\underline{\gamma}_{cr}$	$-\mathbf{1.4}\underline{\gamma}_{cr}$	$\mathbf{1.5}\underline{\gamma}_{cr}$
γ_0 (deg.)	0	-48.99	58.78	63.68	68.58	-68.58	73.48
$\frac{t_s}{t_s^*}$ (%)	100	143	147	157	168	156	274
$\max(n_y, n_z)$	7	14	20	22	23	19	25
$\frac{\max(n_y, n_z)}{\max(n_y^*, n_z^*)}$ (%)	100	200	286	314	329	271	357
$\max\lvert\gamma_{1ss}\rvert$ (deg.)	0	40	43	37	37	44	35
$\min y$ (m)	-0.03	-0.25	-0.32	-0.34	-0.4	-0.33	-0.78
$\frac{\lvert\min y\rvert}{y_0}$ (%) Overfalling with respect to y	1.4	12.5	16.0	17.0	20.0	16.5	39.0
$\min z$ (m)	-0.03	-0.09	-0.08	-0.08	-0.09	-0.15	-1.07
$\frac{\lvert\min z\rvert}{z_0}$ (%) Overfalling with respect to z	1.4	4.5	4.0	4.0	4.5	7.5	53.5
$\min y(\infty)$ (m)	0	-0.19	-0.18	-0.19	-0.20	-0.18	-0.21
$\max y(\infty)$ (m)	0	0.03	0.05	0.09	0.13	0.12	0.11
$\min z(\infty)$ (m)	0	-0.05	-0.04	-0.04	-0.04	-0.05	-0.04
$\max z(\infty)$ (m)	0	0.08	0.12	0.09	0.11	0.13	0.09

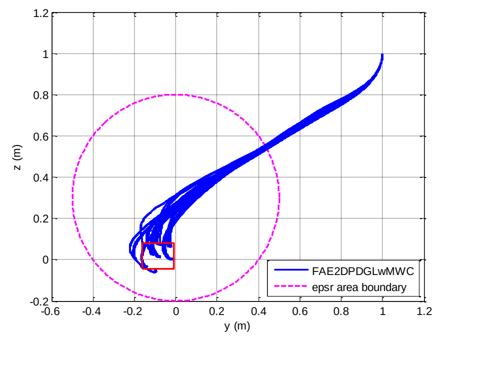

a) $\gamma_0 = \underline{\gamma}_{cr} = 48.99$ deg.;

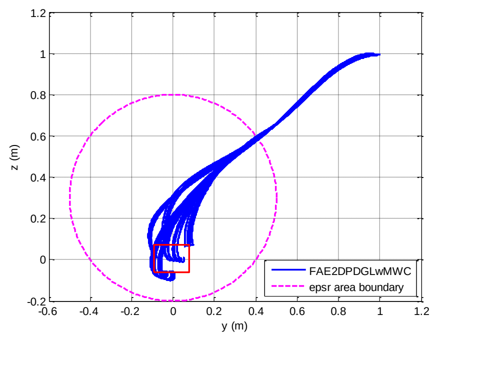

b) $\gamma_0 = -1.2\underline{\gamma}_{cr} = -58.78$ deg.;

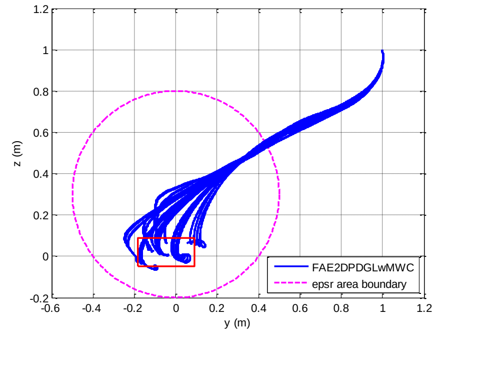

c) $\gamma_0 = 1.4\underline{\gamma}_{cr} = 68.58$ deg.;

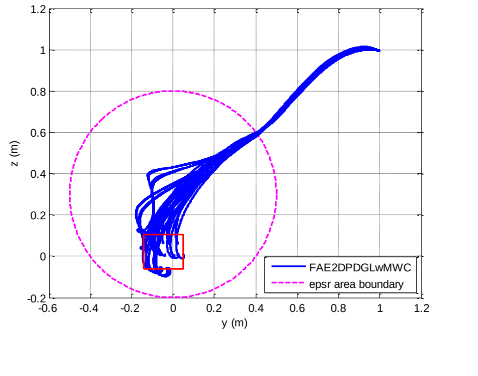

d) $\gamma_0 = -1.5\underline{\gamma}_{cr} = -73.48$ deg.;

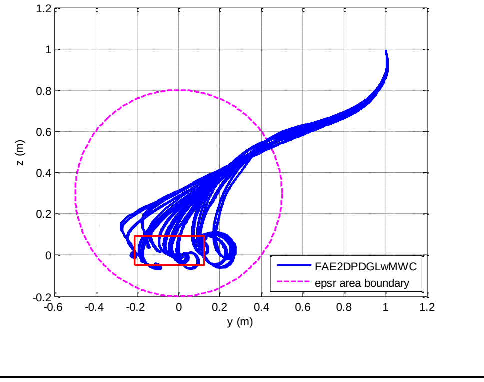

e) $\gamma_0 = 1.7\underline{\gamma}_{cr} = 83.27$ deg.;

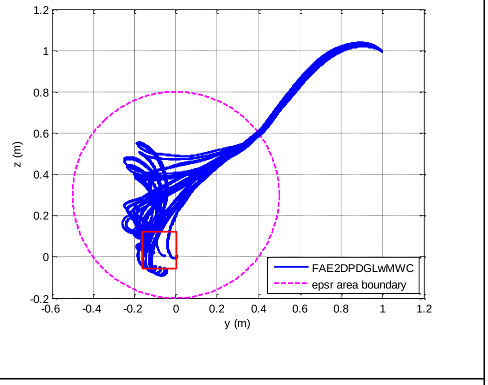

f) $\gamma_0 = -1.8\underline{\gamma}_{cr} = -88.17$ deg.

Figure 6.23 Summary of all extremal trajectories in the picture plane of the spatial closed loop system with the SAE2DPDGLwMWC with initial point $(y_0, z_0) = (1, 1)$ at different values of the phase coupling angle γ_0 : a) $\gamma_0 = \underline{\gamma}_{cr} = 48.99$ deg.; b) $\gamma_0 = -1.2\underline{\gamma}_{cr} = -58.78$ deg.; c) $\gamma_0 = 1.4\underline{\gamma}_{cr} = 68.58$ deg.; d) $\gamma_0 = -1.5\underline{\gamma}_{cr} = -73.48$ deg.; e) $\gamma_0 = 1.7\underline{\gamma}_{cr} = 83.27$ deg.; f) $\gamma_0 = -1.8\underline{\gamma}_{cr} = -88.17$ deg.

Table 6.13 Summary of some performance indicators of the spatial closed loop guidance system with the SAE2DPDGLwMWC when the initial trajectory point in the picture plane $(y_0, z_0) = (1, 1)$ regarding the phase coupling angle γ_0.

γ_0	0	$\underline{\gamma}_{cr}$	$-1.2\underline{\gamma}_{cr}$	$1.4\underline{\gamma}_{cr}$	$-1.5\underline{\gamma}_{cr}$	$1.7\underline{\gamma}_{cr}$	$-1.8\underline{\gamma}_{cr}$
γ_0 (deg.)	0	48.99	−58.78	68.58	−73.48	83.27	−88.17
$\frac{t_s}{t_s^*}$ (%)	100	145	132	146	142	150	211
$\max(n_y, n_z)$	3.5	8	6	12	9	14	15
$\frac{\max(n_y, n_z)}{\max(n_y^*, n_z^*)}$ (%)	100	229	172	343	257	400	429
$\max\lvert\gamma_{1ss}\rvert$ (deg.)	0	31	19	31	36	36	42
$\min y$ (m)	−0.01	−0.22	−0.12	−0.25	−0.18	−0.28	−0.26
$\frac{\lvert\min y\rvert}{y_0}$ (%) Overfalling with respect to y	1.4	22.0	12.0	25.0	18.0	28.0	26.0
$\min z$ (m)	−0.01	−0.06	−0.10	−0.07	−0.10	−0.07	−0.09
$\frac{\lvert\min z\rvert}{z_0}$ (%) Overfalling with respect to z	1.4	6.0	10.0	7.0	10.0	7.0	9.0
$\min y(\infty)$ (m)	0	−0.16	−0.09	−0.19	−0.14	−0.21	−0.16
$\max y(\infty)$ (m)	0	−0.01	0.08	0.09	0.05	0.12	0.01
$\min z(\infty)$ (m)	0	−0.05	−0.06	−0.05	−0.06	−0.05	−0.06
$\max z(\infty)$ (m)	0	0.08	0.07	0.09	0.10	0.09	0.12

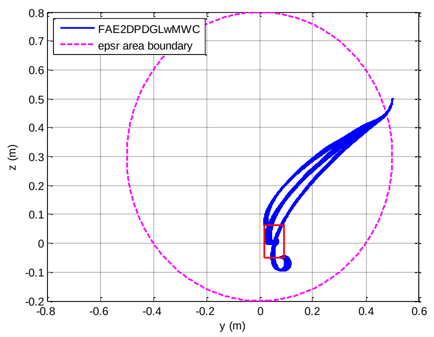

a) $\gamma_0 = \underline{\gamma}_{cr} = 48.99$ deg.;

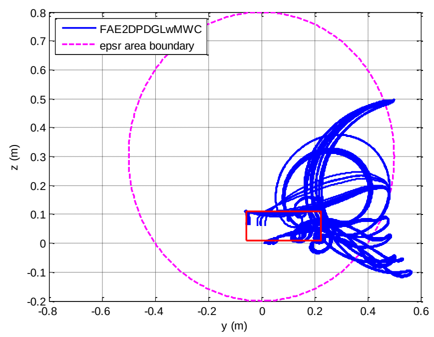

b) $\gamma_0 = -1.2\underline{\gamma}_{cr} = -58.78$ deg.;

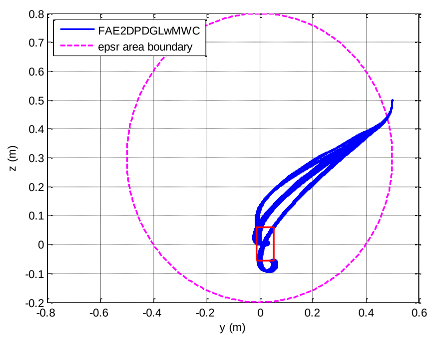

c) $\gamma_0 = 1.4\underline{\gamma}_{cr} = 68.58$ deg.;

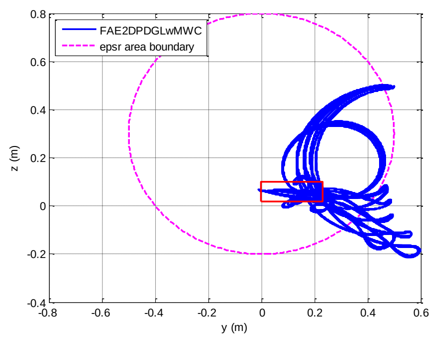

d) $\gamma_0 = -1.5\underline{\gamma}_{cr} = -73.48$ deg.;

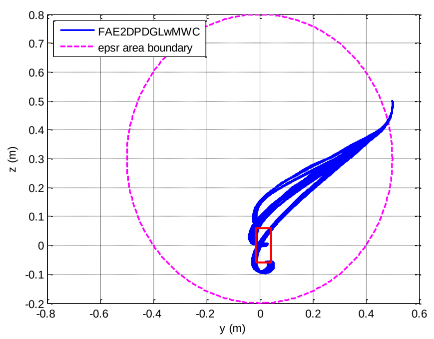

e) $\gamma_0 = 1.7\underline{\gamma}_{cr} = 83.27$ deg.;

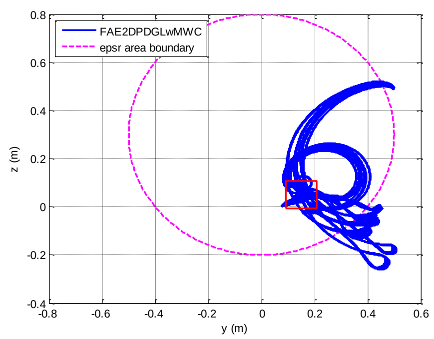

f) $\gamma_0 = -1.8\underline{\gamma}_{cr} = -88.17$ deg.

Figure 6.24 Summary of all extremal trajectories in the picture plane of the spatial closed loop system with the SAE2DPDGLwMWC with initial point $(y_0, z_0) = (0.5, 0.5)$ at different values of the phase coupling angle γ_0 : a) $\gamma_0 = \underline{\gamma}_{cr} = 48.99$ deg.; b) $\gamma_0 = -1.2\underline{\gamma}_{cr} = -58.78$ deg.; c) $\gamma_0 = 1.4\underline{\gamma}_{cr} = 68.58$ deg.; d) $\gamma_0 = -1.5\underline{\gamma}_{cr} = -73.48$ deg.; e) $\gamma_0 = 1.7\underline{\gamma}_{cr} = 83.27$ deg.; f) $\gamma_0 = -1.8\underline{\gamma}_{cr} = -88.17$ deg.

Table 6.14 Summary of some performance indicators of the spatial closed loop guidance system with the SAE2DPDGLwMWC when the initial trajectory point in the picture plane $(y_0, z_0) = (0.5, 0.5)$ regarding the phase coupling angle γ_0.

γ_0	$\mathbf{0}$	$\underline{\gamma}_{cr}$	$-1.2\underline{\gamma}_{cr}$	$1.4\underline{\gamma}_{cr}$	$-1.5\underline{\gamma}_{cr}$	$1.7\underline{\gamma}_{cr}$	$-1.8\underline{\gamma}_{cr}$
γ_0 (deg.)	0	48.99	−58.78	68.58	−73.48	83.27	−88.17
$\frac{t_s}{t_s^*}$ (%)	100	169	354	151	361	147	283
$\max(n_y, n_z)$	1.73	4	7	5	8	7	8
$\frac{\max(n_y, n_z)}{\max(n_y^*, n_z^*)}$ (%)	100	231	405	289	462	405	462
$\max\lvert\gamma_{1ss}\rvert$ (deg.)	0	15	39	9	40	7	37
$\min y$ (m)	−0.01	0.02	−0.06	−0.02	−0.01	−0.04	0.08
$\frac{\lvert\min y\rvert}{y_0}$ (%) Overfalling with respect to y	1.4	3.2	12.4	4.7	2.3	8.1	NO
$\min z$ (m)	−0.01	−0.10	−0.12	−0.10	−0.21	−0.10	−0.09
$\frac{\lvert\min z\rvert}{z_0}$ (%) Overfalling with respect to z	1.4	20.0	23.4	19.0	42.8	19.3	52.0
$\min y(\infty)$ (m)	0	0.02	−0.06	−0.01	−0.00	−0.02	0.09
$\max y(\infty)$ (m)	0	0.09	0.23	0.05	0.23	0.04	0.20
$\min z(\infty)$ (m)	0	−0.05	0.01	−0.06	0.02	−0.06	−0.00
$\max z(\infty)$ (m)	0	0.06	0.11	0.06	0.10	0.06	0.11

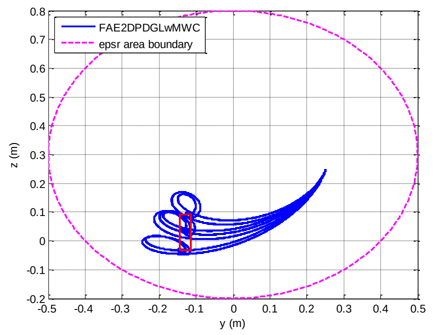

a) $\gamma_0 = \underline{\gamma}_{cr} = 48.99$ deg.;

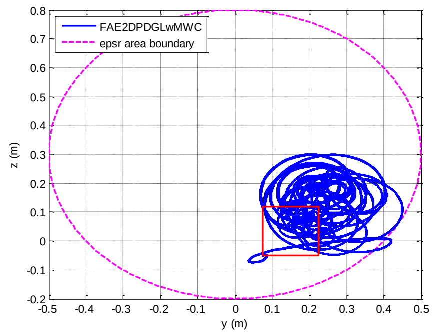

b) $\gamma_0 = -1.2\underline{\gamma}_{cr} = -58.78$ deg.;

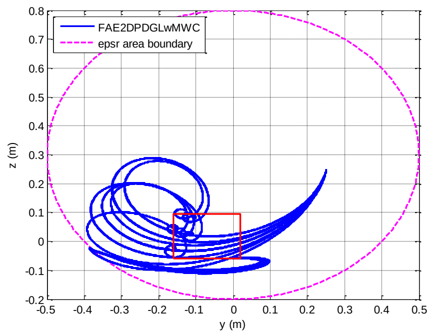

c) $\gamma_0 = 1.4\underline{\gamma}_{cr} = 68.58$ deg.;

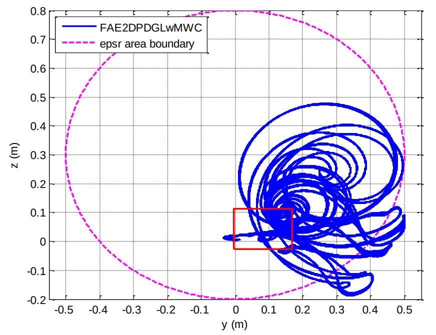

d) $\gamma_0 = -1.5\underline{\gamma}_{cr} = -73.48$ deg.;

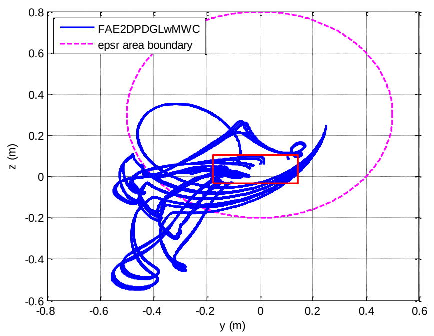

e) $\gamma_0 = 1.7\underline{\gamma}_{cr} = 83.27$ deg.;

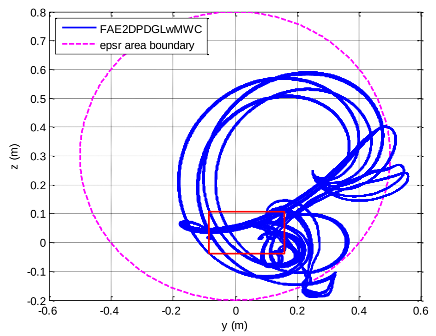

f) $\gamma_0 = -1.8\underline{\gamma}_{cr} = -88.17$ deg.

Figure 6.25 Summary of all extremal trajectories in the picture plane of the spatial closed loop system with the SAE2DPDGLwMWC with initial point $(y_0, z_0) = (0.25, 0.25)$ at different values of the phase coupling angle γ_0 : a) $\gamma_0 = \underline{\gamma}_{cr} = 48.99$ deg.; b) $\gamma_0 = -1.2\underline{\gamma}_{cr} = -58.78$ deg.; c) $\gamma_0 = 1.4\underline{\gamma}_{cr} = 68.58$ deg.; d) $\gamma_0 = -1.5\underline{\gamma}_{cr} = -73.48$ deg.; e) $\gamma_0 = 1.7\underline{\gamma}_{cr} = 83.27$ deg.; f) $\gamma_0 = -1.8\underline{\gamma}_{cr} = -88.17$ deg.

Table 6.15 Summary of some performance indicators of the spatial closed loop guidance system with the SAE2DPDGLwMWC when the initial trajectory point in the picture plane $(y_0, z_0) = (0.25, 0.25)$ regarding the phase coupling angle γ_0.

$\boldsymbol{\gamma_0}$	$\mathbf{0}$	$\underline{\boldsymbol{\gamma}}_{cr}$	$-1.2\underline{\boldsymbol{\gamma}}_{cr}$	$1.4\underline{\boldsymbol{\gamma}}_{cr}$	$-1.5\underline{\boldsymbol{\gamma}}_{cr}$	$1.7\underline{\boldsymbol{\gamma}}_{cr}$	$-1.8\underline{\boldsymbol{\gamma}}_{cr}$
γ_0 (deg.)	0	48.99	−58.78	68.58	−73.48	83.27	−88.17
$\frac{t_s}{t_s^*}$ (%)	100	166	865	262	659	412	384
$\max(n_y, n_z)$	1	2	4	5	9	13	12
$\frac{\max(n_y, n_z)}{\max(n_y^*, n_z^*)}$ (%)	100	200	400	500	900	1300	1200
$\max\lvert\gamma_{1ss}\rvert$ (deg.)	0	30	44	32	39	36	37
$\min y$ (m)	−0.004	−0.25	0.04	−0.39	−0.03	−0.56	−0.18
$\frac{\lvert\min y\rvert}{y_0}$ (%) Overfalling with respect to y	1.4	98.0	NO	157	13.5	223	73.6
$\min z$ (m)	−0.004	−0.05	−0.08	−0.11	−0.19	−0.55	−0.19
$\frac{\lvert\min z\rvert}{z_0}$ (%) Overfalling with respect to z	1.4	19.4	30.2	44.5	74.9	220	75.6
$\min y(\infty)$ (m)	0	−0.14	0.08	−0.16	−0.00	−0.18	−0.09
$\max y(\infty)$ (m)	0	−0.11	0.22	0.02	0.17	0.14	0.16
$\min z(\infty)$ (m)	0	−0.03	−0.05	−0.06	−0.03	−0.03	−0.04
$\max z(\infty)$ (m)	0	0.09	0.12	0.10	0.11	0.10	0.11

7 FINAL NOTES

The synthesis of the spatial command to the-line-of-sight anti-tank guided missile's (CLOS ATGM's) closed loop guidance system based on the presentation of the missile's trajectory equations in the $Y_L Z_L$-plane, the picture plane, in polar or pseudo-polar coordinates alongside with introducing a feedback linearization was proposed for the first time by the author dating back more than 20 years. This technique allows decoupling the missile dynamics into two new separated linear looking new channels with regard to the polar radius and the polar angle as well as straightening the missile trajectory in the $Y_L Z_L$-plane, the picture plane.

The accepted initially way of developing the original idea faces theoretical obstacles connected with the need to deal with the inverse trigonometric arctangent function and the smooth transition through the picture plane's origin. These obstacles are resolved partly by introducing pseudo-polar coordinates allowing also negative values of the polar radius as well as keeping the kinematic relations in Cartesian coordinates, but the theoretical stability justification of the new spatial closed loop guidance system remains open despite the promising simulation results.

The presented here set of five new command to line-of-sight (CLOS) guidance laws do overcome the previous theoretical issues. They all are nonlinear two-dimensional proportional-derivative guidance laws, where four of them are variable structure guidance laws but not sliding mode control laws. They possess the following main features.

It is proposed for the first time the approach of combining the advantages of joint application of both Cartesian and polar coordinates in the command to line-of-sight guidance law based on the presentation of the missile's trajectory equations in the $Y_L Z_L$-plane, the picture plane. Thus, alongside with a variable structure guidance law the following effects/benefits are achieved. The synthesis of two new separate linear looking channels with regard to the polar radius and polar angle, as well as the synthesis of two traditional horizontal and vertical channels at one application become possible.

For the first time, it is proposed the approach of dealing with the worsen performance indicators of the spatial closed loop system of a command to line-of-sight guided missile with losing system's stability while the transition process of putting the missile onto the line of sight observed as spiraling trajectory in the picture plane by dealing first with the case of no coupling between the control channels with next upgrade of the obtained control for the case with phase coupling between the horizontal and vertical control channels of the missile and providing global stability of the spatial closed loop system.

It is synthesized a new nonlinear variable structure guidance law (but no sliding mode control law) called „Expanded two-dimensional proportional-derivative guidance law" – E2DPDGL for the case of command to line-of-sight guided missile with no coupling between the channels which straightens the system trajectory in the $Y_L Z_L$-plane, the picture plane, in case of non-proportional to each other initial conditions at starting the controlled missile flight to the target. The global asymptotical stability of the spatial closed loop guidance system is theoretically rigorously proven by a specially synthesized for this purpose unique positive definite Lyapunov function. An improvement of the performance indices of the transition process of putting the missile onto the line-of-sight is achieved which results into an improvement of the near field operational range of the anti-tank guided missile's (ATGM's) system.

In order to deal effectively with the extremely unfavorable cases of spiraling system trajectory in the $Y_L Z_L$-plane, the picture plane, while the transition process of putting the missile onto the line-of-sight and losing system's stability due to the phase coupling between the horizontal and vertical channels caused by the phase coupling angle γ_0 as well as non-proportional to each other initial conditions a second new nonlinear adaptive variable structure guidance law (but no sliding mode control law) called "Adaptive expanded two-dimensional proportional-derivative guidance law" – AE2DPDGL is synthesized. The global stability of the spatial closed loop system with the adaptive expanded two-dimensional proportional-derivative guidance law (AE2DPDGL) is theoretically proven. An improvement of the performance indices of the transition process of putting the missile onto the line-of-sight in the picture plane by the adaptive expanded two-dimensional proportional-derivative guidance law (AE2DPDGL) is achieved which represents straightening the system trajectory in the picture plane overcoming the spiral type trajectory and losing system's stability caused by the angle γ_0 of phase coupling between the channels for a very broad range of the angle γ_0 and far beyond the classical narrow limitations for it. In the ideal case of the spatial closed loop guidance system with phase coupling between the channels this new range regarding the phase coupling angle γ_0 represents the whole interval $[-\pi, \pi]$.

In order to deal effectively but in a simple way with the extremely unfavorable cases of spiraling system trajectory in the $Y_L Z_L$ -plane, the picture plane, during the transition process of putting the missile onto the line-of-sight and losing system's stability in case of phase coupling between the horizontal and vertical channels caused by the phase coupling angle γ_0 as well as non-proportional to each other initial conditions a new simplified adaptive nonlinear command to line-of-sight guidance law called "Simplified adaptive two-dimensional proportional-derivative guidance law" – SA2DPDGL is synthesized. The SA2DPDGL represents the rotated summary vector of the two CPDGLs of y and z-channels in the complex plane by the angle ψ whose angular velocity $\dot{\psi}$ is directly proportional to an introduced index of disproportionality $\varphi_{1r} = \dot{z}y - \dot{y}z$ in m^2/s with a coefficient of proportionality k_ψ. The stability of the closed loop system with the SA2DPDGL is theoretically established.

In order to achieve an even better performance of the spatial closed loop guidance system with phase coupling between the horizontal and vertical missile channels caused by the phase coupling angle γ_0 while putting the missile onto the LOS by the AE2DPDGL the so called command to line-of-sight "Sophisticated adaptive Expanded Two-Dimensional Proportional-Derivative Guidance Law" – SAE2DPDGL is developed. This fourth new guidance law combines the benefits of the AE2DPDGL and the SA2DPDGL and reduces or ceases the transitions trough the predetermined ε_r area around the picture plane origin. The guidance law is a nonlinear variable structure guidance law but not sliding mode control law. It represents the AE2DPDGL outside the predetermined ε_r area around the picture plane origin while within the ε_r area the guidance law turns into the SA2DPDGL. As a result there is a full control of the guidance law's vector rotation in the complex plane in order to compensate for the phase coupling between the channels not only outside the ε_r area around the picture plane origin by the AE2DPDGL but also within it by the SA2DPDGL. The global stability of the spatial closed loop guidance system is theoretically proven. The SAE2DPDGL provides a better effectiveness of the spatial closed loop system with phase coupling between the horizontal and vertical channels compared to the the AE2DPDGL.

In order to achieve a better accuracy of the closed loop guidance system with the SAE2DPDGL with respect to the influence of the missile weight as an external disturbance a feedforward control for the missile weight compensation is included into the guidance law. The inclusion concerns only the input data for the guidance law. It represents a replacement of the vertical component of the missile position in the picture plane with a modified shifted value while the other input data for the guidance law representing the horizontal component and both derivatives of the vertical and horizontal components remain the same. The result is a very high accuracy and a zero steady state with respect to the vertical component of the missile position when the steady state of the summary phase coupling between the channels becomes zero while the horizontal component of the steady state remains the same. This modified guidance law is named "Sophisticated adaptive Expanded Two-Dimensional Proportional-Derivative Guidance Law with Missile Weight Compensation" – SAE2DPDGLwMWC. It is the most developed fifth new command to line-of-sight guidance law of the set of new developed guidance laws.

A methodology for upgrading the classical spatial closed loop guidance and control system with phase coupling between the two horizontal and vertical missile channels with the new set of guidance laws is developed. Based on this methodology an example with a hypothetical but more realistic model of an ATGM is presented. The model takes into consideration the transfer functions of both yaw and pitch channels (the horizontal and vertical channels) including the missile fin control actuation system, the phase coupling between the channels, aerodynamics, missile velocity, the CLOS kinematic relations and existence of some external disturbances as the missile weight, a target's movement and a wind gust. As a result the new spatial closed loop guidance and control system with the most developed of the new set of guidance laws – the SAE2DPDGLwMWC possesses:

- Robust asymptotic stability within a very broad range of phase coupling angle compared to the classical spatial closed loop guidance system;

The established here interval of stability of the spatial closed loop guidance and control system with the SAE2DPDGLwMWC for the considered case of varying coefficients is 1.8 times wider than the classical interval of stability for the same case of varying coefficients;

- Excellent performance indices within a very broad range of the phase coupling angle compared to the classical spatial closed loop guidance system;

The classical system provides acceptable performance when the phase coupling between the channels is around zero and far from the boundaries of the classical stability interval regarding the phase coupling angle while the new spatial closed loop guidance and control system possesses an excellent performance even beyond the boundaries of the classical interval of stability. The established interval with excellent performance for the considered case of varying coefficients is more than four times wider than the classical interval with acceptable performance.

- High steady state accuracy;

The numerical experiments for the full set of extremal varying coefficients, initial trajectory points and phase coupling angles fully comply with the estimations: $-0.28 < y(\infty) < 0.28\ (m), -0.06 < z(\infty) < 0.15\ (m)$.

If we have to describe the new spatial closed loop guidance and control system of the ATGM based on the SAE2DPDGLwMWC in one word this is excellence.

It could be concluded finally that the goals of the monograph formulated in Section 1.4 “Monograph’s main goals” (page 27) have been achieved. There exist all theoretical preconditions for a prospective realization of the new powerful advanced two-dimensional command to line-of-sight (CLOS) guidance laws.

8 APPENDICES

8.1 Analysis of the stability of the closed loop system (1.30) - (1.31) with control (1.3) in function of the parameter γ

Let us define the following complex variables:

$p = y + iz\,,$	(8.1)
$a_p = a_y + ia_z\,,$	(8.2)
$u_p = u_y + iu_z\,.$	(8.3)

The system (1.30) - (1.31) in terms of the variables (8.1) - (8.3) is presented in the following way:

$\ddot{p} = a_p\,,$	(8.4)
$a_p = \left(u_y \cos\gamma + u_z \cos\left(\frac{\pi}{2} + \gamma\right)\right) + i\left(u_y \sin\gamma + u_z \sin\left(\frac{\pi}{2} + \gamma\right)\right) =$	
$= \left(u_y \cos\gamma + iu_y \sin\gamma\right) + i\left(u_z \sin\left(\frac{\pi}{2} + \gamma\right) - i\,u_z \cos\left(\frac{\pi}{2} + \gamma\right)\right) =$	
$= \left(u_y \cos\gamma + iu_y \sin\gamma\right) + i(u_z \cos\gamma + i\,u_z \sin\gamma) =$	
$= \left(u_y e^{i\gamma}\right) + i\left(u_z e^{i\gamma}\right) =$	
$= e^{i\gamma}\left(u_y + iu_z\right) =$	
$= e^{i\gamma} u_p\,.$	(8.5)

Taking into account (1.31) - $\gamma = \gamma_0 = const$, for (8.5) we obtain

$a_p = \quad {}^{i\gamma_0} u_p\,.$	(8.6)

The control (1.3) in terms of (8.1) - (8.3) represents:

$$u_p = u_y + iu_z = \left(\frac{-1}{a_0}(y + a_1\dot{y})\right) + i\left(\frac{-1}{a_0}(z + a_1\dot{z})\right) =$$

$$= \left(\frac{-1}{a_0}\left((y + iz) + a_1(\dot{y} + i\dot{z})\right)\right) =$$

$$= \left(\frac{-1}{a_0}(p + a_1\dot{p})\right). \tag{8.7}$$

So the closed loop system (1.30) - (1.31) with control (1.3) in terms of the complex variables (8.1) - (8.3) represents the system:

$$\begin{aligned} &\ddot{p} = a_p\,, \\ &a_p = e^{i\gamma_0}u_p\,, \\ &u_p = \left(\frac{-1}{a_0}(p + a_1\dot{p})\right). \end{aligned} \tag{8.8}$$

The Laplace transform of the above system (8.8) at zero initial conditions is:

$$\begin{aligned} &s^2p(s) = a_p(s)\,, \\ &a_p(s) = e^{i\gamma_0}u_p(s)\,, \\ &u_p(s) = \left(\frac{-1}{a_0}(1 + a_1 s)\right)p(s)\,. \end{aligned} \tag{8.9}$$

The above system (8.9) determines the open loop transfer function

$$L(s) = e^{i\gamma_0}\frac{\left(\frac{1}{a_0}(1+a_1 s)\right)}{s^2}. \tag{8.10}$$

Denote the open loop transfer function in case of absence of crosslinks, no coupling, between the y and z-channels – $\gamma_0 = 0$ (1.32) – as

$$L_0(s) = L(s)|_{\gamma_0=0} = \frac{\left(\frac{1}{a_0}(1+a_1 s)\right)}{s^2}. \tag{8.11}$$

Thus, the open loop transfer function (8.10) represents also (8.12) and the relations between corresponding frequency response functions $L(i\omega)$ and $L_0(i\omega)$ stemmed from (8.12) are (8.13).

$L(s) = e^{i\gamma_0} L_0(s)$	(8.12)
$L(i\omega) = e^{i\gamma_0} L_0(i\omega)$	(8.13)

Denote the gain and phase functions of the open loop frequency response function $L(i\omega)$ as $A(\omega)$ (8.14) and $\varphi(\omega)$ (8.15) and the gain and phase functions of the frequency response function $L_0(i\omega)$ as $A_0(\omega)$ (8.16) and $\varphi_0(\omega)$ (8.17).

$A(\omega) = \lvert L(i\omega)\rvert$	(8.14)
$\varphi(\omega) = arg\big(L(i\omega)\big)$	(8.15)
$A_0(\omega) = \lvert L_0(i\omega)\rvert$	(8.16)
$\varphi_0(\omega) = \ arg\big(L_0(i\omega)\big)$	(8.17)

It follows from (8.13) the relation (8.18) is valid for the gain functions $A(\omega)$ and $A_0(\omega)$ and the relation (8.19) is valid for the phase functions $\varphi(\omega)$ and $\varphi_0(\omega)$.

$A(\omega) = \lvert L(i\omega)\rvert = \lvert L_0(i\omega)\rvert = A_0(\omega)$	(8.18)
$\varphi(\omega) = arg\big(L(i\omega)\big) = arg\big(L_0(i\omega)\big) + \gamma_0 = \varphi_0(\omega) + \gamma_0$	(8.19)

8.1.1 Case of no coupling between the y and z-channels – absence of crosslinks at $\gamma_0 = 0$

Let us first consider the open loop transfer function $L_0(s)$ (8.11) and its respective open loop frequency response function $L_0(i\omega)$. Because of (1.3), where both the coefficients a_0 and a_1 are chosen to be positive (8.20), the relations (8.21), (8.22), and (8.23) are valid.

$a_0 > 0\ (s^2), a_1 > 0\ (s)$	(8.20)
$L_0(-i\omega) = \overline{L_0(\iota\omega)}$	(8.21)
$A_0(-\omega) = \lvert L_0(-i\omega)\rvert = \lvert L_0(i\omega)\rvert = A_0(\omega)$	(8.22)
$\varphi_0(-\omega) = arg\big(L_0(-i\omega)\big) = -arg\big(L_0(i\omega)\big) = -\varphi_0(\omega)$	(8.23)

Thus, because of the above relations (8.21), (8.22), and (8.23), considering the range of $\omega \in [0, \infty)$ is sufficient for the stability analysis of the closed loop system. In that case the gain and phase functions are presented by the expressions (8.24) and (8.25). The gain function is a decreasing one and according to (8.24) it varies from ∞ at $\omega \to 0^+$ to 0 at $\omega \to \infty$. Therefore, there is only one frequency, which satisfies the condition (8.27) - the gain crossover frequency ω_{cg_0}. The real positive solution of the equation (8.27) or (8.28) is (8.29). The phase function is an increasing one and according to (8.25) it varies from $-\pi$ at $\omega \to 0^+$ to $-\frac{\pi}{2}$ at $\omega \to \infty$.

The open loop transfer function $L_0(s)$ comprises a double integrator. Because of that, we traverse the Nyquist contour [46] (Chap. 9, Figure 9.5), [43] (Chap 6, §6.4), [47] (Chap. 3, §3.6), [48] (Chap. 10, §10.3) clockwise with a small semicircle around the double pole $s = 0$. Thus the Nyquist plot of $L_0(i\omega)$ for the range of $\omega \in [0, \infty)$ is completed by a semicircle of infinite radius starting from the infinity of the real axis at $\omega = 0$ moving clockwise to the infinity of negative part of the real axis, where this arc conjugates with the plot of $L_0(i\omega)$ at $\omega \to 0^+$. Figure 8.1 shows the Nyquist plot for the range of $\omega \in (-\infty, \infty)$. The plot is symmetric about the real axis and for the range of $\omega \in [0, \infty)$ it is below the real axis. The arc of infinite radius (dashed line) represents the image of $L_0(s)$ when s traverses around the double pole $s = 0$ with a small radius in the clockwise direction. The Nyquist plot tends asymptotically to the infinity of the negative part of the real axis at $\omega \to 0^+$ and tends asymptotically to the origin of negative part of the imaginary axis at $\omega \to \infty$ (solid line). Thus the plot of $L_0(i\omega)$ for the range of $\omega \in [0, \infty)$ lies wholly in the fourth and third quadrants of the complex plane, not crossing the negative part of the real axis at a finite positive frequency. Such a Nyquist plot has no encirclements of the critical point $s = -1$ and determines an asymptotically stable closed loop system [46] (Chap. 9), [43] (Chap 6, §6.4), [47] (Chap. 3, §3.6), [48] (Chap. 10, §10.3).

Figure 8.2 shows the Nyquist diagram for the pair of coefficients (8.26), which corresponds to (1.7) and (1.15). As mentioned above the plot of $L_0(i\omega)$ is symmetric about the real axis, the upper branch (dashed line) is the plot for the negative frequencies, but the lower branch (solid line) is the plot for the positive frequencies.

Figure 8.3 shows the corresponding Bode diagram for the pair of coefficients (8.26). The plot of the magnitude has two asymptotes - the first one is on the left of the conjugate frequency $1/a_1$ and represents a straight line with a slope of -40 dB/decade and the second asymptote is on the right of the conjugate frequency $1/a_1$ and represents a straight line with a slope of -20 dB/decade.

Both Nyquist and Bode diagrams are typical illustration of the properties of such frequency response function $L_0(i\omega)$ of the loop transfer function $L_0(s)$ (8.11).

The gain and phase margins are calculated by (8.30) and (8.31). For the pair (8.26) the values of the gain crossover frequency and phase margin are (8.32).

$A_0(\omega) = \begin{cases} \dfrac{\sqrt{1 + {a_1}^2\omega^2}}{a_0\omega^2} & ,\omega > 0 \\ \infty & ,\omega \to 0^+ \\ 0 & ,\omega \to \infty \end{cases}$	(8.24)
$\varphi_0(\omega) = \begin{cases} -\pi + \tan^{-1}(a_1\omega) & ,\omega > 0 \\ -\pi & ,\omega \to 0^+ \\ -\dfrac{\pi}{2} & ,\omega \to \infty \end{cases}$	(8.25)
$a_0 = 0.04\ (s^2), a_1 = 0.16\ (s)$	(8.26)
$A_0(\omega) = \lvert L_0(i\omega)\rvert = 1$	(8.27)
$\dfrac{1}{a_0\omega^2}\sqrt{1 + {a_1}^2\omega^2} = 1$	(8.28)
$\omega_{cg_0} = \sqrt{\dfrac{{a_1}^2 + \sqrt{{a_1}^4 + 4{a_0}^2}}{2{a_0}^2}}$	(8.29)
$GM_0 = 20\log\left(\dfrac{1}{\infty}\right) = -\infty\ (\text{dB})\ \text{at}\ \omega \to 0^+$	(8.30)
$PM_0 = \varphi_0(\omega_{cg_0}) - (-\pi) = \left(-\pi + \tan^{-1}(a_1\omega_{cg_0})\right) + \pi = $ $= \tan^{-1}(a_1\omega_{cg_0})$	(8.31)
$\omega_{cg_0} = 5.8522\ \left(\dfrac{rad}{s}\right),$ $PM_0 = 0.75254\ (rad)$ or $PM_0 = 43.1176$ deg.	(8.32)

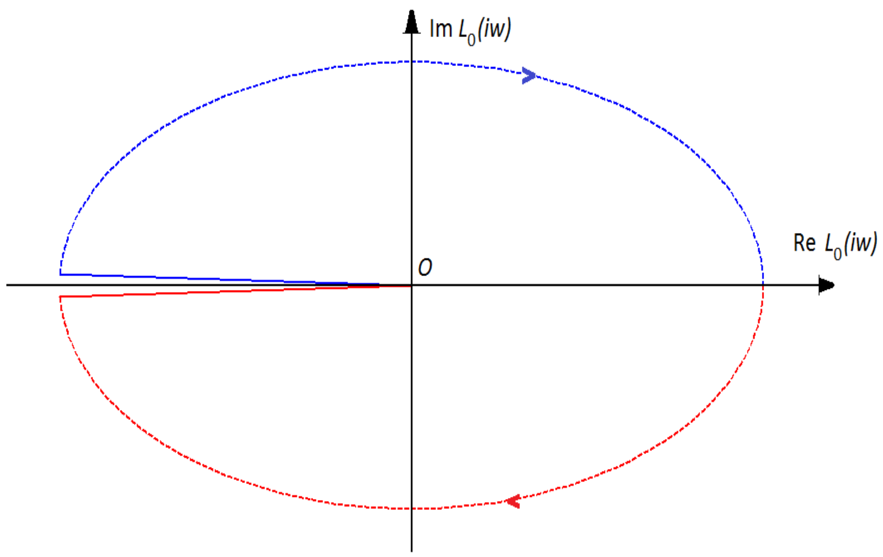

Figure 8.1 Nyquist diagram of the frequency response function $L_0(i\omega)$ for the range of $\omega \in (-\infty, \infty)$. The plot is symmetric about the real axis and for the range of $\omega \in [0, \infty)$ it is below the real axis.

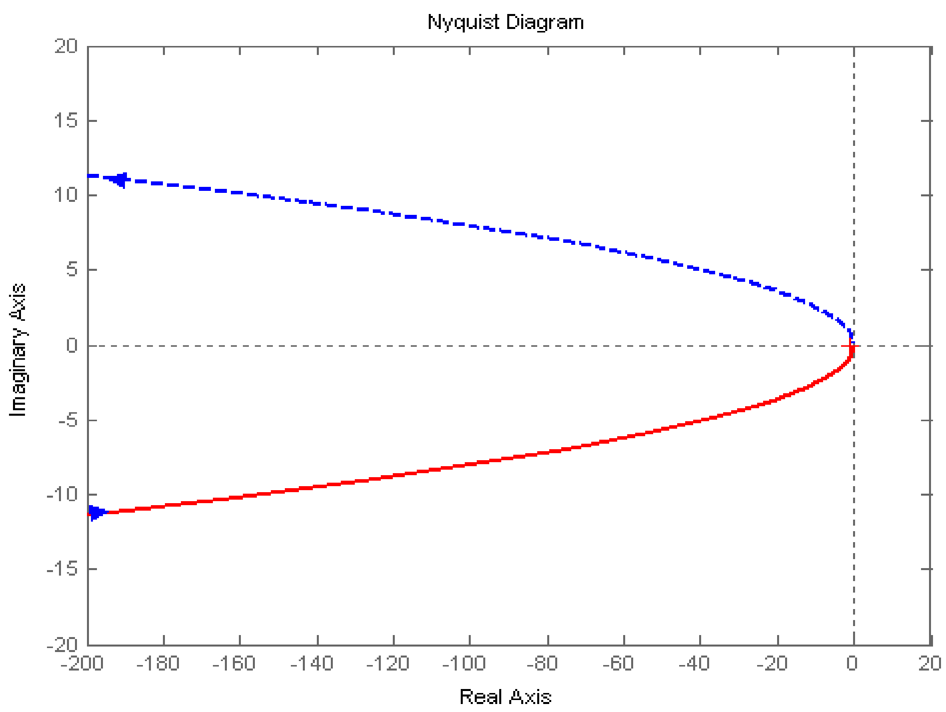

Figure 8.2 Nyquist diagram of the frequency response function $L_0(i\omega)$ at coefficients (8.26).

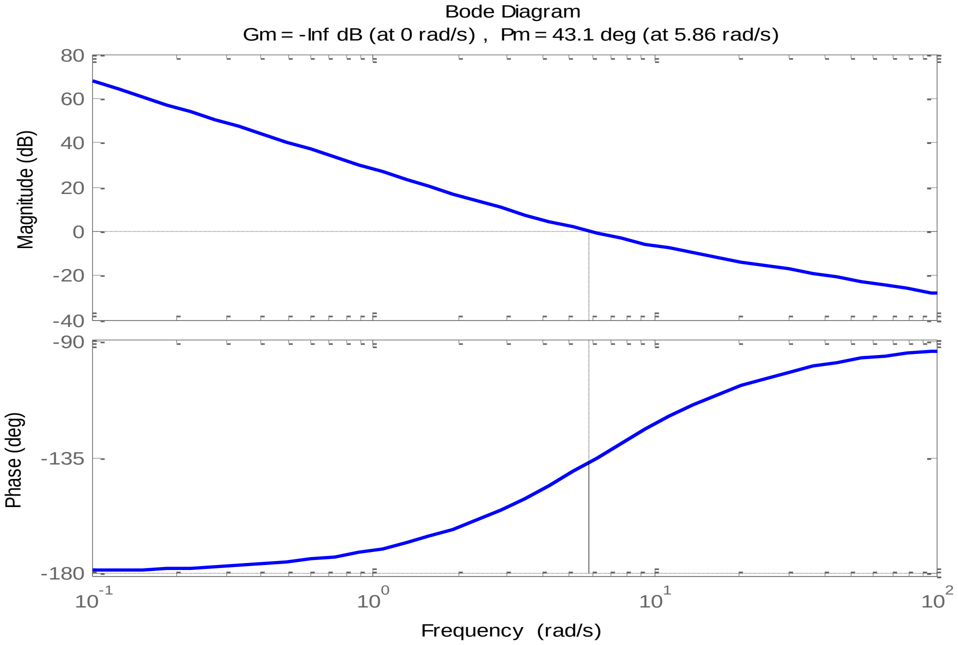

Figure 8.3 Bode diagram of the frequency response function $L_0(i\omega)$ at coefficients (8.26).

8.1.2 Common case with phase coupling between the y and z-channels

Let us deal now with the common case of the open loop transfer function $L(s)$ (8.10) or (8.12) and its frequency response function $L(i\omega)$ (8.13). Having in mind (8.18) and (8.19) the relations (8.33) - (8.35) are valid. According to them the gain function $A(\omega)$ is an even function (8.34), but the condition for the phase function $\varphi(\omega)$ (8.35) of being an odd function is satisfied only when $\gamma_0 = 0$ (8.36).

$L(-i\omega) = e^{i\gamma_0} L_0(-i\omega) = e^{i\gamma_0} \lvert L_0(-i\omega) \rvert e^{i \arg L_0(-i\omega)} =$	
$= e^{i\gamma_0} \lvert L_0(i\omega) \rvert e^{-i \arg L_0(i\omega)} =$	
$= e^{i\gamma_0} A_0(\omega) e^{-i\varphi_0(\omega)} = A_0(\omega) e^{-i(\varphi_0(\omega)-\gamma_0)} =$	
$= A_0(\omega) e^{i(-(\varphi_0(\omega)+\gamma_0)+2\gamma_0)} = A_0(\omega) e^{-i(\varphi_0(\omega)+\gamma_0)} e^{i2\gamma_0} =$	
$= A(\omega) e^{-i\varphi(\omega)} e^{i2\gamma_0} =$	
$= \overline{L(i\omega)} e^{i2\gamma_0}$	(8.33)
$A(-\omega) = A_0(-\omega) = A_0(\omega) = A(\omega)\,,$	(8.34)

$\varphi(-\omega) = -\varphi(\omega) + 2\gamma_0$	(8.35)
$\varphi(-\omega) = -\varphi(\omega)$ only when $\gamma_0 = 0$.	(8.36)

Thus the stability analysis of the closed loop system requires consideration of the Nyquist plot of the frequency response function $L(i\omega)$ (8.13) for the whole range of $\omega \in (-\infty, \infty)$. Based on (8.13), (8.18), and (8.19) the Nyquist plot of the frequency response function $L(i\omega)$ is obtained by rotating the Nyquist plot of the frequency response function $L_0(i\omega)$ counterclockwise about the plane origin by the angle γ_0. That means, keeping the plot of $L_0(i\omega)$ still, we have to rotate both the real and imaginary axis about the plane origin clockwise by the angle γ_0. Thus in case of $\gamma_0 > 0$ we have to rotate both the real and imaginary axis around the plane origin clockwise by the angle $|\gamma_0|$, but in case of $\gamma_0 < 0$ we have to rotate both the real and imaginary axis around the plane origin counterclockwise by the angle $|\gamma_0|$. Let us consider consequently both cases.

8.1.2.1 Case $\gamma_0 > 0$

In that case the upper branch of the Nyquist plot for the range of frequencies $\omega \in (-\infty, 0]$ crosses the negative part of the real axis in two points C_1 and C_2 with coordinates (8.39) and (8.40) at the frequencies (8.37) and (8.38) respectively. At increase of ω the crossing in C_1 is bottom up but the crossing in C_2 is from top to bottom; the point C_2 moves from minus infinity of the real axis towards the critical point $(-1, i0)$ at increase of $\gamma_0 > 0$.

$\omega_{1_\pi} = 0^-$	(8.37)
$\omega_{2_\pi} = \dfrac{1}{a_1}\tan(-\gamma_0) < 0$	(8.38)
$C_1 = (-\infty, i0)$	(8.39)
$C_2 = \left(-\dfrac{\sqrt{1 + {a_1}^2\left(\omega_{2_\pi}\right)^2}}{a_0\left(\omega_{2_\pi}\right)^2}, i0\right)$	(8.40)

In case $\gamma_0 > 0$ the lower branch of the Nyquist plot for the range of frequencies $\omega \in [0, \infty)$ does not cross the negative part of the real axis.

So the closed loop system becomes neutrally stable when the point C_2 reaches the critical point $(-1, i0)$. In other words, the closed loop system becomes neutrally stable when the frequency ω_{2_π} (8.38) coincides with the negative gain crossover frequency $\omega_{cg}^{-} = -\omega_{cg_0}$ (8.41), which case represents the equation (8.42). The solution of (8.42) is (8.43).

$\omega_{cg}^{-} = -\omega_{cg_0} = -\sqrt{\dfrac{{a_1}^2 + \sqrt{{a_1}^4 + 4{a_0}^2}}{2{a_0}^2}}$	(8.41)
$\omega_{2_\pi} = \dfrac{1}{a_1}\tan(-\gamma_0) = \omega_{cg}^{-} = -\omega_{cg_0} = -\sqrt{\dfrac{{a_1}^2 + \sqrt{{a_1}^4 + 4{a_0}^2}}{2{a_0}^2}}\ ,$ $where\ \gamma_0 > 0$	(8.42)
$\gamma_0 = \tan^{-1}\left(a_1 \omega_{cg_0}\right) > 0$	(8.43)
$PM^{-} = \pi - \varphi\left(\omega_{cg}^{-}\right) = \pi - \varphi\left(-\omega_{cg_0}\right) = \pi - \left(\varphi_0\left(-\omega_{cg_0}\right) + \gamma_0\right) =$	
$= \pi - \left(-\varphi_0\left(\omega_{cg_0}\right) + \gamma_0\right) = \pi - \left(\pi - \tan^{-1}\left(a_1\omega_{cg_0}\right) + \gamma_0\right) =$	
$= \tan^{-1}\left(a_1\omega_{cg_0}\right) - \gamma_0$	(8.44)
$\omega_{cg}^{+} = \omega_{cg_0}$	(8.45)
$PM^{+} = \varphi\left(\omega_{cg_0}\right) - (-\pi) = \varphi_0\left(\omega_{cg_0}\right) + \gamma_0 + \pi =$	
$= -\pi + \tan^{-1}\left(a_1\omega_{cg_0}\right) + \gamma_0 + \pi =$	
$= \tan^{-1}\left(a_1\omega_{cg_0}\right) + \gamma_0$	(8.46)

Thus, the conclusion in case of $\gamma_0 > 0$ is that the closed loop system remains asymptotically stable when (8.47) and becomes neutrally stable at γ_0 (8.43).

$\gamma_0 < \tan^{-1}\left(a_1\omega_{cg_0}\right)$	(8.47)

8.1.2.2 Case $\gamma_0 < 0$

In that case the lower branch of the Nyquist plot for the range of frequencies $\omega \in [0, \infty)$ crosses the negative part of the real axis in two points D_1 and D_2 with coordinates (8.50) and (8.51) at the frequencies (8.48) and (8.49) respectively. At increase of ω the crossing in D_1 is bottom up but the crossing in D_2 is from top to bottom; the point D_2 moves from minus infinity of the real axis towards the critical point $(-1, i0)$ at decrease of $\gamma_0 < 0$.

$\omega_{1_{-\pi}} = 0^+$	(8.48)
$\omega_{2_{-\pi}} = \frac{1}{a_1}\tan(-\gamma_0) > 0$	(8.49)
$D_1 = (-\infty, i0)$	(8.50)
$D_2 = \left(-\frac{\sqrt{1 + {a_1}^2\left(\omega_{2_{-\pi}}\right)^2}}{a_0\left(\omega_{2_{-\pi}}\right)^2}, i0\right)$	(8.51)

In case $\gamma_0 < 0$ the upper branch of the Nyquist plot for the range of frequencies $\omega \in (-\infty, 0]$ does not cross the negative part of the real axis.

So the closed loop system becomes neutrally stable when the point D_2 reaches the critical point $(-1, i0)$. In other words, the closed loop system becomes neutrally stable when the frequency $\omega_{2_{-\pi}}$ (8.49) coincides with the positive gain crossover frequency $\omega_{cg}^+ = \omega_{cg_0}$ (8.45), which case represents the equation (8.52) with solution (8.53). The phase margin PM^+ at the positive gain crossover frequency $\omega_{cg}^+ = \omega_{cg_0}$ (8.45) is presented by (8.46) and PM^+ decreases at decrease of γ_0 and at γ_0 (8.53) this phase margin becomes zero. The phase margin PM^- at the negative gain crossover frequency $\omega_{cg}^- = -\omega_{cg_0}$ (8.41) represents (8.44) and it only increases at decrease of $\gamma_0 < 0$.

$\omega_{2_{-\pi}} = \frac{1}{a_1}\tan(-\gamma_0) = \omega_{cg}^+ = \omega_{cg_0} = \sqrt{\frac{{a_1}^2 + \sqrt{{a_1}^4 + 4{a_0}^2}}{2{a_0}^2}}$, $where\ \gamma_0 < 0$	(8.52)
$\gamma_0 = -\tan^{-1}\left(a_1\omega_{cg_0}\right) < 0$	(8.53)

Thus in case of $\gamma_0 < 0$ the closed loop system remains asymptotically stable when γ_0 satisfies the condition (8.54) and becomes neutrally stable at γ_0 (8.53).

$\gamma_0 > -\tan^{-1}(a_1\omega_{cg_0})$	(8.54)

8.1.3 General conclusion on the stability of the closed loop system

Let us denote the critical crossover value of $|\gamma_0|$ as γ_{cr} (8.55) having in mind (8.31), (8.47), and (8.54) obtained at the consideration of all three cases of γ_0 : Case 8.1.1 for $\gamma_0 = 0$, Case 8.1.2.1 for $\gamma_0 > 0$, and Case 8.1.2.2 for $\gamma_0 < 0$.

$\gamma_{cr} = PM_0 = \tan^{-1}(a_1\omega_{cg_0})$	(8.55)

Summarizing it could be concluded that the closed loop system (1.30) - (1.31) with control law (1.3) (or the system (8.8) in terms of the complex variables (8.1) - (8.3)) is asymptotically stable if γ_0 satisfies (8.56). The closed loop system becomes neutrally stable at the boundaries (8.57) of (8.56) and becomes unstable at (8.58).

$\gamma_0 \in (-\gamma_{cr}, \gamma_{cr})$	(8.56)
$\|\gamma_0\| = \gamma_{cr}$	(8.57)
$\|\gamma_0\| > \gamma_{cr}$	(8.58)

8.1.4 Example

In order to illustrate the above conclusion about the stability of the closed loop system (1.30) - (1.31) with control law (1.3) (or the system (8.8) in terms of the complex variables (8.1) - (8.3)) in function of the parameter γ_0 let the parameters of the control (1.3) be the pair (8.26) used already for illustration here in Section 8.1. For all the processes, the initial conditions are (1.16). Figure 8.4 - Figure 8.12 show the processes on y and z as well as the processes in the yz-plane consequently at $\gamma_0 = 0$, $\gamma_0 = \pm 0.5\gamma_{cr}, \gamma_0 = \pm 0.75\gamma_{cr}, \gamma_0 = \pm\gamma_{cr}$ and $\gamma_0 = \pm 1.01\gamma_{cr}$, where $\gamma_{cr} =$ 43.1176 deg. calculated according to (8.55). The increase of $|\gamma_0|$ worsens the stability of the closed loop system, which becomes neutrally stable at $\gamma_0 = \pm\gamma_{cr}$ as shown in Figure 8.9 and Figure 8.10, and becomes unstable at $|\gamma_0| > \gamma_{cr}$, as illustrated in Figure 8.11 and Figure 8.12 at $\gamma_0 = \pm 1.01\gamma_{cr}$.

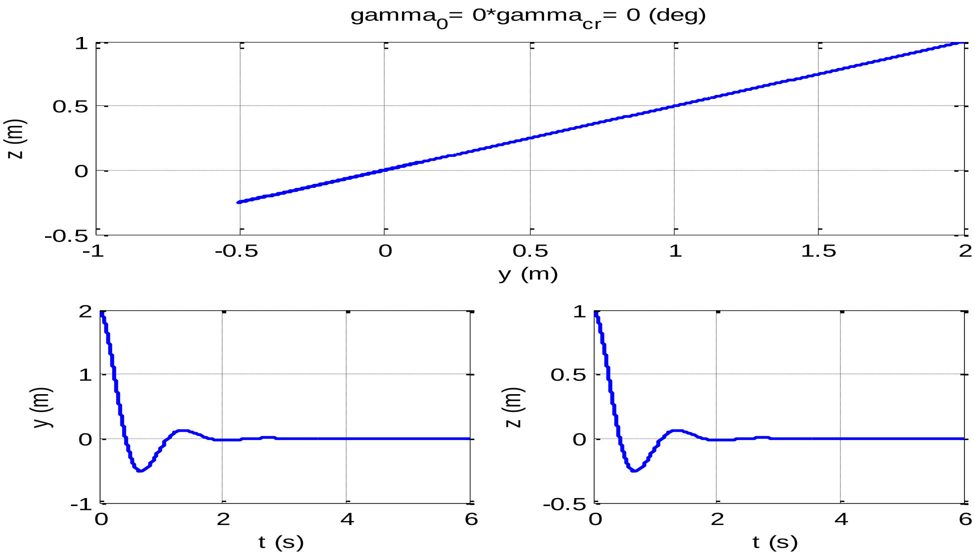

Figure 8.4 **The system trajectory in the yz-plane and the processes with respect to y and z of the closed loop system (1.30) - (1.31) with control law (1.3) with parameters (8.26) at initial conditions (1.16) in case of absence of coupling between the channels – $\gamma_0 = 0$. Case (8.56) of asymptotically stable closed loop system.**

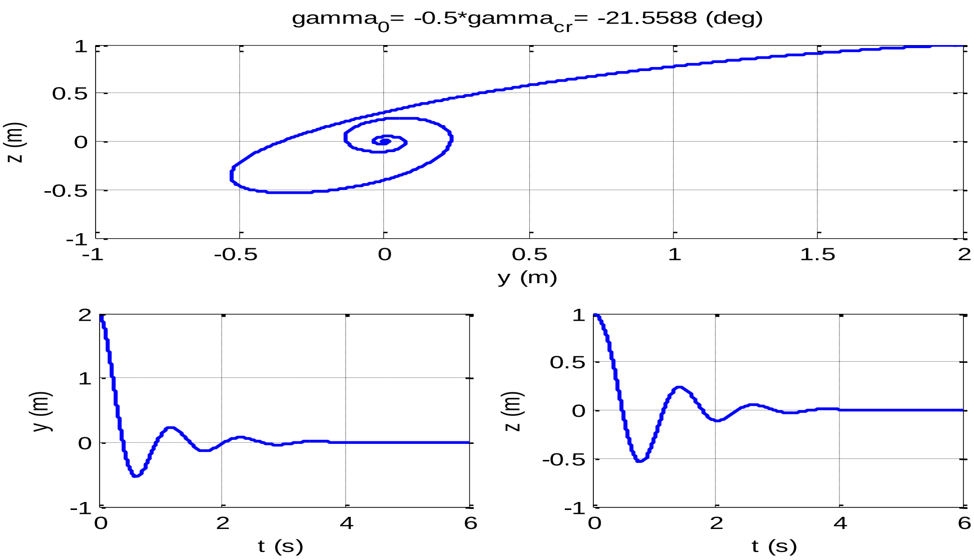

Figure 8.5 **The system trajectory in the yz-plane and the processes with respect to y and z of the closed loop system (1.30) - (1.31) with control law (1.3) with parameters (8.26) at initial conditions (1.16) in case of phase coupling between the channels – $\gamma_0 = -0.5\gamma_{cr} = -21.5588$ deg. Case (8.56) of asymptotically stable closed loop system.**

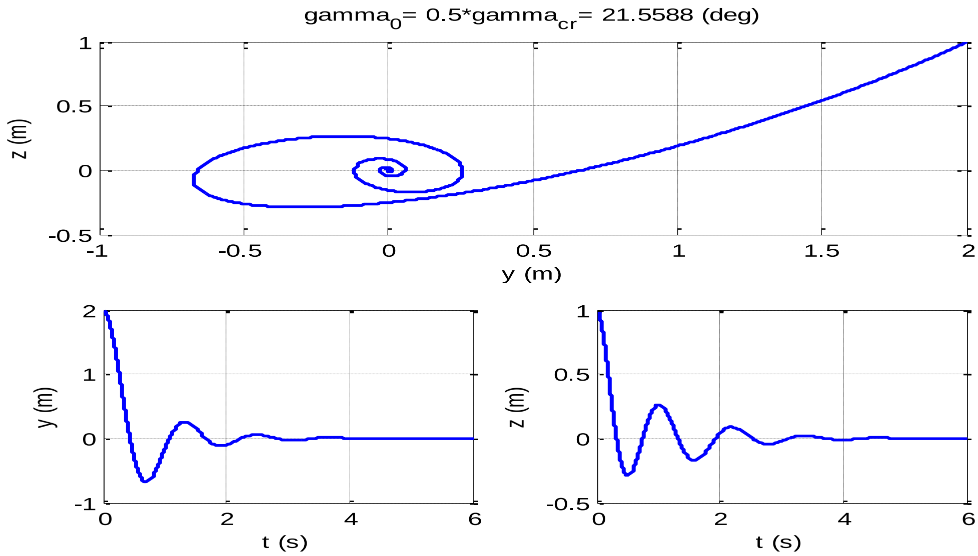

Figure 8.6 The system trajectory in the yz-plane and the processes with respect to y and z of the closed loop system (1.30) - (1.31) with control law (1.3) with parameters (8.26) at initial conditions (1.16) in case of phase coupling between the channels – $\gamma_0 = 0.5\gamma_{cr} = 21.5588$ deg. Case (8.56) of asymptotically stable closed loop system.

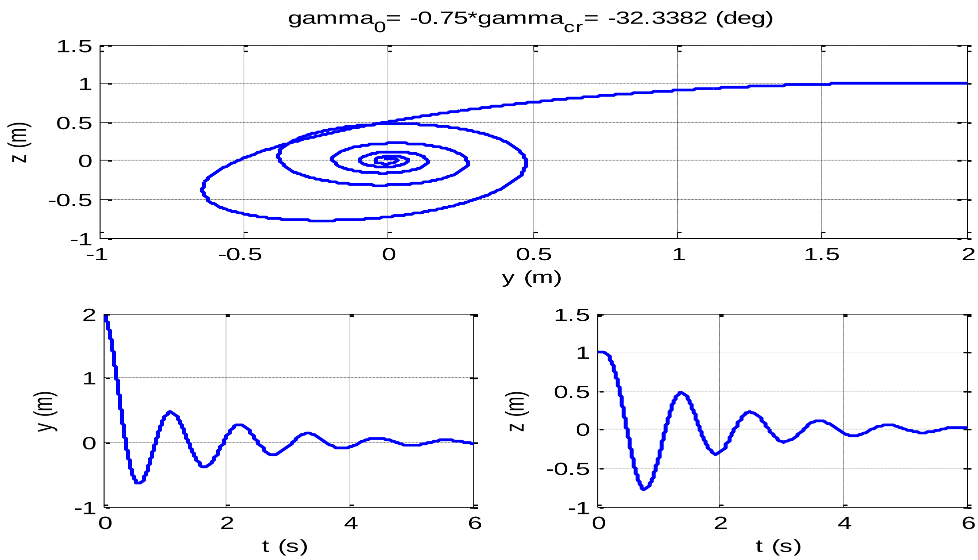

Figure 8.7 The system trajectory in the yz-plane and the processes with respect to y and z of the closed loop system (1.30) - (1.31) with control law (1.3) with parameters (8.26) at initial conditions (1.16) in case of phase coupling between the channels – $\gamma_0 = -0.75\gamma_{cr} = -32.3382$ deg. Case (8.56) of asymptotically stable closed loop system.

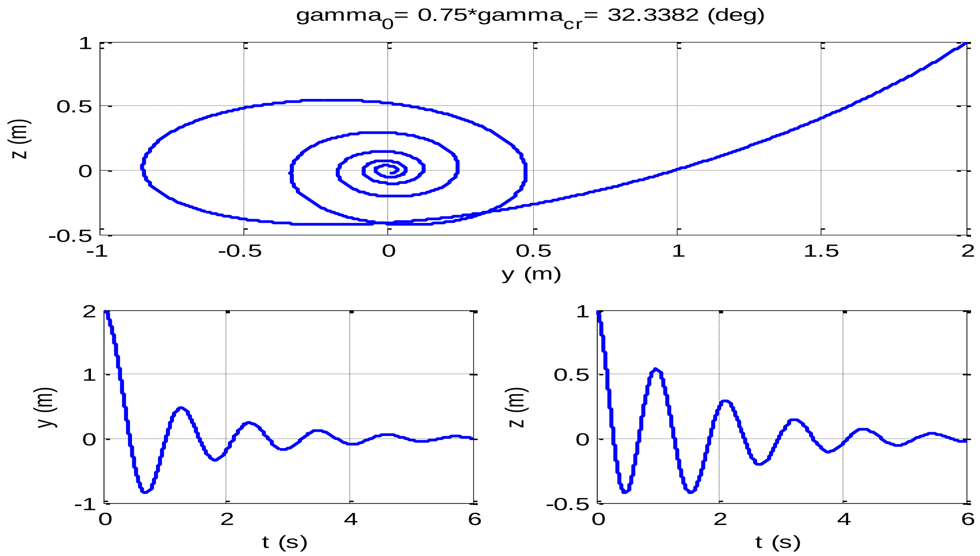

Figure 8.8 The system trajectory in the yz-plane and the processes with respect to y and z of the closed loop system (1.30) - (1.31) with control law (1.3) with parameters (8.26) at initial conditions (1.16) in case of phase coupling between the channels – $\gamma_0 = 0.75\gamma_{cr} = 32.3382$ deg. Case (8.56) of asymptotically stable closed loop system.

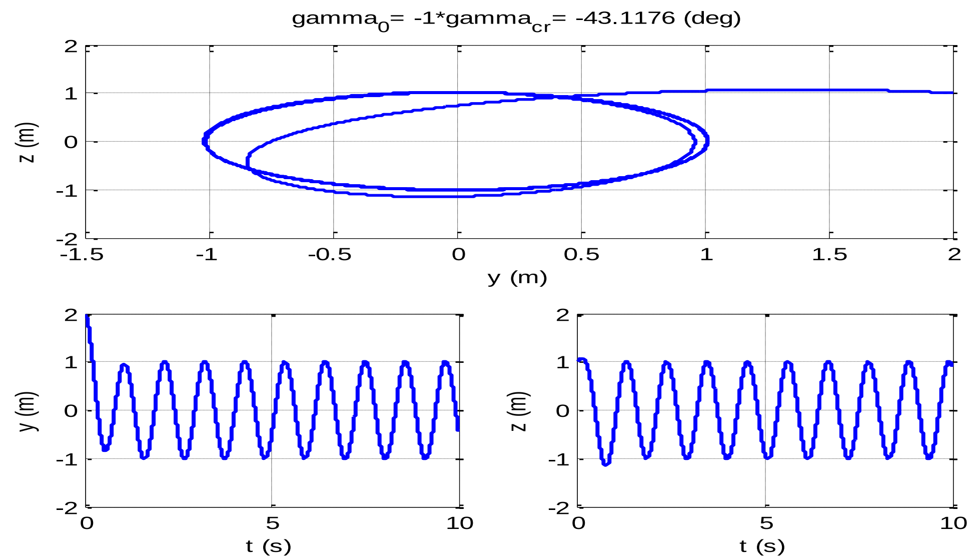

Figure 8.9 The system trajectory in the yz-plane and the processes with respect to y and z of the closed loop system (1.30) - (1.31) with control law (1.3) with parameters (8.26) at initial conditions (1.16) in case of phase coupling between the channels – $\gamma_0 = -\gamma_{cr} = -43.1176$ deg. Case (8.57) of neutrally stable closed loop system.

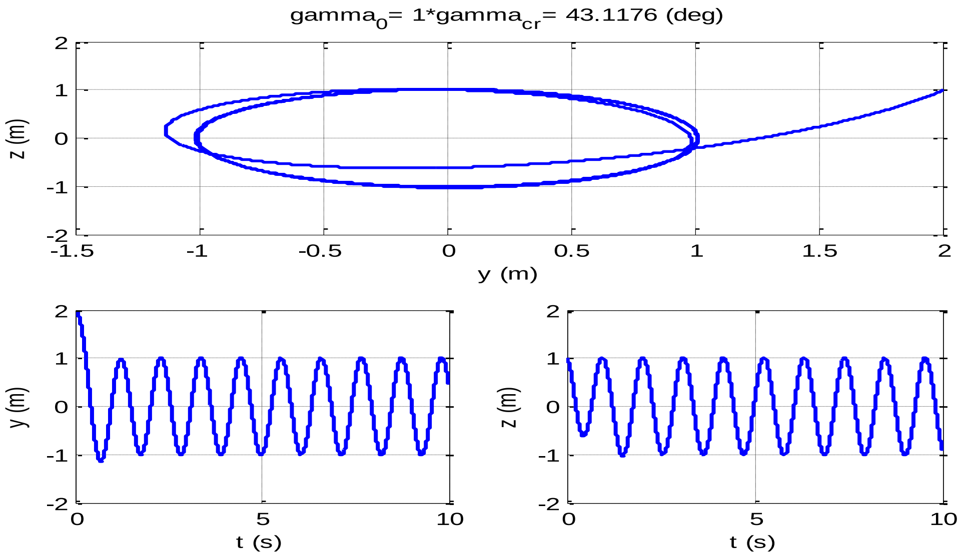

Figure 8.10 The system trajectory in the yz-plane and the processes with respect to y and z of the closed loop system (1.30) - (1.31) with control law (1.3) with parameters (8.26) at initial conditions (1.16) in case of phase coupling between the channels – $\gamma_0 = \gamma_{cr} = 43.1176$ deg. Case (8.57) of neutrally stable closed loop system.

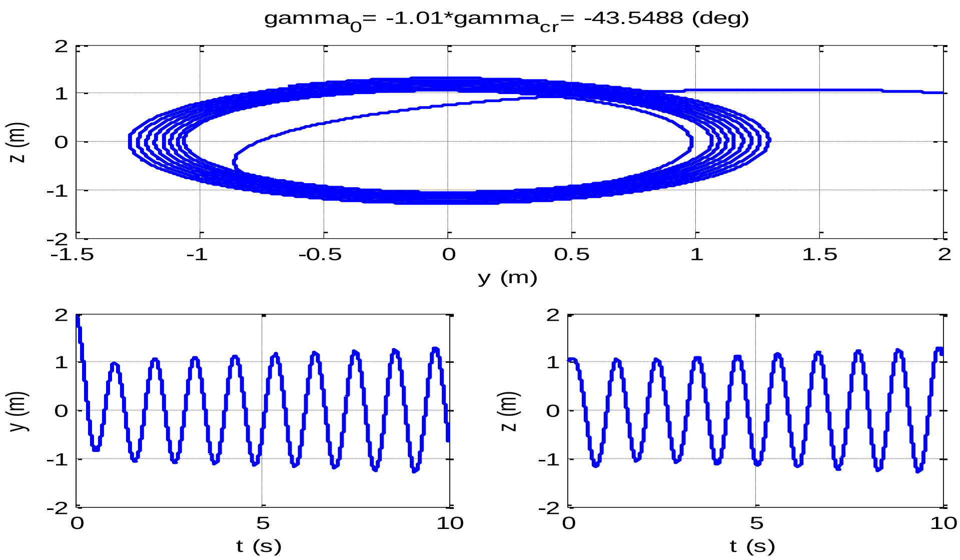

Figure 8.11 The system trajectory in the yz-plane and the processes with respect to y and z of the closed loop system (1.30) - (1.31) with control law (1.3) with parameters (8.26) at initial conditions (1.16) in case of phase coupling between the channels – $\gamma_0 = -1.01\gamma_{cr} = -43.5488$ deg. Case (8.58) of unstable closed loop system.

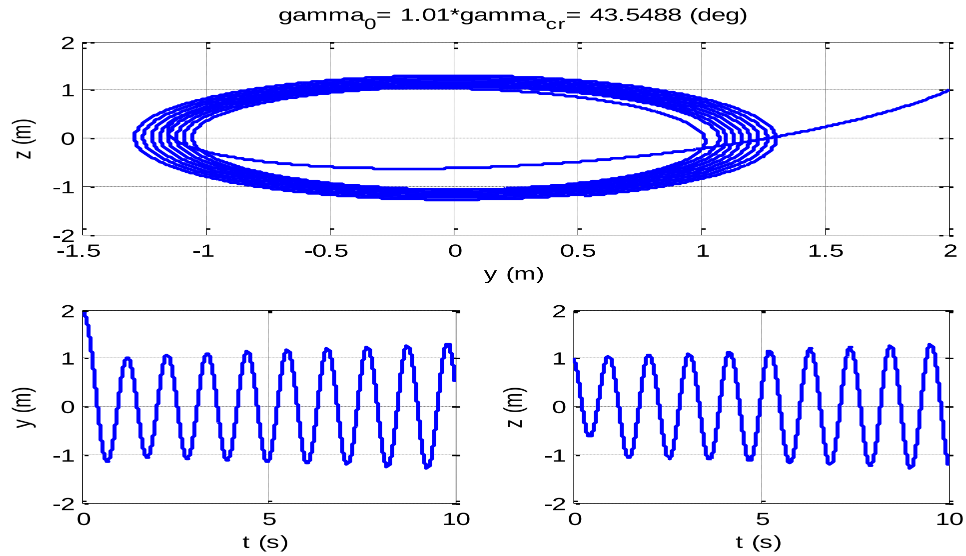

Figure 8.12 The system trajectory in the yz-plane and the processes with respect to y and z of the closed loop system (1.30) - (1.31) with control law (1.3) with parameters (8.26) at initial conditions (1.16) in case of phase coupling between the channels – $\gamma_0 = 1.01\gamma_{cr} = 43.5488$ deg. Case (8.58) of unstable closed loop system.

LIST OF ABBREVIATIONS, ACRONYMS AND SYMBOLS

2D	-	two-dimensional
AE2DPDGL	-	adaptive expanded 2D PD guidance law
ATGM	-	anti-tank guided missile
BTT	-	bank-to-turn
CLOS	-	command to line-of-sight
CPDGL	-	classical PD guidance law
E2DPDGL	-	expanded 2D PD guidance law
E2DPDGL1	-	a version of the E2DPDGL with value of the time constant T_{φ} (2.31)
E2DPDGL2	-	a version of the E2DPDGL with value of the time constant T_{φ} (2.32)
SAE2DPDGL	-	sophisticated adaptive expanded 2D PD guidance law
SAE2DPDGLwMWC	-	sophisticated adaptive expanded 2D PD guidance law with missile weight compensation
IGC	-	integrated guidance and control
LOS	-	line-of-sight
PD	-	proportional-derivative
PN	-	proportional navigation

SA2DPDGL	-	simplified adaptive 2D PD guidance law
STT	-	skid-to-turn
a_0	=	coefficient in s^2
a_1	=	coefficient in s
a_{dy}	=	acceleration, external disturbance in the y-channel in m/s^2
a_{dy0}	=	constant, the value of a_{dy} when it is considered as constant
a_{dz}	=	acceleration, external disturbance in the z-channel in m/s^2
a_{dz0}	=	constant, the value of a_{dz} when it is considered as constant
a_{dp}	=	complex variable for representation of acceleration in a complex form, the external disturbance in complex form
a_p	=	complex variable for representation of acceleration
a_{yc}	=	the component of the acceleration in the y in m/s^2
a_{zc}	=	the component of the acceleration in the z direction in m/s^2
a_y	=	the y component of the acceleration in m/s^2
a_z	=	the z component of the acceleration in m/s^2
$A(\omega)$	=	gain function of the frequency response function $L(i\omega)$
$A_0(\omega)$	=	gain function of the frequency response function $L_0(i\omega)$
c_{y1}	=	constant of integration determined by the initial conditions on y – y_0 and y_{10}
c_{y2}	=	constant of integration determined by the initial conditions on y – y_0 and y_{10}
c_{z1}	=	constant of integration determined by the initial conditions on z – z_0 and z_{10}

c_{z2}	=	constant of integration determined by the initial conditions on $z - z_0$ and z_{10}
C_1	=	point, the intersection of the plot of the frequency response function $L(i\omega)$ with the negative part of the real axis in the complex plane (8.39) at the frequency ω_{1_π} (8.37)
C_2	=	point, the intersection of the plot of the frequency response function $L(i\omega)$ with the negative part of the real axis in the complex plane (8.40) at the frequency ω_{2_π} (8.38)
$D(s)$	=	polynomial with respect to s
D_{GTT}	=	the distance between the ground tracker and the target
D_1	=	point, the intersection of the plot of the frequency response function $L(i\omega)$ with the negative part of the real axis in the complex plane (8.50) at the frequency $\omega_{1_{-\pi}}$ (8.48)
D_2	=	point, the intersection of the plot of the frequency response function $L(i\omega)$ with the negative part of the real axis in the complex plane (8.51) at the frequency $\omega_{2_{-\pi}}$ (8.49)
$f(s)$	=	characteristic polynomial with respect to the variable s
F_{11}, F_{21}	=	the left parts of the first and second differential equations of the system (3.13) or the system (4.19)
F_{12}, F_{22}	=	the opposite right parts of the first and second differential equations of the system (3.13) or the system (4.19)
F_{23}	=	an extraction from the opposite right part F_{22} of the system (4.19)
G_+	=	Group of interval polynomials with all positive coefficients
GM_0	=	gain margin for a closed loop system with the open loop frequency response function $L_0(i\omega)$ in dB

H	=	class of the real Hurwitz polynomials, i.e. the polynomials with real coefficients and all their roots belonging to the open left half of the complex plane
i	=	the imaginary unit, $i = \sqrt{-1}$
j	=	counter /which indicates the jth time when the system stays in the area B – outside the ε_r area/
k	=	coefficient of proportionality, non-dimensional, $k \neq 0$
k_c	=	coefficient in $1/s^2$, $k_c = const > 0$
k_ψ	=	coefficient, $k_\psi = const > 0$. When k_ψ is related to the AE2DPDGL it is non-dimensional, but when it is with the SA2DPDGL it is in m^{-2}
$k_{\psi 1}$	=	coefficient in m^{-2}
$k_{\psi 2}$	=	coefficient, non-dimensional
$k_{\varphi 1}$	=	coefficient in s^{-1}
$L(i\omega)$	=	open loop frequency response function
$L_0(i\omega)$	=	open loop frequency response function, $L(i\omega)$ at $\gamma_0 = 0$
$L(s)$	=	open loop transfer function
$L_0(s)$	=	open loop transfer function, $L(s)$ at $\gamma_0 = 0$
$N(s)$	=	polynomial with respect to s
n_y	=	normal overload in the y-channel, non-dimensional
n_z	=	normal overload in the z-channel, non-dimensional
p	=	complex variable
PM_0	=	phase margin for a closed loop system with the open loop frequency response function $L_0(i\omega)$ in rad

PM^{-}	=	phase margin for a closed loop system with the open loop frequency response function $L(i\omega)$ at the negative crossover frequency ω_{cg}^{-} in rad
PM^{+}	=	phase margin for a closed loop system with the open loop frequency response function $L(i\omega)$ at the positive crossover frequency ω_{cg}^{+} in rad
r	=	variable, a radial coordinate or radius in polar coordinate system in m
r_1	=	variable in s^{-1}
r_{ss}	=	variable, the steady state of r in m
$\dot{r}_{ss}$	=	variable, the steady state of $\dot{r}$ in m/s
s	=	the Laplace transform variable s
$s_{1,2,3,4}$	=	roots of characteristic polynomial $f(s)$ with respect to s
t	=	variable, time in s
t_1	=	variable, time in s
t_2	=	variable, time in s
t_s	=	settling time in s
T	=	time constant in s, $T > 0$
T_1	=	time constant in s, $T_1 > 0$
T_2	=	time constant in s, $T_2 > 0$
T_c	=	time constant in s, $T_c > 0$
T_{φ}	=	time constant in s, $T_{\varphi} > 0$
$T_{\varphi 1}$	=	time constant in s, $T_{\varphi 1} \geq 0$
u_{1p}	=	complex variable, control

u_{1y}	=	variable, control in m/s^2
u_{1z}	=	variable, control in m/s^2
u_r	=	variable, control in m/s^2
u_p	=	complex variable, control
u_y	=	variable, control of the y-channel in m/s^2
u_z	=	variable, control of the z-channel in m/s^2
u_φ	=	variable, control in $(m.rad)/s^2$
u_ψ	=	variable, control in rad/s
$V(x, y, \dot{x}, \dot{y})$	=	positive definite function
V_M	=	missile velocity in m/s
$W(s)$	=	transfer function
y	=	variable, missile deviation on y-axis of the picture plane in m
$y(0)$	=	initial condition on y in m
y_0	=	value of the initial condition on y in m
$\dot{y}(0)$	=	initial condition on the first derivative of y in m/s
y_{10}	=	value of the initial condition on the first derivative of y in m/s
z	=	variable, missile deviation on z axis of the picture plane in m
$z(0)$	=	initial condition on z in m
z_0	=	value of the initial condition on z in m
$\dot{z}(0)$	=	initial condition on the first derivative of z in m/s
z_{10}	=	value of the initial condition on the first derivative of z in m/s
$\dot{\beta}_{LOS}$	=	angular velocity of azimuth angle of the line-of-sight in rad/s

$\ddot{\beta}_{LOS}$	=	angular acceleration of azimuth angle of the line-of-sight in rad/s^2
γ	=	parameter in rad
γ_0	=	constant parameter in rad
γ_1	=	variable in rad
γ_{10}	=	initial condition on γ_1 in rad
γ_{1ss}	=	variable, the steady state of γ_1 in rad
γ_{cr}	=	critical crossover value of the parameter γ_0 in rad
Δt_j^A	=	the length of the jth time of stay in the area A – within the ε_r area in s
Δt_j^{AC}	=	in case there is crossing the ε_r area boundary from inside by the system trajectory then the length of the jth time interval of stay within the ε_r area till crossing this boundary is defined as $\Delta t_j^{AC} = \Delta t_j^A$ in s
Δt_{sum}^{AC}	=	the summary time of stays Δt_{j-1}^{AC} with next crossing the ε_r area boundary in s
Δt_j^B	=	the length of the jth time of stay in the area B – outside the ε_r area in s
Δt_j^{BC}	=	in case there is crossing the ε_r area boundary from outside by the system trajectory then the length of the jth time interval of stay outside the ε_r area till crossing this boundary is defined as $\Delta t_j^{BC} = \Delta t_j^B$ in s
Δt_{sum}^{BC}	=	the summary time of stays outside the predetermined ε_r area in s
ε_r	=	positive parameter in m
ξ	=	damping ratio, non-dimensional, $\xi \in (0, 1)$

φ	=	variable, an angular coordinate or polar angle in polar coordinate system in rad
φ_1	=	variable in rad/s
φ_{1r}	=	variable, index of disproportionality in m^2/s
φ_{1ss}	=	variable, the steady state of φ_1 in rad/s
$\dot{\varphi}_0$	=	initial condition on the first derivative of the polar angle φ in rad/s
$\varphi(\omega)$	=	phase function of the frequency response function $L(i\omega)$ in rad
$\varphi_0(\omega)$	=	phase function of the frequency response function $L_0(i\omega)$ in rad
ψ	=	variable in rad
ψ_{ε_r}	=	the value of ψ at the boundary of the ε_r area outside it when $r \to \varepsilon_r$ in rad
ψ_{ss}	=	variable, the steady state of ψ in rad
ω	=	frequency in rad/s,
ω_{1_π}	=	frequency, the frequency (8.37), at which the phase function $\varphi(\omega) = \pi$ and the plot of the frequency response function $L(i\omega)$ intersects the negative part of the real axis in the complex plane in the point C_1 (8.39), in rad/s
$\omega_{1_{-\pi}}$	=	frequency, the frequency (8.48), at which the phase function $\varphi(\omega) = -\pi$ and the plot of the frequency response function $L(i\omega)$ intersects the negative part of the real axis in the complex plane in the point D_1 (8.50), in rad/s
ω_{2_π}	=	frequency, the frequency (8.38), at which the phase function $\varphi(\omega) = \pi$ and the plot of the frequency response function $L(i\omega)$ intersects the negative part of the real axis in the complex plane in the point C_2 (8.40), in rad/s

$\omega_{2_{-\pi}}$	=	frequency, the frequency (8.49), at which the phase function $\varphi(\omega) = -\pi$ and the plot of the frequency response function $L(i\omega)$ intersects the negative part of the real axis in the complex plane in the point точката D_2 (8.51), in rad/s
ω_{cg_0}	=	frequency, the gain crossover frequency for the frequency response function $L_0(i\omega)$ in rad/s
ω_{cg}^{-}	=	frequency, the negative gain crossover frequency for the frequency response function $L(i\omega)$ in rad/s
ω_{cg}^{+}	=	frequency, the positive gain crossover frequency for the frequency response function $L(i\omega)$ in rad/s
Ω	=	frequency in rad/s
(X_L, Y_L, Z_L)	=	LOS frame

BIBLIOGRAPHY

[1]	Blakelock, J. H., *Automatic control of aircraft and missiles*, Wiley-Interscience, 1991.
[2]	Neupokoev, F. K., *Shooting by anti-aircraft missiles,* Voennoe izdatelstvo, Moskow, 1991, (in Russian).
[3]	Siouris, G. M., *Missile Guidance and Control Systems*, Springer-Verlag New York, 2004.
[4]	Shneydor, N. A., Missile Guidance and Pursuit: Kinematics, Dynamics and Control, Horwood Publishing, 1998.
[5]	Ha, I.-J., Chong, S., “Design of a CLOS Guidance Law via Feedback Linearization,” *IEEE Trans. Aerosp. Electron. Syst.*, Vol. 28, Issue 1, 1992, pp. 51-63. doi: 10.1109/7.135432
[6]	Penev, B. G., “Variant of a system for automatic control of antitank guided missile in polar coordinates,” *Proceedings of Conference “Weapons and military equipment of the year 2000”*, Conference of the Military Scientific and Technological Institute of the Ministry of Defense, 18-20 December 1995, Sofia, Vol. 1 "Weapons, ammunition and surveillance devices", 1995, pp. 54-56. (in Bulgarian) Available on URL: http://e-university.tu-sofia.bg/e-publ/search-det.php?id=2556
[7]	Penev, B. G., Lashnev, A. T., Iliev, I. Ya., “Control of the vector of normal acceleration of anti-tank guided missile in pseudo-polar coordinates,” *Proceedings of Jubilee Conference ”120 years of the April Uprising” of the*

	Higher Air Force School, Dolna Mitropoliya, 22-23 May 1996, Vol. 1 "Aviation and Aerospace", 1996, pp. 336-342. (in Bulgarian) Available on URL: http://e-university.tu-sofia.bg/e-publ/search-det.php?id=2587
[8]	Penev, B. G., "Two-dimensional closed loop control system of an anti-tank guided missile with nonlinear control in pseudo-polar coordinates," *Scientific Session "Prospects for the Development of Armaments and Equipment" of the Military Scientific and Technological Institute of the Ministry of Defence*, Scientific direction #1 - "Weapons, ammunition and surveillance devices", 17-19 December 1997, Sofia. (in Bulgarian)
[9]	Pastrick, H. L., Seltzer, S. M., Warren, M. E., "Guidance Laws for Short-Range Tactical Missiles," *Journal of Guidance, Control, and Dynamics*, Vol. 4, No. 2, 1981, pp. 98-108. doi: 10.2514/3.56060
[10]	Guerchet, P., Estival, J. L., "Line of Sight Guidance Law by Predictive Functional Control for High Velocity Short-Range Tactical Missile," *Proceedings of the European Control Conference 1991,* July 2-5, 1991, Grenoble, France, Vol. 2, pp. 1759-1764.
[11]	Huang, J., Lin, C.-F., "A modified CLOS guidance law via right inversion," *IEEE Trans. Aerosp. Electron. Syst.*, Vol. 31, 1995, pp. 491-495. doi: 10.1109/7.366334
[12]	Lin, C-M., Hsu, C-F., "Guidance Law Design by Adaptive Fuzzy Sliding-Mode Control," *Journal of Guidance, Control, and Dynamics*, Vol. 25, No. 2, 2002, pp. 248-256. doi: 10.2514/2.4905
[13]	Menon, P. K. A., Duke, E. L., "Time-optimal aircraft pursuit evasion with a weapon envelope constraint," *Journal of Guidance, Control, and Dynamics*, Vol. 15, No. 2, March 1992, pp. 448-456.

	doi: 10.2514/3.20856
[14]	Nobahari, H., Pourtakdoust, S. H., “Optimal Fuzzy CLOS Guidance Law Design Using Ant Colony Optimization,” *Lecture Notes in Computer Science*, Vol. 3777 LNCS, 2005, pp. 95-106. doi: 10.1007/11571155_10
[15]	Nobahari, H., Pourtakdoust, S. H., “An optimal-fuzzy two-phase CLOS guidance law design using ant colony optimization,” *Aeronautical Journal*, Vol. 111, Issue 1124, 2007, pp. 621-636.
[16]	Yamasaki, T., Balakrishnan, S. N., Takano, H., "Modified Command to Line-of-Sight Intercept Guidance for Aircraft Defense," *Journal of Guidance, Control, and Dynamics*, Vol. 36, No. 3, 2013, pp. 898-902. doi: 10.2514/1.58566
[17]	Ratnoo, A., Shima, T., "Line of Sight Guidance for Defending an Aircraft," *AIAA Guidance, Navigation, and Control Conference,* 02 August 2010 - 05 August 2010, Toronto, Ontario, Canada, 2010. doi: 10.2514/6.2010-7877
[18]	Tsalik, R., Shima, T., "Inscribed Angle Guidance," *Journal of Guidance, Control, and Dynamics*, Vol. 38, No. 1, January 2015, pp. 30-40. doi: 10.2514/1.G000468
[19]	Cho, N., Kim, Y., Park, S., "Three-Dimensional Nonlinear Differential Geometric Path-Following Guidance Law," *Journal of Guidance, Control, and Dynamics*, Vol. 38, No. 12, December 2015, pp. 2366-2385. doi: 10.2514/1.G001060
[20]	Elhalwagy, Y. Z., Tarbouchi, M., “Fuzzy logic sliding mode control for command guidance law design,” *ISA Transactions*, Vol. 43, 2004, pp. 231-242.

[21]	Elhalwagy, Y. Z., “Guidance Law Design Using Intelligent Non-Linear Controller,” *13th International Conference on AEROSPACE SCIENCES & AVIATION TECHNOLOGY (ASAT- 13),* May 26 - 28, 2009, Military Technical College, Kobry Elkobbah, Cairo, Egypt, 2009, Paper: ASAT-13-CT-32.
[22]	Sadeghinasab, E., Koofigar, H. R., Ataei, M., “Design of robust command to line-of-sight guidance law: A Fuzzy adaptive approach,” *Journal of Engineering Science and Technology*, Vol. 11, No. 11, 2016, pp. 1528-1542.
[23]	Alrawi, A. A. A., Graovac, S., Ahmad, R. B., Rahman, M. M., “Modified guidance law based on a sliding mode controller for a missile guidance system,” *Tehnički vjesnik*, Vol. 23, No. 3, 2016, pp. 639-646. doi: 10.17559/TV-20130625173047
[24]	Zaidi. H., Wu, P., Bellahcene, A., “Missile Guidance Law Design via Backstepping Technique,” *International Journal of Engineering and Applied Sciences*, Vol. 3, Issue 4, 2016, pp. 85-90.
[25]	Yanushevsky, R. T., “Generalized Missile Guidance Laws against Maneuvering Targets,” *Proceedings of 25th Congress of the International Council of the Aeronautical Sciences,* Hamburg, Germany, 3-8 September 2006, Vol. 5, 2006, pp. 3043-3050.
[26]	Davies, D. R., “Line of sight missile guidance”, U.S. Patent 4750688, Issued June 14, 1988.
[27]	Shipunov, A. G., Morozov, V. I., Petrushin, V. V., "Method of Control Signal Forming for Double-Channel Rocket Rotating Around Longitudinal Axis," Russian Federation Patent RU 2511610 C1, Issued 10.04.2014 Bull. 10.
[28]	Gusev, A. V., Morozov, V. I., Nedosekin, I. A., Minakov, V. M., Tarasov, V. I., “Method of beam control over rolling missile and beam-controlled rolling missile”, Russian Federation Patent RU 2460966 C1, Issued March 14, 2011.

[29]	Mandić, S., Stojković, S., Milenković, D., Milošević, M., “Aerodynamic Compensation of the Modified Guided Anti-Tank Missile Configuration,” *Scientific Technical Review*, Vol. 64, No. 1, 2014, pp. 3-12.
[30]	Pavic, M., Mandic, S., Cuk, D., Pavkovic, B., "A new type of flight simulator for manual command to line-of-sight guided missile," *Optik - International Journal for Light and Electron Optics*, Vol. 125, Issue 21, November 2014, pp. 6579-6585. doi: 10.1016/j.ijleo.2014.06.163
[31]	Xin, M., Balakrishnan, S. N., Stansbery, D. T., Ohlmeyer, E.J., “Nonlinear Missile Autopilot Design with Theta - D Technique,” *Journal of Guidance, Control, and Dynamics*, Vol. 27, No. 3, 2004, pp. 406-417. doi: 10.2514/1.1217
[32]	Balakrishnan, S. N., Stansbery, D. T., Evers, J. H., Cloutier, J. R., "Analytical guidance laws and integrated guidance/autopilot for homing missiles," *Proceedings of IEEE International Conference on Control and Applications*, Vol. 1, 1993, pp. 27-32.
[33]	Liu, X., Huang, W., Du, L., Lan, P., Sun, Y., "Three-Dimensional integrated guidance and control for BTT aircraft constrained by terminal flight angles," *Proceedings of the 2015 27th Chinese Control and Decision Conference, CCDC 2015,* May 23 - 25, 2015, Qingdao Haiqing Hotel, Qingdao, China, Session SatA04: Nonlinear Systems (I). doi: 10.1109/CCDC.2015.7161675
[34]	Levy, M., Shima, T., Gutman, S., "Linear Quadratic Integrated Versus Separated Autopilot-Guidance Design," *Journal of Guidance, Control, and Dynamics*, Vol. 36, No. 6, 2013, pp. 1722-1730. doi: 10.2514/1.61363
[35]	White, B., Zbikowski, R., Tsourdos, A., "Direct Intercept Guidance using Differential Geometry Concepts," AIAA Guidance, Navigation, and Control

	Conference and Exhibit, Guidance, Navigation, and Control and Co-located Conferences, 2005. doi: 10.2514/6.2005-5969
[36]	White, B, Zbikowski, R., Tsourdos, A., "Direct Intercept Guidance using Differential Geometry Concepts," *IEEE Transactions on Aerospace and Electronic Systems*, Vol. 43, Issue 3, July 2007, pp. 899-919. doi: 10.1109/TAES.2007.4383582
[37]	Li, D., Poh, E.K., "Nonlinear integrated steering and control of flight vehicles," *Guidance, Navigation, and Control Conference and Exhibit*, 1998. doi: 10.2514/6.1998-4210
[38]	Balakrishnan, S. N., "Analytical missile guidance laws with a time-varying transformation," *Journal of Guidance, Control, and Dynamics*, Vol. 19, No. 2, March 1996, pp. 496-499. doi: 10.2514/3.21646
[39]	Balakrishnan, S. N., Tsourdos, A., and White, B. A., *Advances in Missile Guidance, Control, and Estimation,* CRC Press, 2016.
[40]	Taur, D., "Nonlinear Guidance and Navigation of a Tactical Missile with High Heading Error," *AIAA Guidance, Navigation, and Control Conference and Exhibit (2002),* 05 August 2002 - 08 August 2002, Monterey, California, 2002. doi: 10.2514/6.2002-4773
[41]	Khruslov, V. N., Feofilov, S. V., Goryachev, O. V., Lavit, I. M., and Indyukhin, A. F., "Missile Control in the Polar Coordinate System Using a Scalar Radius," *Gyroscopy and Navigation*, Vol. 6, No. 1, 2015, pp. 66-72. doi: 10.1134/S207510871501006X
[42]	Pontryagin, L. S., and Lohwater, A. J., *Ordinary Differential Equations*, Addison-Wesley Publishing Company, 1962.

[43]	Besekerskiy, V. A., Popov, E. P., *Theory of automatic control systems*, Professiya, Moscow, 2003, (in Russian).
[44]	Khalil, H. K., *Nonlinear systems*, 2nd ed., Prentice Hall, 1996.
[45]	Харитонов, В. Л., “Об асимптотической устойчивости положения равновесия семейства систем линейных дифференциальных уравнений”, Дифференц. уравнения, 14:11 (1978), 2086-2088. Kharitonov, V. L., "Asymptotic stability of an equilibrium position of a family of systems of linear differential equations" Differentsial'nye Uraveniya , Vol. 14, No. 11, 1978, pp. 2086-2088, (In Russian).
[46]	Åström, K. J. and Murray, R. M., *Feedback Systems,* Princeton University Press, Princeton, New Jersey 08540, 2009, ISBN-13: 978-0-691-13576-2.
[47]	Бабаков, Н. А., Воронов, А. А., Воронова, А. А. и др., *Теория автоматического управления. Ч. I. Теория линейных систем автоматического управления.* Высшая школа, Москва, 1986.
[48]	Цыпкин, Я. З., *Основы теории автоматических систем.* Наука, Москва, 1977.
[49]	Penev, B. G., “An Expanded Two-Dimensional Proportional-Derivative Command to Line-of-Sight Guidance Law,” *Gyroscopy and Navigation*, ISSN 2075-1087, Vol. 9, No. 4, pp. 344-351, 2018. DOI: 10.1134/S2075108718040132 Online access to the article has been shared by the author via Springer Nature Sharedit. Please use the following Sharedit link: https://rdcu.be/bfM3Z
[50]	Пенев, Б. Г., „Расширенное двухмерное пропорционально-дифференциальное командное наведение по линии визирования“, *Гироскопия и навигация*. Том 26, № 4 (103), 2018, стр. 58-71. DOI 10.17285/0869-7035.2018.26.4.058-071

9 786199 138212